NASA/CR—1999-208875

NSL–RPT–98–002

Hybrid Active/Passive Jet Engine Noise Suppression System

C.A. Parente and N. Arcas
Northrop Grumman Corporation, Bethpage, New York

B.E. Walker and A.S. Hersh
Hersh Acoustical Engineering, Inc., Westlake Village, California

E.J. Rice
E.J. Rice Consulting, Westlake, Ohio

Prepared under Cooperative Agreement NCC3–379

National Aeronautics and
Space Administration

Lewis Research Center

February 1999

Available from

NASA Center for Aerospace Information
7121 Standard Drive
Hanover, MD 21076
Price Code: A09

National Technical Information Service
5285 Port Royal Road
Springfield, VA 22100
Price Code: A09

FOREWORD

This final report covers the work performed under a National Aeronautics and Space Administration (NASA) Contract No. NCC3-379 for the period February 10, 1995 through February 10, 1997. The work was accomplished by Advanced System & Technology (AS&T) of Northrop Grumman Corporation (NGC), Bethpage, New York, and its team members, Hersh Acoustical Engineering (HAE), Inc. of Westlake Village, California and E. J. Rice Consulting of Westlake, Ohio under the sponsorship of a NASA Aerospace Industry Technology Program Cooperative Agreement.

The work was administered under the technical direction of Mr. Dennis Huff, NASA Lewis Research Center (LeRC) Contracting Officer Technical Representative. Mr. Wayne Girard, LeRC, was the NASA Contract Adminstrator.

Dr. B. E. Walker, VP of HAE was responsible for the design and fabrication of the active control hardware/software components. He was also responsible for conducting the active control ANC and ADP test programs at LeRC. Dr. E. J. Rice of E. J. Rice Consulting was responsible for the design of the passive liner. He was also responsible for conducting the passive ANC and ADP test programs. Mr. M. J. Peter and Mr. C. Weizenecker of NGC were responsible for the structural design and fabrication of the passive components. Mr. C. Parente of NGC was the overall Program Manager responsible for coordinating all the fabrication and test activities. The key personnel associated with the program, and their areas of responsibility include:

- Northrop Grumman Corporation (Team Lead)

C. Parente	Program Manager
N. Arcas	Acoustic Analysis/Test
M. Peter	Structural Design
C. Weizenecker	Materials & Process
C. Auer	Tooling Design
J. Nardiello	Metallic Forming
W. Oelcher	Lead Composite Technican
R. Zambito	Comp. Technician/System Installation
A. Madden	Composite Technician
J. Martorana	Composite Technican

- Hersh Acoustical Engineering, Inc.

Dr. Alan S. Hersh	Program Coordinator/System Integration
Dr. B. Walker	Active/Software Design
J. Celano	Hardware Fabrication
M. Spencer	DSP Programmer

- E. J. Rice Consulting

E. J. Rice	Passive Liner Design

- NASA Lewis Research Center

D. L. Huff	AITP Technical Representative
L. J. Heidelberg	ANCF/ADP Research Coordinator
D. Sutliff	ANCF Research Coordinator
W. Grosser	ADP Operations Engineer
L. Bartos	ADP Operations Engineer
B. Fite	ADP Test Coordinator
D, Elliott	ADP Data Acquisition
S. Wnuk	ANCF Operations Engineer

CONTENTS

Section		Page
1	**INTRODUCTION & SUMMARY**	1
	1.1 Introduction	
	1.1.1 AITP Program and Goals	1
	1.1.2 Background	1
	1.1.3 Proposed Concept	2
	1.1.4 Organization of the Report	3
	1.2 Summary	4
2	**PASSIVE SEGMENTED LINERS**	7
	2.1 Overview of Passive Segmented Liner Concept	7
	2.2 Rice Optimized Impedance Design Code	9
	2.2.1 Eigenvalue Calculation for Attenuating Liner Sections	9
	2.2.2 Segmented Circular Duct Sound Propagation Theory	11
3	**THEORY AND DESIGN OF ACTIVE CONTROL SYSTEM**	13
	3.1 Eigenvalue Decomposition Hardware/Software	13
	3.1.1 Cylindrical Modes	13
	3.1.2 Rotor/Stator Tones - Spinning Waves	13
	3.1.3 Stationary Components of Spinning Waves	14
	3.1.4 Circumferential Mode Separation	14
	3.1.5 Mode Aliasing	15
	3.1.6 Radial Mode Separation	15
	3.1.7 Active Mode Excitation	16
	3.2 Actuator/Noise Source Mode Interaction	16
	3.3 Active Control Actuators and Active Resonators	17
	3.4 Active Control Algorthms	18
	3.4.1 Multi-Channel Filtered X Algorithm	18
	3.4.2 Adaptive Quadrature Algorithm	18
4	**CONCEPT VALIDATION IN NASA LeRC ANCF FAN TEST FACILITY**	21
	4.1 HAE No Flow Calibration Tests	22
	4.1.1 Test Apparatus	22
	4.1.2 Microphone Array Tests	23
	4.1.3 Uniform and Segmented Liner Designs	23
	4.1.4 Passive Liner Insertion Loss Tests	27
	4.1.5 Active and Active/Passive Hybrid Liner Insertion Loss Tests	27
	4.2 ANCF Fan Test Program	28
	4.2.1 ANCF Test Facility	28
	4.2.2 Transducer Array Descriptions	29
	4.2.3 Data Acquisition System	30
	4.2.4 Applied Active Control Alogorithms and Signal Processing	31

Section		Page
	4.2.5 ANCF Acoustic Liner Design	32
	4.2.6 ANC Barrel Fabrication	33
	4.2.7 Modal Measurement Results and Phase Translation	34
	4.2.8 Initial Estimate of ANCF Passive Suppressor Performance	36
	4.2.9 Test Results	36
	4.2.10 Additional Comments	39
5	**CONCEPT VALIDATION IN NASA LeRC 9x15 LOW SPEED WIND TUNNEL FACILITY USING THE ADP FAN**	**43**
	5.1 ADP Test Facility	43
	5.2 ADP Inlet Suppressor Design and Construction	44
	5.2.1 Acoustic Liner Design	44
	5.2.2 Barrel Fabrication	45
	5.3 Data Acquisition System	46
	5.4 ADP Measurement Program	49
	5.5 Modal Phase Measurements and Translation With Position	51
	5.6 Test Results	51
	5.6.1 In-Duct Measurements	51
	5.6.2 Far-Field Radiation Considerations	53
6	**COMMERCIALIZATION OF HYBRID LINER CONCEPT**	**55**
	6.1 Commercialization Plan Summary	55
	6.2 Commercial Product or Service	56
	6.3 Market Assessment	57
	6.4 Aircraft Certification Requirements	59
	6.5 Environmental Requirements	59
	6.6 Development Tasks	60
	6.7 Development Schedule	61
	6.8 Development Task Summary	59
7	**ORGANIZATION DESCRIPTION & VENTURE MANAGEMENT**	**63**
	7.1 Financial Plan	64
8	**REFERENCES**	**65-66**
9	**ILLUSTRATIONS**	**69-142**
A	**APPENDIX A – REVIEW OF ACTIVE HELMHOLTZ RESONATOR CONCEPT**	**143**
	A.1 Basic Concept	143
	A.2 Experimental Validation of the Active Resonator Concept	144
	A.2.1 Anechoic Termination Demonstration	144
	A.2.2 Side-Branch Demonstration	146

ILLUSTRATIONS

Fig.		Page
1.1	Simplified Diagrams of Engine Nacelle, Showing Development of the Adaptive Segmented Liner Concept	69
2.1	Schematic Model of the Axial Segmented Liner	70
3.1a	Radial Pressure Distributions of Modes (-9,0) and (-9,1) and Least Favorable Combination for Interaction with Wall Mounted Passive Treatment	71
3.1b	Radial Pressure Distributions of Modes (-9,0) and (-9,1) and Most Favorable Combination for Interaction with Wall Mounted Passive Treatment	72
3.1c	Ratio of Wall Pressure to Space-Average Sound Pressure vs. Amplitude Ratio and Phase Difference Between Modes (-9,0) and (-9,1)	73
3.2	Active Resonator and Actuator Mounting Detail for Active Segment of Adaptive Segmented Liner in ANCF Test Typical of 32 Spaced 4.5 inches Axially and 22.5° Azimuthally	74
3.3a, b	Amplitude and Phase Response and Deviations for Actuators Used in ANCF Adaptive Segmented Liner Tests	75
4.1	Schematic Diagram of HAE 24-inch Duct for Testing Prototype Liners at Modes (1,0) and (1,1)	76
4.2a, b	HAE Spinning Mode Rig With Test Barrel Installed	77
4.3	Theoretical Sound Pressure Distributions of Radial Modes in HAE, ANCF and ADP Ducts	78
4.4	Optimum Impedance Determination for Uniform Liner HAE 2	79
4.5	Attenuation Sensitivity of Liner 2 of Two Segment Liner HAE 3 Liner 1 Impedance Fixed at 0.076-i1.171	80
4.6	Attenuation Sensitivity of Liner 1 of Two Segment Liner HAE 3 Liner 2 Impedance Fixed at 0.49-i0.34	81
4.7	Attenuation Spectra for Uniform and Two Segment Optimized for 1,050 Hz, D=24.125 inches, HAE No Flow Tests	82
4.8	Attenuation Spectra for Two Segment Liner HAE 3 Showing Effect of Second Radial Mode Phase	83
4.9	Cutaway Diagram of Hybrid Liner Installation on NASA/LeRC ANCF Fan	84
4.10	Hybrid Active/Passive Barrel Installed on the ANCF Rig at NASA LeRC	85
4.11	Rear View of ANCF Rig Located in the NASA LeRC Anechoic Dome	86
4.12a, b	Acoustic Actuator for the ANC and the ADP Test	87
4.13	Schematic Diagram of Active/Passive Segmented Liner Measurements at NASA LeRC ANCF Facility	88
4.14	Optimum Impedance Determination for Uniform Liner ANC 1	89

Fig.	ILLUSTRATIONS (Cont.)	Page
4.15	Attenuation Sensitivity of Liner 2 of Two Segment Liner ANC 2 Liner 1 Impedance Fixed at 0.554-i1.914	90
4.16	Attenuation Sensitivity of Liner 1 of Two Segment Liner ANC 2 Liner 2 Impedance Fixed at 0.788-i0.522	91
4.17	Measured Phase Difference Between the (4,1) and (4,0) Modes Inlet Rake Transducers at 33.94 Inches Ahead of Rotor Tip Leading Edge	92
4.18	Measured Modal Coefficient Magnitude of the (4,0) and (4,1) Modes Inlet Rake Transducers at 33.94 Inches Ahead of Rotor Tip Leading Edge	93
4.19	Phase Difference Between the (4,1) and the (4,0) Modes Estimated at the Beginning of the Acoustic Liner	94
4.20	Phase Difference Between the (4,1) and the (4,0) Modes at the Inlet Lip Probe Location; Measured and Projected	95
4.21	Calculated Attenuation of Inlet Acoustic Liners at 2BPF for All Three Inlet Passive Acoustic Treatments, NASA ANC Fan Stage	96
4.22	Calculated Attenuation of Inlet Acoustic Liners at 2BPF for All Three Inlet Passive Acoustic Treatments, NASA ANC Fan Stage	97
4.23	Calculated and Experimental Attenuation of Inlet Two Segment Passive Acoustic Liner ANC 2 at 2BPF, NASA ANC Fan, 16 Blades With 14 Rods	98
4.24	Calculated and Experimental Attenuation of Inlet Two Segment Passive Acoustic Liner ANC 2 at 2BPF, NASA ANC Fan, 16 Blades With 14 Rods	99
4.25	Measured Modal Coefficient Magnitude of the (4,0) and (4,1) Modes Inlet Rake Transducers Near Inlet Lip	100
4.26	Measured Modal Acoustic Attenuation of the Three ANC Liners at 2BPF NASA ANC Fan Stage	101
4.27	Far-Field Noise Directivity, Baseline and Two-Segment Liner	102
4.28	Far-Field Noise Attenuation for the Two-Segment Passive Liner NASA Lewis ANC Fan Stage, Tone at Twice Blade Passage Frequency	103
4.29	Far-Field Noise Attenuation for Hybrid Active/Passive Liner NASA Lewis ANC Fan Stage, Tone at Twice Blade Passage Frequency	104
4.30	Far-Field Noise Directivity, Hardwall Baseline	105
4.31	Ratios of Mode (4,1) to (4,0) Amplitudes in NASA/LeRC ANCF Fan Inlet as Measured with NASA Rotating Rake and HAE Flush Mounted Microphone Arrays	106
4.32	Differences of Mode (4,1) to (4,0) Phases in NASA/LeRC ANCF Fan Inlet as Measured with NASA Rotating Rake and HAE Flush Mounted Microphone Arrays	106

Fig.	ILLUSTRATIONS (Cont.)	Page
4.33	Comparison of ANCF Baseline Mode Structure of Two Inlet Axial Stations	107
4.34a, b	Comparison of Duct Modes Generated by NGC/HAE Active Liner Segment Upstream and Downstream Actuators with Passive Segment Covered, Fan Stationary	108
4.35a, b	Comparison of Duct Modes in NASA/LeRC ANCF Fan Inlet NGC/HAE Adaptive Segmented Liner, Fan 1886 RPM Control Off vs. Control On	109
4.36a, b	Comparison of Duct Modes in NASA/LeRC ANCF Fan Inlet NGC/HAE Adaptive Segmented Liner, Fan 1886 RPM "Modal" vs. Axial Station Error Microphone Arrays	110
4.37a, b	Comparison of Duct Modes in NASA/LeRC ANCF Fan Inlet NGC/HAE Adaptive Segmented Liner, Fan 1886 RPM Mode (4,0) vs. Mode (4,1) Sensing Error Microphone Arrays	111
4.38a, b	NGC/HAE Adaptive Segmented Liner In-Duct Performance Summary With Passive Segment Covered in NASA/LeRC ANCF Fan Inlet	112
4.39a, b	NGC/HAE Adaptive Segmented Liner In-Duct Performance Summary With Passive Segment Exposed in NASA/LeRC ANCF Fan Inlet	113
4.40	Mode m=4, Insertion Loss Performances of Adaptive Segmented Liner and Its Constituent Elements in NASA/LeRC ANCF 48" Fan Test Facility	114
4.41	Far-Field Forward Directivity of NASA/LeRC ANCF Fan 1886 RPM, Hardwall and NGC/HAE Adaptive Segmented Inlet Liner with Control Off and On	115
4.42	Far-Field Forward Directivity of NASA/LeRC ANCF Fan 1850 RPM, Hardwall and NGC/HAE Adaptive Segmented Inlet Liner with Control Off and On	116
4.43	Far-Field Forward Directivity of NASA/LeRC ANCF Fan 1800 RPM, Hardwall and NGC/HAE Adaptive Segmented Inlet Liner with Control Off and On	117
4.44	Far-Field Forward Directivity of NASA/LeRC ANCF Fan 1750 RPM, Hardwall and NGC/HAE Adaptive Segmented Inlet Liner with Control Off and On	118
4.45a	NASA/LeRC ANCF 48" Fan - Far-Field 0-60 Degree Power Attenuation	119
4.45b	NASA/LeRC ANCF 48" Fan - Far-Field 0-90 Degree Power Attenuation	119
5.1a	View of Hybrid Active/Passive ADP Inlet Mounted for Far-Field Testing in the LeRC 9x15 Wind Tunnel	120
5.1b	ADP Barrel Shown With Acoustic Drivers Mounted Near the Barrel Attachment Flange	121
5.1c	ADP Barrel Mounted on the ADP Engine Core Duct in the LeRC 9x15 Wind Tunnel for Testing	121

Fig.	ILLUSTRATIONS (Cont.)	Page
5.2	Attenuation Contours for Uniform ADP 1 Acoustic Liner 2BPF = 3255 Hz, 5425rpm, mode lobes m=9	122
5.3	Attenuation Contours for Two Segment ADP 2 Liner 2BPF =3255 Hz, 5425 rpm, liner (2) nearest inlet lip is varied here, m=9	123
5.4	Attenuation Contours for Two Segment ADP 2 Liner 2BPF =5425rpm, liner (1) nearest rotor is varied here, m=9	124
5.5	Drawing of the ADP Hybrid Active/Passive Barrel Attached to the ADP Fan Rig	125
5.6a	Schematic Diagram of Dual Active Resonator Actuator Employed in ADP Adaptive Segmented Inlet Liner	126
5.6b	Photograph of an ADP Driver	126
5.7a	ADP Actuator Free Field Sound Pressure Levels	127
5.7b	ADP Actuator Free Field Phase Response	127
5.8	Schematic Diagram of Active/Passive Segment Liner Measurements in P&W ADP Fan	128
5.9	Rotating Rake Installed on the ADP Barrel in the NASA LeRC 9x15 Wind Tunnel	129
5.10a	Circumferential and Radial Mode Sound Powers Produced by NGC/HAE Adaptive Segmented Liner in ADP Fan Inlet with Passive Segment Covered	130
5.10b	Sum of Radial Mode Relative Sound Powers in Circumferential Modes Produced by NGC/HAE Adaptive Segmented Liner in ADP Fan Inlet with Passive Segment Covered	131
5.11a	Circumferential and Radial Mode Relative Sound Powers in ADP Fan Inlet with Hardwall Baseline	132
5.11b	Sum of Radial Mode Relative Sound Powers in Circumferential Modes in ADP Fan Inlet with Hardwall Baseline	133
5.12a	Circumferential and Radial Mode Relative Sound Powers in ADP Fan Inlet with NGC/HAE Adaptive Segmented Liner, Control Off	134
5.12b	Sum of Radial Mode Relative Sound Powers in Circumferential Modes in ADP Fan Inlet with NGC/HAE Adaptive Segmented Liner, Control Off	135
5.10a	Circumferential and Radial Mode Relative Sound Powers in ADP Fan Inlet with NGC/HAE Adaptive Segmented Liner, Control On	136
5.10b	Sum of Radial Mode Relative Sound Powers in Circumferential Modes in ADP Fan Inlet with NGC/HAE Adaptive Segmented Liner, Control On	137

Fig.	ILLUSTRATIONS (Cont.)	Page
5.11	Circumferential Mode m = -9 Sound Power Reduction by Uniform Passive, Segmented Passive, Adaptive Segmented (Control Off) and Adaptive Segmented (Control On) Liners in P&W 22 Inch ADP Fan in NASA/LeRC 9 x 15 Wind Tunnel at Mach 0.1 in the Design (Approach) Speed Range	138
5.15	Calculated and Experimental Attenuation of Inlet Uniform Passive Acoustic Liner NSL960001 at 2BPF	139
5.16	Calculated and Experimental Attenuation of m=-9 Modes Only Segmented Passive Liner	140
5.17	Calculated and Experimental Attenuation of m=-9 Modes Only Hybrid Active/Passive Liner	141
5.18	Tone Protrusion Above Background ADP Hardwall Inlet Far-Field 9x15 Wind Tunnel Tests, Aft Barrier in Place	142
A1	Control Volume Used in Model Derivation of Active Control Helmholtz Resonator Concept	149
A2	Schematic Diagram of Active Control Resonator Calibration Equipment	150
A3	Absorption Coefficient Performance Improvement Achieved With Active Control Resonator	151
A4	Schematic of Active Resonator Side-Branch Attenuation Test Set-up	152
A5	Transmission Loss Performance Improvement Achieved With Side Branch Active Control Resonator	153

TABLES

No.		Page
2.1	Effect of Wall Boundary Condition on Mode Propagation Angle	8
4.1	Summary of HAE/ANCF Experimental Program Test Matrix	21
4.2	NASA/AITP Demonstration Summary	21
4.3	Summary of Mode Generation and Separation Using Inner/Outer Array Synthesizer and Axially Spaced Wall Microphones	23
4.4	HAE Barrel Acoustic Impedance Data	26
4.5	Summary of Active/Passive Treatment Measurements in HAE Duct Facility	28
4.6	Parameters of the NASA ANCF Fan Test Rig Facility	29
4.7	ANC Test Barrel Acoustic Impedance Data	34
5.1	ADP Barrel Acoustic Impedance Values	46
5.2	Summary of Experimental ADP Program Test Matrix	49
6.1a	Total Aircraft in Service	57
6.1b	New Aircraft To Be Manufactured	58
6.1c	Aircraft Forecast	58
6.2	New Aircraft Sales Forecast	58
6.3	Hybrid Suppressor Estimated Development Schedule	61
6.4	Hybrid Active/Passive Development Tasks	62
7.1	Commercialization Cost Estimate	63

1 – INTRODUCTION

1.1 INTRODUCTION

1.1.1 AITP Program and Goals

The Aerospace Industry Technology Program (AITP) was established by the National Aeronautics and Space Administration (NASA) to promote industry research and development ideas and efforts that would focus on dual-purpose aerospace technologies and concepts that have a potential for commercial application. The goal of the AITP program is to "strengthen US industry by advancing high-payoff aerospace technologies defined by industry that will lead to important commercial products and applications in U. S. industries and may significantly support future NASA missions". Grumman Aerospace Corporation (GAC), a subsidiary of the Northrop Grumman Corporation (NGC), as the project lead and its team members, E. J. Rice Consulting (EJR) and Hersh Acoustical Engineering, Inc. (HAE) proposed an innovative program for the development and demonstration of a hybrid active/passive acoustic technology for commercial jet aircraft nacelles. The project titled "Adaptive and Improved Passive Acoustic Suppression of Aircraft Engines" was a two year cost share program that encompassed the investigation of two mutually synergistic technologies of active and passive suppression of turbofan engine noise and was awarded NASA Cooperative Agreement No. NCC3-379. The team coupled the engine liner design and manufacturing expertise of NGC with a team capable of producing the technology for developing the next generation of engine noise suppressors. The end objective was to apply this new innovative technology to achieve the goals, set by NASA, to reduce commercial aircraft noise by the turn of the century. The goals of this program are:

(1) Developing the analytical, manufacturing, and numerical tools to design efficient sound absorbing axially segmented liners,

(2) Validating the hybrid active/passive concept by measuring the performance of candidate axially-segmented liners in laboratory tests at HAE, the Active Noise Control Fan (ANCF) Facility at Lewis Research Center (LeRC) and the ADP fan rig in the NASA LeRC 9' x 15' Wind Tunnel.

1.1.2 Background

The proposed advanced liner nacelle concept was motivated by the excessive and annoying noise to which communities located adjacent to commercial airports are often exposed, from aircraft landing, takeoff and fly-over maneuvers. Recognizing this, NASA has proposed a goal of increasing the efficiency of liner nacelle duct treatment by 25% relative to 1992 technology[1] by the year 2000. It is generally recognized in the aircraft industry that it will be difficult to achieve this using conventional passive liner design technology.

Despite many years of intensive research, jet engine noise remains as one of the major pollution problems facing communities located near military and civilian airports. This is not surprising because the suppression of jet

engine noise is inherently complex, involving the interaction between different physical phenomena such as: (1) radial and spinning modes with three-dimensional flows containing transverse velocity and (in the engine exhaust) thermal gradients which refract the sound, (2) subsonic and supersonic accelerating mean flows, (3) combustion noise and (4) resonance's and natural or forced hydrodynamic and acoustic instabilities. As a consequence of the complexity of these mechanisms and their (nonlinear) interactions, very few "practical" guidelines have evolved to allow the engine designer to predict, let alone control, jet engine noise inlet and exhaust noise in a given design.

The control of jet engine noise is often confronted empirically in the hardware test and development phase by installing arrays of passive sound absorbing liners consisting of fine wire-mesh screens bonded to cavity-backed perforates (i.e., Helmholtz resonators). The need to improve aircraft performance and efficiency while decreasing community noise taxes the acoustic suppression capability of the sound absorbing treatment that line the ducts of turbofan engines. New ultra-high-bypass engines with shorter inlet and exhaust ducts have even less room for acoustic treatment. Thus, more effective treatment is required than is currently available. Much of the treatment used currently has a very limited frequency range over which it is effective; thus multiple areas of treatment are required to address noise in extended frequency ranges. If the treatment could be effective for several or all frequency components simultaneously, then all of the treatment area would be available for each component.

1.1.3 Proposed Concept

The objective of this research program is to assess the potential and practicality of developing the hybrid active-passive sound absorbing liner concept as a scheme to efficiently attenuate excessive turbofan engine noise. The scheme is based upon the idea of combining the recently developed active noise control Helmholtz resonator concept[2] with the multi-segmented passive liner concept originally developed in the 1970's[3-9] to create a hybrid active-passive sound-absorbing segmented liner system.

The sound absorbing hybrid active-passive liner concept is illustrated in Figure 1.1 for an aircraft inlet. The sound field is represented by a vector normal to the wave-front. For this example the initial sound field radiating from the fan is shown propagating at a very small angle to the duct axis. This sound field represents a nearly plane-wave or for a spinning mode a high mode cut-off ratio sound field. As a simplification, the wave does not experience many encounters with the acoustically treated walls and is not highly attenuated in a short duct. Rice[10] has shown that modification of the boundary conditions at the duct wall can alter the propagation angle for a duct mode and that this propagation angle is intimately related to mode cut-off ratio, attenuation in the duct liner, and the far-field radiation angle[11-13]. In the first configuration of Figure 1.1, the uniform acoustic liner configuration, the nearly axial propagating sound field is shown entering the suppressor. The uniform liner can be optimized for this sound field by the proper choice of honeycomb resonator backing depth

and face sheet resistance properties. Some reasonable sound attenuation might be obtained for this uniform dissipative liner. An improved acoustic liner configuration is illustrated by the second configuration in Figure 1.1, the two-segment liner configuration. The properties of the initial segment are selected to increase the effective angle of propagation of the sound entering the second dissipative liner section. The properly designed two-segment liner can provide improved attenuation over the uniform liner of the same total length. However as discussed in Section 2, this tuned system may provide improved performance only over a narrow range of engine speed around the design point. To overcome this limitation, this initial mode conditioning segment can be replaced by an active driver system configuration as shown in Figure 1.1. This is the advanced hybrid liner concept developed and validated in this research program. The active-passive hybrid suppressor system allows the initial mode conditioning section to adapt to compensate for the varying input sound conditions. The output sound signal is monitored and used in a control system to obtain the desired overall suppression results. In addition to substituting for the initial passive system, the active system can provide additional benefits. Some modal cancellation and reflection may be occurring as well as some dissipation in the active resonator cavities.

The hybrid noise reduction method uses active control techniques not to reflect, cancel or absorb noise, but, instead, to scatter or redistribute energy among modes to maximize the effectiveness of the passive sound absorbing element. Less acoustic energy is needed for input into the engine duct relative to conventional active control schemes because the acoustic energy is only redirecting the sound field, not dynamically interacting with it to cancel or absorb it. In addition, the precision required for matching the amplitude and phase, and the problems inherent with complicated higher-order spinning and radial modes, is reduced. The new concept replaces the passive mode scattering segment with arrays of active control Helmholtz resonators to achieve efficient sound absorption over wide RPM bandwidths! As such, the hardware and software demands will be significantly reduced.

1.1.4 Organization of the Report

The report is organized as follows. Following this Introduction, Sections 2 and 3 describe respectively the theory and design of the passive segmented liner and the corresponding theory and design of the active control system. This is followed in Sections 4 and 5 with summaries of the two experimental programs designed to validate the hybrid liner concept. Section 4 describes the research program conducted in the NASA Lewis Research Center ANCF test facility and Section 5 describes the research program conducted in the NASA Lewis Research Center 9' x 15' Wind Tunnel Facility. Section 6 discusses the commercialization of the hybrid liner concept. Section 7 describes the proposed commercialization organization. The report closes with a detailed explanation of the active control Helmholtz resonator concept, an integral component of the active control system, in Appendix A.

1.2 SUMMARY

In the suppression of noise from turbofan engines, the need to provide attenuation of tones generated by rotor wake/stator vane interaction compromises the basic configuration of the engine and affects the design of broadband sound absorbing liners. A novel *adaptive segmented* liner concept has been developed that employs active control elements to modify the in-duct sound field to enhance the tone-suppressing performance of passive liner elements. This could potentially allow engine designs that inherently produce more tone noise but less broadband noise, or could allow passive liner designs to more optimally address high frequency broadband noise.

A proof-of-concept validation program was undertaken, consisting of the development of an adaptive segmented liner that would maximize attenuation of two radial modes in a circular or annular duct. The liner consisted of a leading active segment with dual annuli of axially spaced active Helmholtz resonators, followed by an optimized passive liner and then an array of sensing microphones. A control algorithm minimized acoustic signals at the sensing microphone array by adjusting the excitation of the active resonators. The active resonators included electro-acoustical actuators designed to satisfy specific requirements of resonator excitation in each phase of the development.

Three successively complex versions of the adaptive liner were constructed and their performances tested relative to the performance of optimized uniform passive and segmented passive liners. These began with static tests in a 24-inch diameter duct excited electro-acoustically with modes (1,0) and (1,1) at a single frequency (1050 Hz). This test demonstrated attenuation well in excess of 40 dB and clear superiority of the adaptive segmented liner over the all-passive liners.

The second test series was conducted in the NASA/LeRC 48-inch diameter Active Noise Control Facility (ANCF) facility, using inlet spoiler rods to generate intense twice blade passage frequency (2-BPF) tones with modes (4,0) and (4,1). Comprehensive tests were conducted over an extended fan speed range 1550 - 1886 RPM, corresponding to a 2BPF frequency of 827 - 1006 Hz. The adaptive segmented liner provided attenuation up to 35 dB and was superior to the all-passive liners with the exception that at the optimized design speed, the segmented passive liner provided equal attenuation. The salient result of the test series was that *the attenuation provided by the adaptive segmented liner exceeded by several dB the sum of the active and passive segments measured separately*, demonstrating a synergism that enhances overall liner performance.

The final test was conducted using the Pratt & Whitney 22-inch Advanced Ducted Propulsor (ADP) fan in the NASA/LeRC 9x15 wind tunnel. The liner was designed to operate at 5450 RPM (approach speed), addressing modes (-9,0) and (-9,1) at 2-BPF. Insertion loss tests were conducted over a fan speed range of 5250 - 8450 RPM, corresponding to frequencies 3150 - 5070 Hz at 2-BPF. The adaptive segmented liner provided up to 19 dB attenuation and outperformed the passive liners over the speed range 5250 -

6225 RPM. At speeds over 6000 RPM the adaptive segmented liner also controlled a third radial mode (-9,2). The salient results of the tests were: *The adaptive segmented liner performed well in a high flow speed model fan inlet environment, was successfully scaled to a high sound frequency and successfully attenuated three radial modes using sensor and active resonator arrays that were designed for a two mode, lower frequency environment.*

2 – PASSIVE SEGMENTED LINERS

This section presents a brief overview of the passive segmented liner design concept that was investigated extensively in the 1970's by industry and NASA. It also describes an optimized impedance liner code recently developed by Dr. E. J. Rice that was used to design the segmented passive liner component of the hybrid liner system.

2.1 OVERVIEW OF PASSIVE SEGMENTED LINER CONCEPT

Ducts with multi-segmented acoustic treatment (often called phased treatment) have been extensively studied in the past. Sawdy et al.[3,4], Patterson et al.[5] Lester and Posey[6,7], Clark[8] and Baumeister[9], investigated semi-infinite rectangular ducts with two dimensional sound fields. Cases with no flow and steady flow in the exhaust duct mode were considered. References 3-5 also included experimental programs to verify the theory. The sound was introduced into the flow duct through an exponential horn in an effort to provide plane wave excitation to the uniform and multi-segmented acoustic liners. Reasonable agreement with theory was obtained in most cases. Where agreement was not good, iterative adjustments in the initial modal structure and the wall impedance provided results in good agreement with the experiments. The adjustments were judged to be within the expected error of the experiment.

Lester and Posey[6,7] investigated circular ducts with multi-sectioned acoustic liners with no steady flow in the duct. Most of the studies were conducted with acoustic inputs of a plane wave or of a point source on the duct axis. Both of course produce axisymmetric excitation. However, one very important additional case was studied using the calculated modal output from a high speed twelve inch fan using a computer code developed by Clark et al.[8]. To our knowledge, this is the only investigation in which an attempt was made to simulate an acoustic input to the uniform and segmented acoustic liners which resemble that of the spinning modes produced by the rotor wake-stator interaction of a fan stage.

All of the above studies showed large potential increases in acoustic attenuation for the segmented ducts over that of a uniform acoustic liner for an intermediate frequency or wavelength range. For the two dimensional rectangular ducts the best potential was at a frequency such that the duct height/sound wavelength was about 1.5. For the round duct, the duct diameter/sound wavelength was about 1.3. For the simulated fan stage modes, a reasonable increase in attenuation for the two and three segment liners (three better than two) over that of the uniform liner occurred even though the fan tone frequency was well out of the optimum range.[6,7]

The above studies also provided conclusions regarding why the segmented acoustic treatment worked well. The optimum initial section always tended toward a purely reactive impedance with very low resistance and thus very little dissipation of sound energy. The conclusion was thus that the first section set up the sound modes for later sections to attenuate. It accomplished this by scattering the sound into radial modes combinations that damp faster in the resistive sections. This is certainly part of the answer, but

as mentioned above, the boundary condition can have a substantial effect on the angle of propagation of each individual mode, which can provide increased attenuation in later sections due to increased angles of propagation relative to the duct axis. The following table provides an example of these propagation angle changes.

Table 2.1 Effect of Wall Boundary Condition on Mode Propagation Angle

Duct Mode	Angle in Hard Wall Duct	Angle in Soft Wall Duct
Four lobe, first radial	28.1°	43.3°
Four lobe, second radial	57.0°	88.6°

The calculations are for the first and second radial modes of the four lobed sound pressure pattern in a round duct. All eigenvalues are real since the wall impedance for the hard duct is infinite and for the soft duct it is zero (pressure release boundary). Notice that the conclusion that increased attenuation, due to scattering into the higher radial modes, is reasonable since even within the hard duct the angle of propagation for the second radial is substantially larger than that of the first radial (57.0° vs. 28.1°), which would result in higher attenuation within the resistive section. Also observe that for each individual mode the angle of propagation is increased resulting in increased attenuation in the resistive section. The combined effect of the modal scattering to higher modes and the increased angle of propagation of each individual mode probably provides the increased attenuation of the segmented liners.

To our knowledge, the last publication on segmented liners was provided by Baumeister[9] in November 1979. He conducted a statistical study in which he introduced substantial variations in the input sound modal structure and the wall impedance of the segmented acoustic liners. The loss in performance of the liners due to these variations and the lack of substantial bandwidth improvement over uniform liners led Baumeister to conclude that the segmented liners were not worth pursuing in spite of the large potential increases in the attenuation for properly designed and tuned liners. About this same time the emphasis in noise reduction research shifted to the advanced turboprop with the emphasis on cabin noise. The turboprop has no surrounding shroud and interest in duct acoustics, uniform or segmented, waned and was discouraged.

We believe that no further progress has been made regarding segmented liners for turbofan ducts. The problem of turbofan community noise has again returned with the proposed ultra-high by-pass turbofan. This configuration presents an increased challenge due to the short ducts (relative to the diameter) which makes it very difficult to provide the required fan noise attenuation with conventional acoustic treatment. The large diameter and

structurally restricted blade number has however brought the duct diameter to sound wavelength ratio closer to the optimum for segmented treatment. In addition, better control of manufacturing tolerances on acoustic treatment can overcome some of the acoustic performance degradation calculated by Baumeister[14]. If additional impedance control is required, the recently developed active resonator concept can be used to provide precise tuning and required tracking of the acoustic impedance as duct conditions change. Also the segmented liner concept has not really been optimized for the spinning modes that might be expected from modern high by-pass turbofan engines.

2.2 RICE OPTIMIZED IMPEDANCE DESIGN CODE

The passive segmented duct acoustic suppressor theory is important here because it is used to design the passive portion of the active-passive hybrid suppressor. During this early stage in the development of the active-passive hybrid suppressor the active section is viewed as replacing the first section of the passive segmented acoustic liner. The first section of the segmented liner is considered as a set-up section that conditions the acoustic input to the passive attenuating section to provide the optimum results as defined by the goal of the suppressor design. This goal may be maximum acoustic power attenuation, as used in this concept verification study, or optimum radiation directivity reduction as might be desired to achieve maximum EPNL reduction. The passive segmented acoustic liner theory is summarized here with the details left to the references. The schematic drawing of the two segment circular duct shown in Figure 2.1 will be used in the following discussion.

2.2.1 Eigenvalue Calculation for the Attenuating Liner Sections

At the heart of any acoustic propagation code for soft wall ducts is the eigenvalue search routine which provides the eigenvalues or characteristic numbers for each of the duct modes. The eigenvalues are complex numbers for these modes in the soft wall duct sections[15] as represented by Liner 1 and Liner 2 in Figure 2.1. Extensive effort was invested in developing an eigenvalue search routine that provides reliable results upon which the rest of the codes depend. If an eigenvalue is missed, the modal system is not complete and the pressure and axial velocity matching across the liner interface will not be correct. Omitting an eigenvalue will cause irregularities of contour plots of attenuation in the impedance plane, which have usually been interpreted as local minima or maxima in papers in the literature. If a double value is inadvertently returned (iteration to the same value from different starting values) the matrix determinant will be zero and the solution will "blow up." Iteration is required since the equations can not be solved explicitly for the eigenvalues given the wall impedance. The wall impedance can be solved explicitly given the eigenvalue. For the no-flow code, a very careful assessment of the wall impedance relative to each mode optimum impedance was made to determine the proper iteration strategy. In some regions of the impedance plane relative

to a particular mode optimum, only one mode should be pursued and a proper starting value for the iteration is provided. In another impedance region, two softwall modes should be pursued which have nearly the same eigenvalue amplitude but different phases. In another region two modes must be pursued which have similar phases but different amplitudes. These wall impedance regions are always relative to the optimum impedance of the particular mode under consideration. The efficient calculation procedure is to have a correlating equation for the optimum eigenvalues from which the optimum impedance can then be immediately calculated to start the iteration for arbitrary wall impedance. This correlation was available for the inlet with no-flow and was used to provide a very efficient calculation procedure.

Another eigenvalue problem had to be considered, that reported by Zorumski and Mason[16]. It is well known that at the optimum impedance for each mode, two modal solutions collapse into one. They have shown that these two functions orthogonal to each other merge into the single solution that is orthogonal to itself. This means that the properly weighted Bessel function squared integral, which is essential in the modal coefficient determination (in the denominator) is equal to zero. Zorumski and Mason have shown that an alternate solution exists with a linear modification to the Bessel function. This concept was checked out by evaluating the Bessel function integrals near the optimum impedance. They are certainly correct; the integral goes to zero as the optimum is approached. However, the impedance must be very close to the optimum for the integral to be very small. Thus rather than going to the alternate solution at the optimum, if the optimum should be inadvertently hit the wall impedance is changed slightly to avoid the problem and still provide two distinct modal solutions which are sufficiently different to allow the calculations to proceed.

The eigenvalue search code for no-flow was tested and found to be very robust. Double value problems were essentially eliminated. The routine works to very high lobe number or Bessel function order, perhaps to m = 70 beyond where we would use it. A double precision complex version has also been written to be consistent with the needs in the matrix inversion process.

For the case of flow in the duct, the eigenvalue calculation is considerably more complex. To properly simulate an aircraft inlet a wall boundary layer must also be considered. As in the no-flow case the wall impedance under consideration is compared to the optimum wall impedance for each mode to determine starting values for the iteration procedure. To accomplish this a new correlation of the optimum wall impedance for an arbitrary mode had to be developed. Four correlations were needed for the amplitude and phase for the two wave directions. The two wave directions are required since upstream and downstream waves behave differently when flow and boundary layers are present and both directions must be considered when reflections are considered. Several thousand optimum impedance calculations were performed and stored to provide data for the required correlations. The parameter space includes Mach number M = 0 to +/-0.6, frequency parameter $\eta \equiv fD/c$ = 1 to 20, boundary layer displacement thickness

to effective wavelength ratio $d^*/[\lambda(1 + M)] = 0$ to 2.5, and boundary layer displacement thickness to duct radius ratio $d^*/r_D = 0$ to 0.2. Some definitions are: frequency f, duct diameter D, speed of sound c, boundary layer displacement thickness d^* and sound wavelength λ. The optimum eigenvalues had to be further refined with an additional iteration to ensure proper convergence for wall impedances that might lie near any mode optimum.

2.2.2 Segmented Circular Duct Sound Propagation Theory

The initial computer code was written to solve the acoustic wave equation in a circular duct with no steady flow. The procedure followed that of Zorumski[17] which considers multiple radial mode input to a multiple segmented soft-wall duct as pictured in Figure 2.1. The multi-segmented duct has up to three finite length soft-wall sections with infinite length hard-wall sections as input and output sections. Up to ten radial modes, for any circumferential lobe number mode, can be input in the first hard-wall section. Up to ten radial modes (same number as chosen for the input section) are carried throughout the remaining sections. In the hard-wall sections, the eigenvalues for the modes are just the zero-slope solutions for the Bessel function. In the soft-wall sections, the eigenvalues are complex as determined by the complex wall impedance equation for each section. The number of duct sections and radial modes can of course be increased if desired, but the numbers chosen here should be sufficient for the present purposes. At each duct interface (hard to soft, soft to soft, soft to hard) continuity of acoustic pressure and axial acoustic velocity are required. This provides sufficient equations to solve for reflected modes in the input hard section, transmitted and reflected modes in all of the intermediate soft-wall sections, and for transmitted output waves in the final hard-wall section. The number of equations and unknown modal coefficients is equal to twice the number of modes times the number of liner interfaces. Thus if ten radial modes are used with two acoustic liners (three interfaces) a 60 by 60 matrix must be inverted to solve for the sixty unknown modal coefficients. Axial acoustic power is calculated on each side of each interface to insure continuity of power across the interface. As mentioned in the previous section, extreme care was exercised in the development of the soft-wall eigenvalue solution programs, which are the heart of the acoustic codes. Iterative procedures are required to solve for these complex eigenvalues. Care must be taken to develop routines that do not produce duplicate eigenvalues which will cause the blow-up of the matrix inversion subroutine, or to miss an eigenvalue which can give a false indication of a local maximum or minimum in the attenuation contours. In spite of this attention to precision, occasionally an eigenvalue is missed. For the results to be shown in this report, the contours are smooth with only one maximum indicated showing that the eigenvalue search routine was successfully negotiated over the impedance range shown.

With the addition of duct flow and the wall boundary layer, the procedure developed by Rice[18] was used. Outside of the boundary layer a uniform flow region is used. The solutions in the uniform flow region are the standard Bessel functions. From the interface of the uniform flow region and the boundary layer outer edge, to the acoustic liner wall surface a Runge-Kutta integration is performed using one hundred steps to complete the solution of the wave equation. Within the boundary layer a linear profile is assumed near the wall and this merges into a $1/7^{th}$-power velocity profile away from the wall. The acoustic intensity equation of Goldstein[19] was used to calculate the acoustic power for the hardwall input modes, output modes, and for the softwall modes on the acoustic liner side of each interface (see Figure 2.1). During the check-out phase of the computer code, acoustic power was observed to match across each interface which indicated that the acoustic pressure and axial velocity were properly matched across each interface.

3 – THEORY AND DESIGN OF ACTIVE CONTROL SYSTEM

This section describes the theoretical basis for the design of the active control system, which consists of the following components: (1) eigenmode identification and decomposition hardware/software, (2) mode scattering active control Helmholtz resonator hardware/software and (3) controller hardware/software. A discussion of the active helmholtz resonator concept is provided in the Appendix.

3.1 EIGENMODE DECOMPOSITION HARDWARE/SOFTWARE

3.1.1 Cylindrical modes

The pressure field of sound propagating in cylindrical or annular ducts can be represented as a superposition of eigenmodes in the form

$$P(r,\theta,z,t) = \sum_{m=-\infty}^{\infty}\sum_{n=0}^{\infty} A_{mn}\left[\mathrm{J}_m(\alpha_{mn}r) + \beta_{mn}\,\mathrm{Y}_{mn}(\alpha_{mn}r)\right]e^{i(k_{zmn}z+m\theta-\omega t)} \qquad (1)$$

where J_m and Y_m are Bessel functions of the first and second kind and the axial wavenumber k_{zmn} is

$$k_{zmn} = \frac{-kM \pm \sqrt{k^2 - (1-M^2)\alpha_{mn}^2}}{1-M^2}; \quad k \equiv \omega/c_0 \qquad (2)$$

where M is the flow mach number and with the + sign referring to downstream propagation and - sign to stream propagation. The eigenvalues α_{mn} and coefficients β_{mn} satisfy the boundary conditions at the duct walls [in a circular duct, $\beta_{mn} = 0$]. The index m is the circumferential mode order (number of lobes) while the index n is the radial mode order (number of nodal radii). For purposes of illustration and comparison, the radial distributions for the various circular and annular duct geometry's in this study are presented in Figure 4.3 of Section 4.

Modes with positive values of m are considered "spinning" in the direction of fan rotation and vice versa. Modes with complex values of k_{zmn} are considered to be cut off, which occurs for frequencies lower than

$$(f_{co})_{mn} = \frac{c_0\alpha_{mn}}{2\pi}\sqrt{1-M^2} \qquad (3)$$

3.1.2 Rotor/Stator Tones - Spinning Waves

Tyler and Soffrin[20] demonstrated that an axial flow fan with B rotor blades and V stator vanes radiates periodic sound structured as duct modes at blade passage harmonic h with circumferential indices m_q determined from

$$m_q = hB - qV;\ q = \text{any integer} \qquad (4)$$

For example, a fan with 16 blades and 14 vanes will radiate mode m_q = .., -12, 2, 16, .. etc. at BPF, m_q = ..., -10, 4, 18, .. etc, at 2BPF and so forth. The mixture of radial mode orders n for each of the circumferential modes depends on the details of the sound generation process. Only modes with cut-off frequencies f_{co} below the appropriate blade passage harmonic frequency $hB\Omega/2\pi$ ($\Omega = 2\pi RPM/60$) will actually radiate acoustic power.

3.1.3 Stationary Components of Spinning Waves

In typical fan designs, the radiated field at each blade passage harmonic is often dominated by sound in a single m order with multiple radial orders. The single m order defines a spinning wave in which only the phase is dependent upon the azimuthal angle in the duct:

$$P_{mn}(r,\theta,z,t) = P_{mn}(r,z,t)e^{im\theta} \tag{5}$$

For resolving mode m orders using simple arrays of stationary microphones, it is useful to employ the identity:

$$e^{im\theta} = \cos(m\theta) + i\sin(m\theta) \tag{6}$$

and to note that multiplication by i is equivalent to introducing a phase shift of 90°. This provides two stationary wave components of the m^{th} order spinning wave, which can then be resolved with stationary microphone arrays using real-valued processor weightings.

3.1.4 Circumferential Mode Separation

In a complex sound field in which advance knowledge of the mode content is available, active control approaches that address the modes are preferred to a more general approach because fewer control channels are required. This is the situation in a turbofan engine environment, where the mode structure of rotor/stator noise is dictated by the axisymmetric elements of the sound source. Aside from the controller itself, transducer arrays are required to activate the active Helmholtz resonators and to sample the resultant sound field to provide the appropriate system error signals.

For control addressing a particular m order mode set (possibly with multiple radial orders), it is desired to provide error microphones that separate the addressed m order from others that may be present and also from random noise due to flow and fan broadband radiation. For an array of N azimuthally equally spaced microphones at a given axial position, orthogonality makes it possible to use simple weighting and summing networks to isolate the stationary wave mode components:

$$P_{m,\cos} = \sum_{j=1}^{N} P_j(\theta)\cos(j\theta), \quad P_{m,\sin} = \sum_{j=1}^{N} P_j(\theta)\sin(j\theta) \tag{7}$$

where P_j is the sound pressure at the j^{th} microphone in the annular array. An especially convenient approach is $N = 4m$, in which case the weighting factors are all +1, 0 or -1.

While signals from the addressed modes add coherently in the weighted summing networks, non-addressed modes (see subsequent

discussions on mode aliasing) are rejected by orthogonality. Flow noise adds incoherently so that a signal to noise ratio (SNR) improvement of 10 log($N/2$) is achieved on each of the two stationary mode outputs. Note that if $N = 2m$ (the Nyquist number) only the cosine component may be resolved, but that the signal to noise improvement is 10 log(N). If the circumferential mode order is well known, then $N = 2m$ is viable.

3.1.5 Mode Aliasing

When sampling a sound field with an annular array of N equally spaced microphones and using summations with real weightings to isolate the sine and cosine stationary wave components of arbitrary circumferential mode m, the following series of modes will be measured:

$$\pm m \pm qN; \quad q = \text{any integer} \tag{8}$$

For example, for target mode m = 4 and N = 16, modes m = -28,-20,-12, -4, 4, 12, 20, 28 etc. would all be sensed equally by the array. Using complex weights on the microphones or equivalently by combining the sine and cosine components

$$P_m = P_{m,\cos} + iP_{m,\sin} \tag{9}$$

eliminates the $\pm m$ ambiguity so that the mode aliasing series becomes

$$m \pm qN; \quad q = \text{any integer} \tag{10}$$

or for the prior example, modes m = -28, -12, 4, 20 etc. are sensed equally while all others are rejected due to mode orthogonality.

3.1.6 Radial Mode Separation

In a hard wall circular or annular duct, multiple radial order modes for a given circumferential order may be isolated using weighted combinations of radially spaced microphones. However, the circumferential mode separation must be done first, and this implies a very large microphone array within the duct or else a rotating rake system as is employed by NASA. For application in a real environment, it is necessary to employ an axially/circumferentially spaced microphone array, flush mounted in the duct wall(s). The circumferential elements of the array may be used to separate mode m orders as discussed above. The axial distribution in each m order can then be analyzed one-dimensionally to separate the n or radial orders based on their axial wave number k_{zmn}. The number of axially spaced microphone annuli required to isolate the radial modes is equal to the number of incident modes plus the number of reflected modes. The separation process is then a simultaneous linear equation solution

$$p_{mj} = \sum_n \left(e^{ik_{zmn}z_i} + R_{mn}e^{ik_{-zmn}z_i} \right) P_{mn} \tag{11}$$

where P_{mj} is the (measured) sound pressure in circumferential mode m at axial station z_j and P_{mn} and $R_{mn}P_{mn}$ are the incident and reflected radial mode component amplitudes to be determined.

In the proof-of-performance tests, two radial modes were addressed at a single *m* order. With very weak reflections expected in the 48" ANCF or 22" ADP inlet duct/bell-mouth, two axially spaced microphone arrays would be required to resolve the two radial modes. To allow for reflection of the less cut-on mode in the ANCF test program, a third row of microphones was employed.

3.1.7 Active Mode Excitation

In order to interact with duct modes of circumferential order *m* a sound source array is required that is capable of radiating mode *m* in the duct. Analogous to the microphone array discussion, an annular array of *N* equally spaced actuators, excited with equal amplitude and with phase that follows the trace of the mode at the duct wall, will radiate modes

$$m \pm qN; \quad q = \text{any integer} \tag{12}$$

in the duct. The number of actuators in the array must therefore be selected such that modes $m + N$ and $m - N$ are cut off at the frequency of operation. It should be noted that each actuator in the array individually couples into all cut on *m*-orders. One thus depends upon the orthogonality of the circumferential mode structures and the source phase distribution to eliminate coupling of energy into modes of unwanted *m*-order. This requires that the actuators be equally spaced around the annulus.

The annular source actuator array at a given axial station will radiate energy in a target circumferential or *m*-order, distributed among radial or *n*-order components in a ratio that depend upon the relative mode strengths at the duct wall, the cut-off ratios of the modes and the axial extent of the actuators.

3.2 ACTUATOR/NOISE SOURCE MODE INTERACTION

The intent of the active components of the hybrid liner is to scatter sound energy from lower radial orders to higher radial orders, thus increasing the absorption efficiency of the passive liner elements. Alternatively, the active components can be thought of as re-phasing the modes so that the ratio between wall pressure and total sound energy is maximized in the region of the passive liner.

$$Wall\,Pressure\,Ratio \equiv \frac{P_{wall}^2 R^2}{2\int_0^R P(r)^2 r\,dr} \tag{13}$$

where P is the sum of the sound pressures in the modes. As an example, Figures 3.1a and b illustrate that in a relatively simple two-mode environment, the sum of the two modes can either decrease or increase the degree to which energy is concentrated near the wall. Figure 3.1c shows the nature of the interaction for modes (9,0) and (9,1) as a function of relative mode amplitude and phase, normalized to the case of mode (9,0) alone. When the wall pressure is nearly zero because of destructive interference between modes,

the energy loss to a passive absorber of finite length would be small. By contrast, as shown in Figure 3.1c, when the wall pressure is maximized, the rate of absorption by the passive absorber would be greatly enhanced, offsetting energy added to the system by the actuators. The active control system would be required to seek a balance between added energy and inhanced passive absorption elements.

The simplest approach to the balancing discussed above would be using a single row of active resonators as a scattering impedance acoustically upstream of the passive liner. The effectiveness would be dependent upon the phase relationship between the noise source generated modes at the axial location of the active resonators (or actuators). If the phases between the modes are opposite, the actuators would increase the energy in one mode while reducing it in the other. If the phases of the modes were nearly equal, the actuators could reduce energy in both simultaneously.

A more universal approach would be to incorporate two or more rows of active resonators to form a distributed scattering impedance area. This would have the further advantage of allowing resonator actuators to be phased axially to interact more efficiently with specific modes or groups of modes.

In the actual hybrid liner implementation, two rows of actuators, spaced approximately 3/8 wavelength were installed immediately ahead of the passive liner. The closed loop control system was programmed to minimize sound energy transmitted past the entire assembly, with the active resonator element assuming the role appropriate to the incident mode mixture.

3.3 ACTIVE CONTROL ACTUATORS AND ACTIVE RESONATORS

The above discussions of actuator array configurations are based on modal excitation and anti-aliasing considerations. Equally important are the capabilities to provide acoustic signals of adequate amplitude to interact with the fan noise and to withstand potentially high amplitude pressure fluctuations within the engine fan environment. In addition, with thought toward final application, actuators were sought that were inexpensive, lightweight and compact.

For operation in the frequency range 800 to 1000 Hz, conventional electrodynamic loudspeakers are efficient and reliable, but are neither lightweight nor compact. Further, they typically have lightweight diaphragms that would be susceptible to damage from intense fluctuating pressures.

The next readily available transducer type is piezo-electric or piezo-ceramic, bonded to an aluminum diaphragm. This approach is compact and lightweight and can be designed to have a high mechanical impedance, protecting it form fluctuating ambient pressure. The disadvantage is that the high mechanical impedance restricts vibration amplitude. At frequencies of 800 to 1000 Hz, the approximately 120 dB sound pressure levels expected in the ANCF test facility are indicative of acoustic particle displacement on the order 1-mil, readily attained in electro-dynamic drivers, but requiring high drive levels and robust construction in a piezo-ceramic/aluminum disc transducer.

Figure 3.2 shows a diagram of the circular piezo-ceramic transducer used for the ANCF demonstration. Each of 32 transducers was used as the base of an active Helmholtz resonator, tuned just above the maximum 2BPF frequency of the ANCF fan (1006 Hz). Figure 3.3a and b are amplitude and phase response plots for the actuators, showing the high degree of uniformity as required for minimal modal aliasing.

For the ADP tests, the design of the active resonator was modified by switching the location of the piezo-ceramic actuator to the wall or nearest the noise source. A slot adjacent to the actuator element and the cavity behind the actuator form the resonator, which act to increase the output at the low end of the desired response range.

3.4 ACTIVE CONTROL ALGORITHMS.

In the simplest sense, the function of the active control system in the hybrid liner is to apply signals to the active resonator actuators with appropriate amplitude and phase to minimize the sound pressure at the array of error microphones. Because the system objective is suppression of the rotor/stator interaction tone, a reference signal is obtained from a fan tachometer or other non-acoustical pickup that produces or can be processed to produce a BPF harmonic tone or tone series. Two different approaches to this function were used.

3.4.1 Multi-Channel Filtered X Algorithm.

Transfer functions are established between the two active resonator arrays and the sine and cosine components of three error microphone annuli using random noise injection at the resonator actuators. The reference signal is processed by one multi-tap finite impulse response (FIR) filter per actuator array channel and sent to the actuator drive amplifiers. The FIR filter has no feedback paths and therefore can synthesize filters with zeros only. The error microphone signals are cross-correlated with the FIR filter tap weights and new tap weights are computed based on the errors and the system transfer functions. The process is repeated until the sum of the squares of the error signals is minimized. For a detailed description of the Filtered-X control algorithm, see (Reference 21).

3.4.2 Adaptive Quadrature Algorithm

The filtered-X algorithm uses delay lines to model the acoustical transfer functions of the fan and active noise control system elements. For controlling quasi-steady tones, the transfer function can be re-cast as an amplitude ratio and phase shift or two parameters per control channel. In a high frequency environment such as the ADP engine model, a control algorithm that acts on signal parameters instead of the signals themselves offers a significant advantage in processing requirements.

The adaptive quadrature or A-Q algorithm measures the fan signal and the signals from all resonator rows at all error microphone rows using fan BPF harmonic tone injection. The algorithm computes the minimum-norm actuator drive vector (complex) that will combine with the fan noise to produce a minimum in the sum of the squares of the error signals. Following the initial

adaptation, the system sequentially perturbs the real and imaginary parts of the actuator drive signals and determines on-line corrections to maintain the minimization of the error signals.

Unlike the Filtered-X algorithm, which processes a reference signal for application to the resonator actuators, the A-Q algorithm generates the real and imaginary parts of control signals using DSP lookup tables and uses a fan tachometer only for system timing. The results of the "solver" in the algorithm are multipliers for the reference signals, so that the actual control calculations can be carried out at a slower rate than the signal I/O.

4 – CONCEPT VALIDATION IN NASA LeRC ANCF FAN TEST FACILITY

A two-phase test program was undertaken in the NASA Lewis Research Center ANCF 48-inch fan facility to validate the hybrid active-passive segmented liner concept. The first step was a static test in the HAE No-Flow 24-inch duct facility, with the primary purpose of verifying flush mounted microphone techniques for radial mode separation and stable operation of the active element of the segmented liner. Three test liners were designed, constructed and their acoustic performance measured in terms of insertion loss.

The second step was a full diagnostic and verification measurement series in the NASA ANCF fan facility. A series of tests consisting of mode resolution by microphone arrays, mode generation by actuator arrays, insertion loss by active elements, passive elements and hybrid active-passive elements were evaluated. Table 4.1 is a summary of the parameters of the test series, which are subsequently discussed in detail. The demonstration program summary is outlined in Table 4.2.

Table 4.1 Summary of HAE and ANCF Experimental Program Test Matrix

Test Facility	Nominal Diameter (inches)	Sound Source	Target Modes	Active Resonators	Error Microphones	Speed Range (Corr. RPM)	Test Section Mach no.	Frequency Range (Hz)
HAE	24	10 Driver Mode Synthesizer	(±1,0), (±1,1)	2 Rows of 8 each	2 Rows of 8 each	NA	0	800-1050
NASA ANCF	48	14 ea. 1/4" Rods, 16 Blade Rotor	(4,0), (4,1)	2 Rows of 16 each	3 Rows of 16 each	1520-1886	≈ 0.1	810-1006 @ 2BPF

Table 4.2 NASA/AITP Demonstration Program Summary

Test Facility	Test Period	Inlet Liner Diameter (in.)	Total Treatment Length (in.)	Target Frequency (Hz)	In-Duct Mach No.	Mode Order (m, n)	Active Control Drivers	Microphones
Hersh Acoustical Engineering. (HAE)	Aug-Sept. '95	24	12	1050	0	(1,0) (1,1)	2 Rows, 8 Drivers Each Row	2 Rows, 8 Each Row
Active Noise Control Fan (ANCF) NASA LeRC	Dec. '95, Jan '96	48	23	1000	-0.07	(4,0) (4,1)	2 Rows, 16 Drivers Each Row	3 Rows,16 Active Control Mic. Each Row
Advanced Ducted Propulsor (ADP) Rig 9'x15' Wind Tunnel NASA LeRC	Nov. '96	22	7.75	3255	-0.3	(9,0) (9,1)	2 Rows, 36 Drivers Each Row	2 Rows, 18 Active Control Mic. Each Row

4.1 HAE NO FLOW CALIBRATION TESTS

4.1.1 Test Apparatus

As observed on the drawing of Figure 4.1a and b and in the photographs of Figure 4.2a and b, the HAE facility was constructed with two 48-inch lengths and one 24-inch length of fiberglass reinforced plastic duct. The test liners were inserted between the two 48-inch sections and the active resonator elements, when used, were installed in the 24-inch section and inserted acoustically upstream of the liners. The source end of the duct assembly was fitted with a cylindrical duct mode synthesizer on the end wall consisting of eight outer radius (r = 10-inches) drivers and two inner radius (r = 4.1-inches) drivers. These could be driven from controlled amplitude and phase coherent signal sources to allow generation of modes (±1,0) and (±1,1) with predetermined complex ratios. The load end of the duct was terminated with 4-inch thick acoustically absorptive foam for most of the tests, but other terminations, including a hard wall, free radiation and a foam wedge were also used. The 48 inch duct sections were fitted with numerous microphone ports, with axial spacing corresponding to one-half axial wavelength for modes (1,0) and (1,1) at test frequency 1050 Hz. In addition, the facility included four existing eight-element circumferential arrays of microphones, spaced 3-inches axially and radially traversing pressure and pressure gradient sensors at locations immediately upstream and downstream of the test liner insertion point.

Figure 4.3a shows the radial distributions of desired modes (1,0), (1,1) and undesired mode (3,0) in the circular duct. Driver radius ratios were 0.34 and 0.83, resulting in maximum coupling from the inner array to mode (1,1) and weak coupling to unwanted mode (3,0). [Observe that the outer radius array had an adequate number of elements (8) to eliminate coupling to mode (3,0).] Since the two array radii flank the nodal radius for the (1,1) mode and there is no nodal radius for the (1,0) mode, excitation of either mode independently was accomplished with the appropriate inner/outer array drive ratio. Excitation of both modes with predetermined amplitude and phase relationship was then a complex-weighted superposition of the independent drive signal combinations.

$$\begin{bmatrix} OuterDrive \\ InnerDrive \end{bmatrix} = \begin{bmatrix} H_{11}(\omega) & H_{12}(\omega) \\ H_{21}(\omega) & H_{22}(\omega) \end{bmatrix} \begin{bmatrix} Mode(1,0) \\ Mode(1,1) \end{bmatrix} \qquad (14)$$

where Mode(m,n) is the complex amplitude of the mode and H is the complex weight matrix.

It may be noted that for these measurements, spinning modes m = +1 and m = -1 were generated simultaneously, resulting in a stationary mode $\cos(m\theta)$. This simplified the mode synthesis process and resulted in no loss of generality in the linear test system.

4.1.2 Microphone Array Tests

One element in the active control approach was the use of flush mounted wall microphone arrays to separate radial orders in complex sound fields. The simplest way to accomplish this in a two-mode environment was to separate circumferential microphone arrays axially one-half wavelength for each of the two modes, and then recover a signal representative of the opposite mode by summing the outputs of the two arrays. Although only applicable for a single frequency, the approach would allow active control error signals for individual modes at a design point.

At a test frequency of 1050 Hz, the axial one-half wavelengths for modes (1,0) and (1,1) are 7.75 in. and 21.5 in, respectively. With microphones separated by these distances, a slow frequency sweep was made from 950 to 1100 Hz and the summed output of the two microphones was measured with inner/outer drive ratios +2, 0 and -2. At frequencies other than 1050 Hz, response was erratic. At 1050 Hz, the mode level relationships were well behaved and relatively independent of duct termination, as shown in Table 4.3.

The results presented in Table 4.3 as well as numerous other measurements, conducted with the inner and outer source arrays driven separately, indicated that the simple mode synthesizer was capable of generating a wide range of mixtures of modes (1,0) and (1,1) and that the wall-mounted microphone array could be used to discriminate between radial mode components in a composite sound field.

Table 4.3. Summary of Mode Generation and Separation Using Inner/Outer Array Synthesizer and Axially Spaced Wall Microphones

Inner/Outer Drive Ratio	Wedge Termination Mode 1,0: Mode 1,1	Open Termination Mode 1,0: Mode 1,1
2:1	+14 dB	+14 dB
0:1	+4 dB	+5 dB
-2:1	-24 dB	-22 dB

4.1.3 Uniform and Segmented Liner Designs

The multi-modal, multi-segment acoustic suppressor theory discussed in Section 2 was used to design several sets of acoustic liners for increasingly challenging test conditions. The first liner set was designed for test in the HAE duct facility Since the acoustic measurements to validate the active-passive hybrid liner concept were to be made within the inlet duct, maximum attenuation of total acoustic power for the target modes was chosen as the optimization goal for the acoustic suppressors. Each facility presented different modes to its suppressors so each liner set was individually optimized.

The conditions for the acoustic liner design are as follows. The simplest two radial mode configuration is selected with a one circumferential lobe pattern (m = 1) driven at 1050 Hz which provides a frequency parameter $\eta = fD/c = D/\lambda = 1.888$. A total of 12-inches was allowed for the acoustic treatment

either uniform or two sectioned giving a total L/D = 0.5. It was desired that the lower radial mode that is harder to attenuate should carry the largest acoustic power so the zeroth radial mode amplitude A_0 = 2.0 and a first radial mode amplitude A_1 = 1.0 were chosen. It was determined from exercising the liner code that a phase difference between the modes of 135 degrees gave the best results at 1050 Hz so this phase was chosen. These mode amplitudes and phases could be achieved easily in the HAE rig since the sound is produced by driver arrays in one end wall.

The first optimization performed was for a uniform liner under the conditions stated above. A 20 x 20 impedance array was selected around the estimated optimum impedance and the segmented duct code was exercised at each point for the two input modes and five radial modes in each duct section which yields twenty unknown modes. The output array of impedance and attenuation were read into the Axum plotting software and the plotted results are shown in Figure 4.4. A tighter impedance array around the observed optimum area yielded a maximum attenuation of 14.5 dB at a normalized specific acoustic resistance of 0.566 and acoustic reactance of -0.944. The specific acoustic impedance used here is the non-dimensional impedance as normalized by the characteristic impedance of a free air medium given by ρc where ρ is the air density and c is the speed of sound. These values provide the optimum at this particular chosen frequency. The constant decibel attenuation contours in Figure 4.4 show the off-optimum liner performance as well for this frequency. If the optimum impedance is missed somewhat due to design and manufacturing errors, as would be expected in practice, a robust liner such as this would still provide reasonable attenuation. The single segment liner results of Figure 4.4 are intended mainly for comparison to the results of a two-segment liner of the same total length. This uniform liner optimized for 1050 Hz was labeled as HAE 2. HAE 1 was another uniform liner which was not optimized with the present code but which was designed and built for testing in the HAE facility.

The optimized two segment acoustic liner HAE 3 is somewhat more complex than the uniform liner because of the larger number of variables involved. The total length of 12 inches had to be held but the two segments could be any combination of lengths adding to 12 inches. A quite arbitrary split of 6-inches for each segment was chosen to start this study. A parametric study of length spit between the liners has not been made so it is certainly possible that in spite of the excellent results to be shown below, even better results may be possible with further study. For the two segment liner optimization, one liner impedance was held fixed while the second was varied over the impedance plane the same as was done for the uniform liner. The optimum impedance was then held for the second liner and the impedance of the first liner was varied over the impedance plane to find its optimum impedance. The procedure was repeated until no more improvement could be found. The results of the final pass are shown in Figures 4.5 and 4.6. In Figure 4.5 the acoustic impedance of liner 2 was varied as liner 1 was held at its optimum non-dimensional acoustic impedance of 0.076 - i1.171. In Figure 4.6

the reverse occurred with liner 1 being varied as liner 2 was held at its optimum of 0.491 - i0.340. The maximum attenuation observed with this two-segment liner was 26.5 dB. The first obvious result of this study is that the two segment liner has an attenuation at the design point of over twice that of the best uniform liner. For this set of conditions at least, the resistance of liner 1 should be very near zero, a purely reactive liner, which is the same type of result obtained for the plane wave studies as reported in the literature and discussed in the Background section of this report. This near zero resistance is difficult to achieve for a passive liner but is quite reasonable using an active resonator. As seen from Figures 4.5 and 4.6 the liner seems to be quite robust also since the large attenuation contours reach over a fairly large impedance range.

The impedance for each of the three 24 inch diameter barrels used for this phase was defined by E. J. Rice Consulting. These one-splice barrels, were complete cylinders, that were designed with mounting flanges that would mate with the HAE no-flow duct. Each barrel was 24-inches in diameter and was 12-inches long with integral mounting flanges incorporated into each barrel. These aluminum flanges were stretch formed to meet the HAE contour.

The first barrel fabricated HAE 1 (NSL95001) was a uniform all-passive acoustic treatment having a 2.35 inch honeycomb core depth. The impedance for this barrel was defined as 1.147-i0.395. The barrel was constructed as a uniform impedance single degree linear liner with one small (.25) inch) axial core splice. The construction consisted of a woven wire mesh bonded to a perforated aluminum skin which was bonded to an aluminum Flex-Core honeycomb. A solid back-face skin made from graphite epoxy (Gr/Ep) laminates completed the configuration. A two-microphone acoustic impedance test was conducted on the completed panel. The equivalent dc flow resistance for the panel was 47.6 cgs rayls with a non-linearity factor (NLF200/20) of 1.3.
HAE 2 (NSL95002) was also an all-passive barrel with a liner impedance of 0.566-i0.944. The construction of this barrel was similar to the first and analysis indicated that a honeycomb core depth of 1.534 was required. The equivalent dc flow resistance of this barrel was 23.5 cgs Rayls and with a (NLF200/20) of 1.3.

HAE 3 was a segmented (NSL95003) all-passive barrel. The acoustic impedance requirement for the 1.34 inch deep core section that would be installed closest to the acoustic drivers was 0.076-i1.171. This section was two-microphone tested and had an average dc flow resistance of 3.15 cgs Rayls and an (NLF200/20) of 1.3. The second segment, which had a 2.32 inch deep core, had a required liner impedance of 0.49-i0.34. This section was tested and had a dc flow resistance of 20.4 and a (NLF200/20) of 1.3. The HAE barrels were designed with the wire mesh on perforate liners which appears to provide the design flexibility to attain a fairly low resistance to accommodate the two segment liner section with the very low resistance. A summary of the Two-Microphone test results are provided in Table 4.4.

Table 4.4 HAE Barrel Acoustic Impedance Data

Barrel Identification	Type Acoustic Treatment	Liner Impedance	Barrel Dia. (in.)	L/D	Honeycomb Core Depth	Req. R105	Meas. & Extrapolated to 115 dB (Sine)	Meas. & Extrapolated to 115 dB (Broadband)	NLF (R200/ R20)
NSL95001 (HAE1)	Uniform Passive Linear Liner	1.147-0.3947i	24 in.	0.5	2.35	47.6	44.4	41.6	1.3
NSL95002 (HAE2)	Uniform Passive Linear Liner	0.566-0.944i	24 in.	0.5	1.534	23.5	18	15.9	1.3
NSL95003 (HAE3)	Segment 1 Passive Linear Liner (fan face)	0.076-1.171i	24 in.	0.25	1.34	3.15	2.8	2.6	1.3
NSL95003 (HAE3)	Segment 2 Passive Linear Liner	0.49-0.34i	24 in.	0.25	2.35	20.4	16.4	15.7	1.3

The front end of the multi-segment sound propagation code was modified to include the impedance model for this liner construction and a loop to run through a series of frequencies to provide attenuation spectra for these liners. The calculated attenuation spectra for liners HAE 1, 2, and 3 are shown in Figure 4.7. Recall that these results are calculated using the best estimates of the liner impedance as built. The number of radial modes that can propagate in the hard duct sections are shown at the bottom of the scale. The two section liner, HAE 3 is seen to substantially out perform the best uniform liner, HAE 2, over quite a wide frequency range around the design frequency of 1050 Hz. The uniform liner, HAE 2, does have a sharp peak of attenuation just below the second mode cut-on frequency of 954.2 Hz. Actually the bandwidth of the HAE 2 attenuation spike is sharper than shown because of the calculations being made only at every 50 Hz. Closer examination has shown the attenuation to drop sharply between 954.2 and 955 Hz (22.9 to 13.8 dB).

One final result is of significance for both the HAE suppressors and the program in general. This is the effect of the phase between the radial modes upon the attenuation of the two modes by the acoustic suppressor. Recall that we have been using a phase difference of 135 degrees and the reason for this is shown in Figure 4.8 where the liner attenuation spectra for the two segment HAE 3 liner is shown for the range of possible phases. It is seen that the results for 135 degrees phase difference is best with substantial attenuation fall off around the design frequency of 1050 Hz at other phases but with an increase in attenuation at around 850 Hz and at the radial mode cut-on of 954 Hz. This result would be of no great consequence for tests using acoustic drivers since any phase difference can be attained. However, for a real noise source such as an engine, not much control of the phase can be exerted except possibly liner location which must then be traded off against liner length. Also recall that the liner might be re-optimized to recoup part of the loss and also that the uniform liner suffers some loss of performance with change in modal phase difference.

4.1.4 Passive Liner Insertion Loss Tests

Two uniform passive liners and a segmented passive liner were inserted in the HAE test facility and their insertion loss measured using the four circumferential microphone arrays, set to accept mode m = ±1. The duct was terminated with the 4-inch. thick foam. Insertion loss was determined as the ratio of the mean square pressure at the two downstream arrays to the mean square pressure at the two upstream arrays, normalized by the ratio measured with the liner absent. The mode synthesizer was driven to provide a nominal mode (1,0) to mode (1,1) amplitude ratio of 2.0 with a phase difference of 135° at the leading edge of the liner at 1050 Hz (the liner design conditions).

4.1.5 Active and Active/Passive Hybrid Liner Insertion Loss Tests

As a simple test of the functionality of the active control system and the active-passive segmented liner, the HAE dual eight-element active Helmholtz resonator array was installed in the hard duct section and then upstream of uniform liner section designated HAE 3 (NSL95003). The filtered-X controller system was operated, using the cos(θ) and sin(θ) mode decompositions from the two downstream microphone arrays as error signals and the test oscillator signal as a reference. The pressure distributions may be written,

$$P_{m,\cos} = \sum_i P_i \cos(2\pi m \theta_i) \qquad (15a)$$

$$P_{m,\sin} = \sum_i P_i \sin(2\pi m \theta_i) \qquad (15b)$$

where θ_i is the azimuthal angle of the i^{th} microphone in the array.

Independent cos(θ) and sin(θ) control signals were sent to each of the two rows of eight resonators, both individually and simultaneously. The mode synthesizer was driven to provide a nominal mode (1,0) to mode (1,1) amplitude ratio of 2.0 with a phase difference of 135° at the leading edge of the liner at 1050 Hz

Table 4.5 shows the results of these measurements. Here, the Active entries 8-inch and 19-inch refer to the resonator arrays 8-inches and 19-inches upstream of the passive liner, respectively. Microphones A and B are upstream and C and D are downstream of the liner.

Table 4.5. Summary of Active/Passive Treatment Measurements in HAE Duct

Treatment		Microphone Array Amplitude				Average Atten (dB)
Passive	Active	A	B	C	D	
None	None	174.38	337.26	242.32	97.84	3.2
HAE 3	None	132.67	277.72	84.69	40.32	10.3
None	8"	216.29	338.02	35.22	54.00	15.9
None	19"	505.1	449.60	56.71	82.87	16.6
HAE 3	19"	286.07	221.31	30.03	9.92	21.2
HAE 3	8"	219.13	301.31	1.40	5.78	35.9
HAE 3	8" & 19"	462.68	354.47	0.28	2.40	>40
None	8" & 19"	414.61	422.73	0.29	0.30	>40

The results of this preliminary test were indicative of the interactive synergy of the hybrid liner concept. Observe that combined attenuation of passive liner HAE 3 and the active resonators 8-inch. upstream is nearly 10 dB greater than the sum of the attenuation of the two elements measured individually. The two final entries in Table 4.5 suggest that the two active resonator arrays provided greater attenuation with two rows of active resonators was below the system noise floor.

4.2 ANCF FAN TEST PROGRAM

4.2.1 ANCF Test Facility

The Active Noise Control Facility (ANCF) is located in the NASA LeRC's Aeroacoustic Propulsion Laboratory (APL), a hemispherical anechoic (to 125 Hz) test facility. This APL is a 130-foot diameter geodesic dome with a fully anechoic arena with treated walls and floors. This facility has provisions for far-field noise measurements with microphones located at a 50-foot radius at angles of 6°. The ANCF uses a 16-bladed variable pitch rotor and was configured with stator vanes to provide specific mode generation and propagation. The drive consists of a 125 horsepower electric motor, and two drive shafts connected by a belt. The fan and associated structure is located at a centerline height of 10-feet. A maximum tip Mach number of 0.35 can be achieved with the fan which corresponds to a corrected speed of 1886 RPM. The duct has a constant 48-inch diameter. The length of the inlet for the test was adjusted to accommodate the treatment and to move the rotating rake to various positions in the duct. The rotating rake permits measurements of the spinning acoustic mode structure. The rake is mounted to a small section of the wall and is designed to rotate at 1/100 of the fan speed. Microphones are mounted at several radial locations to measure the radial pressure profile. An Inflow Control Device (ICD) was installed for these tests that allowed static

testing. This ICD removes large scale, random turbulence and ground vortices that could interact and cause unwanted tones. A complete description of this facility is contained in Heidelberg et al.[22-23] and the key fan parameters are provided in Table 4.6.

Table 4.6 Operating Parameters of the NASA ANCF Fan Test Rig Facility

Blade Number	16
Spoiler Rods	14
Inlet Duct Diameter	4 ft.
Modes at BPF (*m,n*)	(2,0), Cutoff 273 Hz
Modes at 2-BPF (*m,n*)	(4,0), Cutoff 476 Hz (4,1), Cutoff 830 Hz
Maximum RPM	1886
Maximum BPF	503 Hz
Maximum 2-BPF	1006 Hz

A cutaway diagram of the ANCF fan, as operated in this program, is shown in Figure 4.9. A photograph of the facility viewed from the side of the fan rig is shown in Figure 4.10 and from the rear in Figure 4.11. In order to generate an initial sound field with strong signal-to-noise ratio and a preponderance of energy in a low radial order mode, the stator vanes were removed and 14 rods, each of one-quarter inch diameter, were installed immediately upstream of the rotor. The result was a 2BPF sound field consisting of spinning mode order m = 4, radial orders n = 0 and 1 as shown in Figure 3.1b, with approximately 2.9:1 amplitude ratio of mode (4,0) to mode (4,1) at 1886 RPM (1006 Hz). The blade passage fundamental and other blade passage harmonics were present as well, but were not addressed by the demonstration tests.

4.2.2 Transducer Array Descriptions

The target modes were (4,0) and (4,1) at 2BPF, using 14 spoiler rods and a 16 blade rotor in the inlet of the 48-inch ANCF fan. Fan operating speeds were 1520-1886 RPM, corrected to 59° ambient temperature (1117 ft/sec sound speed), producing mean flow of nominally Mach 0.1 in the fan inlet.

Error microphone arrays consisted of three annuli of 16 equally spaced Knowles Type BT1755 electret condenser microphone, each with individually trimmed preamplifier, flush mounted in the ANCF inlet duct using nylon inserts/ transfer tubes of diameter 0.05-inch and nominal length 0.75-inch. The microphones were spaced axially 0, 7.25 and 11.25-inches relative to the downstream row, corresponding to the axial half wavelength for modes (4,0) and (4,1) respectively at 1886 RPM fan speed. This would allow on-line radial mode separation at this fan speed only. Outputs of the individual microphones in each annulus were weighted by the cosine and/or sine of their modal azimuthal angle and summed to produce mode m = 4 stationary wave outputs. (Note that with 16 microphones, the weighting factors for m = 4 are all either +1,

-1 or 0.) These modal outputs were used for active control error signals and were monitored to indicate control system effectiveness.

Active Helmholtz resonator arrays consisted of two annuli of 16 equally spaced resonators, 4.5-inches diameter and 0.5-inch deep, with a 2-inch diameter orifice covered with 30% open perforated metal and very low resistance wire mesh screen. The base of each resonator was a specially machined aluminum disk with a piezoceramic actuator element cemented to the back side. Each actuator was driven by an individually trimmed pulse-width modulated power amplifier. Figure 4.12a is a photograph of one of the actuators used for the ANC tests shown along side one of the ADP actuators in Figure 4.12b, which will be discussed in a later section.

As discussed previously, terminated tube frequency response measurements were taken for 49 actuators, with results as shown in Figure 3.4a and b, which indicates very uniform response characteristics among the actuators except near the primary mechanical resonance. The best matched 32 actuators were graded and grouped for use in the active resonators. Variations among actuators were trimmed in situ to within 2% amplitude and 2° phase by adjusting voltage/current feedback on the individual power amplifiers.

Initially, the 16 active resonators in each annulus were activated by separate control channels for the cosine and sine stationary wave components for mode $m = \pm 4$. In the final configuration, a single control signal was used for each annulus. The control signal was split into $\cos(\omega t)$ and $\sin(\omega t)$ components using a Hilbert transform processor (two analog delay lines with constant 90° phase difference). These signal components were used to drive the $\cos(m\theta)$ and $\sin(m\theta)$ elements of the active resonator annuli, respectively. [Note that with N = 4m, the cosine and sine resonator arrays are physically separate, alternating around the annulus.]

4.2.3 Data Acquisition System

Performance measurements in the NASA/LeRC ANCF were made using in-duct modal power ("Rotating Rake") and far-field stationary microphone array techniques. Again this rotating rake system is discussed in detail in References 22 and 23. The in-duct system consists of six pressure microphones, spaced on a radial boom that scans the sound field at a fixed axial station in the duct by rotating at a known fraction of the fan rotation speed (one percent in the case of ANCF). Circumferential mode orders are resolved based on Doppler shift of the measured sound spectrum. Radial mode orders are resolved by least-square curve fits of the radial sound distribution to a series of up to six Bessel functions of the appropriate circumferential order. Again this rotating rake system is discussed in detail in References 22 and 23.

The far-field measurement system is a semi-circular array of 28 stationary pressure microphones spaced approximately 6° on an approximately 40-foot radius.

For the hybrid liner tests, electrical drive signals to the active element actuator arrays were recorded on computer disks for assessment of active control solution vectors versus incident sound field characteristics and system performance.

In-duct modal 2BPF tone sound pressure measurements and far field sound pressure measurements were taken over a fan speed range 1520 to 1886 RPM (corrected to 1117 ft/sec sound speed) for the following fan and inlet configurations:

i. Cast aluminum inlet spools for hard-wall baseline data

ii. Uniform passive inlet liner L/D 0.5

iii. Segmented passive inlet liner L/D 0.5

iv. Hybrid active-passive segmented inlet liner, active only, passive element covered

- Active off
- Upstream resonator actuators only
- Downstream resonator actuators only
- Upstream and downstream resonator actuators

i. Hybrid active-passive segmented inlet liner

- Active off
- Upstream resonator actuators only
- Downstream resonator actuators only
- Upstream and downstream resonator actuators

Figure 4.13 is a schematic diagram of the active/passive measurement system utilized in the ANCF Facility.

4.2.4 Applied Active Control Algorithms and Signal Processing

Active control signal processing was completed using a Spectrum, quad Texas Instruments TMS320C40 floating point DSP system, programmed for single reference, four error channel and two/four output channel filtered-X processing.

The active control reference signal was obtained from the 128x pulse train output of the fan shaft encoder. The encoder was divided by 4 in a binary divider, giving a 32 shaft order (2BPF) square wave, which was then filtered to provide a 2BPF sine wave.

All signal paths were conditioned using band pass filtering to restrict signals to the range 400-1200 Hz.

System monitoring was conducted using Data Translation/Hewlett-Packard DT-VEE data acquisition/processing/display software and a Data Translation type DT2821-G-16SE high speed analog I/O interface. The following system signals were monitored and samples thereof stored on disk for subsequent analysis:

- Modal sound pressure signals from six microphone mode separators

- Filtered reference signal
- Control signals to two annular active resonator arrays
- Unprocessed microphone signals from one microphone in each of three annular arrays

The DT-VEE processing and display provided on-line indications of the following information:

- Modal sound pressure PSD display for six microphone mode separators
- Sound pressure waveforms from three unprocessed microphone signals
- Control signal waveforms for two active resonator annuli

These were used for on-line assessment of liner performance and actuator drive levels.

4.2.5 ANCF Acoustic Liner Design

The conditions for the acoustic liner design are as follows. The duct diameter for the ANC facility is nominally 48-inches. Modal information was obtained using the NASA LeRC rotating microphone rig. In order to obtain a dominant lower radial mode for the two mode system, the case where 14 rods mounted in front of the 16 rotor blades must be used. At a rotor rotation of 1886 RPM, the 16 blade rotor produces a tone of 1005.9 Hz at twice the blade passage frequency. With the 14 rods inserted a four lobed circumferential mode is produced with two propagating radial modes. The mode amplitude ratio of $A_0/A_1 = 2.92$ was provided by L. Heidelberg of NASA LeRC. The rotating probe microphones are located 29.16-inches forward of the start of the proposed acoustic treatment. The measured phases were $\phi_0 = -123.186°$ and $\phi_1 = -134.072°$ relative to a reference signal. When these phases are projected 29.16 inches toward the rotor the result is $\phi_1 - \phi_0 = 105°$. The above conditions provide a frequency parameter $\eta = fD/c = D/\lambda = 3.5978$. A total of 23-inches was allowed for the acoustic treatment either uniform or two sectioned giving a total L/D = 0.4792.

The liner optimizations were performed the same as for the HAE acoustic liners. A 20 x 20 impedance matrix was used to provide inputs to the multi-segment circular duct sound propagation code. The acoustic attenuation, at each wall impedance, was calculated and the results fed to AXUM software to perform contour plots. Results for the uniform liner ANC 1 are shown in Figure 4.14. The optimum specific acoustic impedance is 1.159 - i1.324 with the maximum attenuation of 14.3 decibels. In Figure 4.14 again it is seen that the uniform acoustic liner case is quite robust with substantial attenuations being achieved over quite a large portion of the impedance plane. For the two segment acoustic liner, ANC 2, the optimum conditions are shown in Figures 4.15 and 4.16. In Figure 4.15 the impedance of liner 1 is held constant at its optimum value of 0.554-i1.914 while liner 2 is varied throughout the impedance

plane. The very large potential for attenuation with the ANC liner compared to that of the HAE 3 two-segment liner can be seen by comparing Figure 4.15 with Figure 4.5. The scales for the two figures are about the same so a direct comparison can be made. The region of the impedance plane encompassed by the 25 dB contour for the ANC 2 case is much larger than that for the HAE 3 case. The maximum attenuation for the ANC 2 case is 51.0 dB but the impedance region for this high attenuation is quite tight as seen by the close spacing of the higher attenuation contours in Figure 4.15. In Figure 4.16 the ANC 2 liner attenuation in the liner segment 1 impedance plane is shown while holding the liner 2 acoustic impedance at its optimum value of 0.788 - i0.522. The noticeable difference between this result and that for the HAE 3 two segment liner in Figure 4.6 is that for ANC 2 the liner 1 segment is not just reactive at its optimum. The optimum impedance in Figure 4.16 should be quite easy to obtain using passive sections only. This difference is due to the higher circumferential lobe number (4 vs. 1) and the higher frequency parameter (3.60 vs. 1.89) with the latter probably being the most significant.

The third acoustic suppressor used in this concept validation program, the active-passive hybrid suppressor, uses the same liner 2 segment as the two-segment suppressor, ANC 2. This current hybrid liner design philosophy uses the active driver system as a replacement for the set-up or mode conditioning section 1 while retaining the dissipative liner 2.

The theoretical results show dramatic advantages for the two segment liner over the uniform liner of the same length. For the two cases shown so far it appears that the two segment passive liner has the potential to double the decibel attenuation over that of the same length uniform liner.

4.2.6 ANC Barrel Fabrication

Three test barrels were fabricated for the ANC test program. The impedance of each of these barrels was defined as described in the previous section. ANC 1 (NSL95005) was constructed with a 48-inch diameter, a 23-inch acoustic liner length and a constant honeycomb core depth of 1.29-inches. The resistance goal was 48.1 Rayls and the final value achieved was 51.9 (sine testing) and 52.9 broadband testing.

ANC 2 (NSL95006) was a 48-inch diameter barrel with the total 23-inch acoustic liner length divided into two liner segments. The segment adjacent to the fan face was composed of a 10-inch length with a 0.97-inch deep core. The resistance goal for this segment was 23.0 Rayls. The segment closest to the inlet lip was composed of a thirteen inch length with a 2.13-inch core depth having a resistance goal of 32.7 Rayls. Two-microphone tests yielded an average resistance of 40.7 Rayls at 1384 Hz. for the thirteen inch segment and 29.4 Rayls at 2842 Hz. for the ten inch segment. Sine wave excitation tests for the 2.13-inch deep segment were conducted at a frequency of 1400 Hz. An average resistance of 41.8 Rayls was obtained. For the 0.97-inch deep segment a frequency of 2800 Hz. was used and average resistance of 27.4 Rayls was obtained.

ANC 3 (NSL95007) was constructed with a 48-inch diameter, 23-inch liner length and had one liner segment and one segment designed for mounting of the active control drivers. The first segment was composed of a thirteen inch length with a 2.13-inch core depth and resistance goal of 32.7 Rayls. The second segment was composed of a ten inch length that was configured for inserting active control transducers. For the 13-inch liner segment, a series of two random excitation measurements were conducted at each of sixteen evenly spaced circumferential locations. The testing yielded an average resistance of 40.5 Rayls at 1384 Hz. Sine wave testing at a frequency of 1400 Hz yielded an average resistance of 41.1 Rayls. The reference test results were obtained with a hardwall liner. The hardwall was obtained by inserting a solid skin over the acoustic treatment. Table 4.7 is a summary table of the ANC impedance requirements and test results.

Table 4.7 ANC Test Barrel Acoustic Impedance Data

Barrel Identification	Type Acoustic Treatment	Liner Impedance	Barrel Diameter (in.)	L/D	Honeycomb Core Depth (in.)	Required R105	Actual R105 (Sine)	Actual R105 (Broadband)
NSL95005 (ANC1)	Uniform Passive Linear Liner	1.1585-1.3240i	48 in.	0.48	1.29	48.1	51.9	52.9
NSL95006 (ANC 2)	Segment 1 Passive Linear Liner (nearest fan)	0.554-1.914i	48 in.	0.21	0.971	23	27.4	29.4
NSL95006 (ANC 2)	Segment 2 Passive Linear Liner	0.788-0.522i	48 in.	0.27	2.131	32.7	41.8	40.7
NSL95007 (ANC 3)	Segment 1 Active (nearest fan)	Active Driver Section	48 in.	0.21	NA	NA	NA	NA
NSL95007 (ANC 3)	Segment 2 Passive Liner	0.788-0.522i	48 in.	0.27	2.131	32.7	41.1	40.5
Hardwall	Hardwall	NA	48 in.	0.48	NA	NA	NA	NA

4.2.7 Modal Measurement Results and Phase Translation

Some terminology used here is as follows. The first two radial modes of the four lobed circumferential pressure pattern will be expressed as the 4,0 and the 4,1 modes. The coefficients of these modes are complex numbers representing the amplitude and phase of the modal coefficients. The ANC rig instrumentation at the time of these tests could not capture absolute phase but phase difference such as between the 4,0 and the 4,1 modes are measured. This phase difference and the mode amplitude ratio are what is important in the acoustic liner design.

Improved and more complete rotating rake data was obtained by NASA Lewis engineers on the relevant build of the ANC fan stage with 14 rods mounted ahead of the 16 rotor blades and with hard inlet and exhaust ducts. This data was obtained on 10/18/95 and was provided to us for use in our noise suppressor analysis. The phase data does not have a fixed reference so

only phase differences are relevant. Figure 4.17 shows the phase difference between the zeroth and first radials of the four lobed pressure pattern over the range of corrected speeds between first radial mode cut-off and the fan maximum speed. Both the inlet (open symbols) and the exhaust duct (filled symbols) data are shown. The exhaust duct data will not be used in the analysis but is shown only to contrast the smoothness of the aft data to the abrupt variations in the inlet data with fan speed. The solid curve shows the phase difference expected at the inlet probe location if the phase difference between the two radial modes back at the rotor tip leading edge were a constant 64.8°. Several inlet data points, 1700, 1750, 1850, and 1886 RPM match this curve very well with the suggestion that this may be the underlying phase with rod-rotor interaction standing wave problems at 1650 and 1800 RPM. This is just an interesting conjecture which provides a smooth set of data for illustrative purposes and the suppressors are evaluated with both sets of phases. Figure 4.18 shows the mode amplitudes again for the inlet and the exhaust ducts at their respective rotating rake positions. Again the aft duct mode amplitudes are curiously smooth in contrast to the erratic behavior of the inlet duct modes. The inlet data in the form of the ratio between the zeroth and first radial mode amplitudes were used in the noise suppressor analysis. The input needed for the acoustic liner analysis are the phase difference and amplitude ratio at the beginning of the acoustic liner. The mode phase difference evaluated at the liner entrance is shown in Figure 4.19. The phase change with position in the duct for the two modes was calculated using each mode wave number with the small flow Mach number considered for each speed. Two cases are shown, again the assumed idealized case calculated using the constant phase assumption (64.8° all speeds) at the rotor and the case derived from the measured phase difference data. The phase difference at 1886 RPM is close to the preliminary data of 135° which was used as an input to design the acoustic liners. This shows the repeatability of the data over a long time period between builds of the test rig.

Figure 4.20 shows the results of a very interesting experiment. The radial mode phase difference was measured at two locations 24-inches apart on two different days. One measurement location is near the inlet lip the other near the rotor. The two modes have different phase speeds in the duct and this changes with frequency or fan speed. The measurements near the fan have been projected to the position near the inlet lip and compared to the near lip measured phase difference. The agreement is seen to be excellent at fan speeds where both data sets were taken. The older data listed as measured was not taken with the improved frequency resolution of the newer data listed as calculated (from one position to the other). These results show that the phase difference is quite repeatable and that this phase can be calculated quite well at one position from a different measuring position. This calculation must be performed to obtain the mode phase difference at the acoustic liner entrance.

4.2.8 Initial Estimate of ANCF Passive Suppressor Performance

The first evaluation of the performance of the acoustic liners uses the idealized inputs of constant phase difference at the rotor (solid symbols Figure 4.19 and the constant amplitude ratio of 2.92 used for the liner designs. These idealized results are shown in Figure 4.21. The segmented duct provides significantly more attenuation than the uniform duct of the same length at the higher speeds as the design conditions are most closely approached. Recall that ANC 3 represents the 13-inch second section of ANC 2 which is used with a 10-inch active section but which is not considered here. The addition of the 10-inch passive section to ANC 3 (as represented by ANC 2) is seen to quadruple the attenuation dramatically illustrating the benefit of segmented acoustic treatment.

When the radial mode phase differences and amplitudes as derived from the experimental data Figures 4.18 and 4.19 are used in the acoustic liner analysis, more erratic results are obtained as shown in Figure 4.22. The segmented liner still greatly outperforms the other liners at the design speed. It appears that the full length uniform liner is less sensitive to input changes since the performance of ANC 1 in Figures 4.21 and 4.22 are quite similar. It is not surprising that a high performance concept might be more sensitive to requiring the inputs be similar to the design inputs. When the active section is added to complete the liner ANC 3, the erratic modal input will be seen to be accommodated and attenuation maintained over a wide speed range.

4.2.9 Test Results

The ANC liners were tested as follows. In 1996 the hybrid active-passive liner ANC 3 was tested with the 13-inch passive section covered with an aluminum sheet to provide a baseline for the 10-inch active upstream section and to obtain the purely active control performance. Runs 794 to 809 provided far-field noise measurements with the rotating probe removed. The inlet rotating probe located in the near lip position was used for runs 810 to 826. The aft mounted rotating rake was used for runs 827 and 828. Hybrid liner ANC 3 was tested in the true active-passive mode also in 1996. Tests were conducted over the speed range with active control off, two rows of drivers operating, upstream drivers only and then downstream drivers only operating. Runs 834 to 864 utilized the inlet rotating rake in the near lip position and runs 865 to 897 provided far-field noise data with the rotating rake removed. NASA personnel conducted aft rake tests, runs 898 to 903. The segmented passive liner, ANC 2, was tested in 1995 with the inlet rotating rake mounted near the inlet lip for mode measurement runs 904 to 917. Far-field noise data were then obtained in runs 918 to 931 with the rake removed. The uniform 23-inch long liner, ANC 1, was tested in 1995. Inlet mode measurements were taken during runs 932 to 944 and far-field noise measurements during runs 945 to 956. The passive liner tests were taken with corrected speed increments of 25 RPM to provide improved frequency resolution.

The experimental acoustic power attenuation performance of the two-segment liner ANC 2 for the four lobed modes 4,0 and 4,1 at twice the blade passage frequency (2BPF) is shown in Figure 4.23. Also shown is a theoretical attenuation for these modes. The theory is based on the forward or near lip position of the rotating rake data of 10/18/1995 as projected to the input plane of the acoustic liner. This is the same calculation as presented in the Passive Suppressor Theory section. The 25 dB suppression of the acoustic power at the design point 1886 RPM corrected is seen to be quite large and also the agreement with theory is seen to be quite excellent particularly at the higher speeds. The fall off in performance with speed reduction is of no consequence here. The objective was to provide a theory that could predict the liner performance and to show that at an optimum design point the two segment liner is much better than a uniform liner of the same total length. Another objective of the study was to show that a hybrid liner could be developed that would control this performance fall off. This will be shown shortly.

In Figure 4.24 the same experimental results of Figure 4.23 are shown with a slightly different theoretical calculation of the ANC 2 suppressor performance. This calculated performance was based upon modal measurements near the rotor and then projected to the liner input plane. The peak near 1750 RPM is predicted with almost unbelievable accuracy. At the design point of 1886 rpm corrected speed this calculation does not do as well as was shown in Figure 4.23. This is mainly due to the different modal amplitude ratios measured in the two different baselines. A small parametric study was performed and shown by the solid symbols at 1886 RPM. The higher amplitude ratios produce the higher predicted attenuations and this result is consistent with the results of the two baselines. It appears that the theory is quite excellent with only the input choices causing problems.

Most of the erratic behavior of the suppressor performance with engine speed as shown in Figures 4.23 and 4.24 is produced by the equally erratic behavior of the modal amplitudes as shown in Figure 4.25. This modal amplitude data is the same as one of the baselines also shown in the Passive Liner Theory section. The passive liners were designed for a modal amplitude ratio of $A_0/A_1 = 2.9$ at 1886 RPM corrected. The recent baselines have not achieved this ratio even at 1886 RPM and deviate dramatically from this at lower speeds.

A summary of the experimental performance of the three ANC inlet suppressors is shown in Figure 4.26. The erratic nature of the results with fan speed are believed to be produced by the erratic nature of the 4,0 and 4,1 acoustic mode amplitude and phase caused by the rod rotor interaction as was discussed above. The uniform liner is providing about 15 dB of suppression at the design speed. The maximum suppression of about 25 dB is obtained with the passive two-segment liner. The active-passive hybrid suppressor is performing very well at the design speed providing a suppression of about 21 dB. Note that the performance as presented here considers only the reduction of the 4,0 and the 4,1 modes at the blade passage frequency harmonic (2BPF).

These are the only propagating modes with the rods mounted in front of the ANC fan at the design speed. The active element of the suppressor does suffer some mode spill-over which further limits its performance and this behavior is discussed in another section of this report. As the fan speed is reduced, the high performance of the two segment passive liner falls off dramatically probably due to the erratic mode amplitude and phase changes. However, it should be recognized that a finely tuned system like this will in general be more susceptible to input changes than the poorer performing uniform liner. Note that the active-passive hybrid system is able to overcome even these substantial input changes. This is of course the goal of this program to show that the hybrid system can overcome the loss in performance of the highly tuned system.

The performance of the hybrid and the passive liners based upon internal duct mode measurements for the NASA ANC fan stage tests were summarized above. It is also of interest to evaluate the suppressors based upon far-field noise results, especially for the ANC fan since the upstream rods produced fan tones far above the background noise. Figure 4.27 shows the far-field tone noise directivity for the hard-wall baseline and the two-segment passive liner for the two highest fan speeds tested. The tone considered here is twice the blade passage frequency. Significant directivity lobes are observed for the inlet and the aft tone noise for the hard wall baseline case. For the highest speed (1886 RPM) which is the two-segment liner design point, the inlet lobe is seen to be essentially eliminated by the two-segment noise suppressor. No attenuation is seen for the aft lobe which is as expected since no aft duct suppressor was included. Note that at about 41 degrees, a deep cut in the forward noise lobe occurs for the 1886 rpm case. This is due to the cancellation occurring between the two modes (4,0 and 4,1) in the far-field. At 1850 rpm the phase between these two modes is modified somewhat and less cancellation occurs. Liner attenuation can not be evaluated at this angle for the highest speed.

The far-field inlet noise attenuation for the two-segment passive liner is shown in Figure 4.28. At the design speed (1886 rpm) a large attenuation of 25 decibels is observed. This is the same as the modal power reduction measured in the duct. This large noise reduction in the far-field is possible because the tone level is far above (about 35 dB) the broadband noise level and this is due to the strong rod wake-rotor interaction. For 1886 rpm a dashed line has been drawn through the data points bridging the noise cancellation point at 41 degrees. As the fan speed is increased the performance of the two-segment passive liner falls off due to changing modal amplitudes and phases just as occurred in the duct mode power measurements previously reported.

The far-field tone noise attenuation for the hybrid active-passive liner is shown in Figure 4.29. The results are again for the tone at twice the blade passage frequency, and the hybrid liner has just the downstream drivers operating. Large inlet noise lobe attenuation is observed, and this attenuation is seen to be maintained with speed much better than that of the passive liner system. The active control has been able to cope with the dramatic changes in

mode amplitude and phase. These results provide additional confirmation of the superior performance of the hybrid active-passive liner system very similar to that provided by the internal duct mode measurements. Note also that the peak attenuation moves to larger angle with reduced fan speed. This is just the result of the tone modes radiating at larger angle due to the mode cut-off ratios being reduced toward unity as the fan speed is reduced.

The experimental far-field radiation directivity for the design speed of 1886 RPM is again shown in Figure 4.30 along with a theoretical radiation directivity. The theoretical results were obtained following the procedure of Rice[24]. The angle location and breadth of the modal radiation was calculated, but the magnitudes of the two modes were adjusted and a power summation made to best fit the experimental directivity. Notice that the deep plunge in the experimental data at about 43° occurs at about the point where the two modes are of equal magnitude. If the two modes (4,0 and 4,1) are nearly out of phase this would account for the large cancellation in the experimental data. The 4,0 mode radiation peaks at about 25° and the 4,1 mode peaks at about 50°. When the segmented and hybrid suppressor radiation directivity attenuation are compared to the theoretical radiation directivity, the hybrid liner Figure 4.29 appears to mainly attenuate the 4.0 mode and the segmented passive suppressor Figure 4.28 must attenuate both radials to have the attenuation peak at 35°. The far field noise data for the ANCF fan as shown in Figure 4.30 is probably dominated by aft fan noise for angles more than 60 or 70°.

4.2.10 Additional Comments

The following presents a summary of the results of measurements that demonstrate the functional performance of the hybrid active-passive segmented liner and its constituent elements.

Figures 4.31 and 4.32 illustrate the radial mode resolving capability of the flush mounted wall microphone array, as measured in the hardwall baseline duct configuration. Circumferential order spinning mode $m = +4$ sound pressures from the sin/cos components at the three axial stations

$$P_{m,Spinning} = \left(P_{m,\cos} - iP_{m,\sin}\right)/2 \tag{16a}$$

$$P_{-m,Spinning} = \left(P_{m,\cos} + iP_{m,\sin}\right)/2 \tag{16b}$$

were presumed to be a linear combination of upstream traveling (4,0) and (4,1) modes and downstream traveling (reflected) (4,1) modes

$$P_{4,Mic} \approx P_{4,0}e^{ik_{4,0,+z}z_{Mic}} + P_{4,1}e^{ik_{4,1,+z}z_{Mic}} + R_{4,1}P_{4,1}e^{-ik_{4,1,-z}z_{Mic}} \tag{17}$$

where $k_{m,n,\pm z}$ is the axial wave number for mode (m,n) and z_{Mic} is the axial coordinate of the microphone array. Reflection of mode (4,0) was ignored based on the duct dimensions and sound wavelength. Figures 4.31 and 4.32 present the ratio of mode amplitudes and difference in mode phases between modes (4,1) and (4,0) at the downstream edge of the fixed array, together with the mode amplitude ratio and phase difference data measured with the NASA rotating rake. There is a clear agreement between the two sets of

measurements, indicating both that the microphones and mode separation networks provide a faithful indication of the $m = 4$ sound pressure at each axial station and that the low (4,0) reflection presumption is warranted.

Figures 4.33a and b are 3D bar graphs showing the 2BPF mode structure of the baseline measurement at two axial locations for fan speed 1886 RPM. With the exception of some minor differences in the $m \neq 4$ modes, the two are nearly equal. The total 2BPF tone power is approximately 118.8 dB, of which 118.7 dB is mode m = 4. The 103 dB remainder is from spurious modes, most prominently m = +2, -1,-4 and +8 or a "targeted to spurious" mode ratio of about 15.5 dB. At the inlet plane measurement station, mode (4,0) has a power level of 118.2 dB and mode (4,1) a power level of 109.3 dB (amplitude ratio 0.3 on the outer duct wall). This illustrates the utility of the ANCF fan with rods as a test site for active control of sources with specific well defined modal structures.

Figures 4.34a and b are 3D bar graphs showing the modes radiated by the two sets of active resonators when driven from an oscillator signal simulating the 1886 RPM fan reference. The fan was stationary and the passive element of the liner was covered with aluminum sheet. Note that the "Upstream" drivers are the active resonators closer to the (covered) passive liner element. In both cases, modes (4,1) and (4,0) are nearly equal at 109-110 dB (112-113 dB sum). The "targeted to spurious" ratio is 7.5 dB for the upstream resonators and 10 dB for the downstream resonators, poorer than the fan but adequate to demonstrate the functionality of the hybrid liner system. It may be noted by comparison to Figures 4.33a and b that the (4,0) : (4,1) ratio for the active resonators is dissimilar from that of the fan. A single active resonator row would therefore be unable to cancel fan noise.

[Note - As discussed previously, the original system design concept was to provide control channels for the two stationary components of the $m = 4$ spinning mode individually, to allow control of m = -4 energy radiated by the fan. It was determined that this was unnecessary and detrimental to the system operation. The system was revised, using Hilbert transform processors to derive quadrature signals required to drive the spinning mode from a single control signal per resonator array.]

For use in the active-passive hybrid liner, the microphone arrays were positioned such that at the design fan speed of 1886 RPM, separate "error" signals could be derived easily for modes (4,0) and (4,1). This was done by spacing the three arrays (identified as A, B and C in flow-wise order) so that pairs (B, C) and (A, C) were 1/2 wavelength apart for modes (4,0) and (4,1) respectively. Summing the signals from one pair of microphone arrays would then reject that mode, providing an error signal for the opposite mode (as discussed for the HAE tests). Although this approach was the most effective embodiment of the system at the design speed, it was found that at lower fan speeds, more reliable operation was achieved using separate error signals from two of the microphone arrays, with A and C being somewhat preferable and used for all reported test results except as specifically identified otherwise.

Figures 4.35a, b show control on vs. control off modal plots for the full active-passive hybrid liner at the design speed, using the "modal" error signal combinations described above. Observe by comparison to the baseline plots that mode m = 4 power has been reduced by over 33 dB and that total 2BPF sound power has been reduced by over 15 dB. Figures 4.36a, b provide a comparison between the full "modal" error signal and the A & C array errors. The latter achieved approximately 3 dB less attenuation, but still reduced m = 4 by over 30 dB. By contrast, Figures 4.37a and b show the results for individual modal error. Observe that with microphones B + C used for error, mode (4,0) is less well attenuated and vice versa, demonstrating that the system adapts to control the mode for which the error signal is most representative.

Figure 4.38a shows the mode m = 4 sound power level vs. fan speed for baseline, control off, and upstream, downstream and both resonator rows active with the passive liner covered. Figure 4.38b shows the total 2BPF sound power levels under the same conditions. These give an indication of the capability of the active resonator arrays to control the dual mode sound field alone and in pairs. Note that the total attenuation at 2BPF is less than that at mode m = 4 because of modal impurities of both the fan source and the active resonator arrays.

Figure 4.39a shows the mode m = 4 sound power level vs. fan speed for baseline, control off, and upstream, downstream and both resonator rows active, but with the passive portion of the liner exposed. These demonstrate the capability of the hybrid active-passive segmented liner to suppress modal inlet tones with single and dual rows of active resonators, disregarding modal spillover. Observe that the system provides significant attenuation with a single active resonator row but that performance depends strongly on which row is activated.

Figure 4.39b shows the total 2BPF sound power level vs. fan speed for baseline, control off, and upstream, downstream and both resonator rows active, but with the passive portion of the liner exposed. Observe that this demonstrates the total tone reduction, including the effects of modal distortion introduced by the fan and by the liner.

Finally, Figure 4.40 shows a summary of the attenuation in mode m = 4 at 2BPF, relative to baseline, provided by the constituent elements of the hybrid liner, the sum of the constituent attenuation and the overall measured attenuation as a function of fan speed. Over the range of speeds 1750 to 1886 RPM, the overall attenuation exceeded the sum of the constituents by approximately 5 dB, illustrating the synergy of the active/passive segmented liner concept.

On the basis of the 2BPF tone attenuation results shown in Figure 4.39b, approximately 15 dB reduction in far field 2BPF noise radiated toward the fan inlet is expected. Figures 4.41 to 4.44 show forward quadrant directivity patterns for baseline, control-off and control-on (both resonators, microphones A and C) conditions, which illustrate the effect of the hybrid liner on forward radiated noise. Figure 4.45a and b shows the reduction in radiated 2BPF sound power as a function of fan speed.

In general, the degree of far-field 2BPF noise reduction agrees reasonably well with the in-duct measurements for directivity angles up to approximately 60° as shown in Figure 4.45a. For the full 90° quadrant, shown in Figure 4.45b, the overall reduction was significant, but limited by sideline radiation. The far-field levels near 90° were likely contaminated by the radiation coming around from the aft duct and possibly direct radiation from the casing of the hybrid liner, which was fully exposed. In a more practical installation, an outer cowling might reduce this latter flanking radiation.

5 – CONCEPT VALIDATION IN NASA LeRC 9X15 LOW SPEED WIND TUNNEL FACILITY USING THE ADP FAN

Following demonstration of the hybrid active-passive liner in the ANCF 48-inch fan, a series of tests were conducted to investigate the viability of the concept in a high flow speed environment.

5.1 ADP TEST FAN

The Pratt & Whitney 5.9:1 scale "Advanced Ducted Propulsor" (ADP) fan as shown in Figure 5.1a, b and c was selected as a test environment, which required an approximate 4:1 frequency scaling from the ANCF tests. In addition, microphone and active resonator arrays were required to address circumferential mode m = -9 and microphones were required to operate in a 140-150 dB flow noise environment in the Mach ≈ 0.4 inlet flow. The inlet throat of the fan is a circular duct 20.5 inches in diameter, with radial mode structure as shown in Figure 4.3c. The fan spinner protrudes such that at the rotor blades the inlet is an annular duct with radius ratio 0.5.

The ADP fan rig is located in the NASA LeRC 9 x 15 ft. Wind Tunnel. The ADP is a low noise research fan stage that is combined with a nacelle and engine core duct to form a powered fan/nacelle subscale model. The model has a 22-inch leading edge fan diameter that utilizes an existing fan and cowl force balance and drive system. The fan has 18 blades and 45 vanes and is designed to result in minimum noise. The vane number was selected to cutoff blade passage frequency (BPF) and has been optimized for higher harmonics, 2BPF and 3BPF. The rig has a rotating rake measurement system that consists of a rotating drum that supports a rake with 12 inlet pressure transducers. This system rotates at 1/200 of the fan speed. A detailed description of the rake system is contained in a NASA LeRC Reports by Heidelberg et al.[22, 23] The rake system is removed for the far-field measurements in the wind tunnel. In addition, walls are installed along the side and rear to prevent exhaust noise from contaminating the inlet noise.

The ADP fan stage is a 22-inch scale model of a realistic ultra high bypass fan stage of a modern high bypass commercial aircraft turbofan engine. The suppressor design point was chosen at a relatively low fan speed of 5425 RPM since only two radial modes of the minus nine lobed mode can propagate at this speed. Also this was the only fan speed at which preliminary modal data were taken which were needed for the acoustic liner designs. The inlet sound propagation code with flow and a wall boundary layer was used for the suppressor design.

This element of the program suffered from the very preliminary state of the NASA mode measurement capability for high speed fans like the ADP fan stage. This capability improved dramatically prior to the final suppressor test phase, but data needed for the suppressor designs was found to be faulty. Modal data for the first two radials of the m = -9 mode were provided and the suppressors were designed using this very preliminary data. Even the Mach number versus fan speed information was substantially altered from the preliminary data to the final test data. Fortunately, the active-passive hybrid

suppressor is sufficiently adaptable to accommodate these questionable inputs. The following liner designs are based upon the preliminary data inputs.

5.2 ADP INLET SUPPRESSOR DESIGN AND CONSTRUCTION

5.2.1 Acoustic Liner Design

The modal amplitudes and relative phases were provided at the throat of the inlet. The phases were translated to the acoustic liner leading edge using the local wave number based on the local radius and Mach number in a ten step procedure. The design calculations proceeded in a manner similar to that of the HAE and ANC acoustic liners. A 20 x 20 matrix in the wall impedance plane was used to perform a series of acoustic power calculations and the results were plotted as attenuation contours in the impedance plane.

The results of the acoustic design of the passive uniform liner is shown in Figure 5.2. An attenuation of over 10 dB is seen to be possible in spite of the very short liner with L/D = 0.37. The non-dimensional optimum impedance is seen to have a 2.395 resistive component and a -2.224 reactive component. These values are normalized by the free air impedance. The optimum design of the two segment passive liner was performed using an iterative procedure varying one segment while holding the other fixed and then reversing the procedure. The final iterations are shown in Figures 5.3 and 5.4. The impedance characteristics required of the second segment (furthest from the fan stage) are shown in Figure 5.3. About 18 dB attenuation appears to be possible with the two segment liner which would be a very impressive performance with such a short liner. The optimum impedance is seen to be quite usual with a normalized resistance of 1.061 and reactance of -1.567. The first liner section (nearest the fan stage) is seen to be quite unusual as shown in Figure 5.4. A very large negative reactance is required to achieve this high performance. The normalized optimum resistance could be 2.53 while the reactance must be -10.61. This large negative reactance results in a very thin liner for this small scale fan stage. This two segment liner design is specific to the very preliminary design conditions provided for the ADP fan stage at this speed. The modal amplitudes and phase difference as provided by NASA Lewis engineers are shown on the figure. Over the axial length of the liner the duct radius varies somewhat which causes a change in the phase velocity of the modes. The change in the phase difference between the 9,0 and 9,1 modes was calculated over one inch length increments and accumulated over the full length of the liner. An average duct diameter was then used that provided this same phase change over the full length of a constant diameter duct.

The nature of the attenuation-impedance characteristics for the first section of the two section liner as shown in Figure 5.4 are seen to be quite different from those of the other liner sections. No real optimum is found in the high attenuation region. A range for the liner resistance is shown with the lower value probably preferred since this is even quite high (2.53). The usual type of attenuation contours can be found in the lower right side (small

resistance, reactance near zero) of Figure 5.4 where the values for the uniform liner would be approached. The high attenuation region of Figure 5.4 does suffer from a limited number of converged modes which would be considered cut-off if the duct were hard. However, the acoustic power balances very well across the duct segment interfaces and no discontinuous behavior of the liner performance is apparent. The use of the set-up liner for ADP 2 as shown in Figure 5.4 was considered to be high risk due to its very unusual high frequency resonance (thin depth) which may be useless at the lower design frequency if the actual modal inputs were dramatically different than the design inputs. This turned out to be true when the improved data were obtained. However, it was realized that the active section would replace this thin section in the hybrid active/passive barrel and would be adaptive enough to overcome this deficient input data.

Improved modal input data was obtained using a hardwall baseline inlet which was tested during the same NASA 9x15 wind Tunnel entry as the acoustic liner tests. Since no reliable preliminary data was available before this entry, no preliminary suppressor performance calculations were made. The theoretical calculations for the passive ADP suppressors will thus be presented along with the experimental data in a later section.

5.2.2 Barrel Fabrication

Four different barrel sections were designed for testing in the ADP rig. The first barrel, designated as ADP 1 (NSL96001), was designed as an all-passive barrel having a single core depth linear liner acoustic treatment. The second barrel, designated as ADP 2 (NSL96002), is a segmented passive barrel having two different acoustic impedance's. The impedance requirements for the liner segment that is located closest to the fan face of the ADP fan rig were specified as a normalized resistance of 2.53 to 5.05 and normalized reactance of -10.61 at a frequency of 3255 Hz. The impedance tests were conducted with a dual microphone impedance tube. Normalized reactance values averaged minus 10 at 3200 Hz. Resistance values measured using the impedance tube were higher than obtained with dc flow measurements. This is due to experimental error obtained for measurements with a high reactance value. For this small depth liner the dc flow measurements more accurately describe the resistance. The third barrel, designated as ADP 3 (NSL96003), is a hybrid active/passive liner which has the active section located next to the fan and the optimized passive linear liner acoustic treatment forward. The drawing for this component is shown in Figure 5.5. The impedance values for all the barrels are shown in Table 5.1.

Table 5.1 ADP Barrel Acoustic Impedance Values

Barrel ID	Type Acousti Treatme	Liner Impedance	Barrel Diameter	L/D	Hone Core	R105 Goal	Measured 145/150 dB (Sine)	Measured 145/150 dB (Broadband)	NLF (R200/R20)
NSL96007	Hardwall	NA	22.0 in.	0.37	NA	NA	NA	NA	NA
NSL96001 (ADP 1)	Uniform Passive Linear Liner	2.395-2.224i	22.0 in.	0.37	0.2416 in.	126	129.4	110	1.5
NSL96002 (ADP 2)	Segment 1 Passive Linear Liner (nearest fan)	2.53 to 5.05-10.61i	22.0 in.	0.18	0.06 in.		220.3	184.4	2.08
NSL96002 (ADP 2)	Segment 2 Passive Linear Liner	1.061-1.567i	22.0 in.	0.19	0.3132 in.	53.6	57	49.5	1.53
NSL96003 (ADP 3)	Active Section (nearest fan)	NA	22.0 in.	0.18	NA	NA		NA	NA
NSL96003 (ADP 3)	Passive Linear Liner	1.061-1.567i	22.0 in.	0.19	0.3132 in.	53.6	56.6	46.9	1.51

The final barrel consisted of a reference hardwall section, identified as NSL96007, which was used to obtain the baseline induct and far field noise measurements.

The current ADP fans inlet lip "D" nose was not utilized for these tests. Instead a "D" nose that was lengthened by one-inch was designed that would allow the installation of two rows of error microphones. The "D" nose was designed to have mounting flanges to incorporate the two rows of 36 Endevco pressure transducers. Mounting blocks were designed and were installed inside the "D" nose to hold the pressure transducers.

Each of the inlet barrels featured a single splice air passage skin and a no splice backface skin with an integrated attachment flange. The final splice was no greater than 0.075 inches in width. A single "D" nose was utilized for each of the barrels which allowed quicker barrel changes between tests and did not require the removal of the 36 pressure transducers for each configuration change. The "D" nose was a one-piece fiberglass unit having a stretch formed outer cowl splice strap designed to mate with the existing ADP cowl outer skin. A three piece engine attachment flange was fabricated to mate with the existing ADP rig. The inner air passage flow lines matched the current ADP barrels.

5.3 DATA ACQUISITION SYSTEM

The target modes were (-9,0) and (-9,1) at 2BPF, generated by an 18 blade rotor and 45 vane stator row in the nominally 22-inch ADP fan. Fan operating speeds were 5025-9450 RPM, corrected to 59° ambient temperature (1117 ft/sec sound speed), producing mean flow Mach numbers ranging from 0.3 to 0.44 in the fan inlet. Tests conducted at fan speeds exceeding

approximately 6000 RPM included additional radial mode components above and beyond the two for which the demonstration system was designed. At the maximum speed, five radial order modes were cut on in the fan inlet.

The microphone array used in the ADP tests represents a double simplification relative to the ANCF test array. First, the number of annuli was reduced from three to two based on the success of the ANCF tests with two annuli used for error detection. Second, the number of microphones in the annuli were reduced to the Nyquist minimum of 2m, based on NASA data showing that mode m = -9 was heavily predominant over mode m = +9, so that potential for mode aliasing was not a significant issue. Therefore, error microphone arrays consisted of two annuli of 18 equally spaced Endevco type 8510B-1 (1 psi rating) strain gauge pressure transducers, flush mounted in the ADP fan inlet "D" nose. The microphones were spaced axially 1.0-inch, or approximately 1/2 wavelength at the design speed of 5425 RPM (3255 Hz) and approximately 0.4 wavelength at the maximum test speed.

Outputs of the individual microphones in each annulus were weighted by the inverse of their calibration sensitivities and by the cosine and/or sine of their modal azimuthal angle and summed to produce mode m = 9 stationary wave outputs. (Note that with 18 microphones, the weighting factors for m = 9 are all either +1 or -1.) These modal outputs were used for active control error signals and were monitored to indicate control system effectiveness.

Active Helmholtz resonator arrays consisted of two annuli of 36 equally spaced resonators. The resonators were designed and fabricated especially for the high frequency application on the ADP scale model engine and were built in axial pairs to simplify fabrication and installation. As shown in the drawing in Figure 5.6a and b the resonators are approximately 1-inch square and 0.4-inch deep and are designed with the active element on the front, rather than at the base as for the ANCF tests. The size of these drivers are shown in contrast to the ANCF drivers in Figure 4.12a.

The Helmholtz resonator is formed by the slot orifice at the end of the actuator and the cavity behind the actuator. At frequencies between 3,000 and 3,500 Hz, acoustic radiation is primarily due to resonant flow in the orifice. This transitions to direct radiation by the actuator at higher frequencies. The primary mechanical resonance is approximately 5200 Hz and the Helmholtz resonance approximately 3,200 Hz. The operation of the active resonator can be likened to that of the traditional "bass-reflex" loudspeaker, although it has significantly dissimilar mechanical and electrical properties.

Because of the frequency dependent distributed radiation area of the paired active resonators, the effective axial spacing was approximately 2-inches at 3,000-3,500 Hz, with a gradual transition to approximately 1.25-inches at higher frequencies.

Free field frequency response measurements were taken for 41 active resonator pairs. A summary of the results is shown in Figure 5.7a and b, which indicates very uniform response characteristics among the actuators except near the primary mechanical resonance. The best matched 36 pairs of resonators were graded and grouped in sets of three for installation in the liner.

With 36 active resonators per annulus and a control target mode m = -9, there were four resonators per circumferential wavelength, the same as for the ANCF tests. This then requires excitation signals of phase 0°, 90°, 180° and 270° which where provided by the Hilbert transform processor. If the response characteristics of the resonators were perfectly matched, an entire annulus could be driven by four power amplifiers, one for each of the phases, driving nine resonators each. It was elected instead to drive three resonators per amplifier, allowing compensation for minor response variations by amplifier gain and voltage/current feedback adjustments. A total of 24 switching power amplifiers were thus used to drive the 72 miniature active resonators.

Active control signal processing was done on a Spectrum, quad Texas Instruments TMS320C40 floating point DSP system, programmed for externally clocked, two error channel and two output channel Adaptive Quadrature processing.

The active control timing reference signal was obtained from the 128x pulse train output of the fan shaft encoder. Control signals were synthesized by the control algorithm, based on the ratio of the sound frequency to the encoder pulse rate

$$V_{\cos}(q) = V_0 \cos\left(2\pi \frac{nB}{P} q\right); \quad V_{\sin}(q) = V_0 \sin\left(2\pi \frac{nB}{P} q\right) \tag{17}$$

where n is the BPF harmonic, B is the number of rotor blades, P is the number of pulses per fan revolution and q is the encoded pulse count. In the test case, nB/P = 9/32 (i.e., a 32 place lookup table spans nine cycles).

The active control algorithm determined the real and imaginary parts of the drive signal required for each resonator annulus that would combine with the fan 2BPF tone to produce a null at both microphone annuli.

All signal paths were conditioned using band pass filtering to restrict signals to the range 3000-5500 Hz.

System monitoring was done using Data Translation/Hewlett-Packard DT-VEE data acquisition/processing/display software and a Data Translation type DT2821-G-16SE high speed analog I/O interface. The following system signals were monitored and samples thereof stored on disk for subsequent analysis:

- Modal sound pressure signals from two microphone array mode separators
- Filtered cosine reference signal
- Control signals to two annular active resonator arrays
- Unprocessed microphone signals from one microphone in each of two annular arrays
- NASA far field microphone signal during far-field testing

The DT-VEE processing and display provided on-line indications of the following information:

- Modal sound pressure PSD display for two microphone mode separators and (when used) the NASA far field microphone

- Sound pressure waveforms from two unprocessed microphone signals
- Control signal waveforms for two active resonator annuli.

These were used for on-line assessment of liner performance and actuator drive levels.

A schematic diagram of the active/passive segmented liner measurement system is shown in Figure 5.8.

5.4 ADP MEASUREMENT PROGRAM

Table 5.2 is a summary of the parameters of ADP test series, which are subsequently discussed in detail.

Table 5.2. Summary of Experimental ADP Program Test Matrix

Test Facility	Nominal Diameter	Sound Source	Target Modes	Active Resonators	Error Microphones	Speed Range (Corr. RPM)	Test Section Mach no.	Frequency Range (Hz)
ADP	22 in.	18 Blade Rotor, 45 Vane Stator	(-9,0), (-9,1)	2 Rows of 36 each	2 Rows of 18 each	5025-9500	≈0.3-0.45	3000-5500 @ 2BPF

Following installation of the hybrid active-passive liner on the ADP fan inlet, the passive portion of the liner was covered with a heavy plastic septum. The two annuli of active resonators were driven with mode m = -9 signals from the control system, using a pulse generator as an artificial fan shaft encoder, simulating a fan speed of 5425 RPM. The output of the pulse generator was also used to synchronize the NASA rotating microphone rake system shown mounted in front of the inlet in Figure 5.9. The sound field produced by each row of resonators was measured in the absence of the fan rotation, flow and the passive liner element, with results as shown in the modal diagram, Figure 5.10a and b. It may be noted, although only the upstream drivers are shown, that for both active resonator rows, mode *m* = -9 dominated the radiated sound field, with very little modal distortion (spillover).

Following this demonstration of actuator modal output, the active control system was connected to the fan shaft encoder output and the cover was removed from the passive liner sections. Tests were conducted of the active-on vs. active-off duct modes at the fan inlet, again as measured with the NASA rotating rake microphone system. These levels were then compared to measurements taken with the hard-wall baseline inlet, the uniform passive liner and the segmented passive liner.

Two sets of results were determined from these in-duct measurements. First, the distribution of acoustical energy among the propagating m-order modes was plotted for the 5425 RPM (approach) design fan speed, as shown in Figures 5.11 to 5.13. These indicate that the active-passive liner caused a small increase in non-target mode levels, both with control on and control off. Second, the m = -9 target mode attenuation (sound power relative to hard-wall baseline) was plotted, in Figure 5.14 as a function of fan speed over a range

that included between two and five radial components. Figure 5.14 presents a summary of the results of the ADP measurements of the adaptive segmented liner as compared to the optimized uniform passive and segmented passive liners. It shows the attenuation achieved by each liner over the design fan speed range of the system, as well as one speed above this range. It may be noted from the figure that all tested liners appear to perform poorly at fan speed 5625 RPM. This is the result of a partial null in fan rotor/stator tone generation at this speed. The important results demonstrated by Figure 5.14 are as follows:

1. The adaptive segmented liner consistently outperforms the passive liners over the range of speeds 5225-6225 RPM. This is particularly true at the system target design speed 5425 RPM and below, where the adaptive segmented liner outperformed the optimized uniform passive liner by 8 to 10 dB.
2. On average, the uniform passive liner outperforms the adaptive segmented liner when the active control element is inactive. This is expected, as the passive portion of the adaptive segmented liner is only approximately 60% as long as the uniform liner, and they are of the same design. However, it may be noted that at the lowest test speed, 5225 RPM, the inactive adaptive segmented liner performance exceeds that of the uniform passive by over 3 dB. This results from passive absorption of the active Helmholtz resonators, whose natural tuning frequency is approximately 3 kHz (5000 RPM). This is an important aspect of the active resonator approach to active control actuator implementation. It provides an acoustical boundary that does not remove effective area from the passive liner, but rather allows a re-tuning to frequency ranges for which the passive liner may be ineffective.
3. The successful performance of the adaptive segmented liner at 6225 RPM bodes well for the potential simplification of active control systems using the synergistic active/passive hybrid approach for addressing multiple radial modes. At this speed, three radial modes are well cut on in the fan inlet duct, whereas the active system with two rows of actuators and two rows of error microphones was designed only for control of fields with up to two radial mode components.
4. The ineffective performance of the passive segmented liner resulted from use of incorrect mode mixture data in the design of the liner. The design was based on preliminary measurements of the amplitude and phase relationships between modes (-9,0) and (-9,1) in the fan inlet. These proved to differ substantially from the actual mode mixtures, and led to incorrect specification for the impedance of the initial, scattering liner segment.

Two series of measurements were conducted using the NASA far-field microphone traverse system. In the first series, measurements were taken of the full radiation pattern of the fan, fore and aft, for active control on and off conditions with the active-passive liner. A barrier wall was then installed to block aft-radiated noise and far-field measurements were taken for active control on and off conditions with the active-passive liner as wall as for the hard-wall baseline, uniform passive and segmented passive liners. Because the ADP fan inlet noise is dominated by broadband components, these measurements indicate no clear reduction of far-field noise with the active control system on vs. off.

5.5 MODAL PHASE MEASUREMENTS AND TRANSLATION WITH POSITION.

The modal amplitudes and phases were measured at the ADP inlet throat using the rotating rake in the same manner as in the ANC fan tests. A computer code was written to calculate the modal phase at any position in the inlet given the throat phase measurement and Mach number. The internal contours of the inlet, including the center-body, were programmed into the code. One hundred small steps were used to calculate the phase change with each step representing a short cylinder using the local average Mach number and inner and outer radii. The distances from the throat included a one inch constant radius throat section, a four inch passive dissipative liner, and a 3.696-inch initial or set-up liner for the segmented liner case. Unfortunately the segmented and hybrid liner tests had a different baseline than the uniform liner with the latter inadvertently having an interstage liner in place during the test. A fully hard interstage section was installed before the segmented and hybrid liner tests.

Recall that some initial questionable input data was supplied by NASA Engineers early in the program to allow design of the ADP suppressors. This initial data was throat Mach number, $M_{thrt} = -0.3$, mode amplitude ratio, $A_1/A_0 = 0.72$, and mode phase difference at the liner entrance, $\phi_1 - \phi_0 = 17.7°$ at corrected fan speed of 5425 RPM. More reliable data were taken during the test entry in the 9 x 15 Anechoic Wind Tunnel during which the suppressors were tested. The baseline tests for the uniform liner provided $M_{thrt} = -0.3773$, $A_1/A_0 = 0.427$, $\phi_1 - \phi_0 = 3.23^0$. The completely hardwall baseline tests to be used for the segmented liner provided $M_{thrt} = -0.3773$, $A_1/A_0 = 1.33$, and $\phi_1 - \phi_0 = -21.37^0$. Recall that the phase values have been translated to the leading edge of the liners 8.696-inches downstream from the throat where the measurements were made. Note that the input data "as tested" are considerably different than the "as designed" values. As shown in the discussion of the HAE and ANC suppressors, performance is very sensitive to input conditions. Thus optimized passive liner designs for the ADP inlet were not achieved.

5.6 TEST RESULTS

5.6.1 In-Duct Measurements

For each fan speed, the data measured at the inlet lip were translated to the leading edge (nearest fan) of the uniform liner NSL96001 and these results were used in the segmented liner sound propagation code discussed earlier in this report. The measured acoustic impedance as provided by Northrop Grumman engineers for liner NSL96001 were used for the theoretical calculations. The experimental acoustic power attenuation for the m = -9 modes and the theoretical comparison are shown in Figure 5.15. Note that there are two radials at the lower speeds and six radial modes at the higher speeds considered here. The comparison is seen to be very good considering the highly complex experimental and theoretical procedures required here. The one point at 6225 RPM may involve a resonance and reflection (third mode just cut-on) from the fan or termination that is not considered in the theory.

The same procedure was used for the segmented passive liner NSL96002. Again the acoustic impedance for the two liner sections as measured by Northrop Grumman were used in the theoretical calculations.

The comparison of the experimental and theoretical acoustic power attenuation for the m = -9 radial modes are shown in Figure 5.16. The comparison is seen to not be as good as for the uniform liner shown above. At low fan speeds where only two modes are present, the agreement is reasonable, but as more modes propagate at the higher speeds the experiment is showing greater attenuation than the theory predicts. Any explanation of the theory-data comparison is pure conjecture at this time, but it should be recalled that the segmented liner is very sensitive to the modal input values and these are not known with great precision.

Some interesting calculations were performed for the 4-inch long passive section of the active-passive hybrid suppressor NSL96003. The amplitude and phase of all of the input radial modes were varied to provide maximum acoustic power attenuation of the m = -9 radial modes. The calculation started at the low frequencies where only two radial modes propagate and progressed to the higher frequencies where four radial modes propagate using the previous optimized calculation as the new starting point. This calculation represents an attempt at estimating the performance of the active-passive hybrid suppressor if the active section acts only to modify the input modal structure which is then fed to the passive section for suppression. The calculations are shown in Figure 5.17 as the solid round symbols. The experimental results for the active-passive hybrid suppressor are also shown with the drivers on and off. With the drivers off the suppression is provided by the passive section and by the passive effect of the driver resonator cavities. These experimental results in general are considerable but lower than the theoretical results. With the drivers turned on the experimental results are seen to generally exceed the calculated results. The experimental results now encompass several mechanisms. One is of course the modification of the input modes to maximize the passive liner suppression as was included in the calculations. In addition there is the passive suppression of the driver resonators and probably a modal reflection effect due to the active section which all together produce the high observed attenuation.

5.6.2 Far-Field Radiation Considerations

The ADP fan noise tones at twice blade passage (2BPF) are the tones of interest in the far-field especially near the suppressor design speed where only two radial modes of the m = -9 mode propagates. The protrusion of these tones above the broadband background are shown in Figure 5.18. It is seen that the tones stand out only about 9 dB above the background for the maximum case and only about 4 to 6 dB around the design speed. This is not enough margin to adequately study the large attenuation achieved by the active-passive hybrid suppressor. Since the in-duct measurements have shown the validity of the suppressor concept, the far-field data will not be used at this time.

6 – COMMERCIALIZATION OF HYBRID LINER CONCEPT

Aircraft noise is one of the most serious long-term environmental problems facing the aviation industry today. Vehement opposition by airport neighbors and community groups has constrained capacity and limited operations at many of the nation's major airports. Airport proprietors and civic officials, in turn, are pressuring the US Congress and the federal government to adopt stricter aircraft noise rules. Air carriers, frustrated by the multiplicity of restrictive local airport rules, are also pressuring the US Government to preempt the rights of airport proprietors to restrict aircraft operations.

Given the strong sentiments in the US and Europe for strong new rules on aircraft noise, it is clear aircraft owners and operators will be forced either to replace noisier non-compliant aircraft or retrofit them to meet the new regulations. The exact timetables vary among the proposals, but all would have the effect of cutting short the normal lives of these aircraft.

The overall objective of this venture is to develop superior jet engine acoustic treatments that will reduce noise emissions and satisfy or exceed anticipated future federal and local noise regulations. Northrop Grumman Corporation (NGC) has vast amounts of experience in designing and building acoustic treatments for commercial jet engine nacelles. Many of the worlds commercial aircraft including the B747, B767, MD11, Fokker 100, A300, A310, and A330 have acoustic treatments designed and manufactured by NGC. Current Federal Aviation Administration (FAA) Federal Aviation Regulation (FAR) Part 36 Stage 3 and impending new noise regulations being implemented in Europe and Asia threaten to render obsolete many of the worlds current commercial aircraft, some less than 20 years old. There are still many older higher noise level Stage 2 aircraft that have a productive economic life expected to be over 40 years. In addition, more stringent noise regulations, "Stage 4", are being debated within the international aviation groups as local airport communities, especially in Europe, demand restricted hours of operation and even quieter aircraft. New commercial aircraft designs are now specifying noise margins, beyond Stage 3, of at least 4-6 dB for each of the three required ground measurement locations (takeoff, sideline and approach), thus making the use of an all-passive acoustic treatment difficult. Limitations in inlet acoustic area and aerodynamic considerations dictate that a new technology will be needed to meet future aircraft noise requirements.

6.1 COMMERCIALIZATION PLAN SUMMARY

An economical solution is needed to reduce aircraft engine noise to levels that will meet FAR 36 Stage 3 and future noise regulations. Based on economic analysis for a mid-sized aircraft, hush kits sell for $3M and new engine costs are $12M. The cost of replacement aircraft range from $35M (737-600) to $175M (747-400). Hush kit development is the cost-effective solution if aircraft performance is not compromised. In addition, low cost, lightweight, and highly efficient duct attenuators for new aircraft offer a unique solution to future noise requirements. Based on economic analysis there are a

number of items in the Hybrid Active/Passive system that will be more expensive due to added weight and complexity over a passive acoustic liner system. However, this is offset by a reduced nacelle length since shorter duct acoustic treatments are required for the active liner components.

The use of Hybrid Active/Passive acoustic liners will buttress US competitiveness in the world market and insure that commercial transport aircraft meet current and new proposed noise requirements. A successful program will lead to an entirely new business since this technology is non-existent in the aircraft industry today. The required capital investment, excluding the development cost, is estimated to be approximately $3-4M over a 3 year period. The investment is for the engineering and tool design required prior to production start-up. The dollar figure utilized is based on actual expenditures for previous acoustical treatment programs and adjusted for the added complexity of the active control components. Current resources that will be required to be committed include manufacturing capabilities and facilities, composite capabilities, electronic laboratories, engineering personnel, and the capability in acoustic liner design.

Today's big-fan engines have many advantages over earlier generation low bypass engines including superior performance per pound of fuel burned and considerably smaller noise footprints. The length-to-diameter (L/D) of the inlet cowl on these big-fan engine inlets is decreased which results in reduced acoustic areas when compared with previous inlet designs. However, as the engine fan grows in size and the total fan noise increases, ways to reduce this increased noise must be considered. A current engine and airframe noise reduction study being conducted by the European Alliance (a consortium of aerospace companies and research organizations) has concluded that "improved acoustic liners will not achieve the noise reduction targets industry needs" and "other technologies, such as active noise control, may offer further benefits."[25]

Currently the FAA is collecting Passenger Facility Charges (PFC) that are designated for noise mitigation purposes. A total of 52 US airports are imposing PFCs to support airport noise mitigation projects.[26] Approximately one-billion dollars has been collected and approved for this purpose. These PFC's will be used for land purchases, home buyouts, soundproofing, noise monitoring systems, and other noise mitigation projects. Expenditure of these funds would not be required if quiet aircraft were in service.

The projected market for the new aircraft engines that could benefit from this technology averages 1200 units per year. It is estimated that a 30% market share is attainable, however, for the financial calculations a conservative number of 20% of the projected market was utilized.

6.2 COMMERCIAL PRODUCT OR SERVICE

The patented technology of our one-splice inlet barrel, that demonstrated a 3 EPNdB noise reduction, will be utilized in combination with our Hybrid System to achieve the desired technology goals. The aircraft noise reduction

goals set by federal and local governments will be used to satisfy community aircraft noise requirements well into the next century.

The initial plan for commercial products is to introduce this technology on a new aircraft being developed for introduction into service during the years 2003 to 2006. The lead time is required for meeting all the FAA and DOT requirements. This will be a new technology and both the commercial operators and public must be introduced to the benefits of such a system for reducing aircraft noise pollution.

A team experienced in all aspects of these technologies has been assembled to implement and execute this program. Authorities on composite structures, electronic controllers, flow noise, noise control engineering and duct acoustics will be used to achieve the required goals. In addition, we will work with a major commercial jet engine manufacturer to incorporate the system. The team will develop a cost competitive advanced technology system for reducing jet engine noise.

6.3 MARKET ASSESSMENT

The potential market for a noise reduction system is very large. US Carriers have been installing huskiest on older aircraft that do not meet the Stage 3 criteria. At year-end 1996, 560 airplanes in the US fleet had been modified to meet Stage 3. By year-end 1999, the Stage 2 deadline, an additional 1080 airplanes will be modified. After 1999 approximately 880 Stage 2 aircraft must be removed from US operations. However, hushkit application usually results in an aircraft that barely meets Stage 3 with small probability of meeting new, more stringent regulations. Indications are that European operators will not install husk kits on their older Stage 2 aircraft as extensively as the US. European airports have greater latitude in setting acceptable noise limits and penalizing aircraft configured with huskiest that fail to meet regulations. This will lead to sales for new aircraft. Therefore, because of the Stage 3 requirements for current US aircraft, the window of opportunity for this technology for older type aircraft is small.

The following tables, Table 6.1a and b, represent a survey of passenger and freight aircraft that are projected to be in worldwide service through the year 2016. The first table represents the total aircraft in service and the second table lists the number of new aircraft expected to be manufactured during that period. This list includes a mixture of both two and four engine mid-size and large commercial aircraft. Commuter aircraft are not considered in this survey. These aircraft have less severe far-field noise problem, and would not require the Hybrid System.

Table 6.1a Total Aircraft in Service

YEAR	1996	2001	2006	2011	2016
PASSENGER A/C	10271	12471	15270	18199	21239
FREIGHT A/C	1234	1373	1652	1926	2359
TOTAL A/C	11505	13844	16922	20122	23598

Table 6.1b New Aircraft To Be Manufactured*

YEAR	1997-2001	2002-2006	2007-2011	2012-2016	CUM TOTAL
PASSENGER A/C	3626	3509	4040	4364	15539
FREIGHT A/C	82	111	212	218	623
TOTAL A/C	3708	3620	4252	4582	16162

* 90% Two-engines, 10% Four engines

Market studies forecast approximately 730 new aircraft per year for the next ten years or 7300 aircraft with 16,000 engines as listed in Table 6.1c.

Table 6.1c Aircraft Forecast

	Currently	1998-2007	2007 Year-End Fleet
Aircraft	11,500	7300	16,800*
Engines	>25,000	16,000	36,500

* Assumes 2000 aircraft retired

Of the foregoing total market, financial projections were based on production start up in 2000 and obtaining a very conservative 12.9% of the new aircraft market, as shown in Table 6.2.

Table 6.2 New Aircraft Sales Forecast

YEAR	2000	2001	2002	2003	2004	TOTAL
NEW AIRCRAFT SALES	730	730	730	730	730	3650
ENGINES	1460	1460	1460	1460	1460	7300
FORECAST SALES	91	152	213	245	245	946
% OF MARKET	6.25%	10.42%	14.58%	16.67%	16.67%	12.90%

It is estimated that during the years from 2002-2006 we will be able to capture 10-15% of the new aircraft markets. This percentage will increase in succeeding years as the airport traffic volume increases and the overall noise levels increase. During the years 2007-2011 the market percentage is expected to rise to 25% and hold through the year 2016.

There are three known solutions to the noise problem, re-engine the aircraft, install hush kits, and purchase replacement aircraft. A re-engine program will cost approximately $12M per engine. Hush kits cost $1-3M per kit but increase fuel consumption. They require hush kit ejectors which impose drag and weight penalties. Replacement aircraft start at $35M or greater and are designed to meet Stage 3 requirements. These new aircraft would have a

difficulty meeting a "Stage 4" criteria. Our solution will cost approximately $1-1.3M per unit (depending on the type engine) and provide "Stage 4" results for these new aircraft.

There is a major opportunity to capture a large share of the market given the absence of technological and economic solutions currently available. This opportunity would also apply to the foreign marketplace. Based on projections of commercial aircraft engine active noise control research being conducted in Europe, we have a two year lead on their research development.

6.4 AIRCRAFT CERTIFICATION REQUIREMENTS

Certification of the Hybrid System requires the approval of a number of federal organizations prior to introduction into the commercial aircraft fleet. In addition, the flight safety issues for this system must be understood and implemented. Airworthy requirements for the nacelle, engine, and aircraft must be determined and tests conducted in order to meet compliance.

The issue of fan blade-out requirements for the system is an additional concern because of the potential of installing the acoustic drivers in the critical blade-out zone. Fan blade fragments must not penetrate the nacelle if the acoustic drivers are installed within +/-15° angle of the center of the fan plane of rotation. These requirements must be satisfied by blade-out qualification tests and/or analysis.

The matter of system durability will affect the sale of the system. The acoustic drivers, controllers and error microphones must have sufficient durability to convince the operators to purchase this system. Aspects such as component repair and ease of replaceability must be addressed. During the next stage of development, on-site calibration procedures of the individual and combined components must be developed.

6.5 ENVIRONMENTAL REQUIREMENTS

Aircraft nacelles are exposed to severe environments. Each of the hybrid system components must be tested under conditions that will be defined by FAA regulations. The FAA or company Designated Engineering Representative (DER) will specify which of the components will require test and which can be qualified by analysis. It is expected that components that are totally new in commercial use will undergo extensive testing for specific life cycles. A sampling of some of the environmental conditions that must be considered are listed below:

- Sonic fatigue
- Vibration
- Impact resistance
- Erosion resistance
- Salt spray
- Freeze/thaw effects
- Lightening strike
- EMI protection
- Water and skydrol absorption resistance and drainage requirements

6.6 DEVELOPMENT TASKS

The development of the technology into a mature production program will require the close association of three companies, the nacelle manufacturer, the engine manufacturer and the airframe manufacturer. Northrop Grumman Corporation will coordinate and manage the entire development and demonstration phase. The initial stage, development of improved drivers, is ongoing. A commercial engine manufacturer must be involved early in the program. The company selected must have in service a large fan engine and must have the capability to provide an engine ground test facility with an acoustic far field acoustic array setup. In addition, they must have data acquisition and analysis capabilities for providing the far field noise level comparisons between current passive acoustic treatments and the hybrid system. During the latter phase of the engine test program a commercial airframe manufacturer must join the team. This company must have an on-going flight test program, to lower the cost of the demonstration phase, with an aircraft configured with an engine suitable for the hybrid demonstration. The second phase of the demonstration will be a flight test program. This phase is more critical because it involves safety of flight issues and involvement with the FAA in all aspects of the systems operation. Flight worthy equipment will be pre-tested and qualified during this phase. The engine manufacturer will closely interface with the airframe manufacturer to determine cable routes, power requirements, cabin space requirements and test procedures. Northrop Grumman will monitor the driver and electronic manufacturers and establish equipment qualification requirements. Operating manuals will be prepared for each of the components and for operation of the entire system. An overall test plan will be prepared for the flight test evaluation. A successful flight test program will lead to the final phase of commercialization. This will involve the development of a strong marketing plan for the system. This plan will detail the benefits on the active system over existing passive treatments. Successful implementation of the marketing plan will generate a new manufacturing base for this technology.

6.7 DEVELOPMENT SCHEDULE

A development schedule, which carries the technology through to full production is provided below. It accounts for the teaming required to demonstrate the technology, on an engine ground test followed by the more difficult task of demonstrating the technology in a flight test program monitored by the FAA.

Table 6.3 Hybrid Suppressor - Estimated Development Schedule

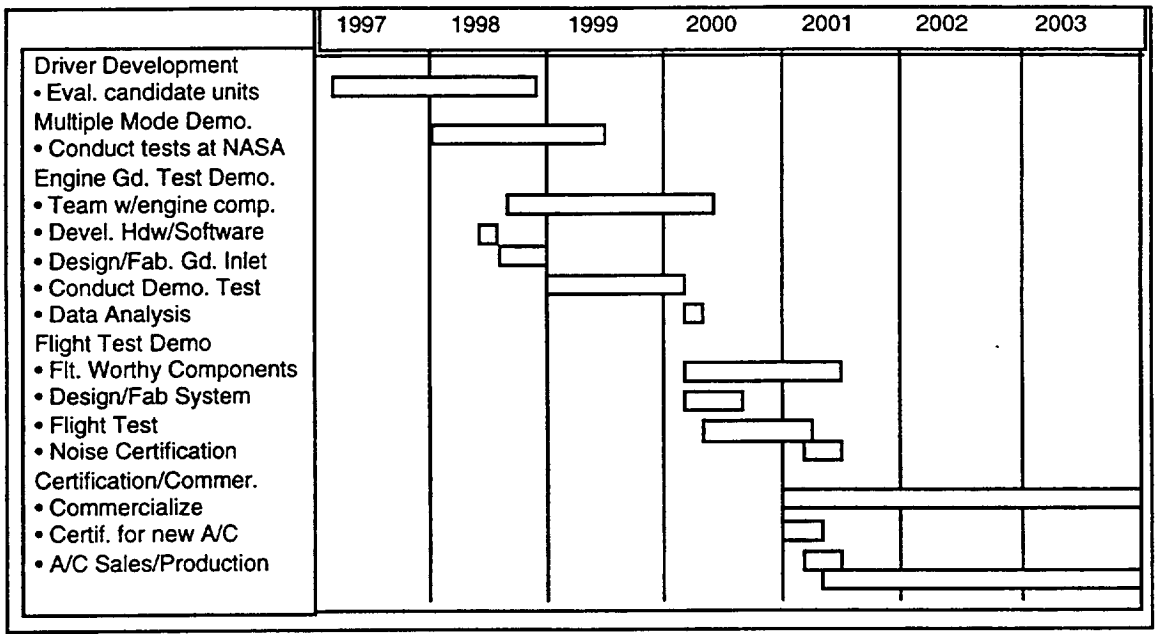

6.8 DEVELOPMENT TASK SUMMARY

The following table (Table 6.4) summaries the tasks for the overall hybrid liner development program.

Table 6.4

Hybrid Active/Passive Noise Suppressor
Development Tasks

TASK	Northrop Grumman Responsibility	Engine Company Responsibility	Airframe Manufacturer Responsibility
• Program Management and Coordination	Prime	Collaboration	Collaboration
• **Phase I** Feasibility Study	Development of high intensity acoustic drivers.	Provide induct noise levels to permit the design of the Hybrid Suppressor treatment. Provide induct noise levels for driver development. Conduct additional mode testing as part of the NASA AST Program.	None
• **Phase II** Full Scale Engine Ground Test	Overall design and fabrication of inlet modifications required for installation of Hybrid System. Hardware and software development. Coordination of all test activities.	Provide induct noise levels to permit design of Hybrid treatment. Provide an engine and engine test stand for static ground test. Provide data acquisition, data reduction, and evaluation of results. Provide operational consultation as required.	None
• **Phase III** Flight Test Demonstration Program	Overall design and fabrication of inlet and flight worthy modification of hardware. Hardware/software modification for flight. Coordination of all test activities.	Provide induct noise levels to permit the design of the Hybrid Suppressor treatment. Provide operational consultation as required.	Provide aircraft for flight test program. Provide acoustic test site for noise certification program.
• **Phase IV** Certification and Commercialization	Overall design and fabrication of Hybrid System for environmental tests. All documentation for certification of Hybrid system and components.	Provide induct noise levels to permit the design of the Hybrid Suppressor treatment. All engine related certification activities including engine control and hardware modifications and certification documentation.	Prime responsibility for certification activities. Provide certification test plan, aircraft and associated support.

7 – ORGANIZATIONS DESCRIPTION & VENTURE MANAGEMENT

Northrop Grumman's ability to perform successfully on this commercialization is based on more than 30 years of experience in the commercial nacelle market and 15 years of acoustic liner design for commercial aircraft. Currently we are building both commercial and military jet engine nacelles at several sites. Our plans for production make use of our Milledgeville, Georgia and Dallas, Texas facilities. The electronics for the system will be provided by outside vendors manufacturing to our specifications. The entire product line will benefit workers in a number of technologies and develop the US commercial manufacturing of a currently non-existent product.

The company's acoustic laboratory is fully equipped to perform the acoustic quality control test, required for certification of the liners for the customer. The integration of the Hybrid System will be overseen by an experienced Nacelle Program Manager.

7.1 FINANCIAL PLAN

An estimate has been made for the cost of introducing the Hybrid Active/Passive noise suppression system into the commercial aircraft industry. Table 7.1 shown below provides that estimate.

Table 7.1 Commercialization Cost Estimate

.COMPANY	PHASE I FEASIBILITY	PHASE II ENGINE GROUND. TEST	PHASE III FLIGHT TEST	PHASE IV COMMERCIALIZATION & MANUFACTURING	TOTAL ESTIMATE
Duration	12 months	18 months	18 months	12 months	5 years
Northrop Grumman Corp.	$ 350,000	$ 800,000	$ 800,000	$ 800,000	$2,750,000
Engine Company	$ -	$ 200,000	$ 100,000	$ 100,000	$400,000
Air Frame Mfg.	$ -	$ -	$ 300,000	$ 200,000	$500,000
TOTAL	$ 350,000	$ 1,000,000	$ 1,200,000	$ 1,100,000	$3,650,000

A more detailed cost analysis is also being prepared which will attempt to determine the costs of qualification and durability tests.

REFERENCES

1. Published goals of the NASA Advanced Subsonic Transport program.
2. US Patent 5,119,477, Hersh et al., issued June 2, 1992.
3. Sawdy, D.T., Beckemeyer, R.J., and Patterson, J.D., "Optimum Segmented Acoustic Liners for Flow Ducts," A76-25129, Paper D6, 90th Meeting Acoustical Society of America, San Francisco, Ca., November 3-7, 1975.
4. Sawdy, D.T., Beckemeyer, R.J., and Patterson, J.D., "Analytical and Experimental Studies of an Optimum Multisegment Phased Liner Noise Suppression Concept," NASA CR-134960, 76N22976, May 1976.
5. Patterson, J.D., Sawdy, D.T., and Beckemeyer, R.J., "Experimental-Analytical Correlation of Optimum Duct Acoustic Liner Performance," A76-25856, ASME Preprint 76-GT-126, ASME Gas Turbine Conference and Product show, New Orleans, La., March 21-25, 1976.
6. Lester, H.C., and Posey, J.W., "Duct Liner Optimization for Turbomachinery Noise Sources," NASA TM X-72789, November 1975.
7. Lester, H.C., and Posey, J.W., Optimal One-Section and Two-Section Circular Sound-Absorbing Duct Liners for Plane-Wave and Monopole Sources without Flow," NASA TN D-8348, December 1976.
8. Clark, T.L., Ganz, U.W., Graf, G.A., and Westall, J.S., "Analytic Models of Ducted Turbomachinery Tone Noise Sources," NASA CR-132443, 1974.
9. Baumeister, K.J., "Evaluation of Optimized Multisectioned Acoustic Liners", AIAA Journal, Vol. 17, No. 11, pp.1185-1192, November 1979.
10. Rice, E.J., "Modal Propagation Angles in Ducts with Soft Walls and Their Connection with Suppressor Performance," AIAA Paper 79-0624, March 1979.
11. Rice, E.J., "Inlet Noise Suppressor Design Method Based Upon the Distribution of Acoustic Power with Mode Cutoff Ratio," NASA CP-2001, Vol. 3, p. 883, 1976.
12. Rice, E.J., "Multimodal Far-Field Acoustic Radiation Pattern Using Mode Cutoff Ratio," AIAA Journal, Vol. 16, pp. 906-911, September 1978.
13. Rice, E.J., "Optimum Wall Impedance for Spinning Modes-A Correlation with Mode Cutoff Ratio," Journal of Aircraft, Vol. 16, No. 5, pp. 336-343, May 1979.
14. Baumeister, K.J., "Generalized Wave Envelope Analysis of Sound Propagation in Ducts With Stepped Noise Source Profiles and Variable Axial Impedance," NASA TM X-71674, March 1975.
15. Rice, E.J., "Attenuation of Sound in Soft-Walled Circular Ducts," AFOSR-UTIAS Symposium on Aerodynamic Noise, Toronto, Canada, May 20-21, 1968.

16. Zorumski, W.E., and Mason, J.P., "Multiple Eigenvalues of Sound-Absorbing Circular and Annular Ducts," Journal Acoustic. Soc. Am., Vol. 55, No. 6, June 1974.

17. Zorumski, W.E., "Acoustic Theory of Axisymmetric Multisectioned Ducts," NASA TR R-419, May 1974.

18. Rice, E.J., "Spinning Mode Sound Propagation in Ducts with Acoustic Treatment and Sheared Flow," AIAA 75-519, also NASA TM X-71672, March 1975.

19. Goldstein, M.E., Aeroacoustics, McGraw-Hill International Book Company, New York, NY.

20. Tyler, J.M., Sofrin, T.G., "Axial Flow Compressor Noise Studies," SAE Trans., Vol. 70, 1962, pp. 309-332.

21. Morgan, D.R.,, "Analysis of Multiple Correlation Cancellation Loop With a Filter in the Auxiliary Path," IEEE Trans. Acoustic., Speech, Signal Processing, Vol. ASSP-28, pp. 454-467, August 1980.

22. Heidelberg, L.J., Hall, D.G., "Inlet Acoustic Mode Measurements Using a Continuously Rotating Rake," Journal of Aircraft, Vol. 4 No. 32 pp. 761-763, July-August 1995.

23. Heidelberg, J.J., Hall, D.G., Bridges, J.E., and Nallasamy, M., "A Unique Ducted Fan Test Bed For Active Noise Control and AeroAcoustics Research," NASA TM 107213, AIAA-(6-1740, Second AIAA/CEAS Aeroacoustics Conference, May, 1996.

24. Rice, E.J., "Aircraft Inlet Noise Radiation Model, Static, Flight and Bellmouth Effect," AIAA 96-1774, May 1996.

25. "Europe Eyes Further Noise Control Studies", Aviation Week & Space Technology, p. 49, March 24,1997.

26. "PFS's," Airport Noise Report, Vol. 9, Number 8, May 19, 1997.

ILLUSTRATIONS

Figure 1.1

Simplified Diagrams of Engine Nacelle, Showing Development of the Adaptive Segmented Liner Concept

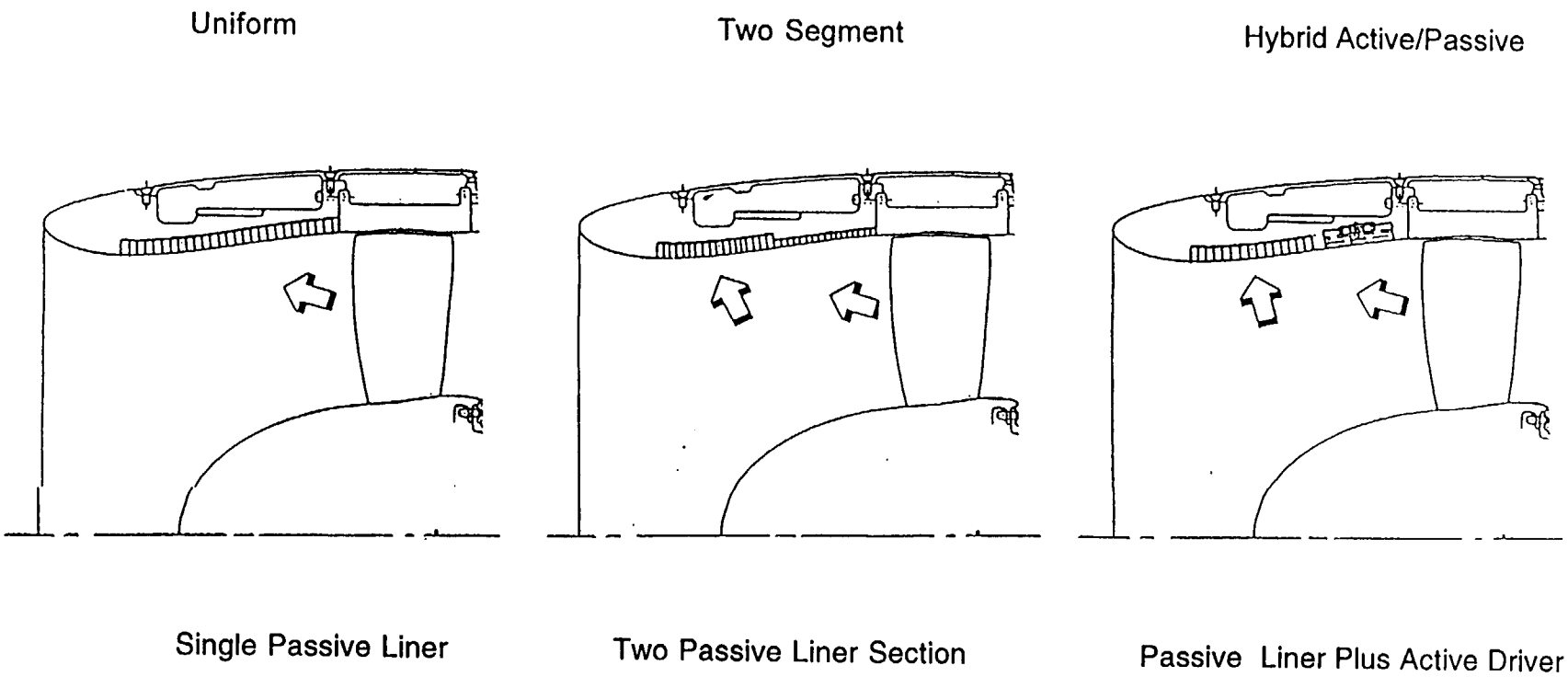

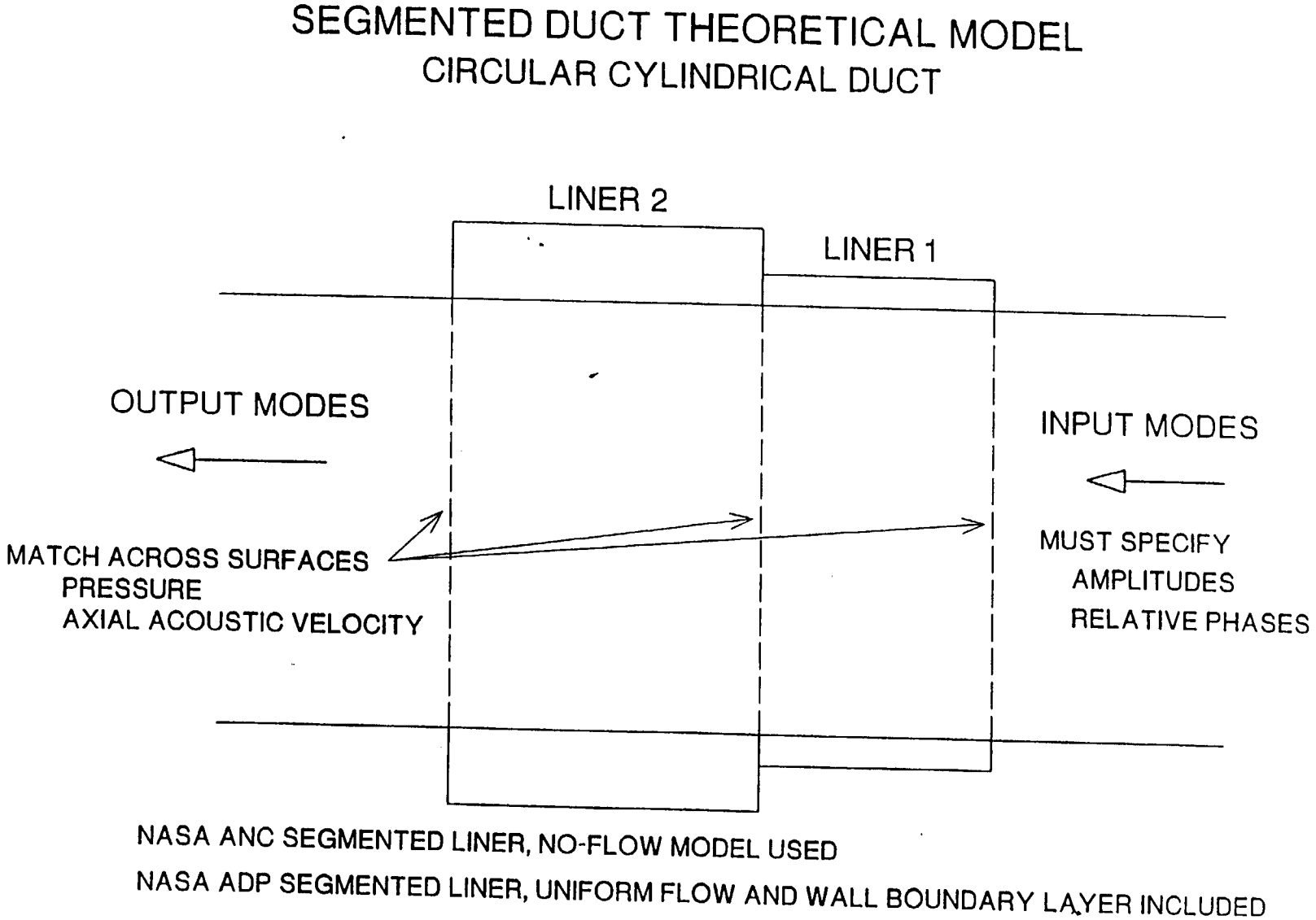

FIGURE 2.1
Schematic Model of the Axial Segmented Liner

FIGURE 3.1 a
Radial Pressure Distributions of Modes (-9,0) and (-9,1) and Least Favorable Combination for Interaction with Wall Mounted Passive Treatment

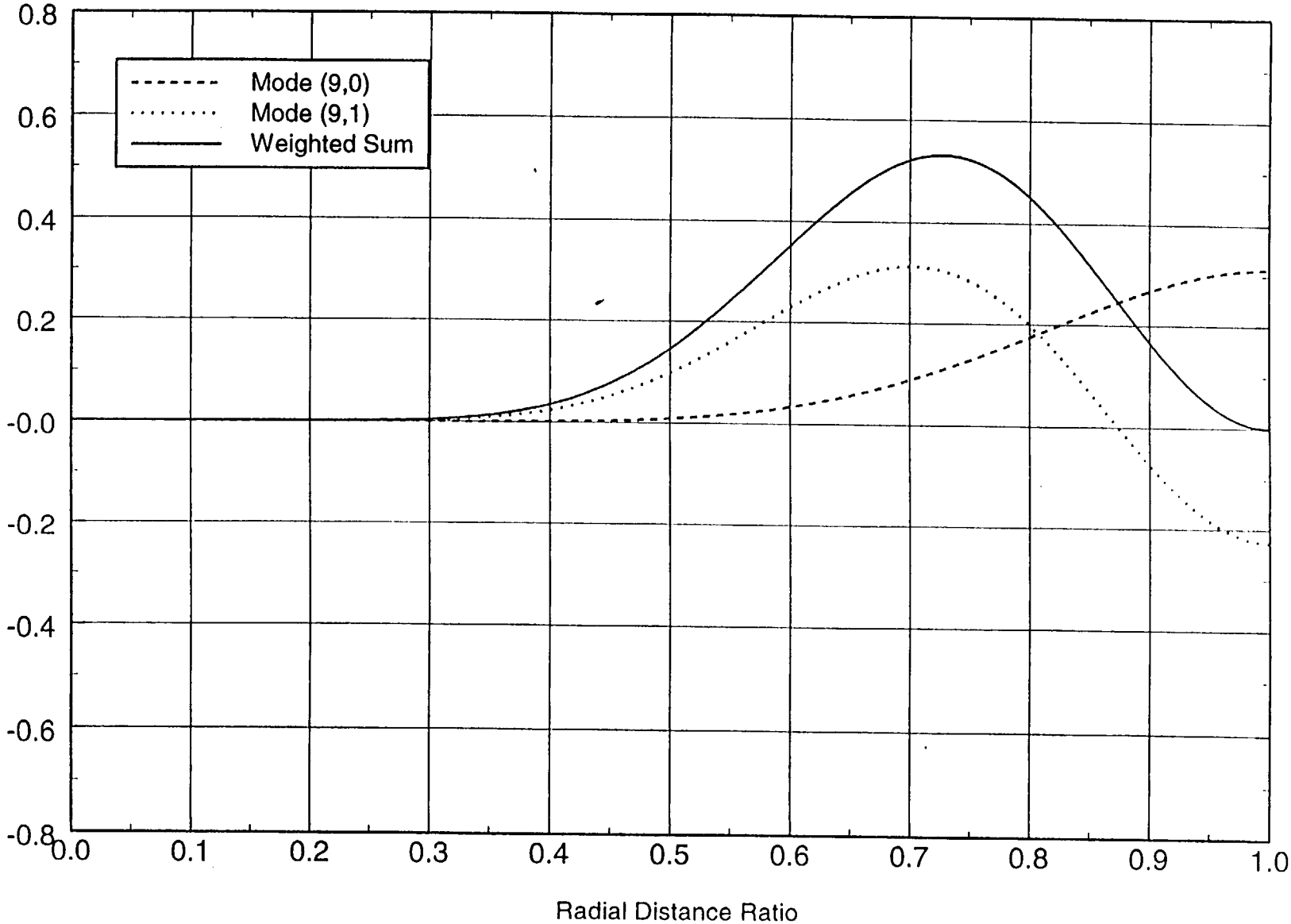

FIGURE 3.1 b
Radial Pressure Distributions of Modes (-9,0) and (-9,1) and Most Favorable Combination for Interaction with Wall Mounted Passive Treatment

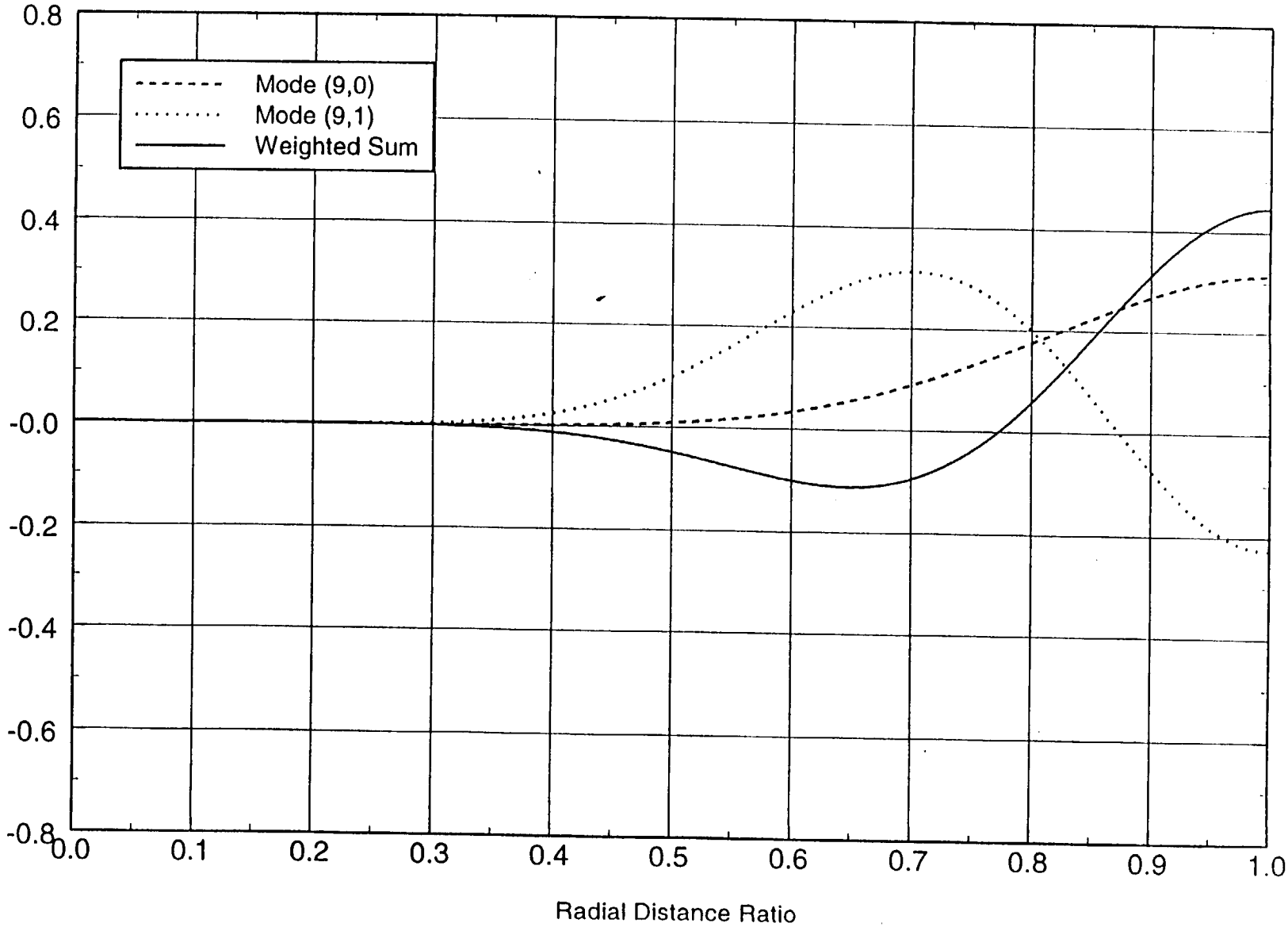

FIGURE 3.1 c
Ratio of Wall Pressure to Space-Average Sound Pressure vs. Amplitude Ratio and Phase Difference Between Modes (-9,0) and (-9,1)

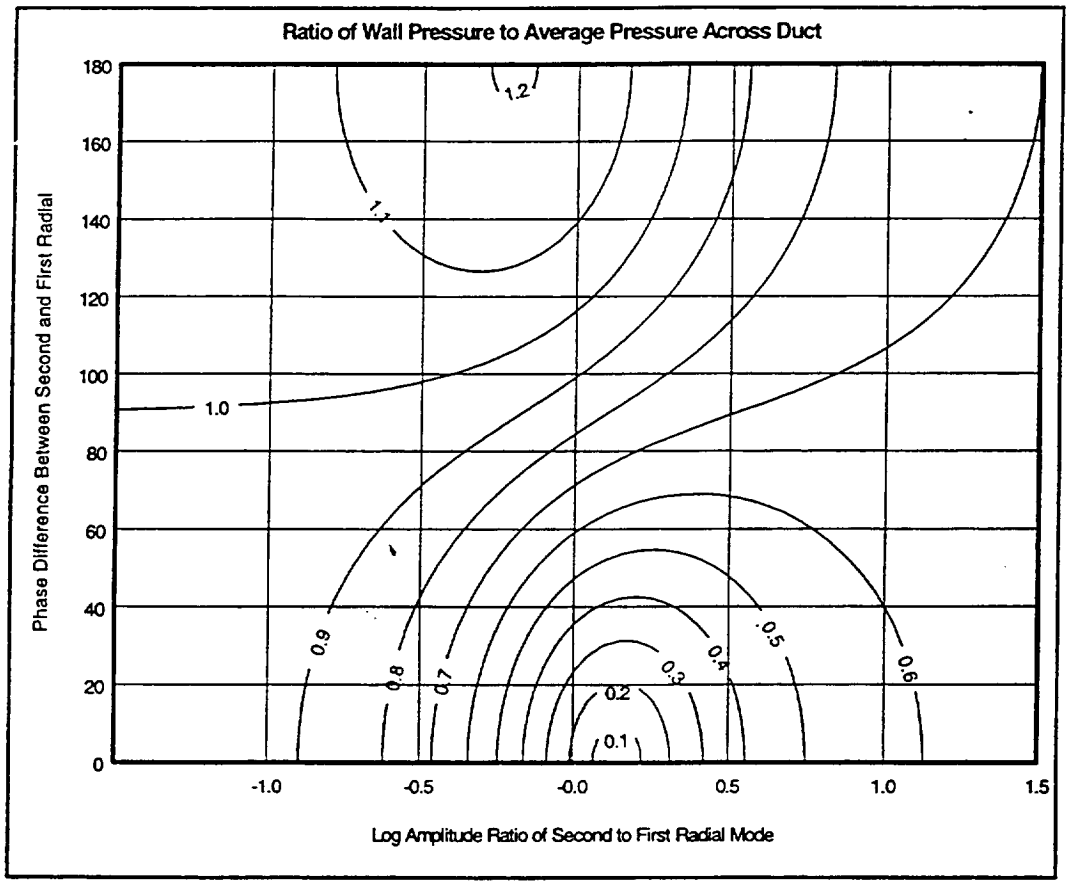

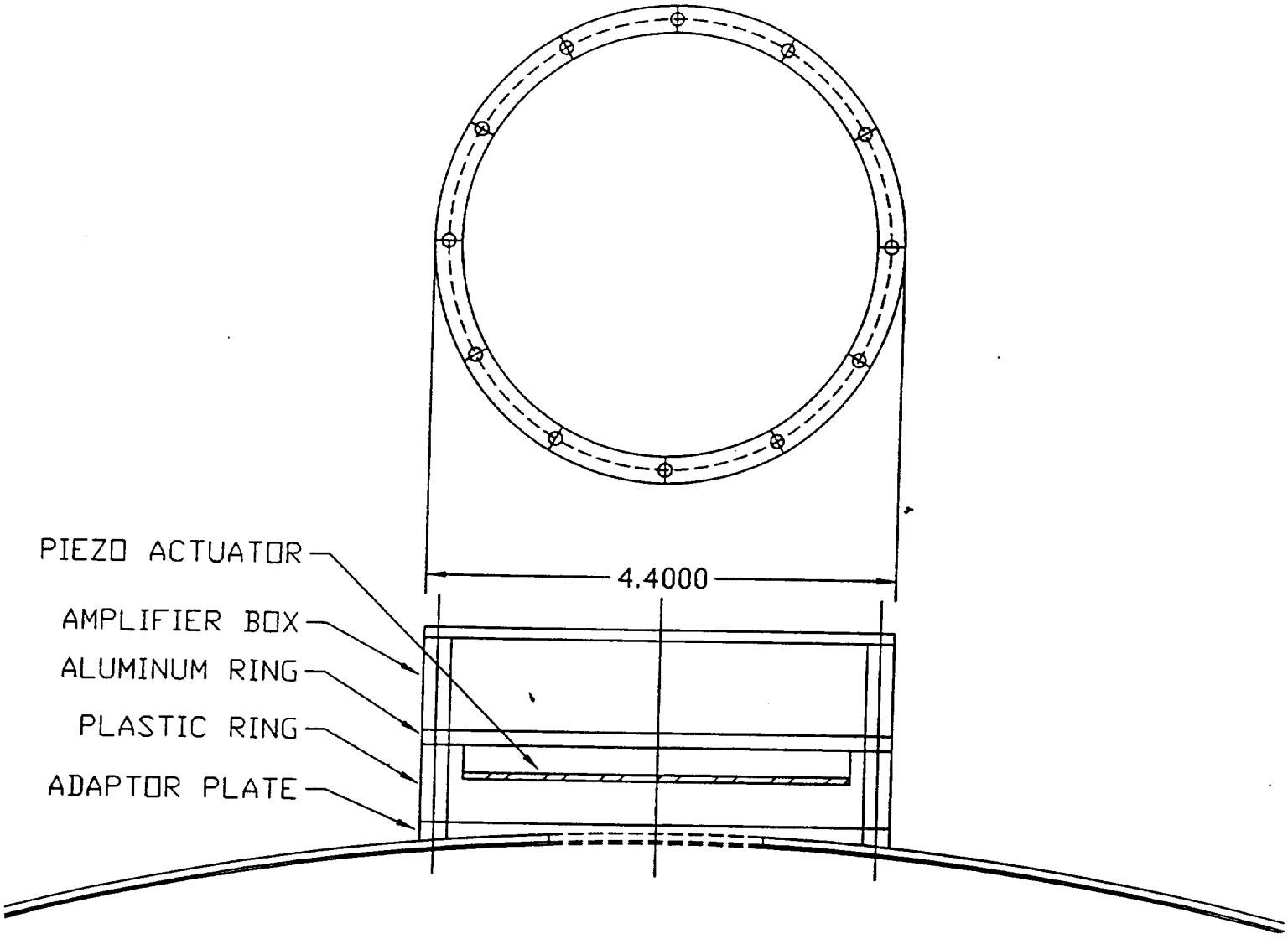

FIGURE 3.2
Active Resonator and Actuator Mounting Detail for Active Segment of Adaptive Segmented Liner in ANCF Test
Typical of 32 Spaced 4.5 inches Axially and 22.5° Azimuthally

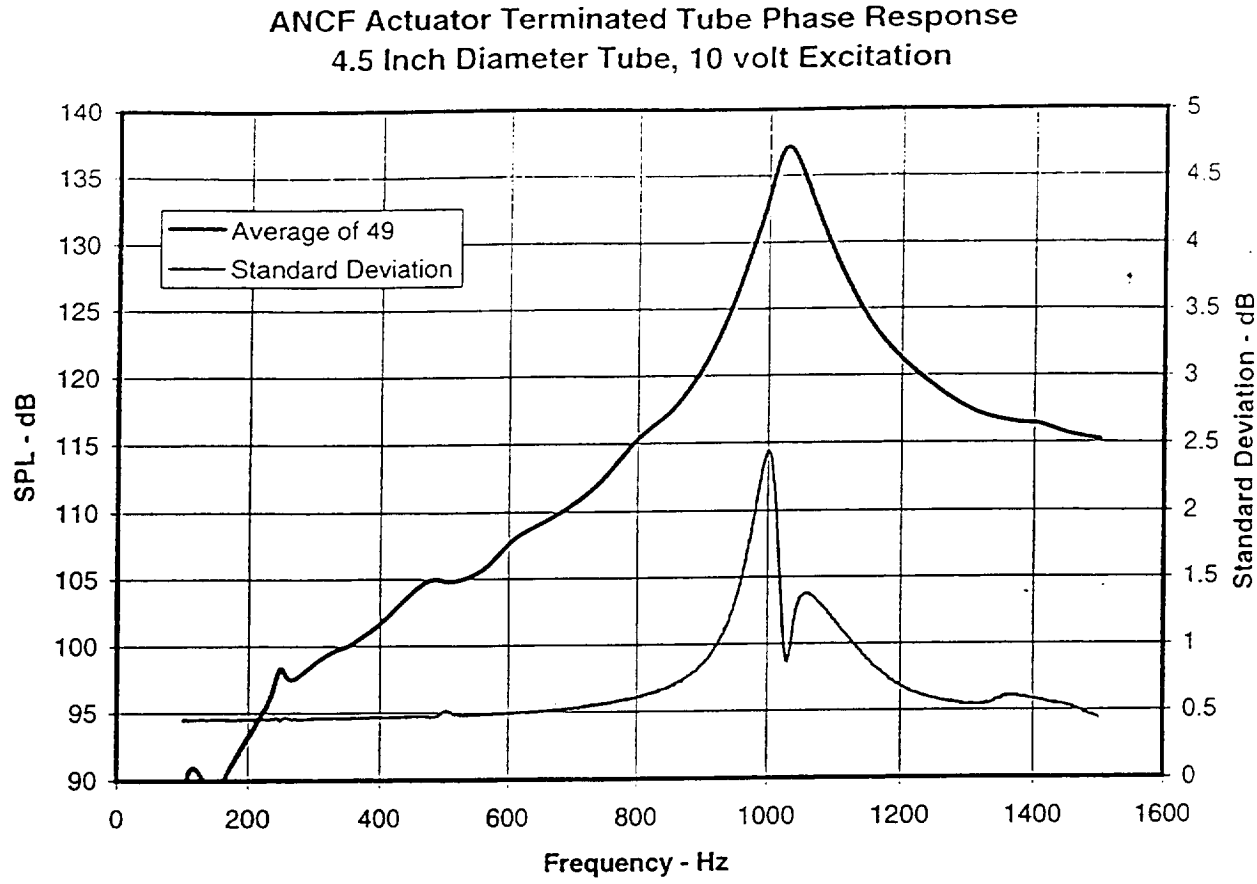

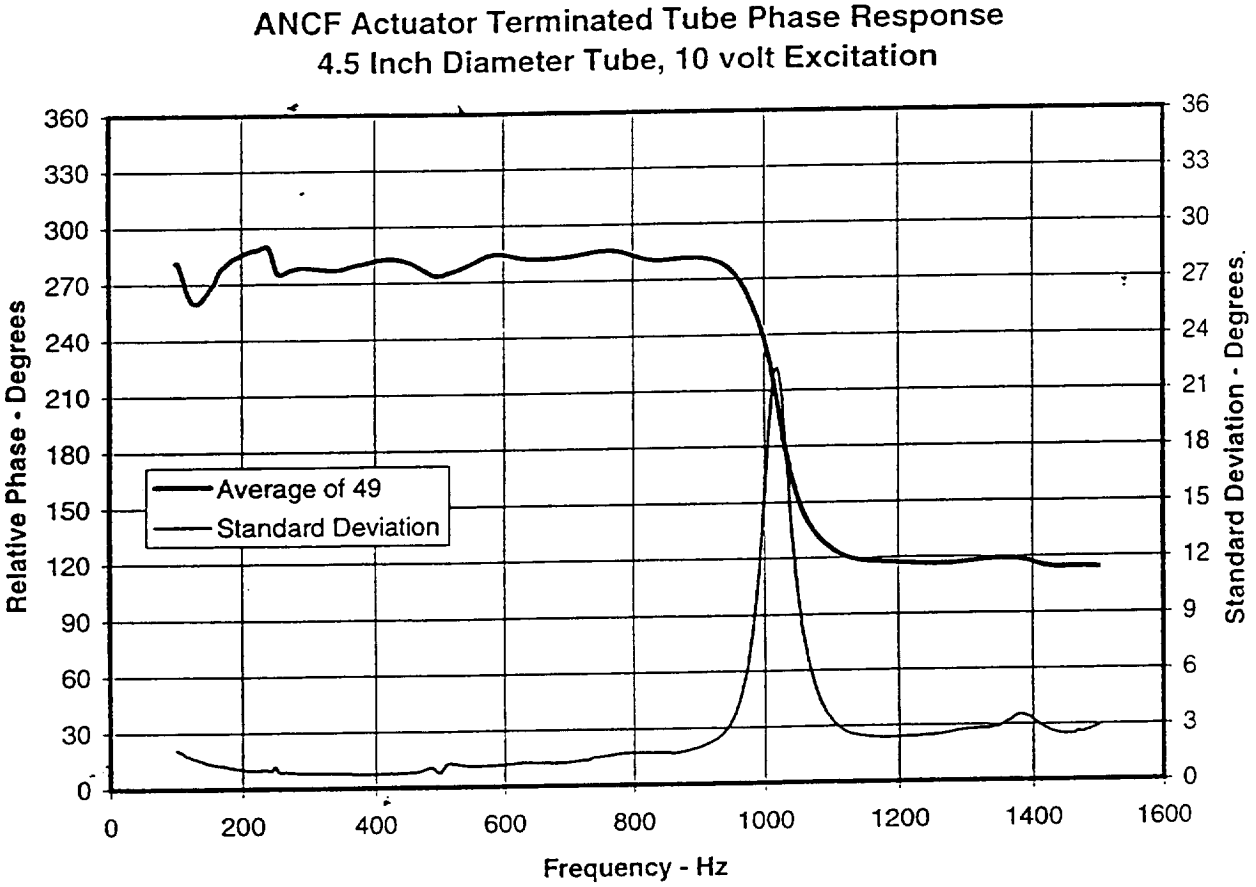

FIGURE 3.3 a, b
Amplitude and Phase Response and Deviations for Actuators
Used in ANCF Adaptive Segmented Liner Tests

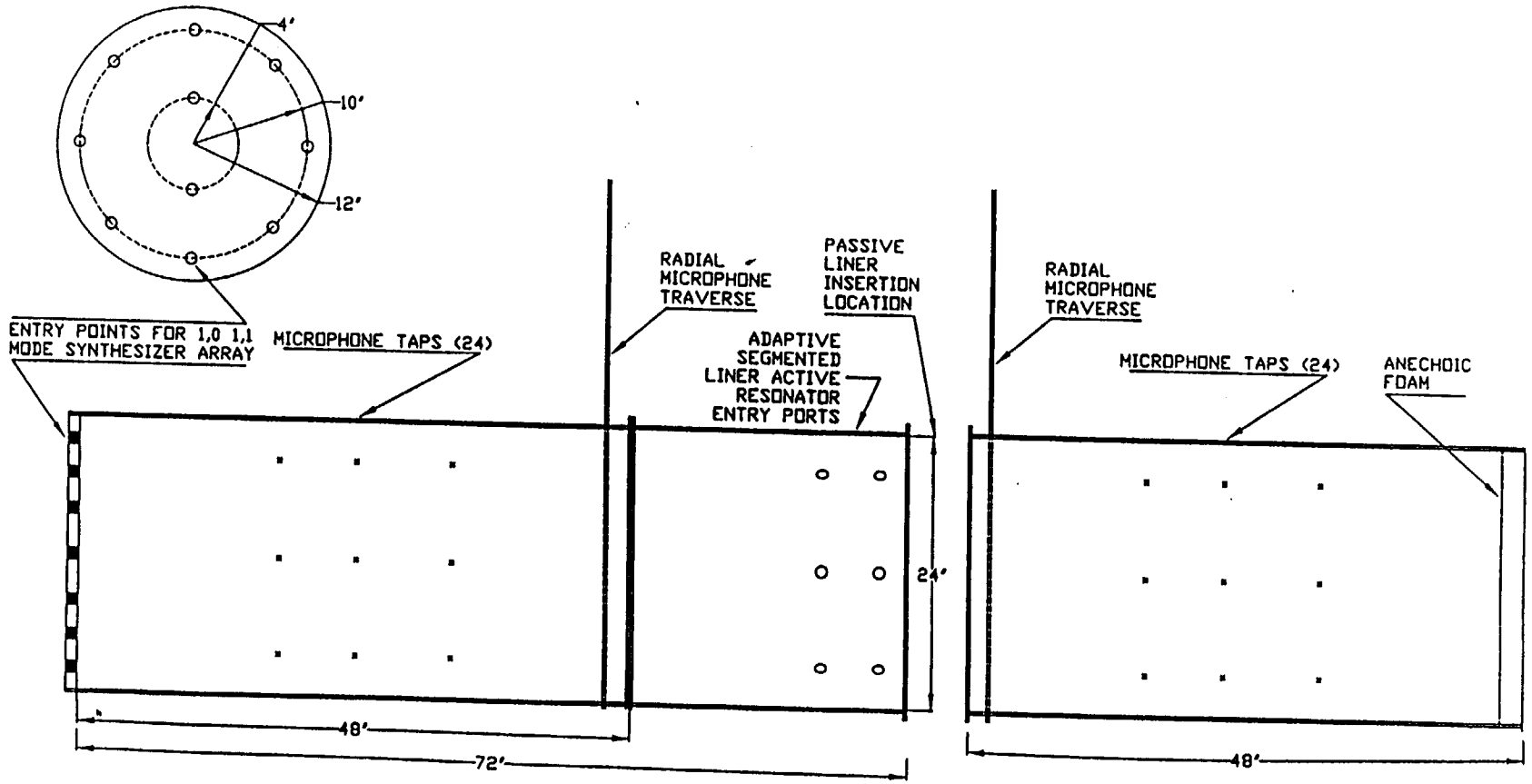

FIGURE 4.1
Schematic Diagram of HAE 24-inch Duct for Testing Prototype Liners at Modes (1,0) and (1,1)

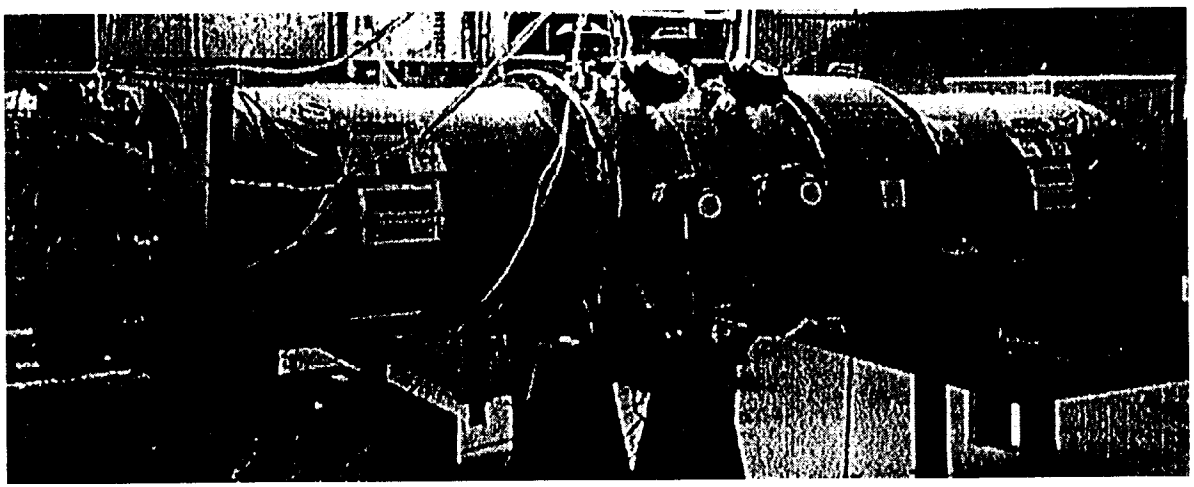

(a)

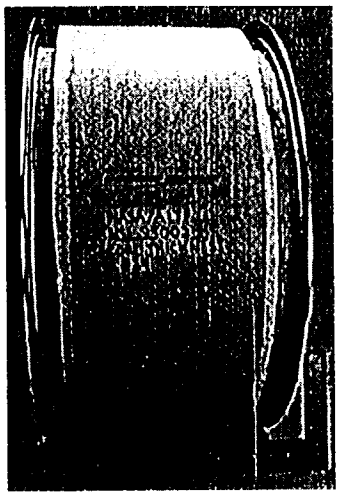

(b)

Figure 4.2a, b
HAE Spinning Mode Rig (a) With Test Barrel (b) Installed

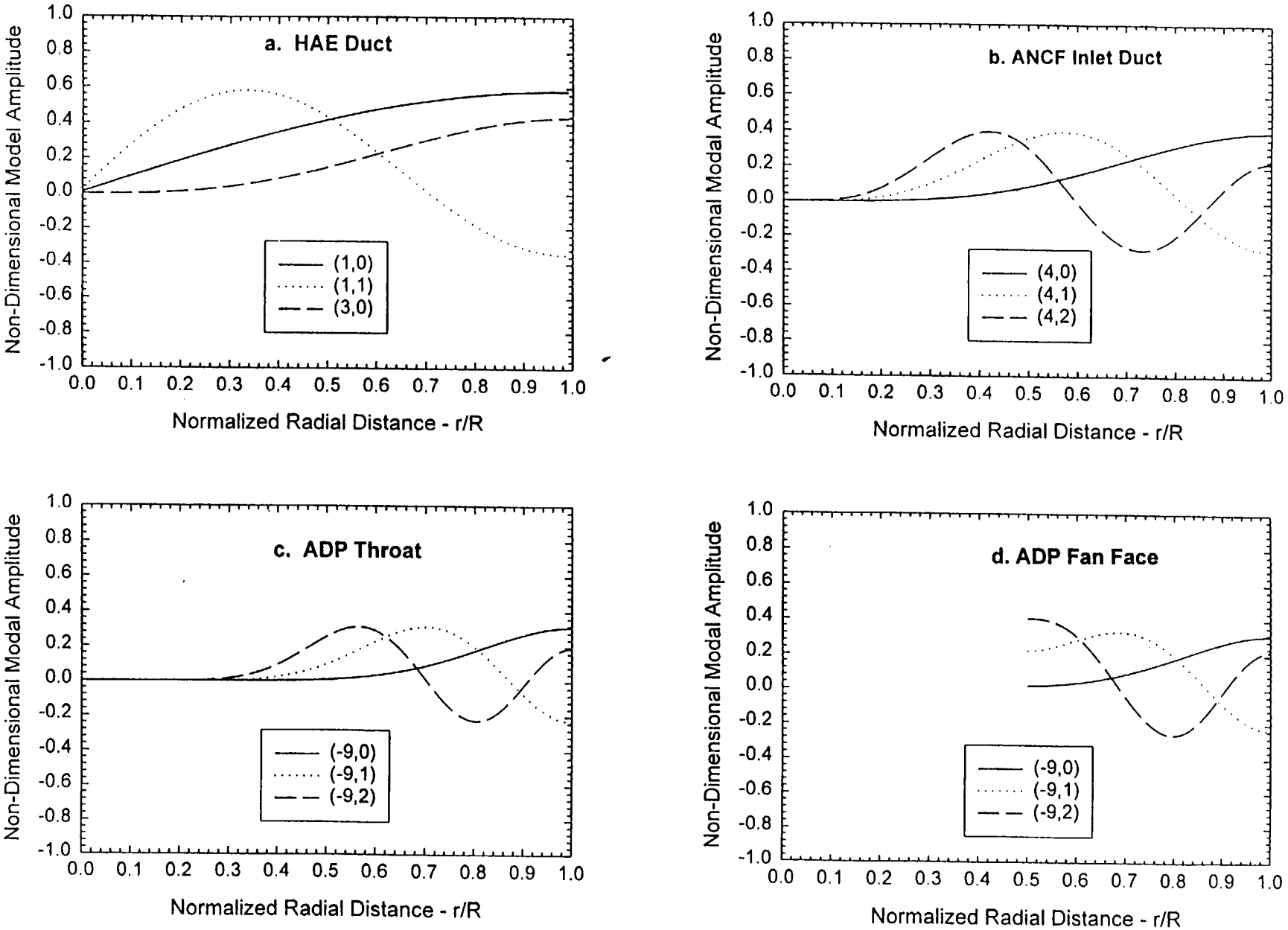

FIGURE 4.3
Theoretical Sound Pressure Distributions of Radial Modes in HAE, ANCF and ADP Ducts

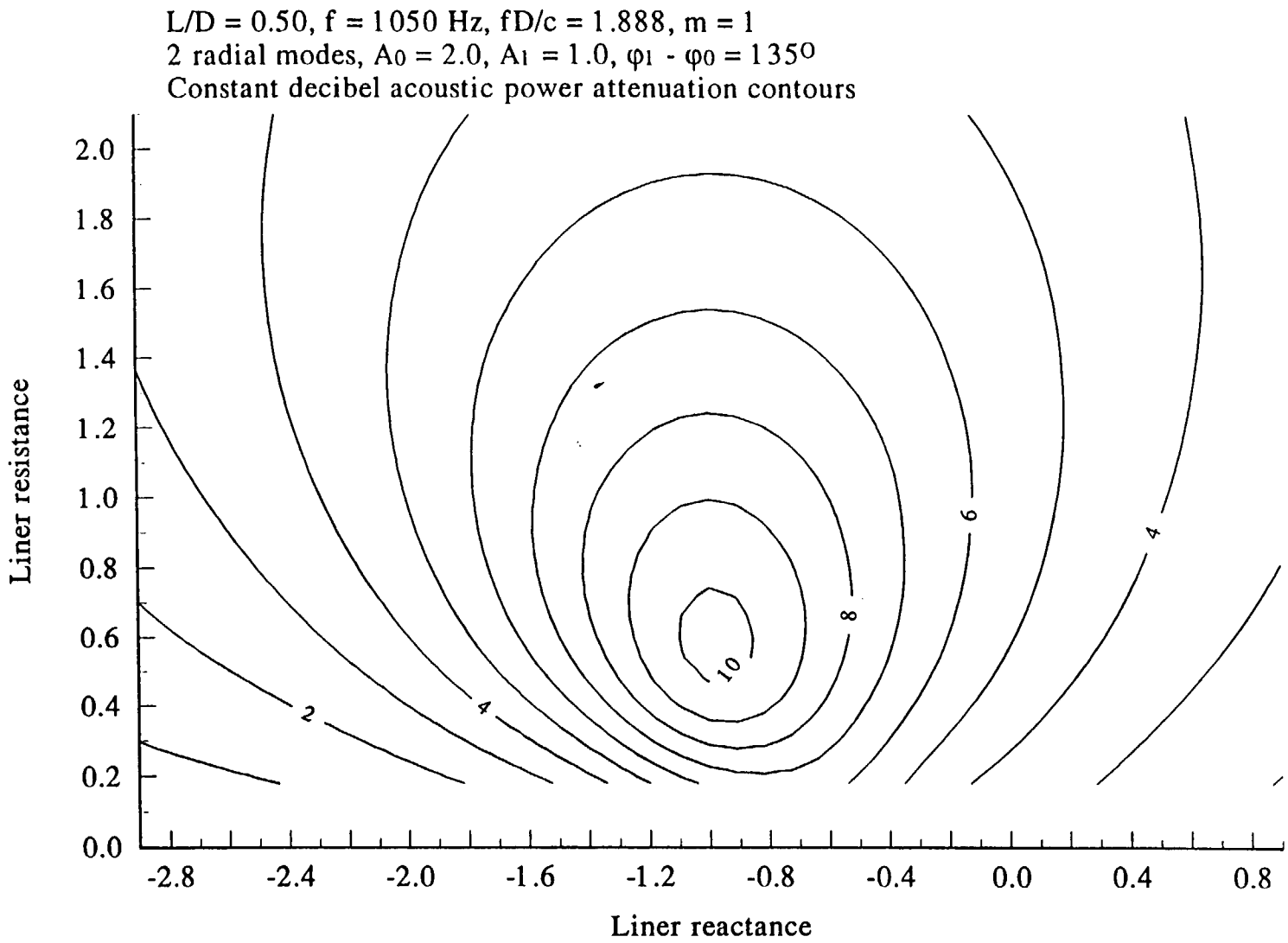

Figure 4.4. Optimum impedance determination for uniform liner HAE 2

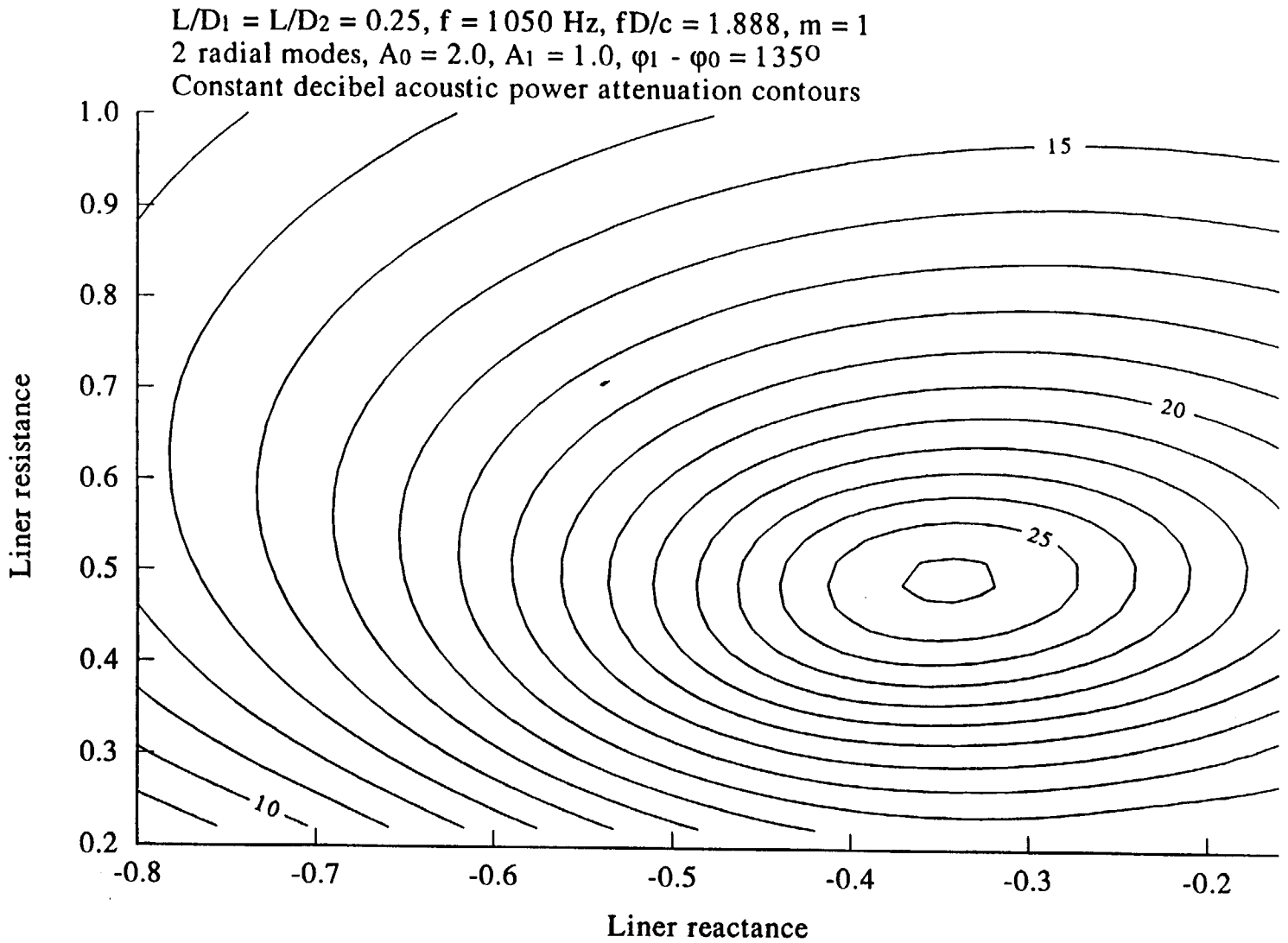

Figure 4.5. Attenuation sensitivity of liner 2 of two segment liner HAE 3
liner 1 impedance fixed at 0.076 - i1.171

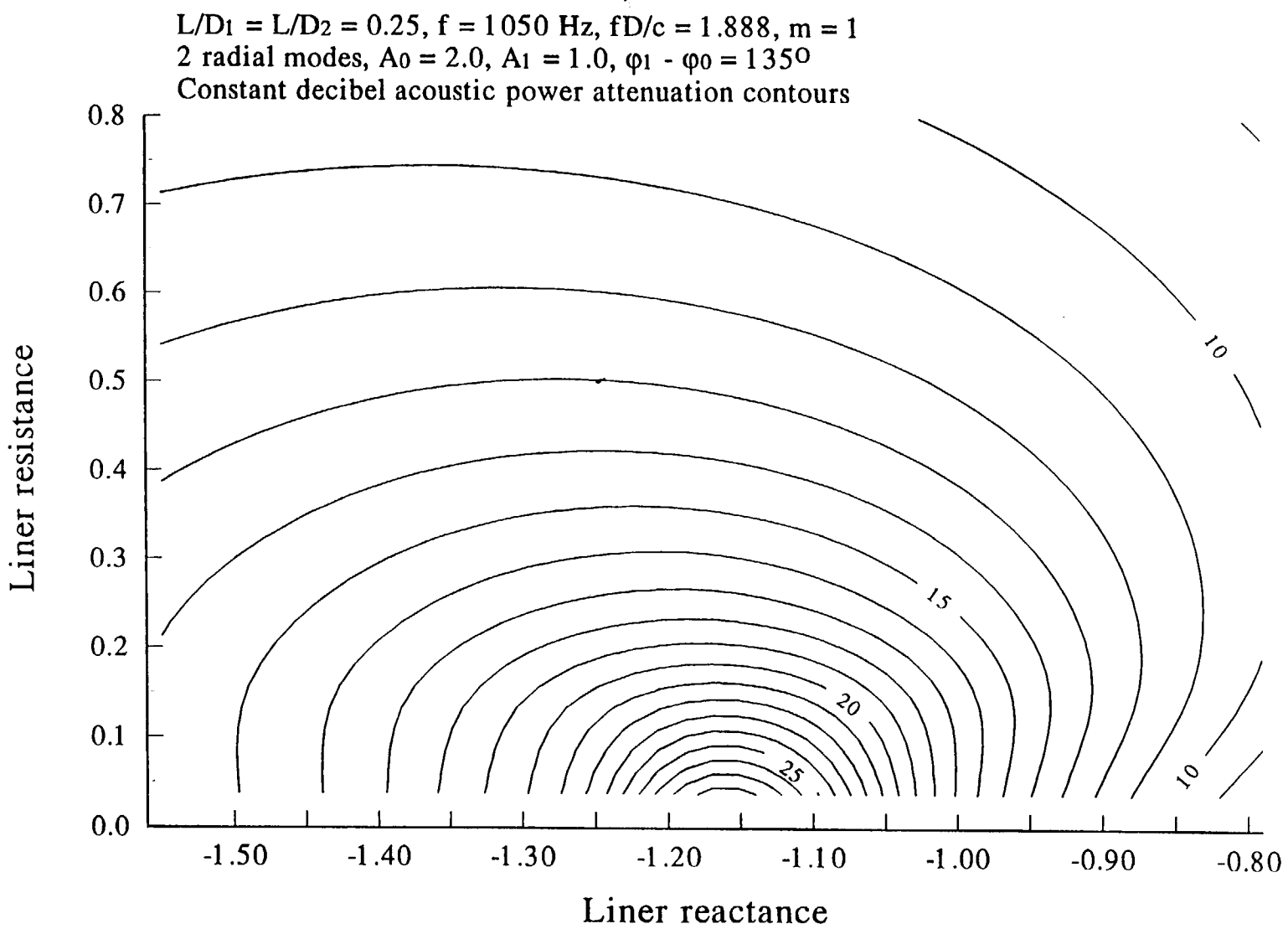

Figure 4.6. Attenuation sensitivity of liner 1 of two segment liner HAE 3 liner 2 impedance fixed at 0.49 - i0.34

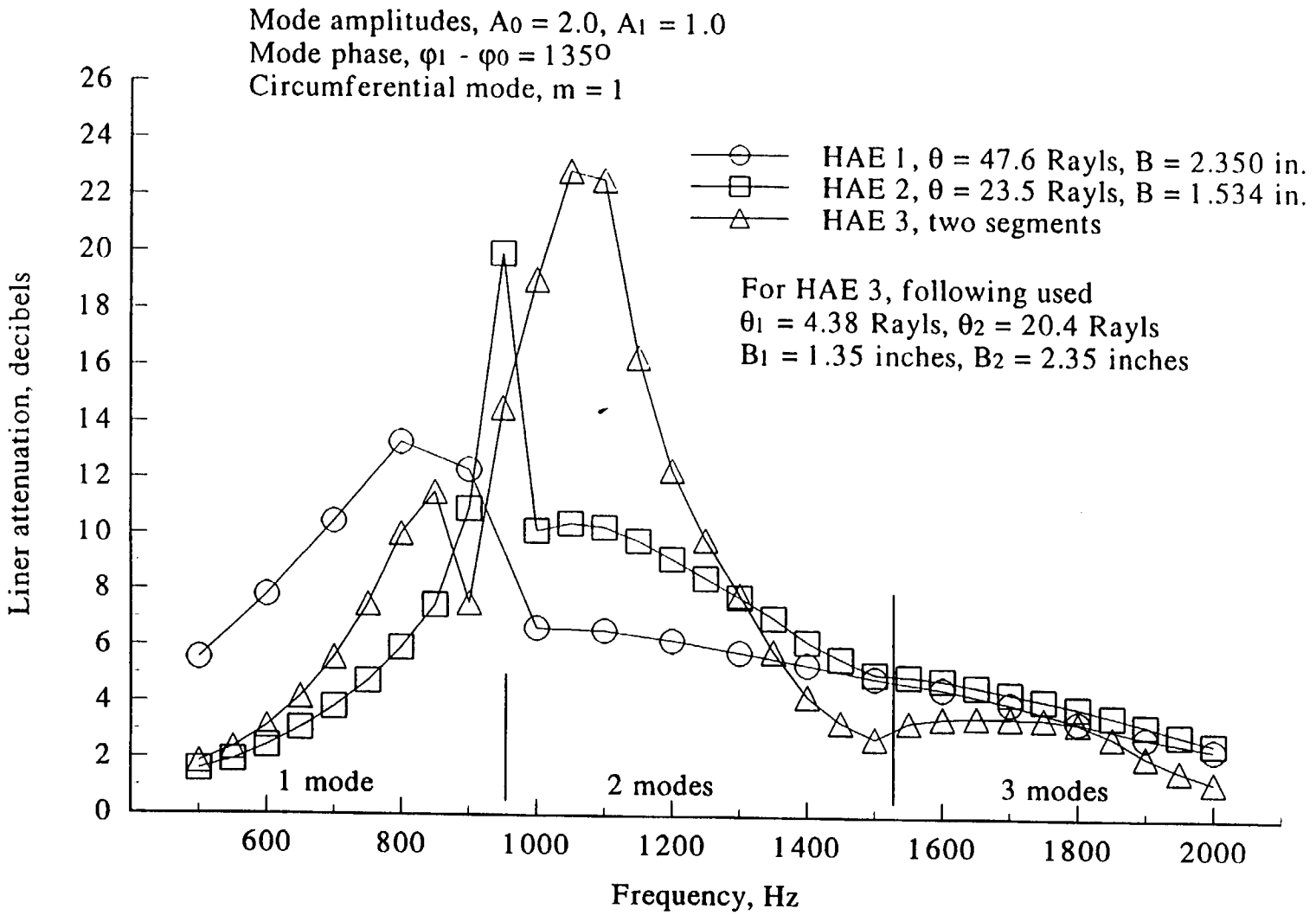

Figure 4.7. Calculated attenuation spectra for uniform and two segment liners optimized for 1050 Hz, D = 24.125 inches, HAE no flow tests

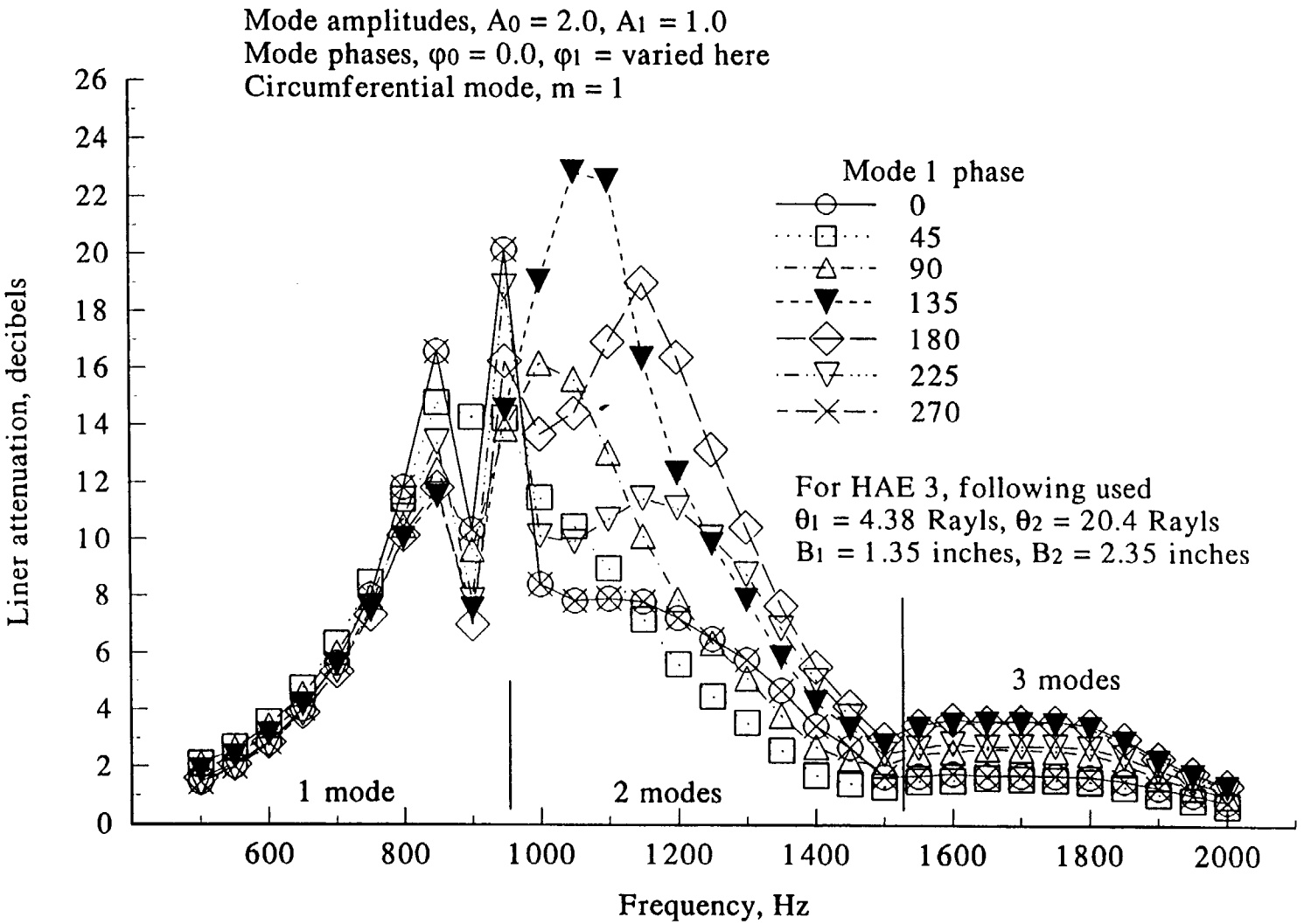

Figure 4.8. Attenuation spectra for two segment liner HAE 3 showing effect of radial mode phase

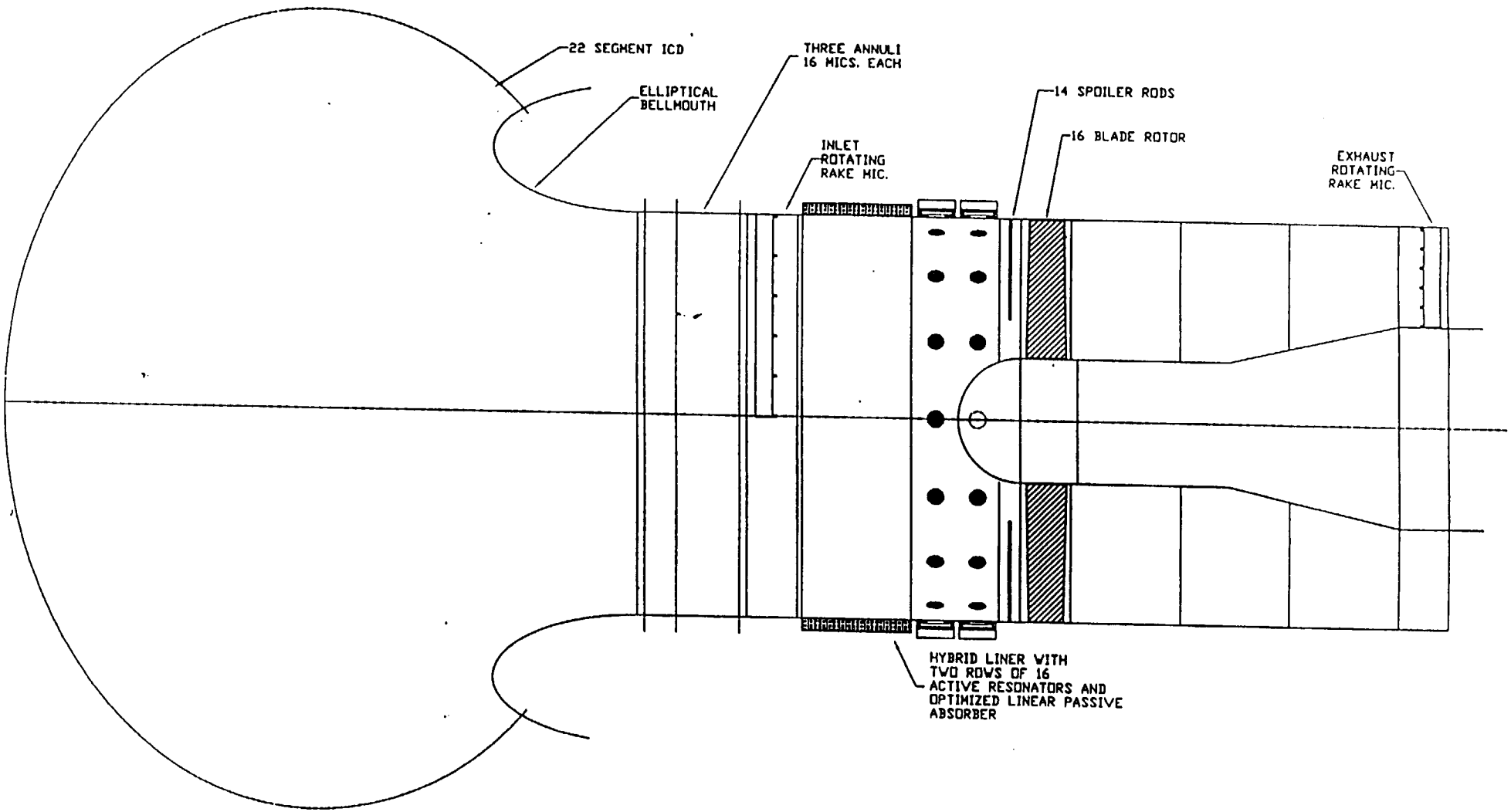

Figure 4.9
Cutaway Diagram of the Hybrid Liner Installation
on the NASA LeRC ANCF Fan

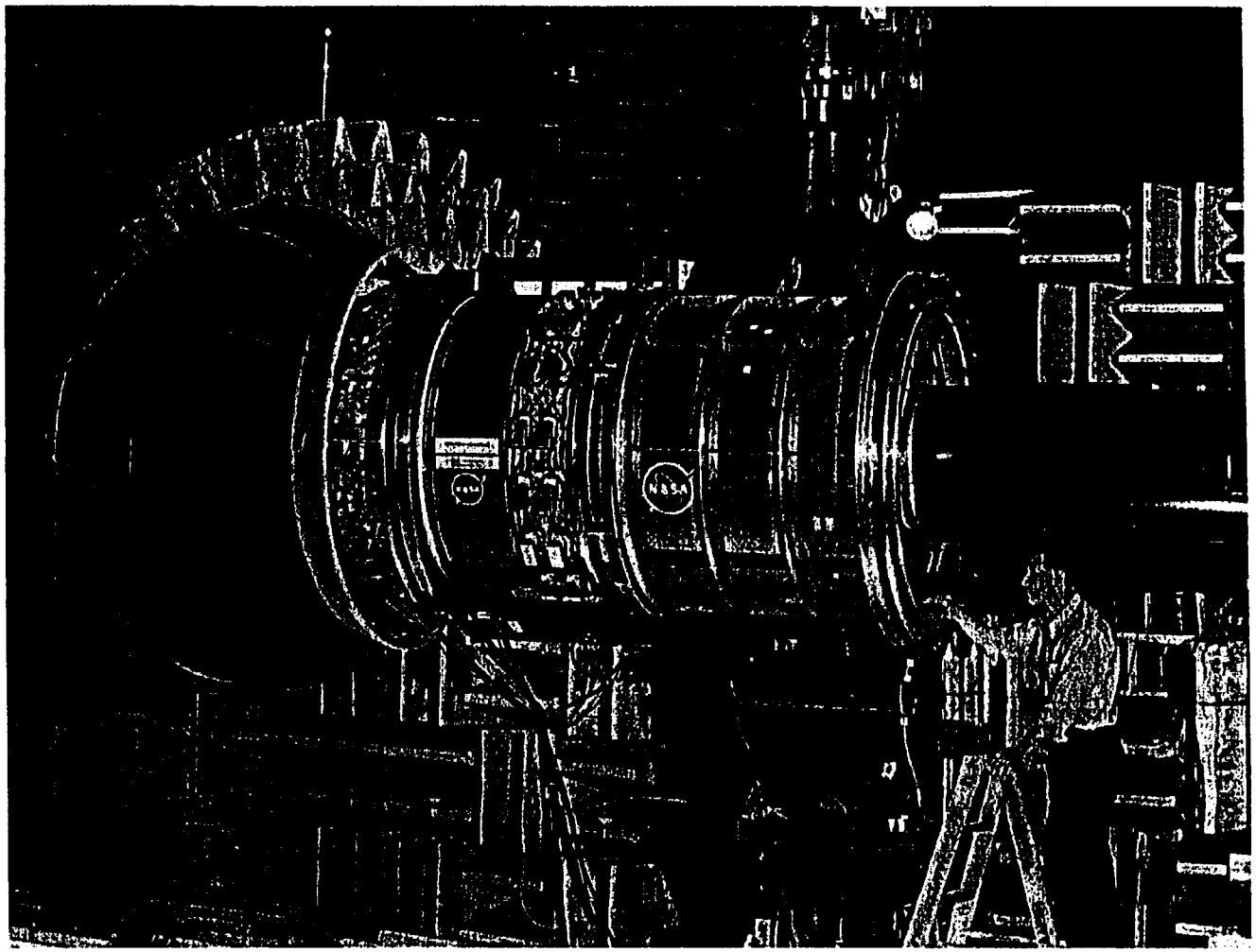

Figure 4.10
Hybrid Active/Passive Barrrel Installed on the ANCF Rig at NASA LeRC

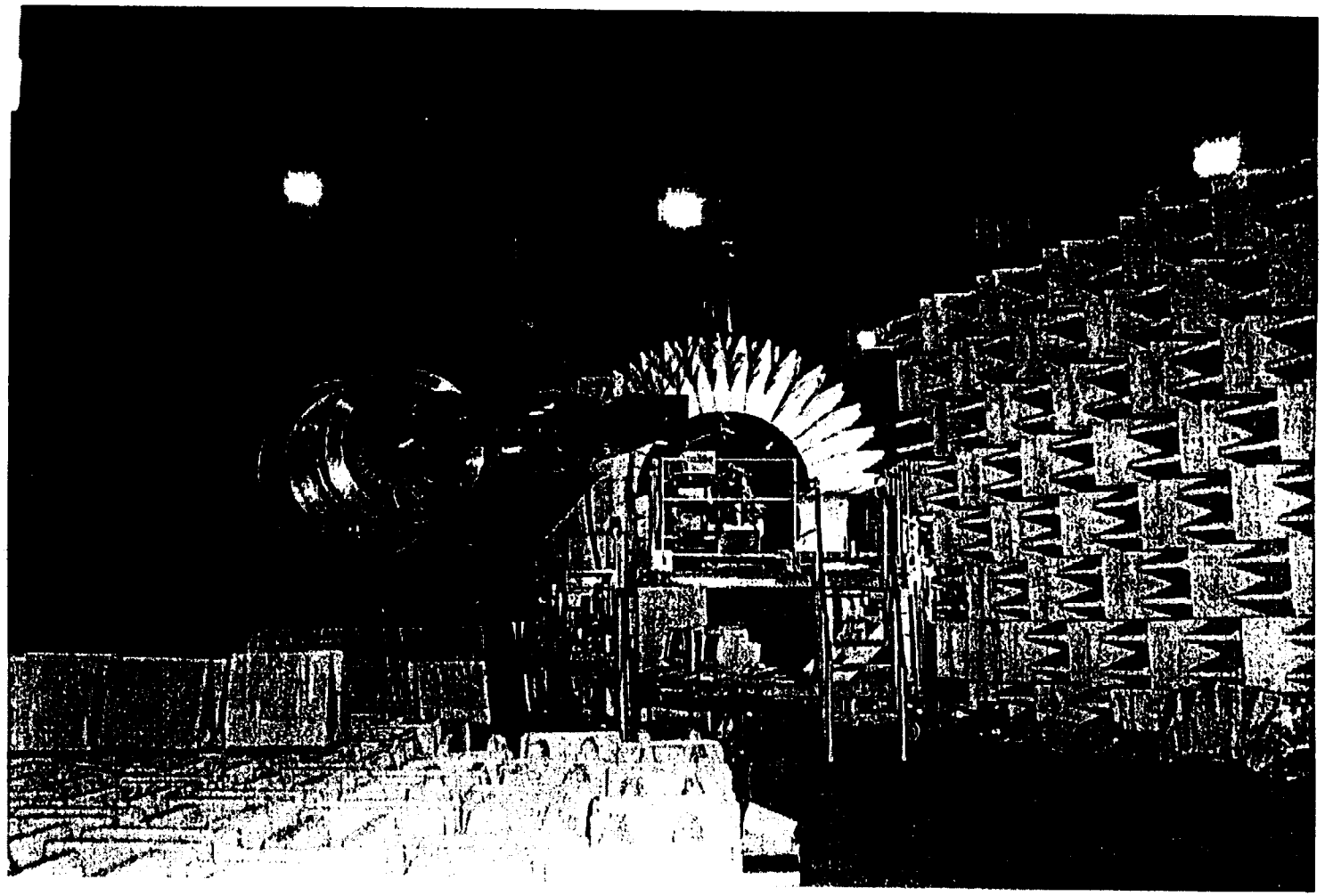

Figure 4.11
Rear View of ANCF Rig Located in the NASA LeRC Anechoic Dome

Figure 4.12a, b
Acoustic Actuator for the ANC Test (a)
and the ADP Test (b)

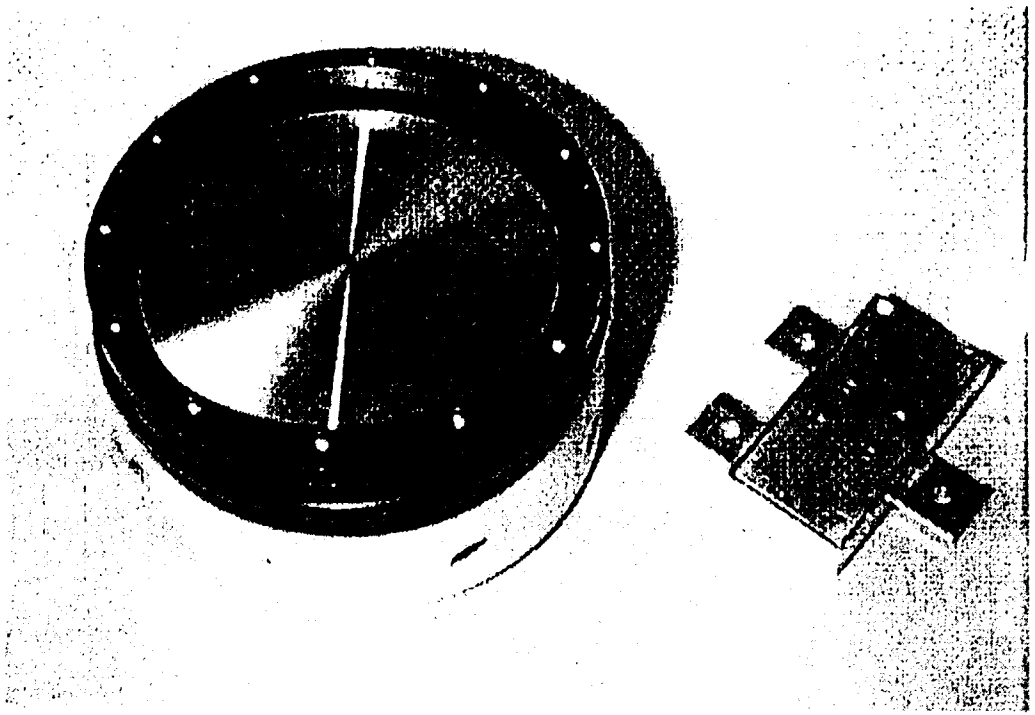

(a) 4 inch Diameter ANC Actuator (b) 1 in. x 2 in. ADP Actuator

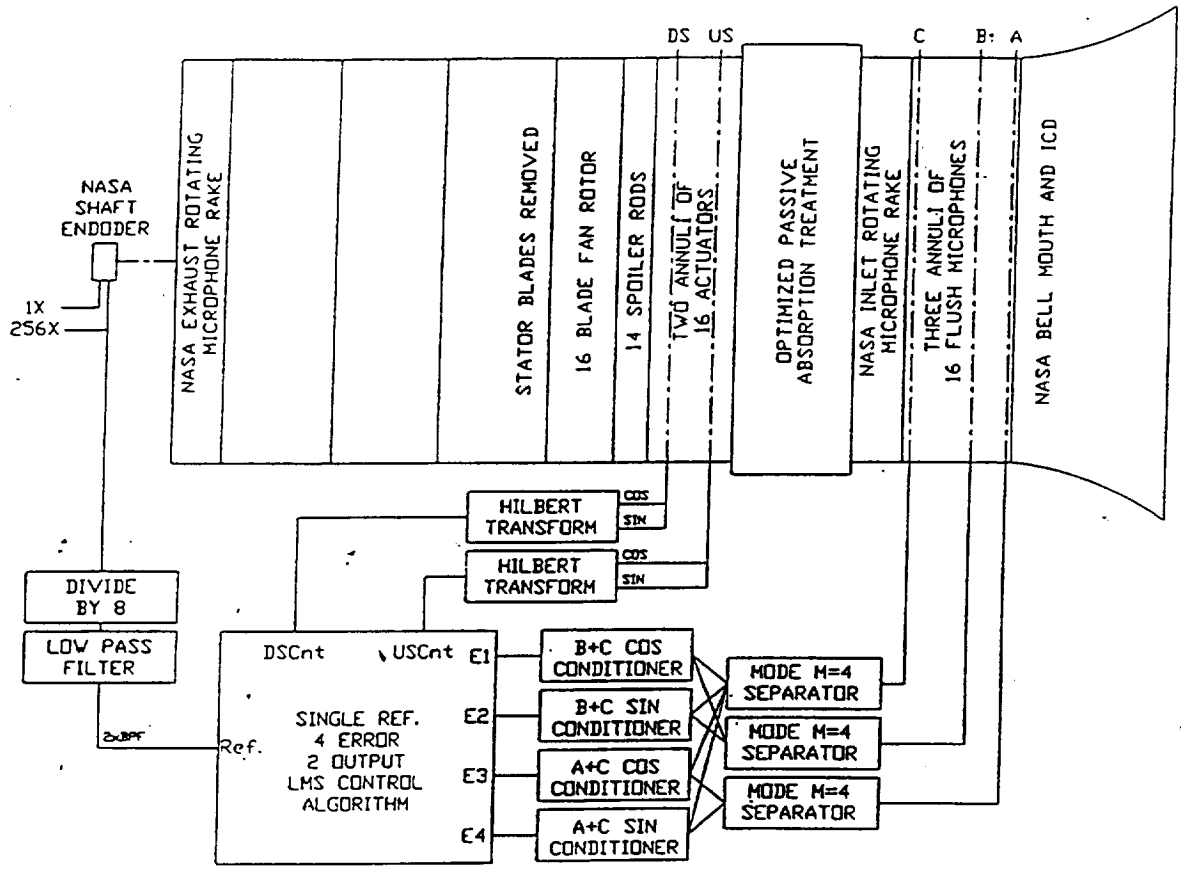

Figure 4.13
Schematic Diagram of Active/Passive Segmented Liner
Measurements at NASA LeRc ANCF Facility

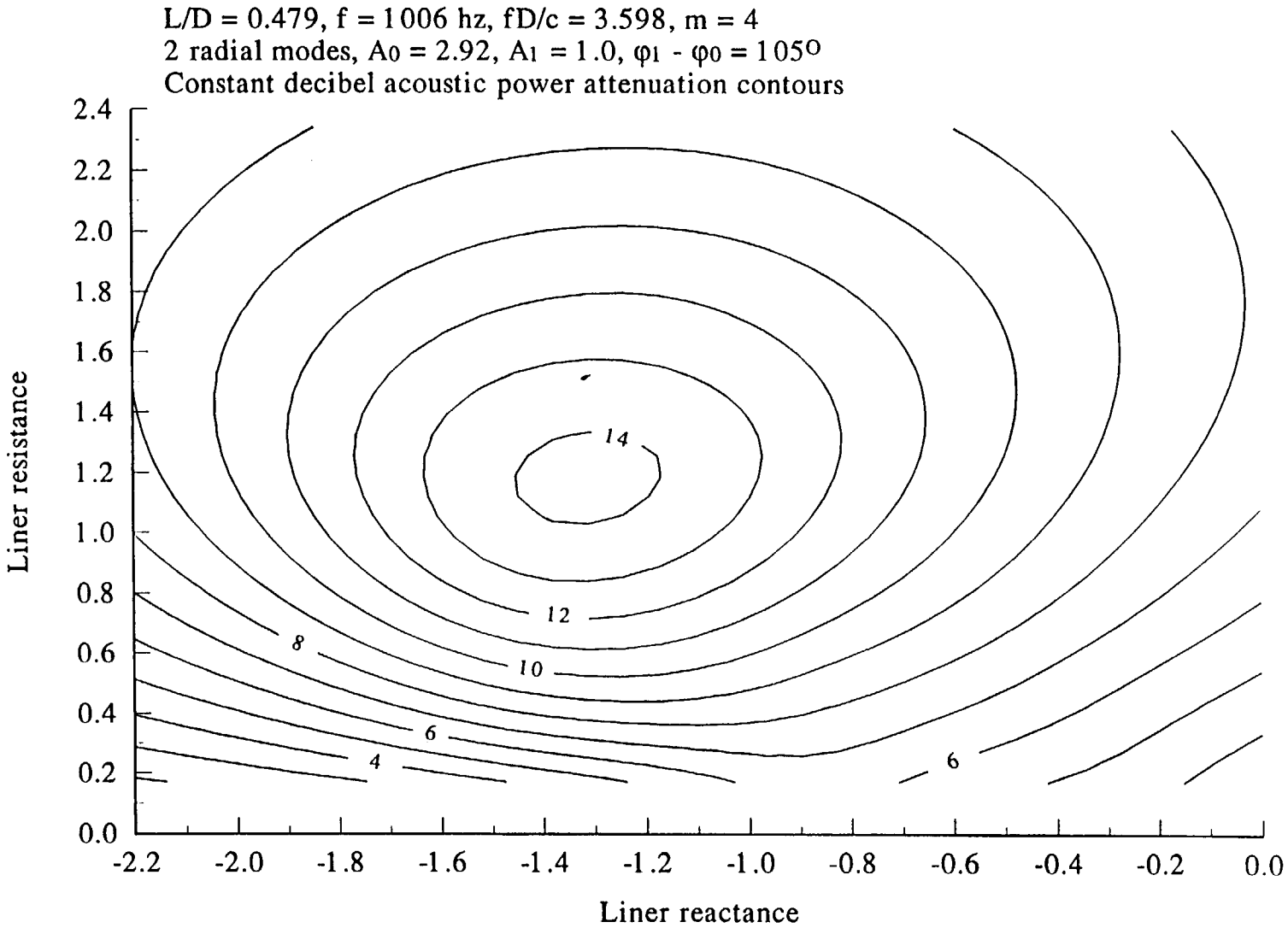

Figure 4.14. Optimum impedance determination for uniform liner ANC 1

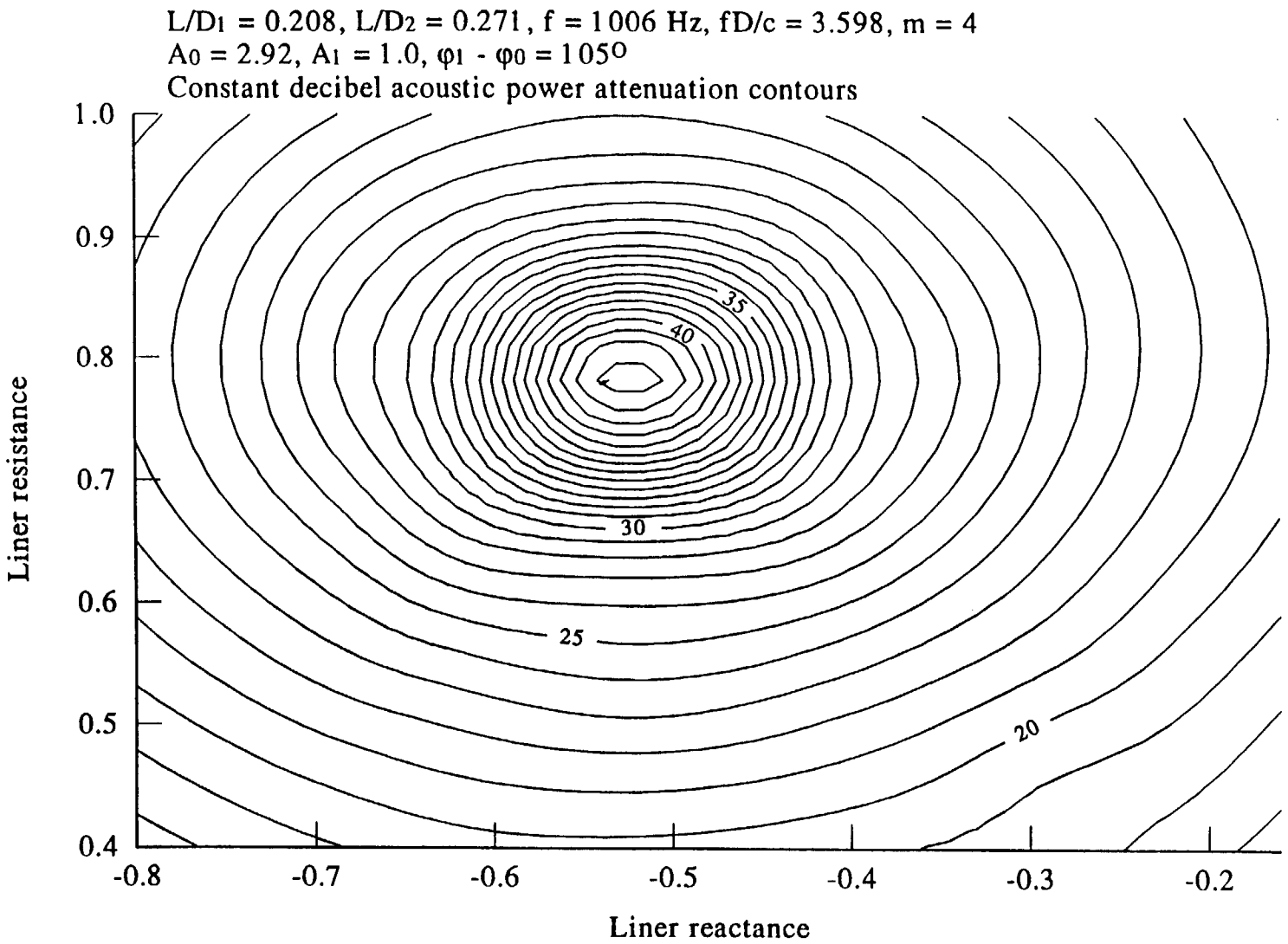

Figure 4.15. Attenuation sensitivity of liner 2 of two segment liner ANC 2
liner 1 impedance fixed at 0.554 - i1.914

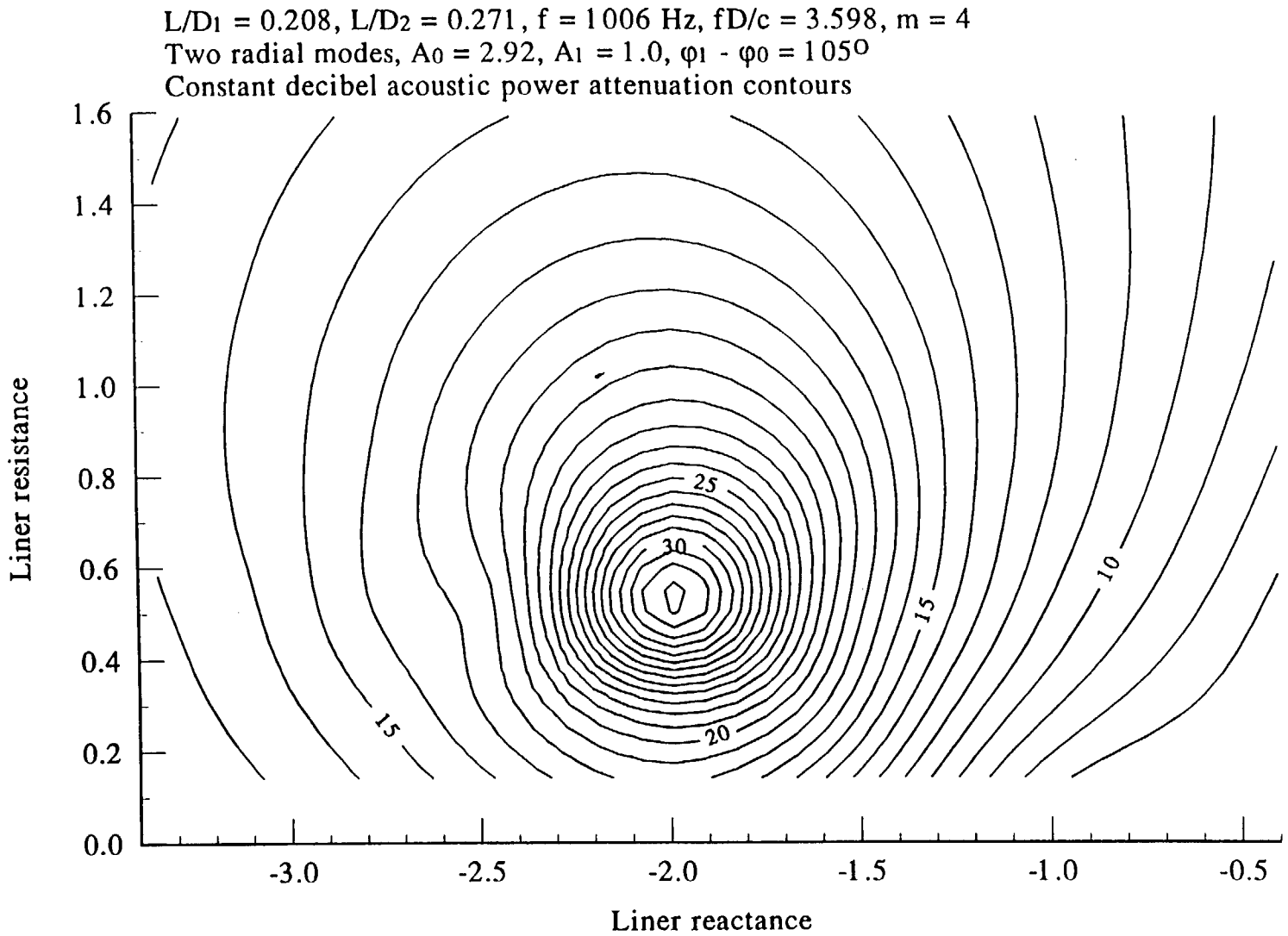

Figure 4.16. Attenuation sensitivity of liner 1 of two segment liner ANC 2
liner 2 impedance fixed at 0.788 - i0.522

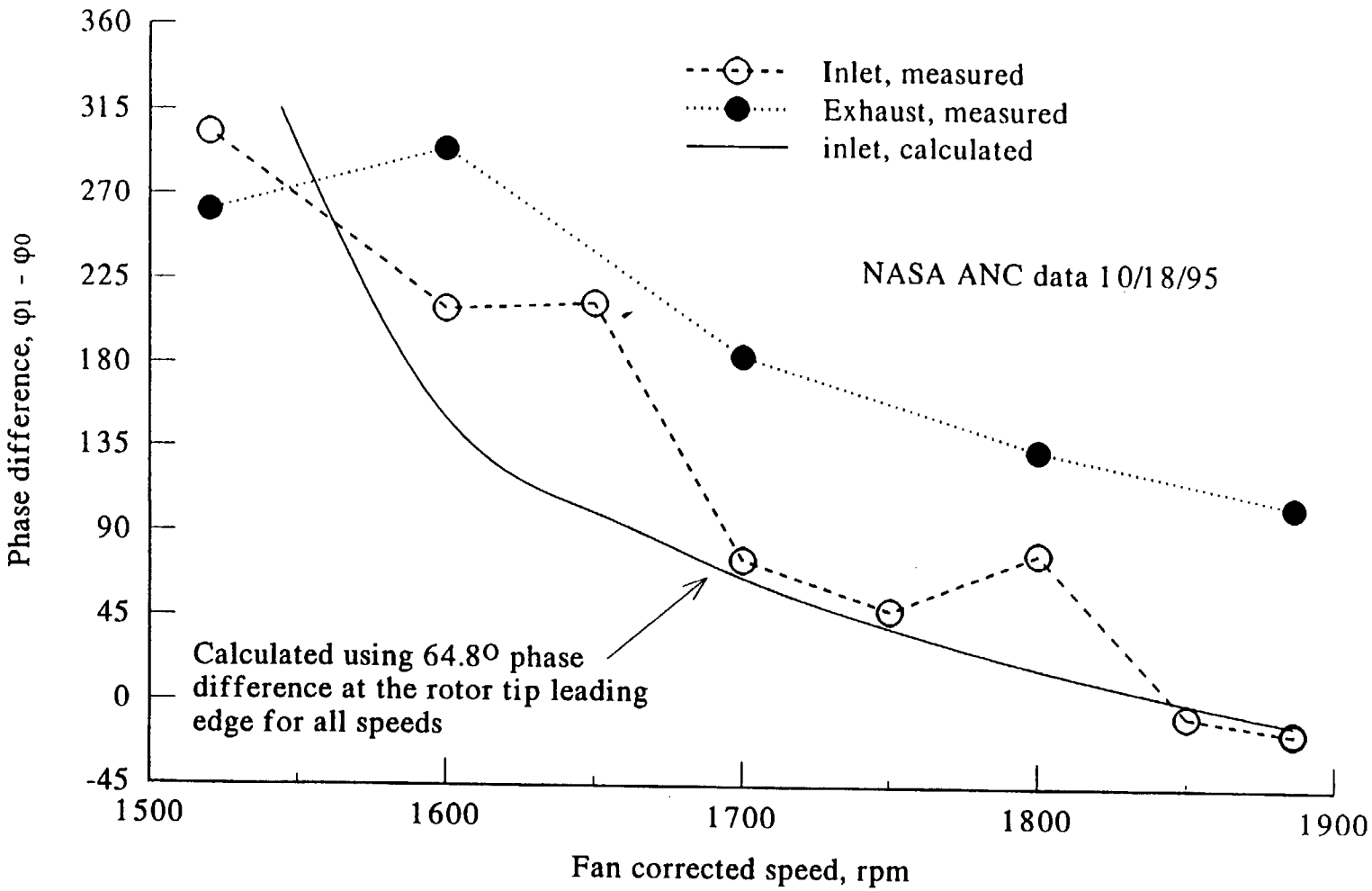

Figure 4.17. Measured phase difference between the 4,1 and the 4,0 modes inlet rake transducers at 33.94 inches ahead of rotor tip leading edge

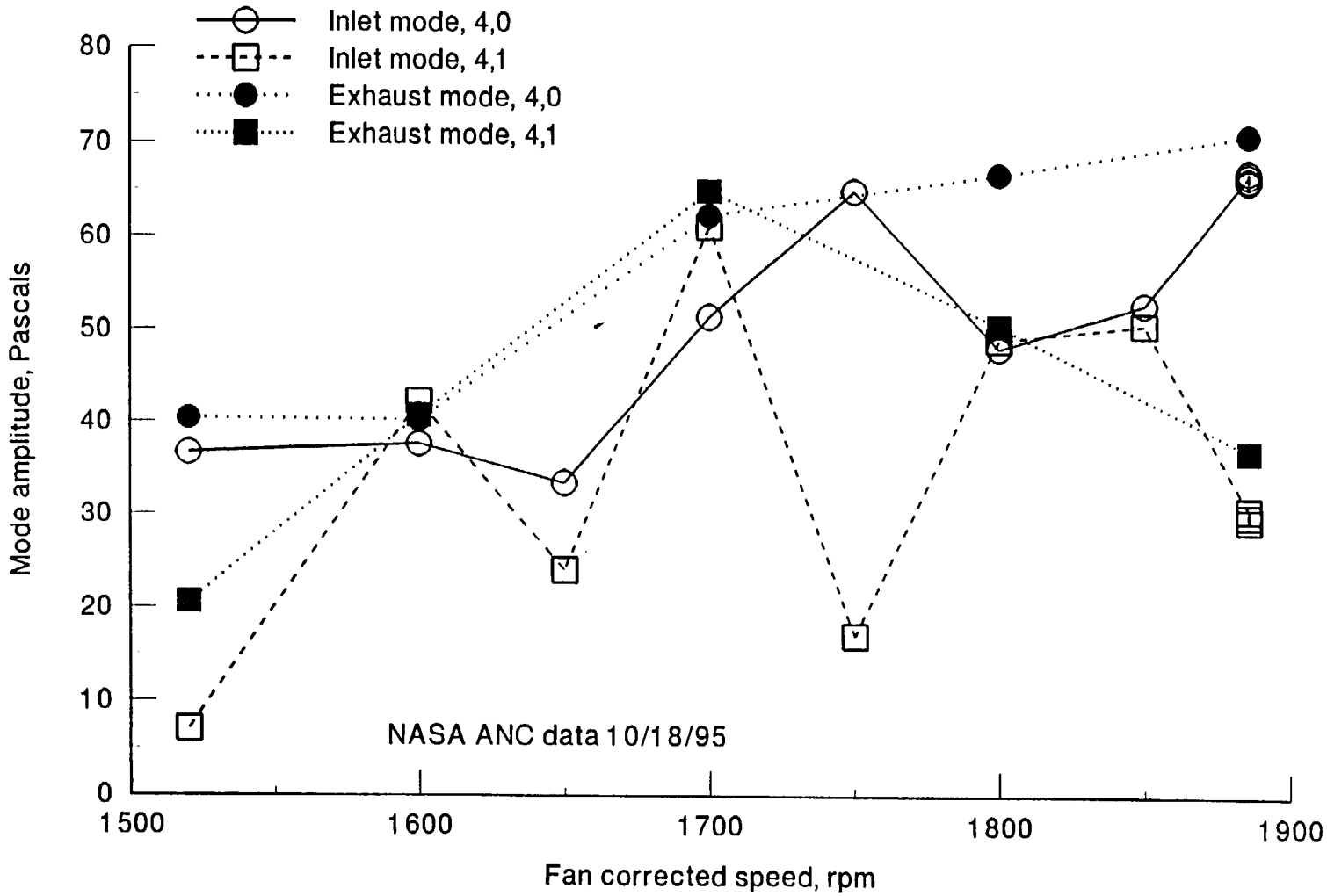

Figure 4.18. Measured modal coefficient magnitude of the 4,0 and 4,1 modes inlet rake transducers at 33.94 inches ahead of rotor tip leading edge

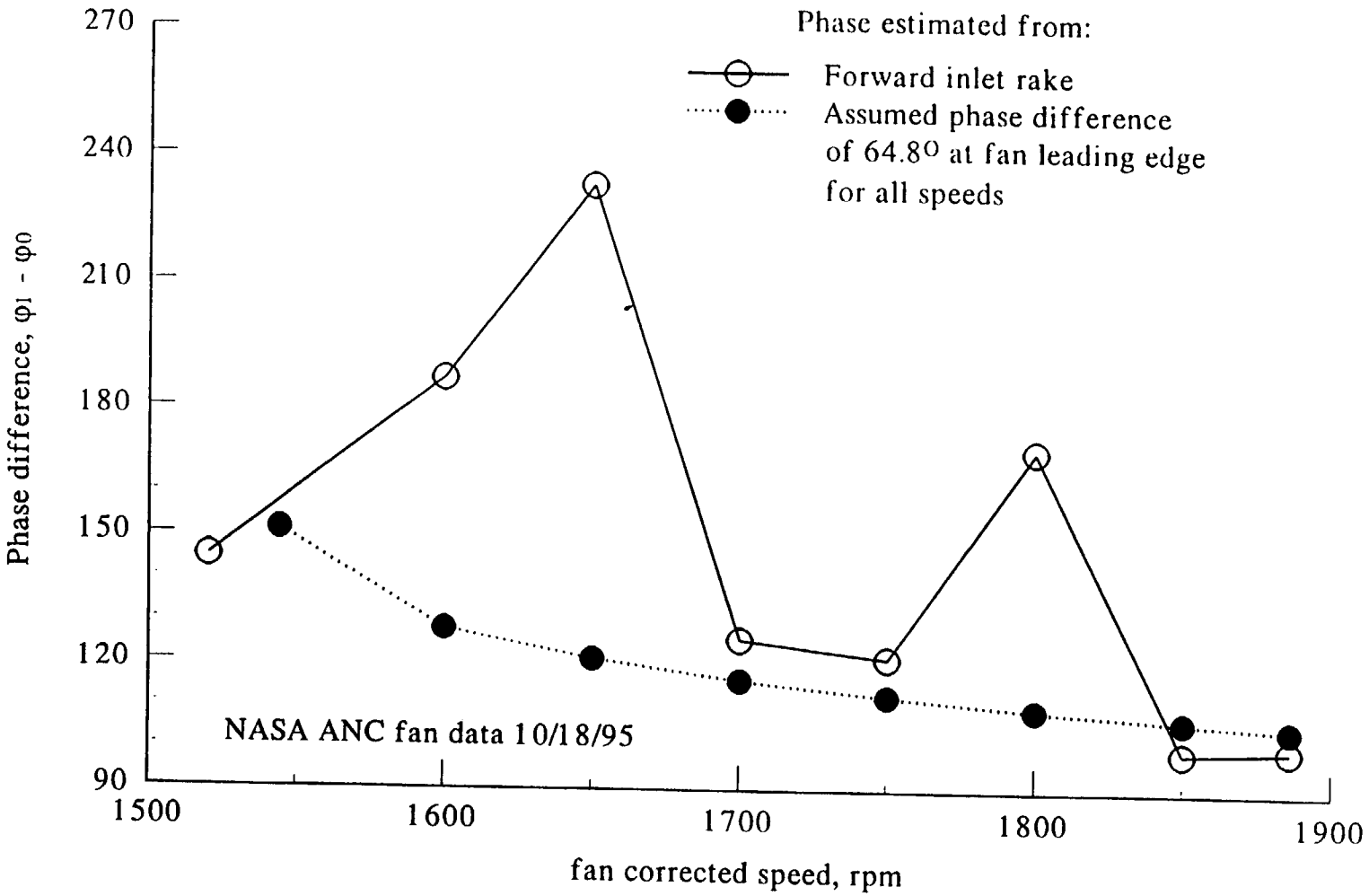

Figure 4.19. Phase difference between the 4,1 and the 4,0 modes estimated at the begining of the acoustic liner

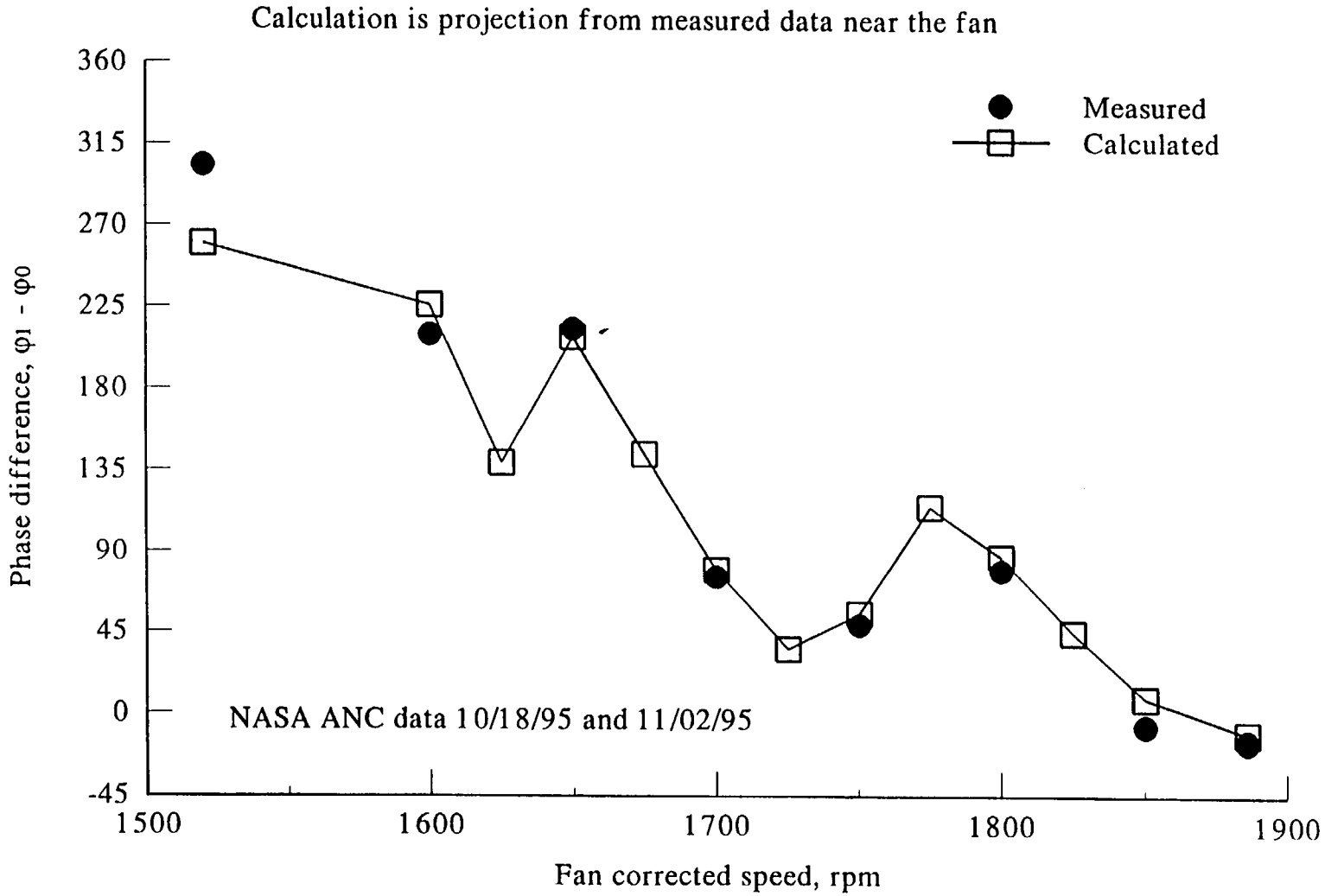

Figure 4.20. Phase difference between the 4,1 and the 4,0 modes at the inlet lip probe location, measured and projected

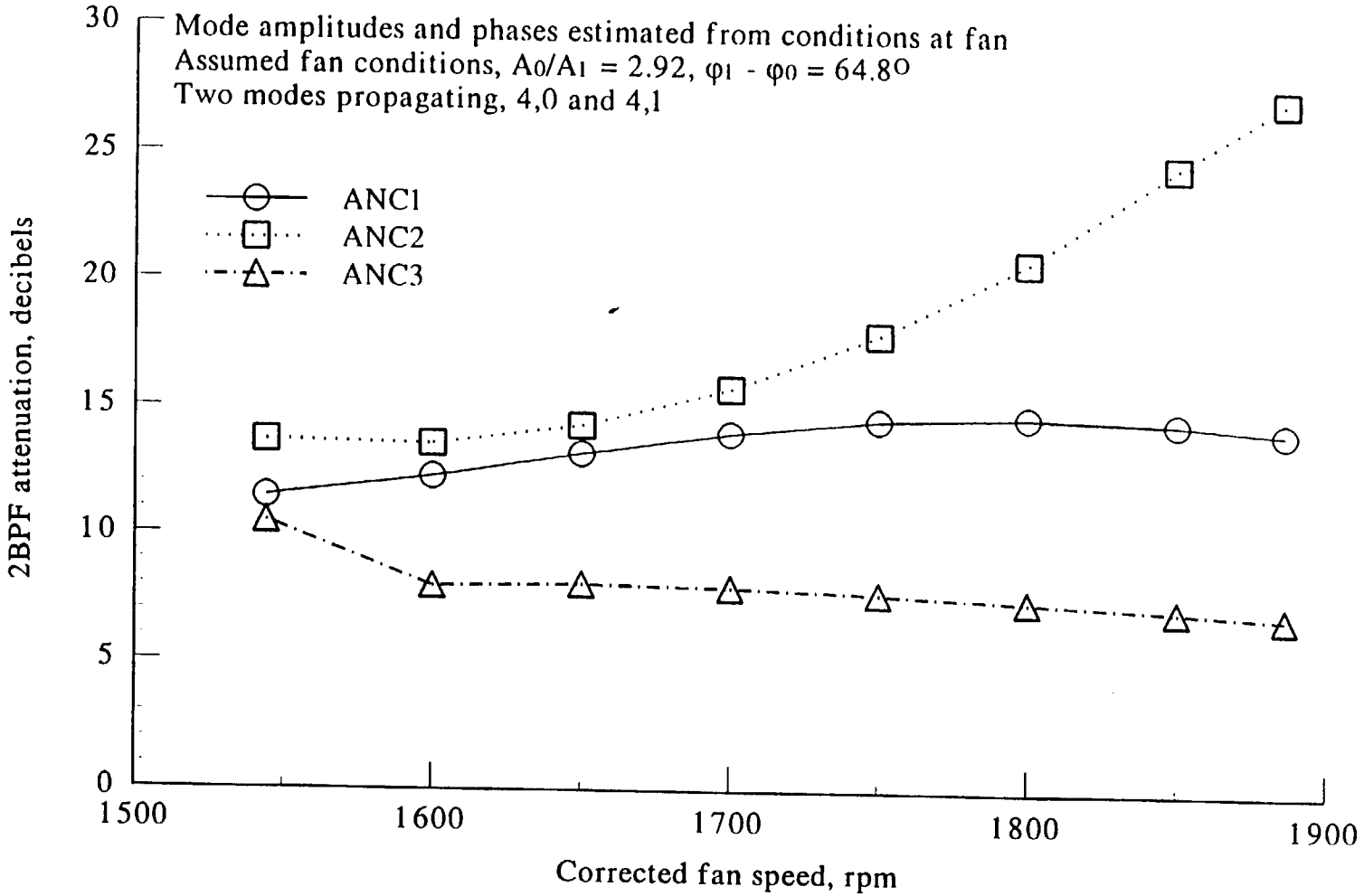

Figure 4.21. Calculated attenuation of inlet acoustic liners at 2BPF for all three inlet passive acoustic treatments, NASA ANC fan stage

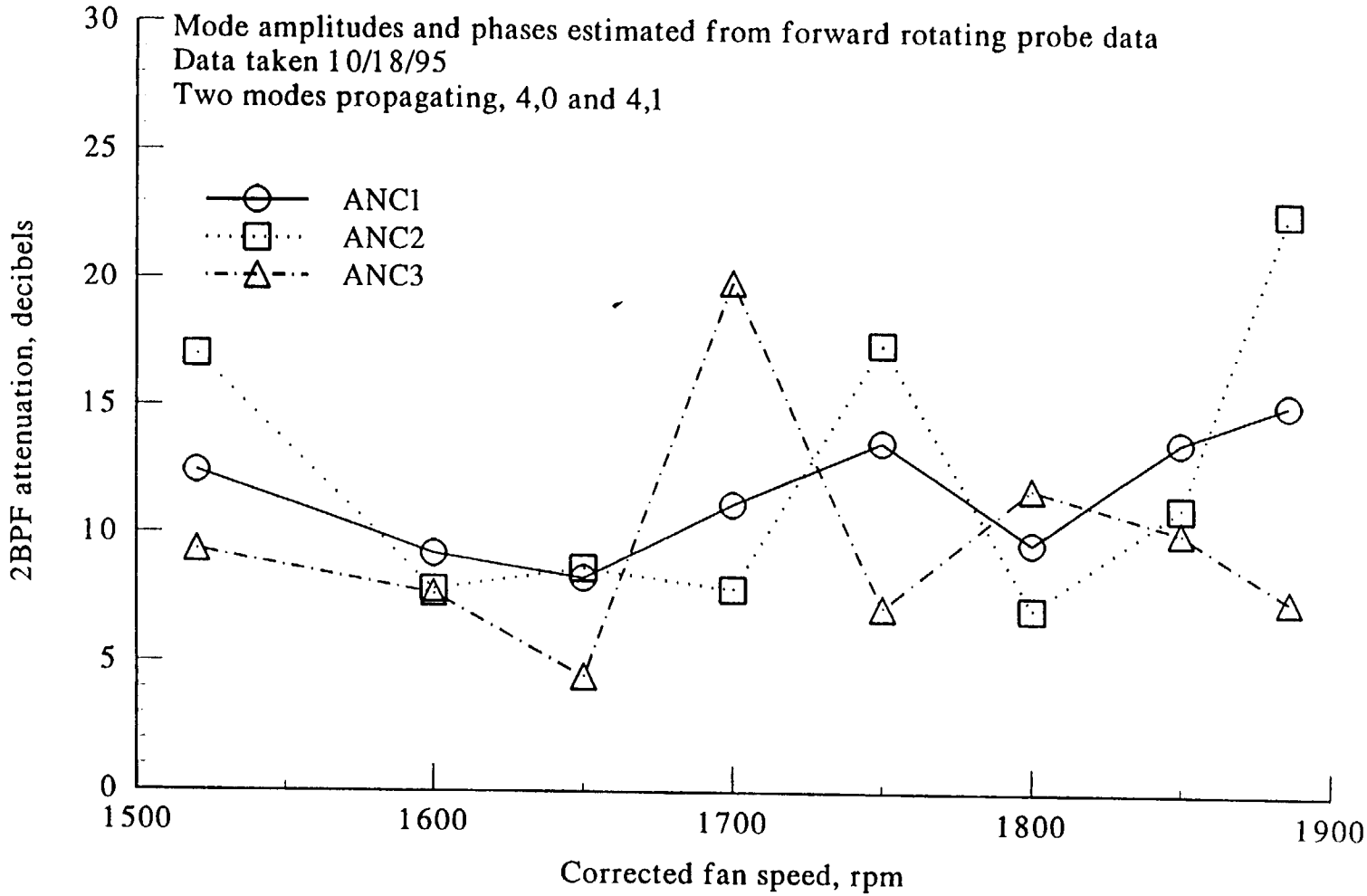

Figure 4.22. Calculated attenuation of inlet acoustic liners at 2BPF for all three inlet passive acoustic treatments, NASA ANC fan stage

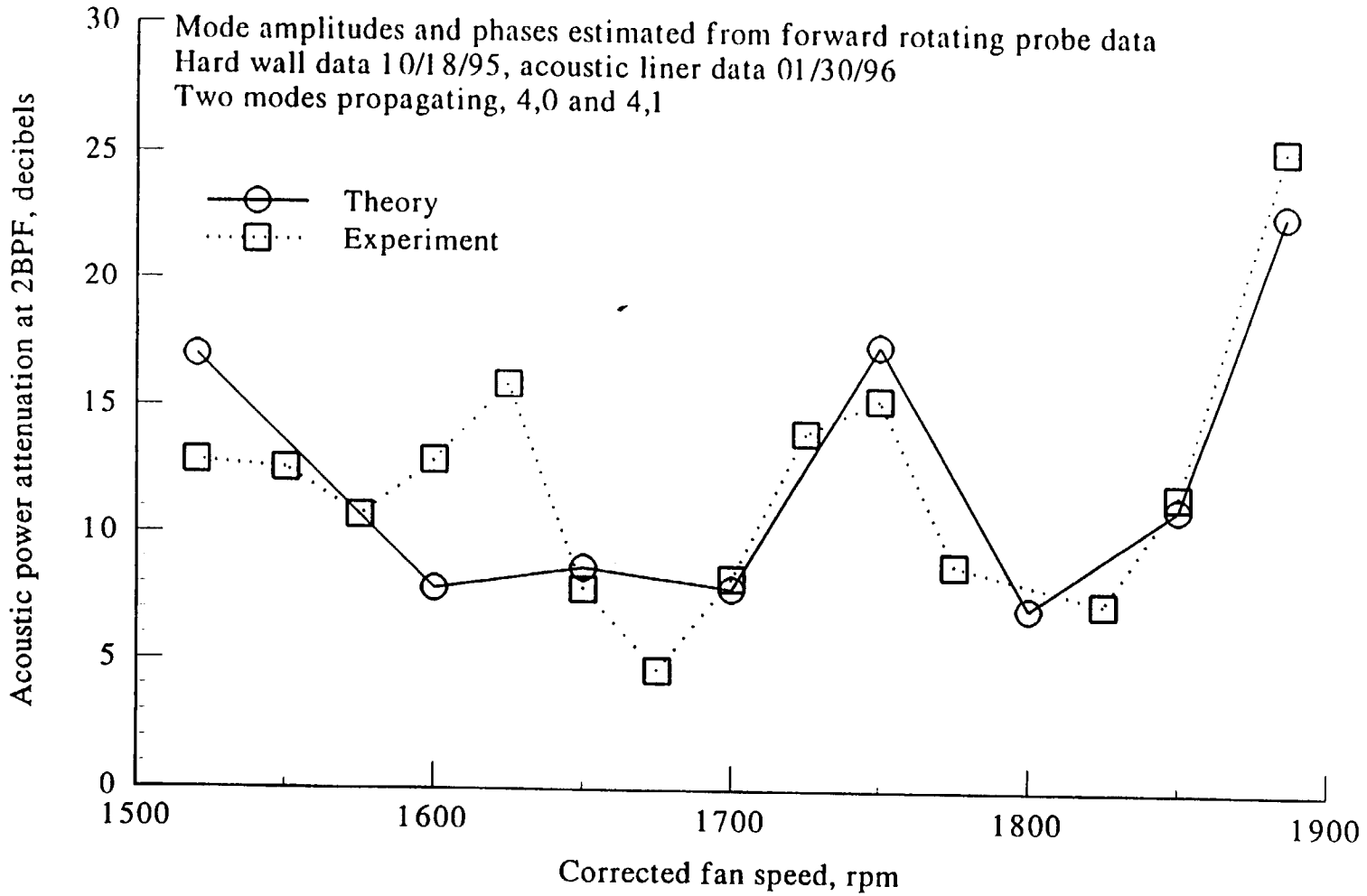

Figure 4.23. Calculated and experimental attenuation of inlet two segment passive acoustic liner ANC2 at 2BPF, NASA ANC fan, 16 blades with 14 rods

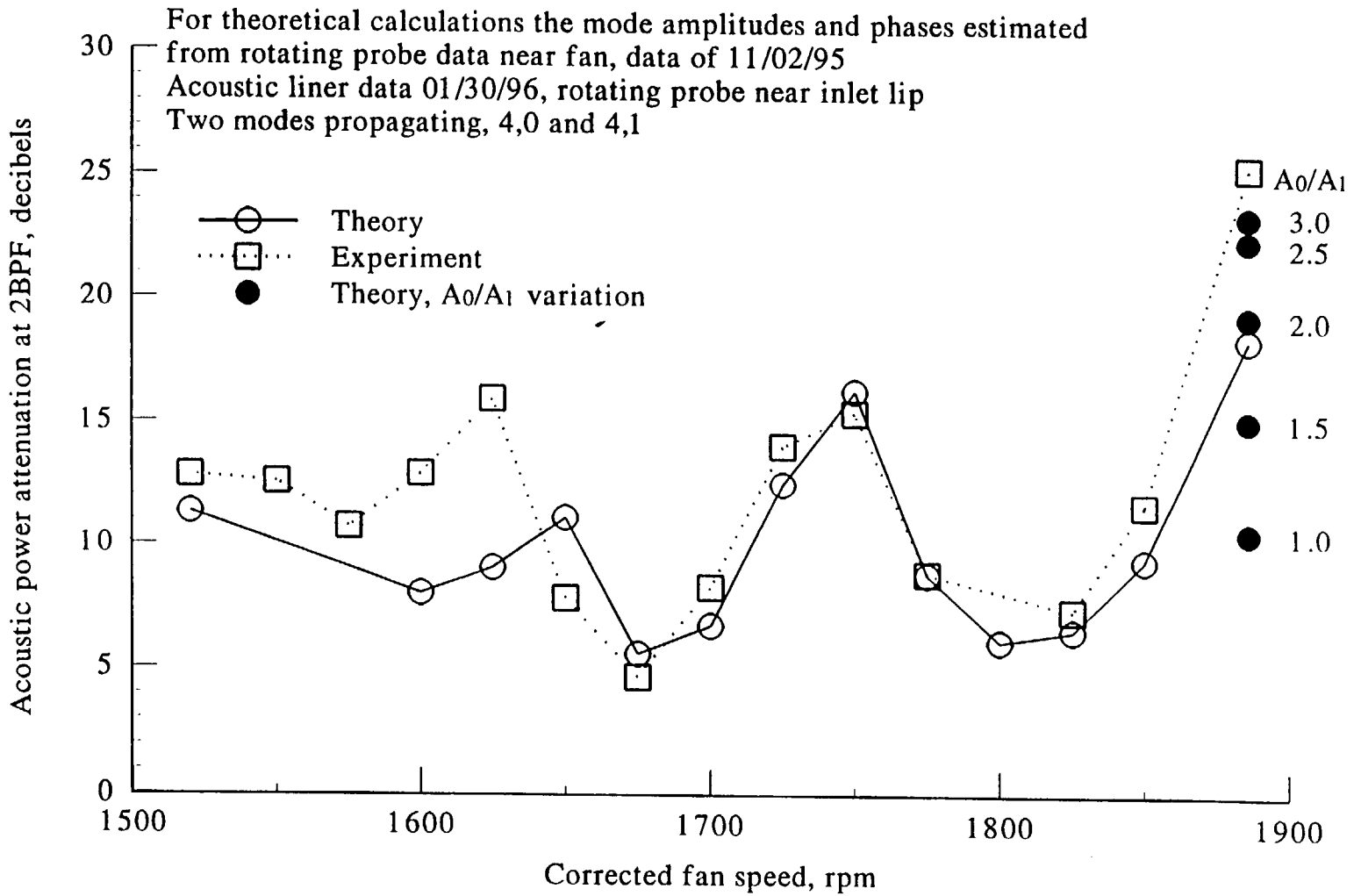

Figure 4.24. Calculated and experimental attenuation of inlet two segment passive acoustic liner ANC2 at 2BPF, NASA ANC fan, 16 blades with 14 rods

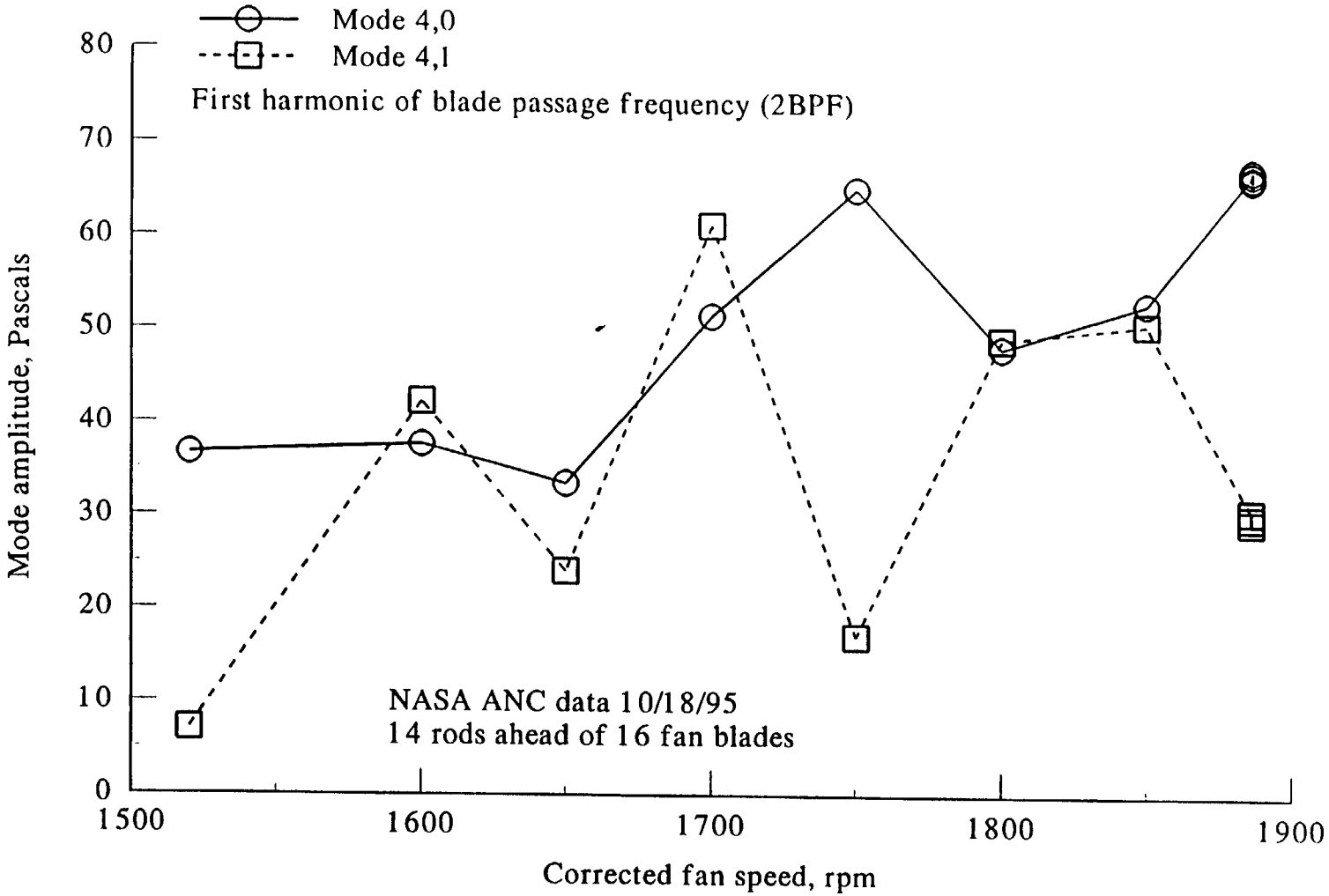

Figure 4.25. Measured modal coefficient magnitude of the 4,0 and 4,1 modes inlet rake transducers near inlet lip

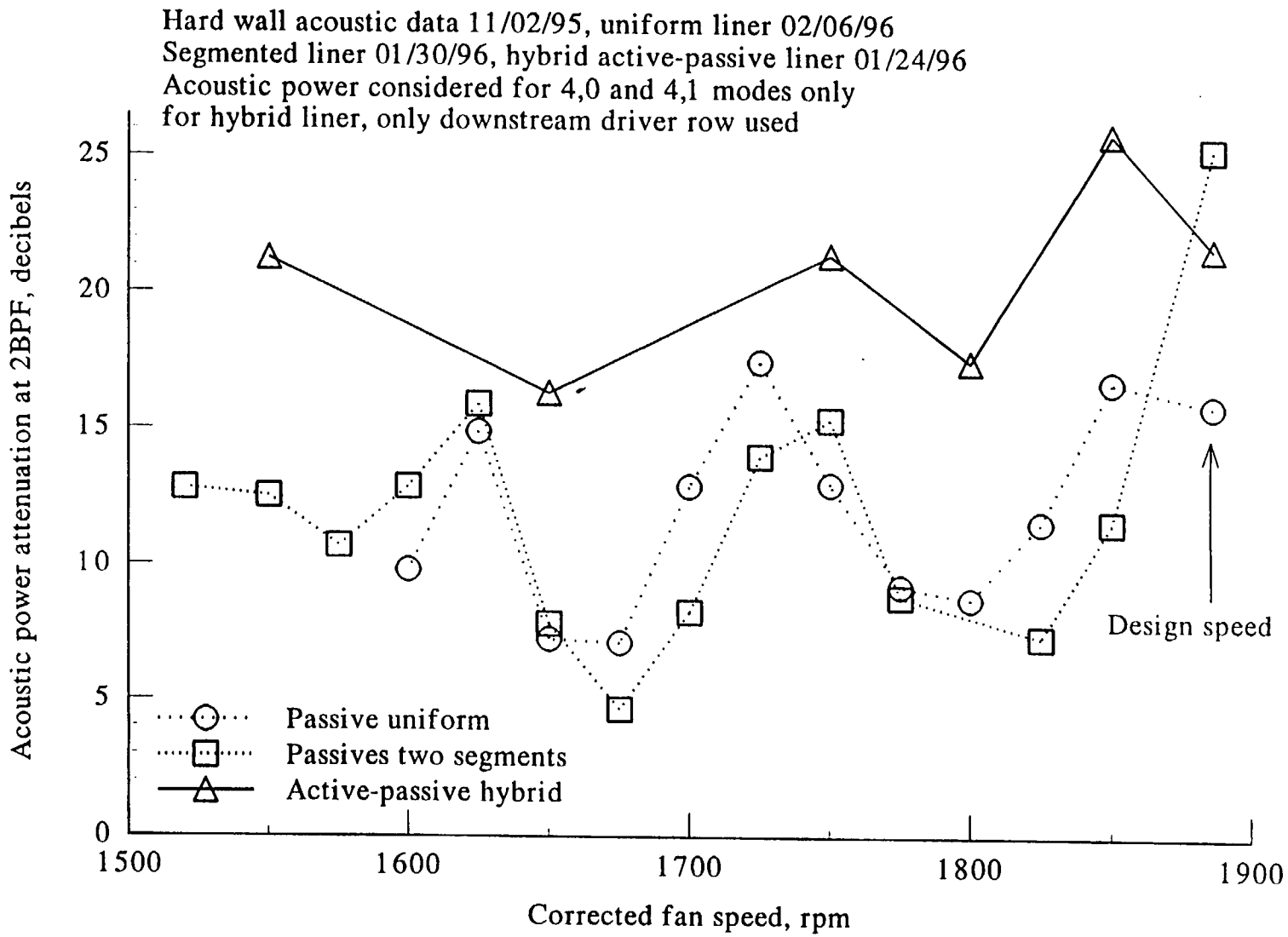

Figure 4.26. Measured modal acoustic attenuation of the three ANC liners at 2BPF, NASA ANC fan, 16 blades with 14 upstream rods

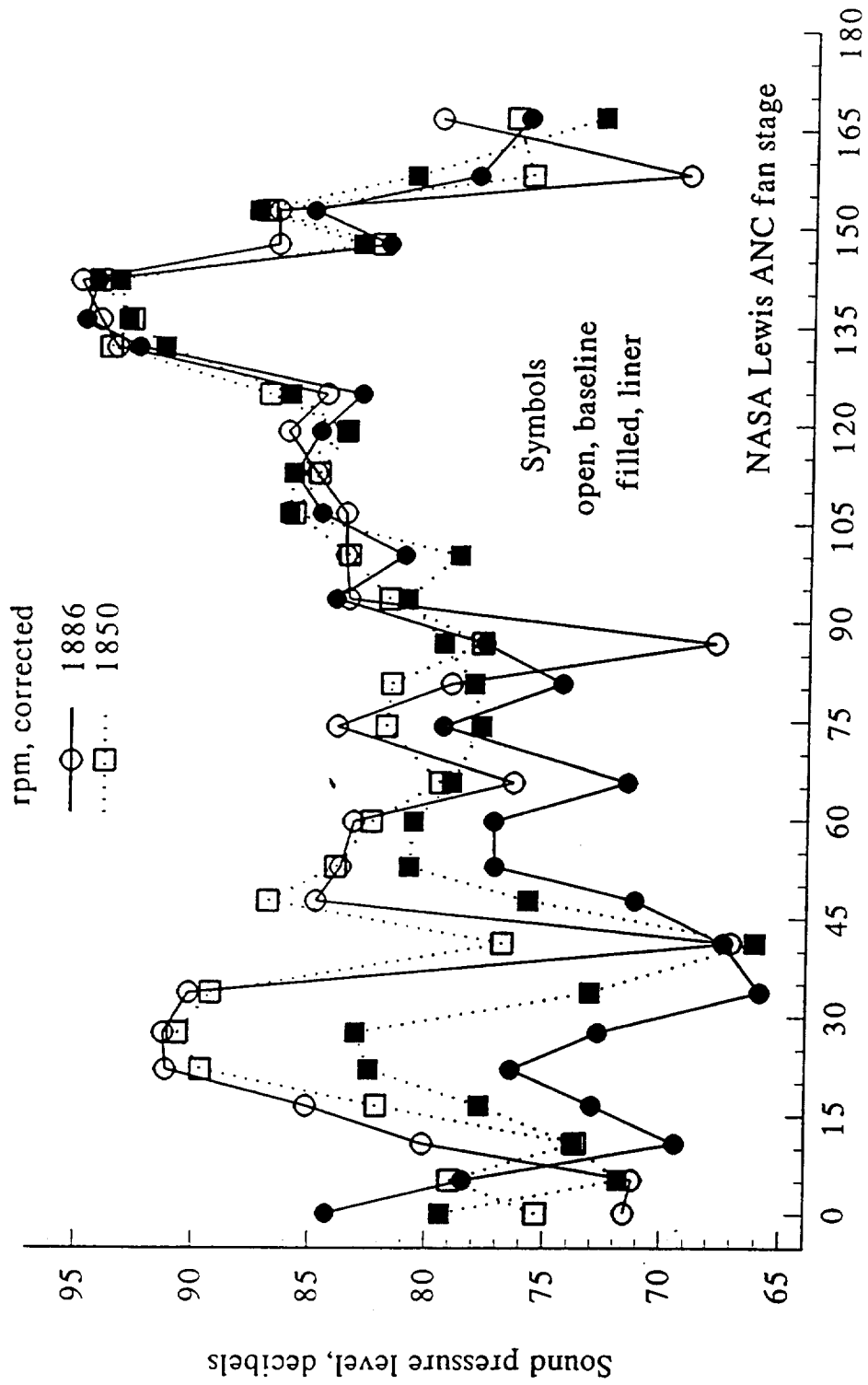

Figure 4.27. Far-field noise directivity, baseline and two-segment liner at 2BPF

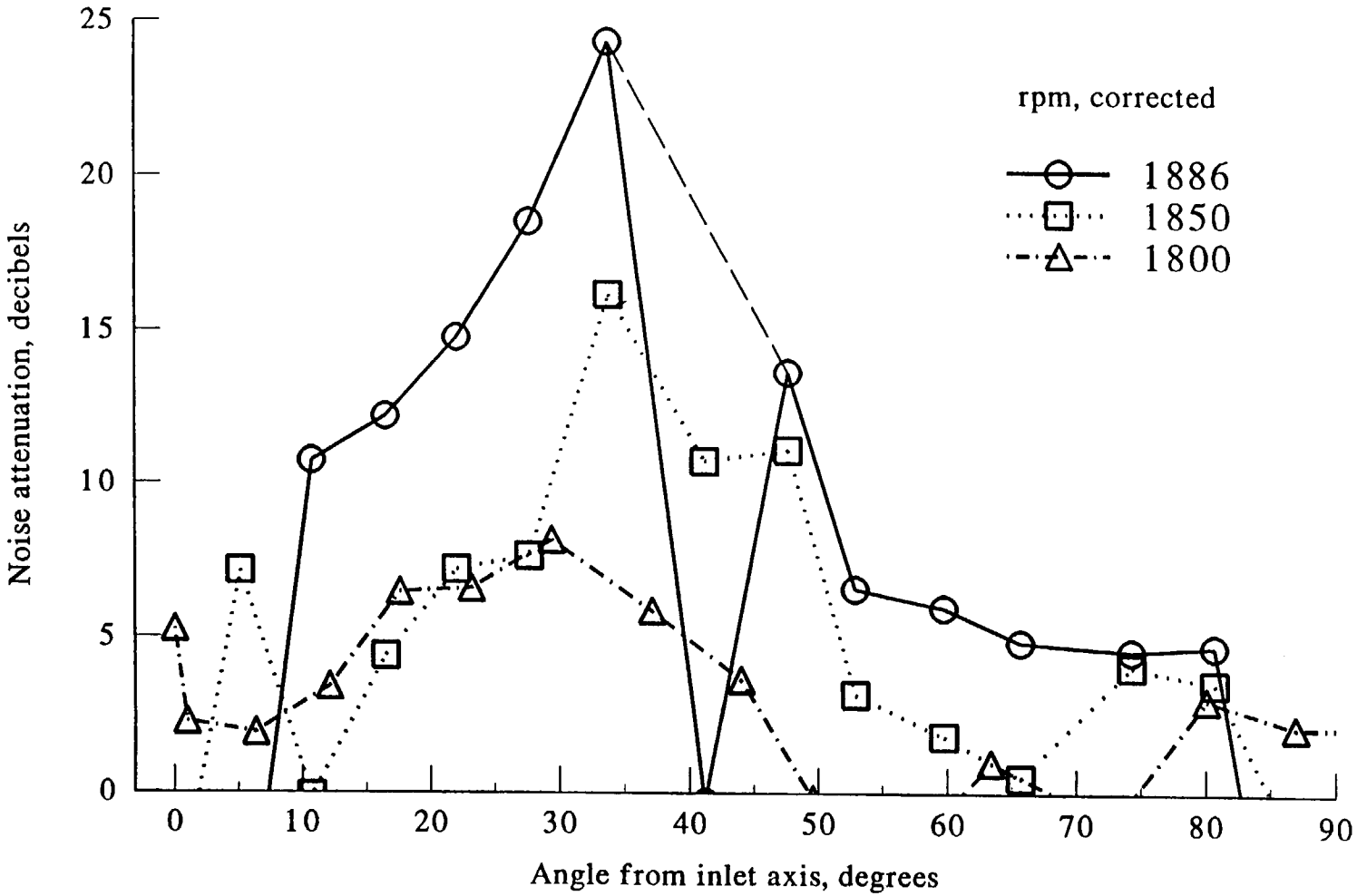

Figure 4.28. Far-field noise attenuation for the two-segment passive liner
NASA Lewis ANC fan with 14 upstream rods, tone at 2BPF

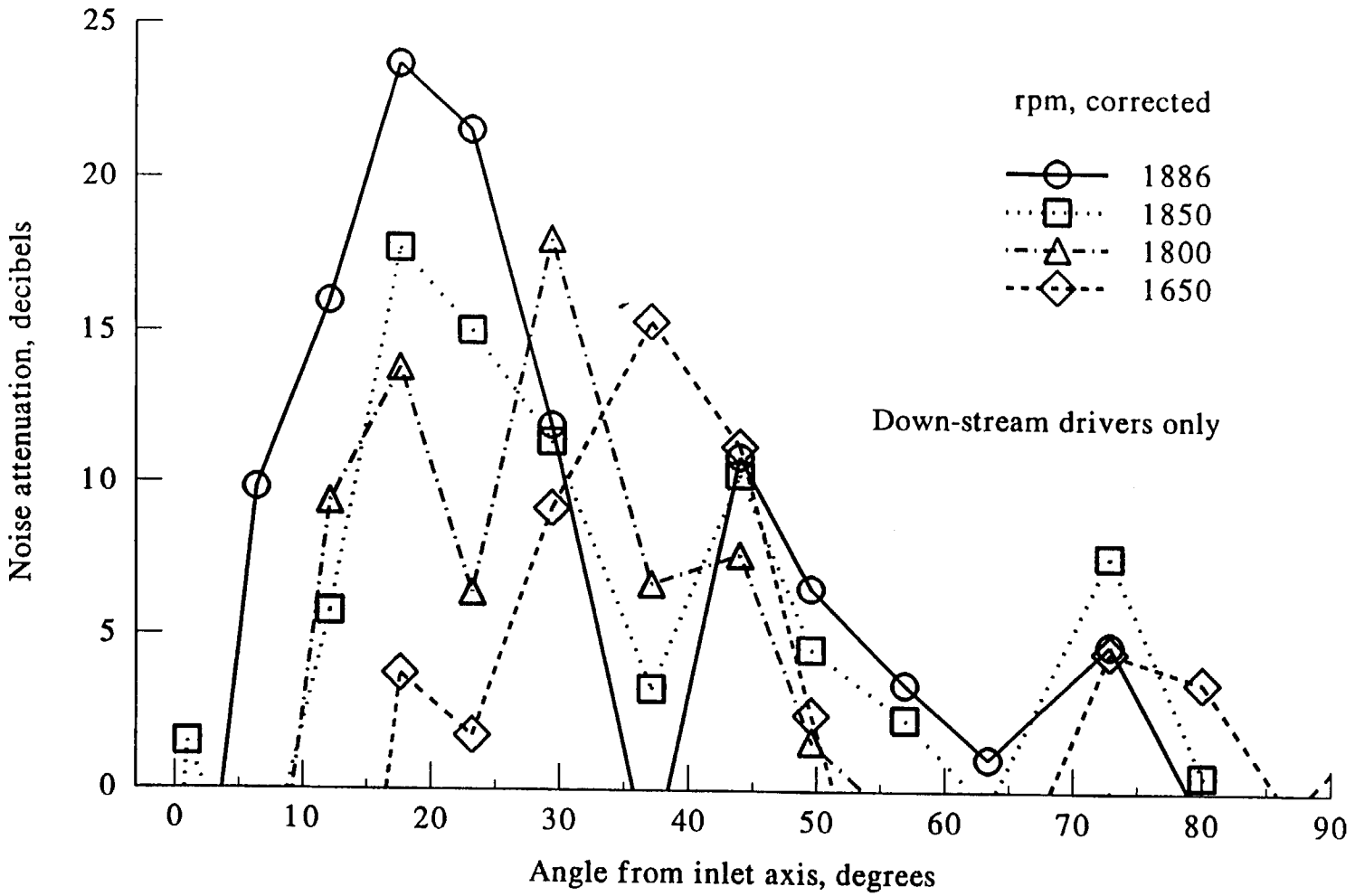

Figure 4.29. Far-field noise attenuation for hybrid active-passive liner
NASA Lewis ANC fan with 14 upstream rods, tone at 2BPF

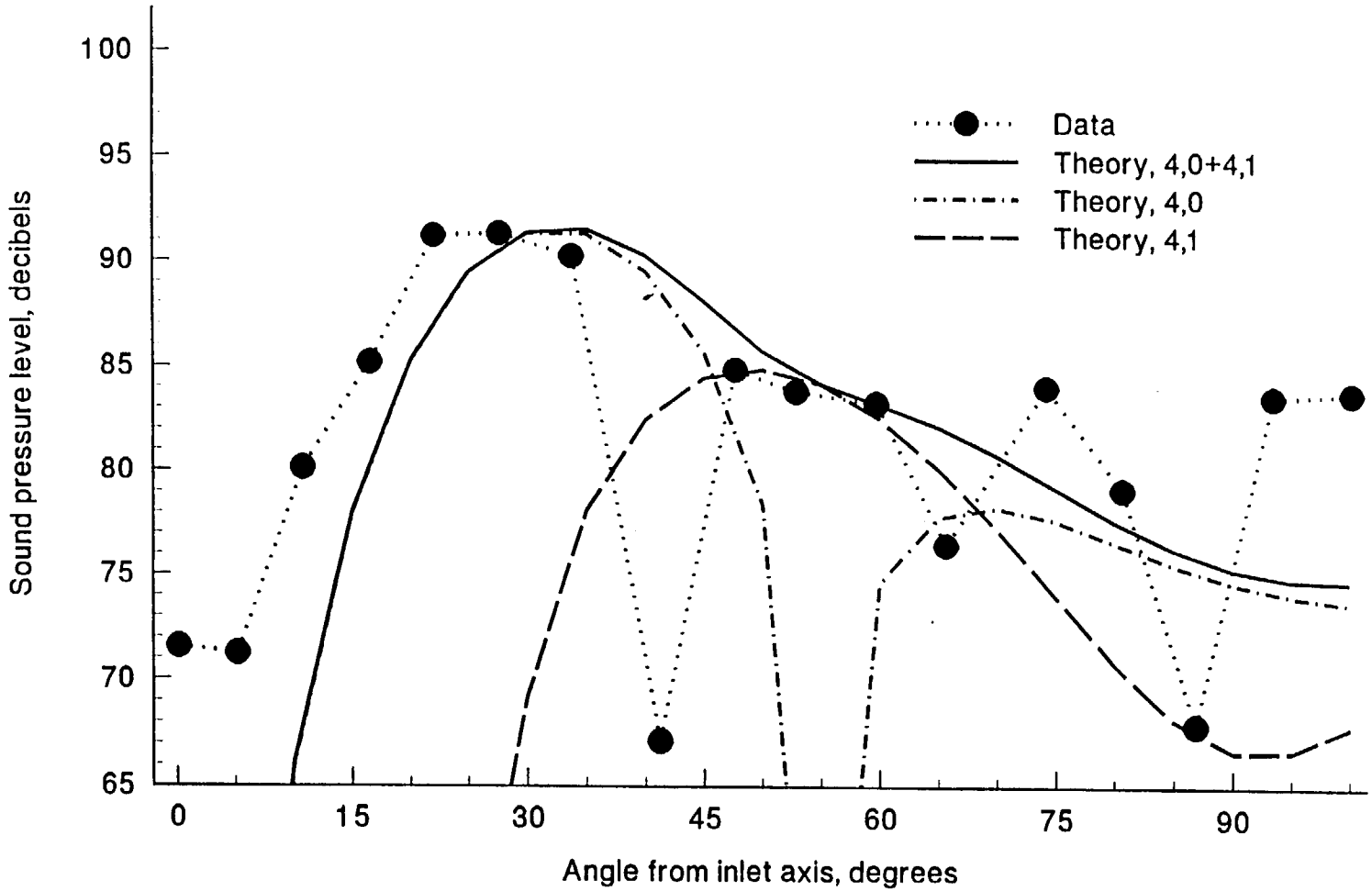

Figure 4.30. Far-field noise directivity, hard wall baseline, NASA Lewis ANC fan with 14 upstream rods, tone at twice blade passing frequency

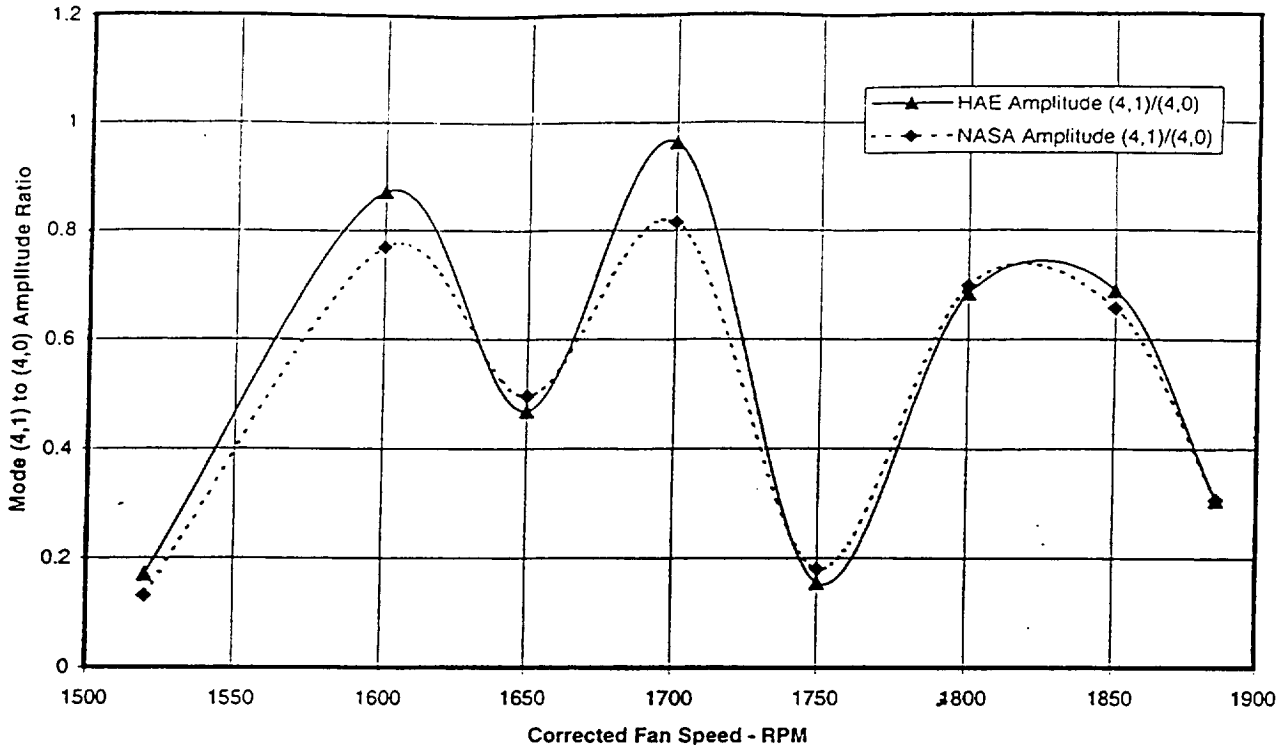

FIGURE 4.31
Ratios of Mode (4,1) to (4,0) Amplitudes in NASA/LeRC ANCF Fan Inlet as Measured with NASA Rotating Rake and HAE Flush Mounted Microphone Arrays

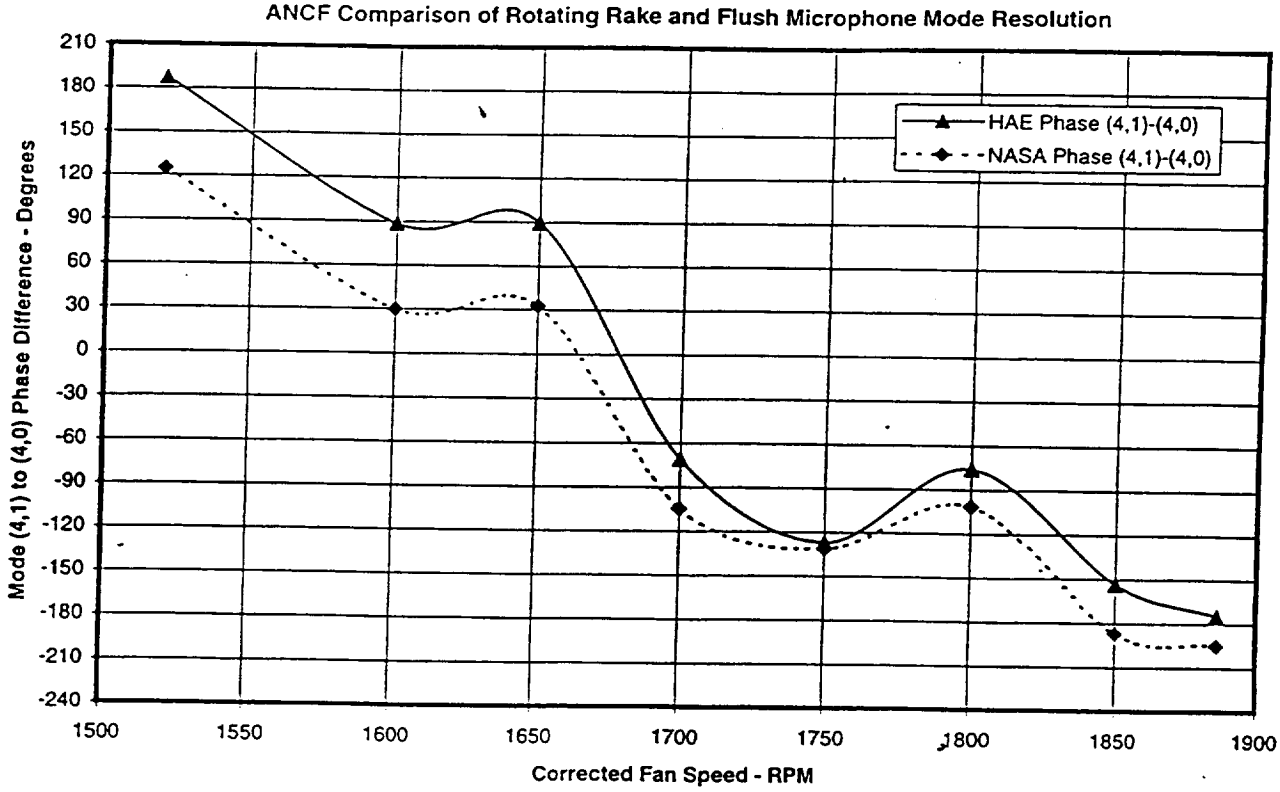

FIGURE 4.32
Differences of Mode (4,1) to (4,0) Phases in NASA/LeRC ANCF Fan Inlet as Measured with NASA Rotating Rake and HAE Flush Mounted Microphone Arrays

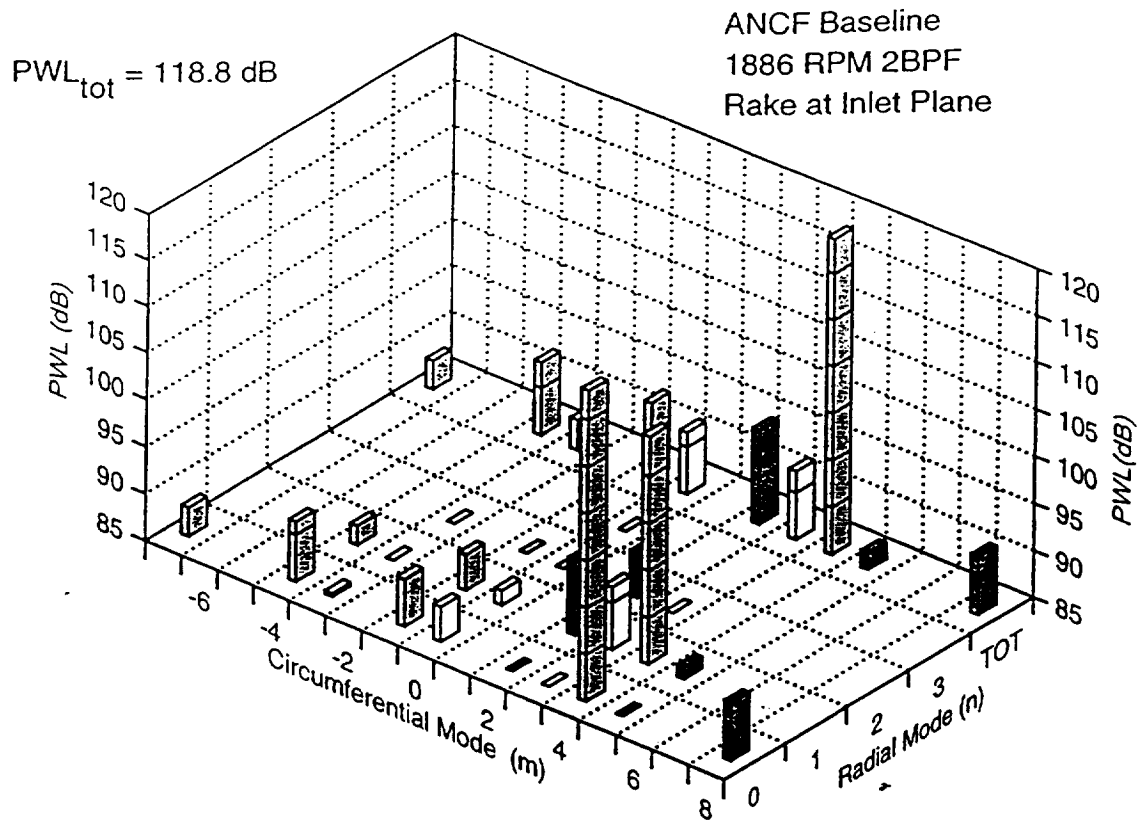

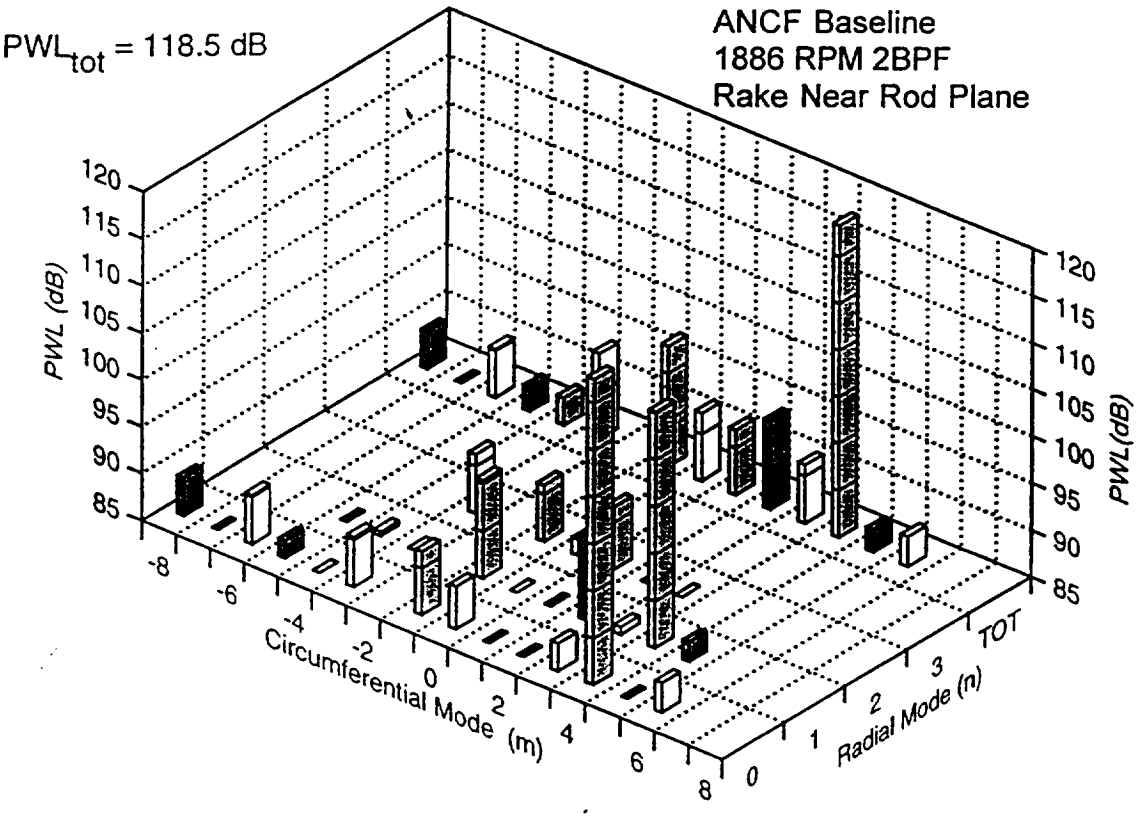

FIGURE 4.33 a, b
Comparison of ANCF Baseline Mode Structure at Two Inlet Axial Stations

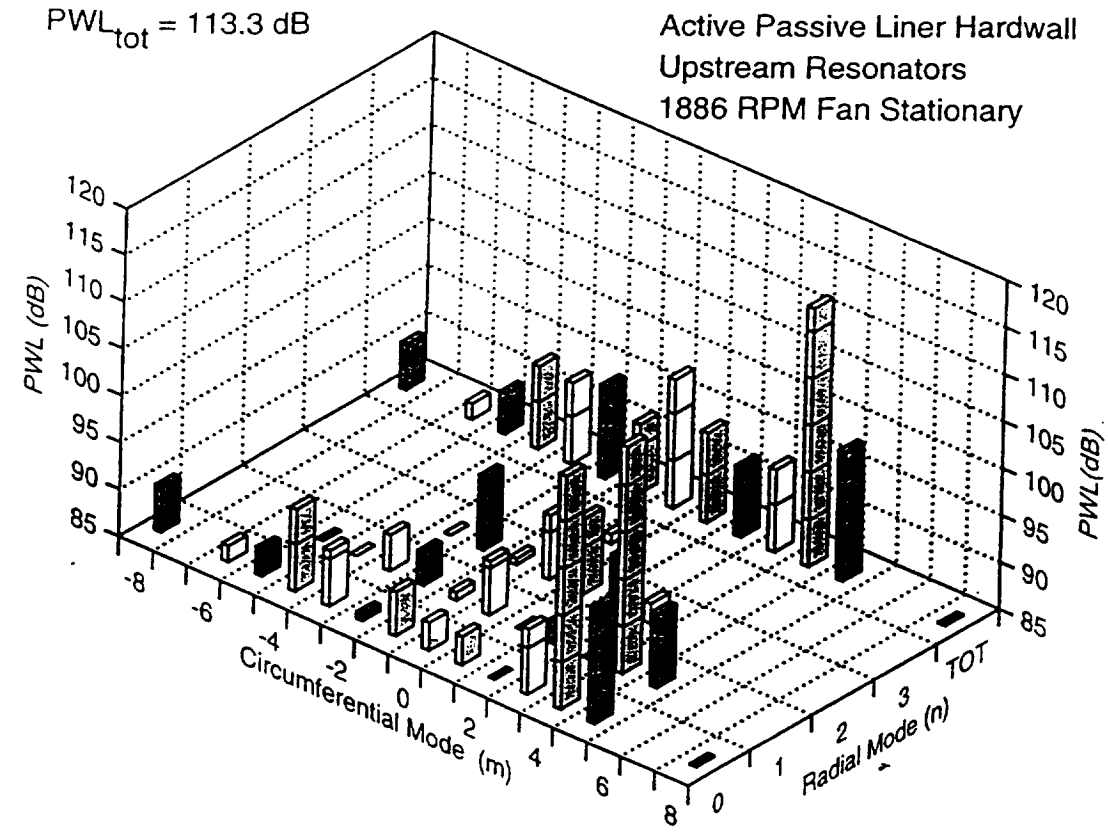

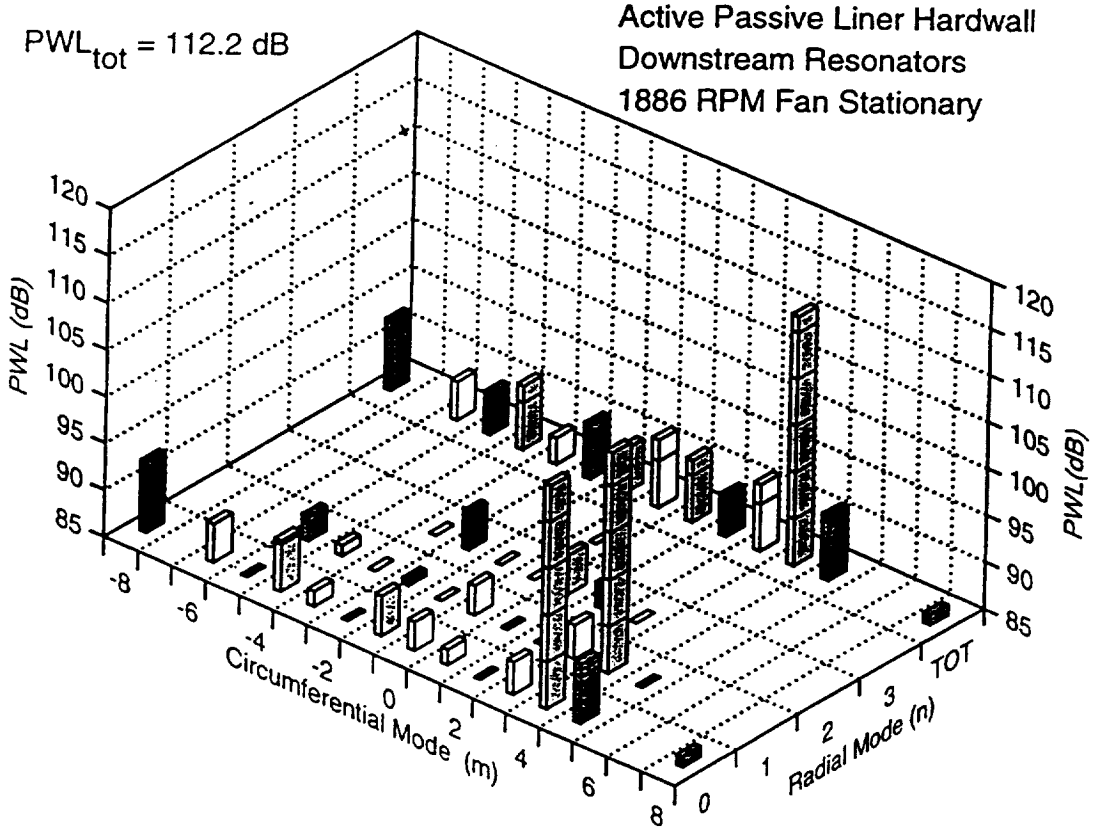

FIGURE 4.34 a, b
Comparison of Duct Modes Generated by NGC/HAE Active Liner Segment Upstream and Downstream Actuators with Passive Segment Covered, Fan Stationary

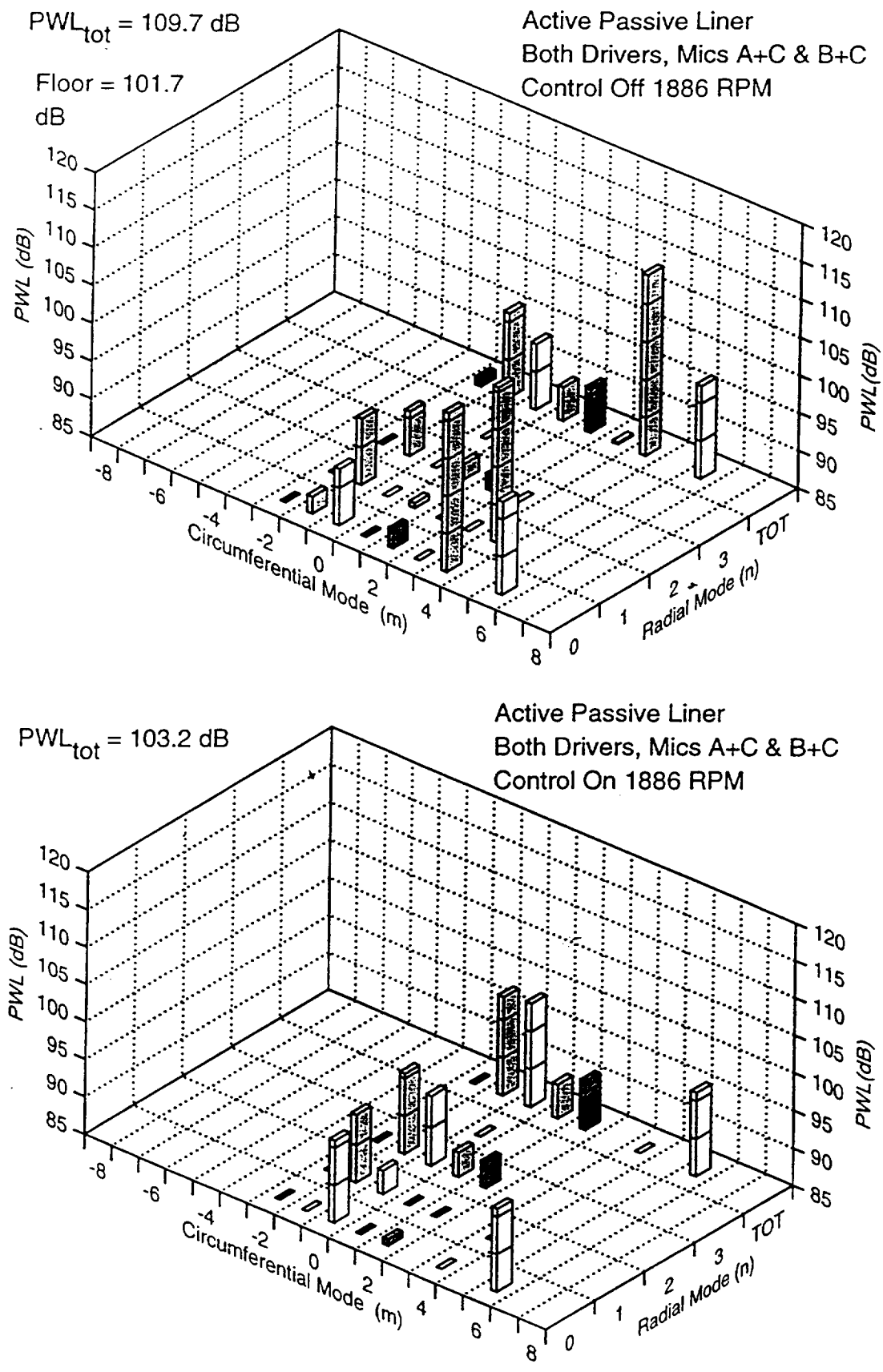

FIGURE 4.35 a, b
Comparison of Duct Modes in NASA/LeRC ANCF Fan Inlet
NGC/HAE Adaptive Segmented Liner, Fan 1886 RPM
Control Off vs. Control On

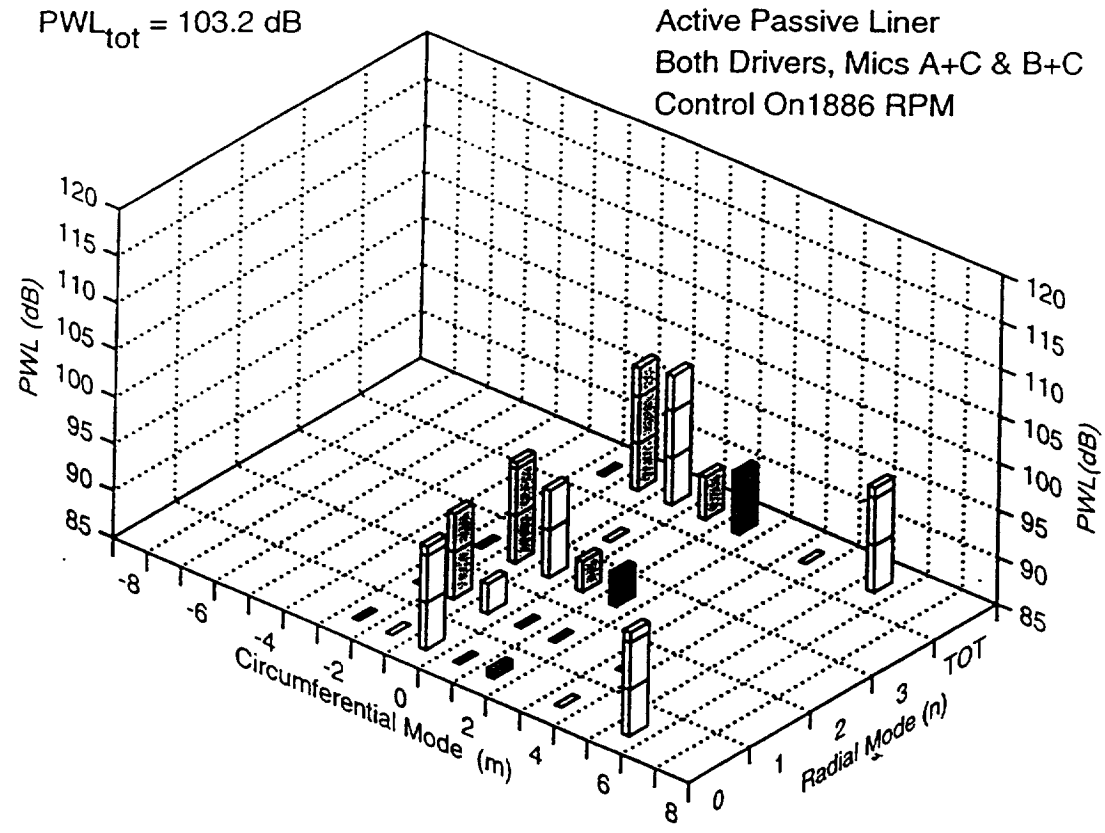

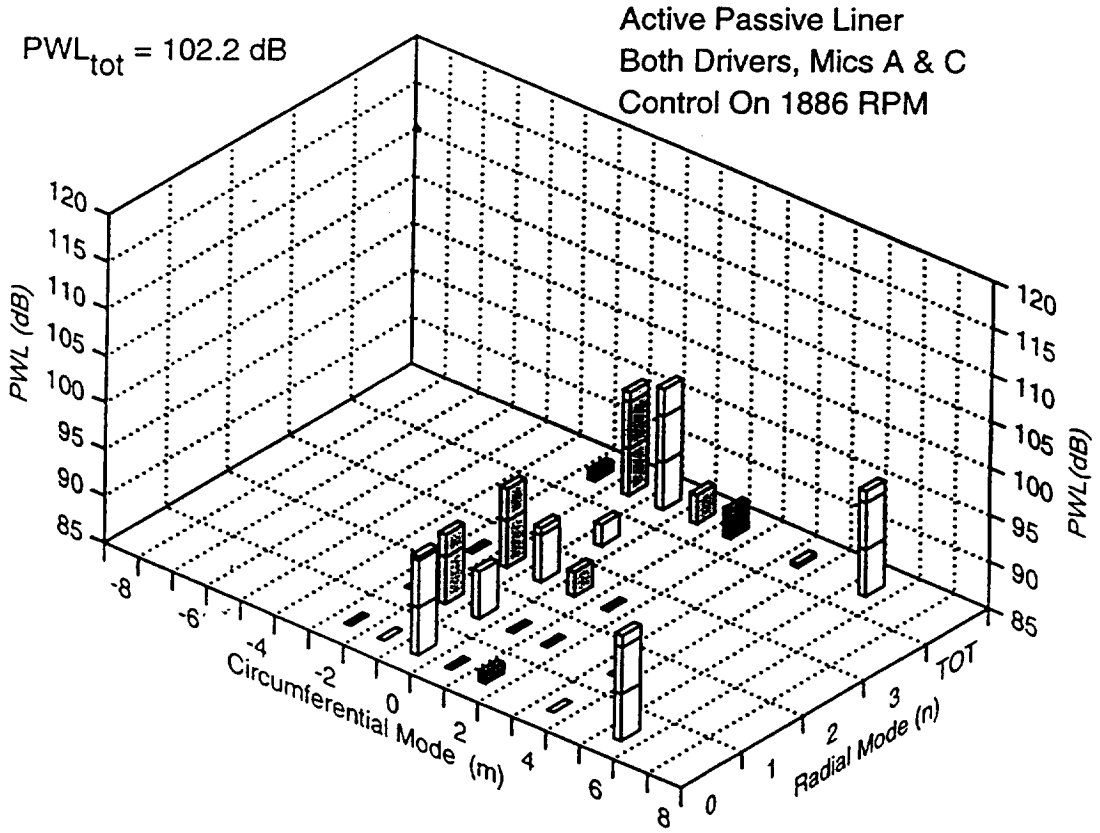

FIGURE 4.36 a, b
Comparison of Duct Modes in NASA/LeRC ANCF Fan Inlet
NGC/HAE Adaptive Segmented Liner; Fan 1886 RPM
"Modal" vs. Axial Station Error Microphone Arrays

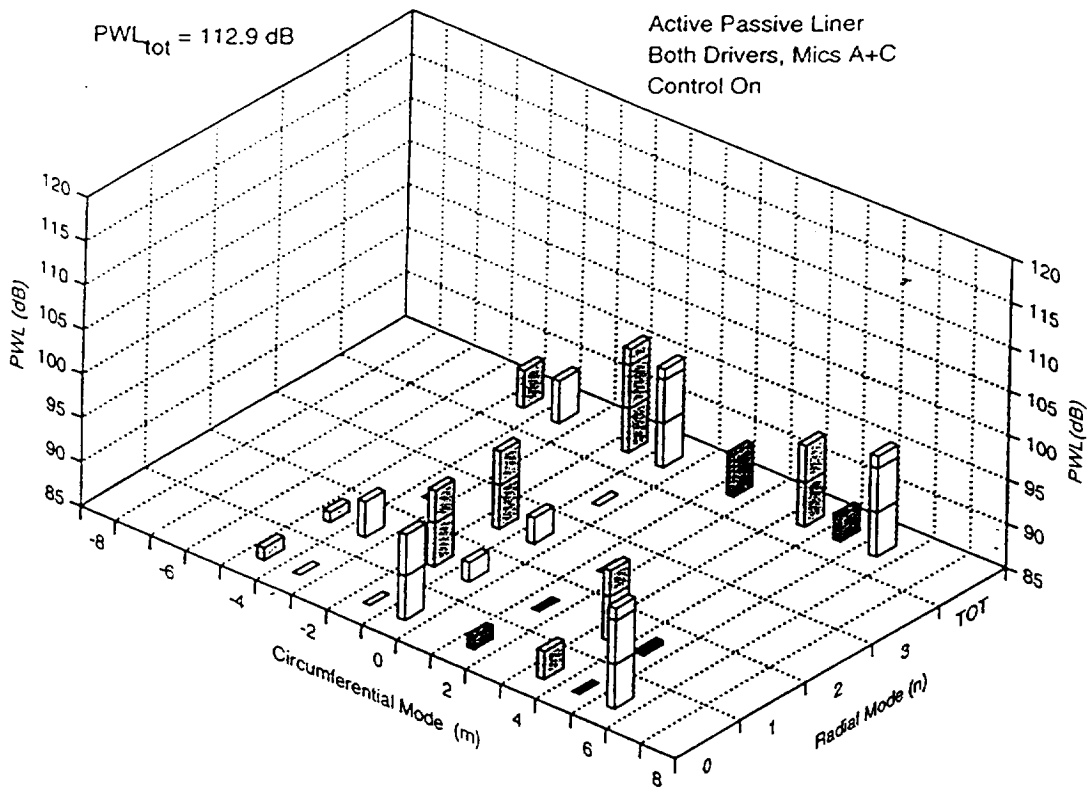

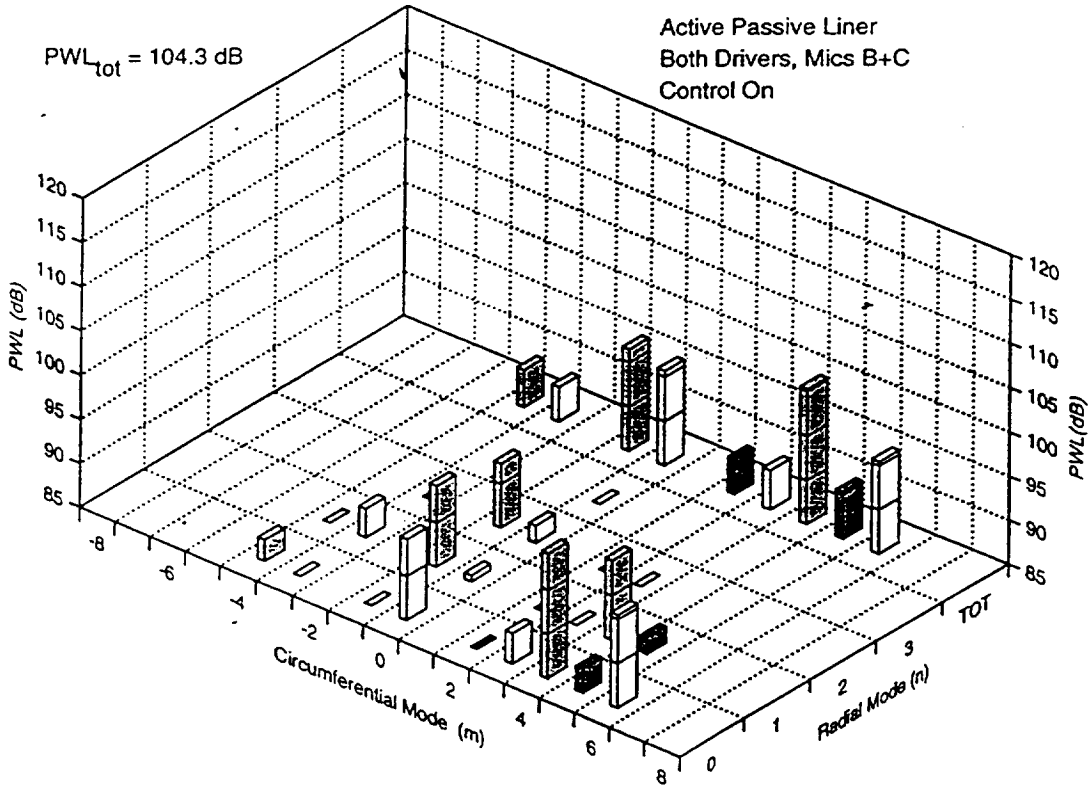

FIGURE 4.37 a, b
Comparison of Duct Modes in NASA/LeRC ANCF Fan Inlet
NGC/HAE Adaptive Segmented Liner, Fan 1886 RPM
Mode (4,0) vs. Mode (4,1) Sensing Error Microphone Arrays

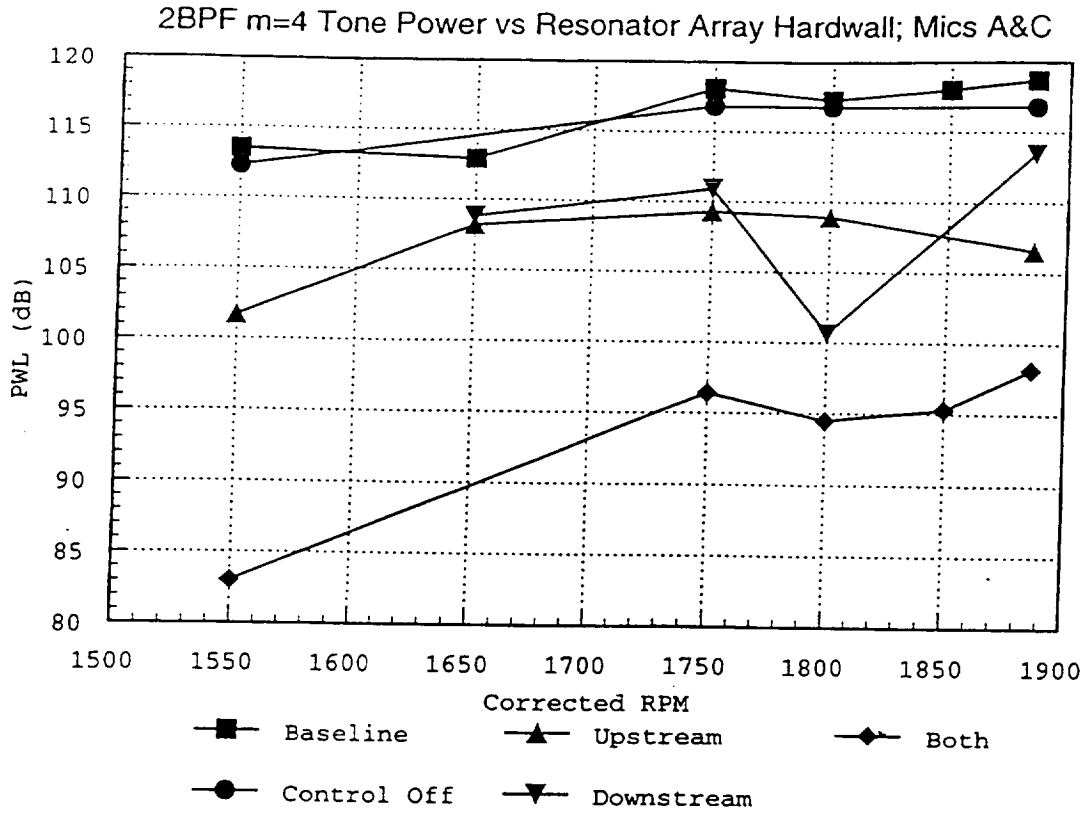

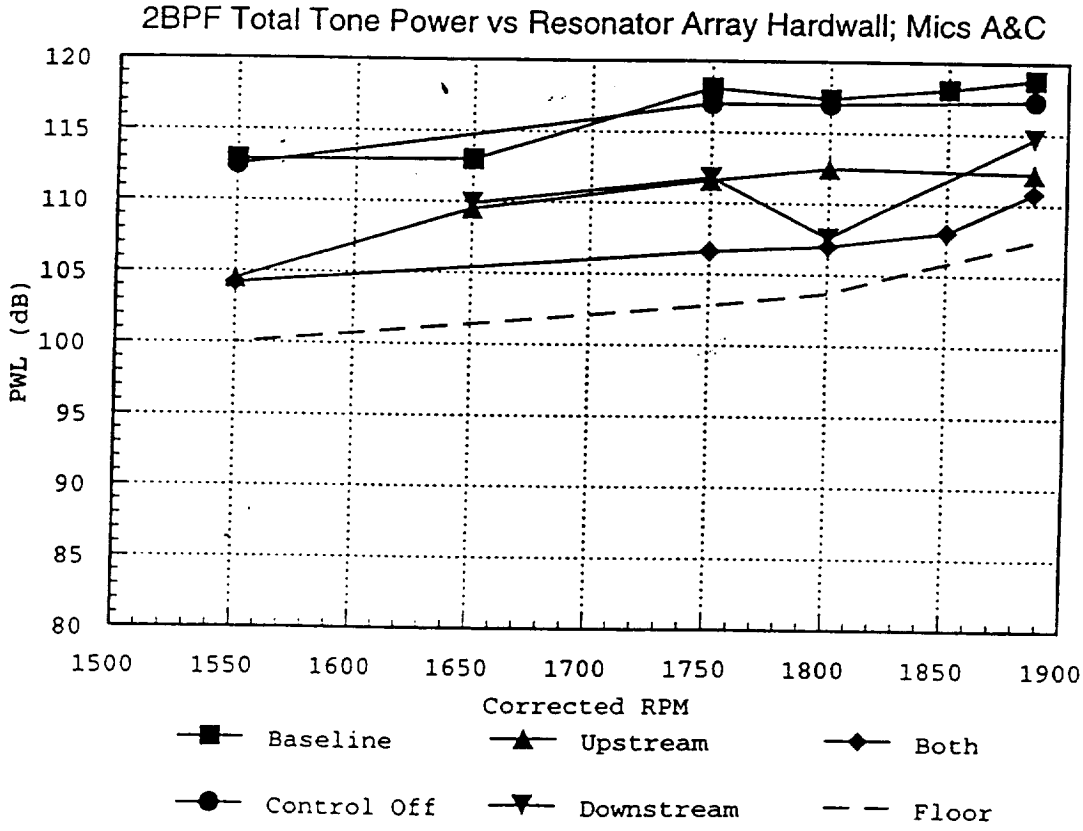

FIGURE 4.38 a, b
NGC/HAE Adaptive Segmented Liner In-Duct Performance Summary
with Passive Segment Covered in NASA/LeRC ANCF Fan Inlet

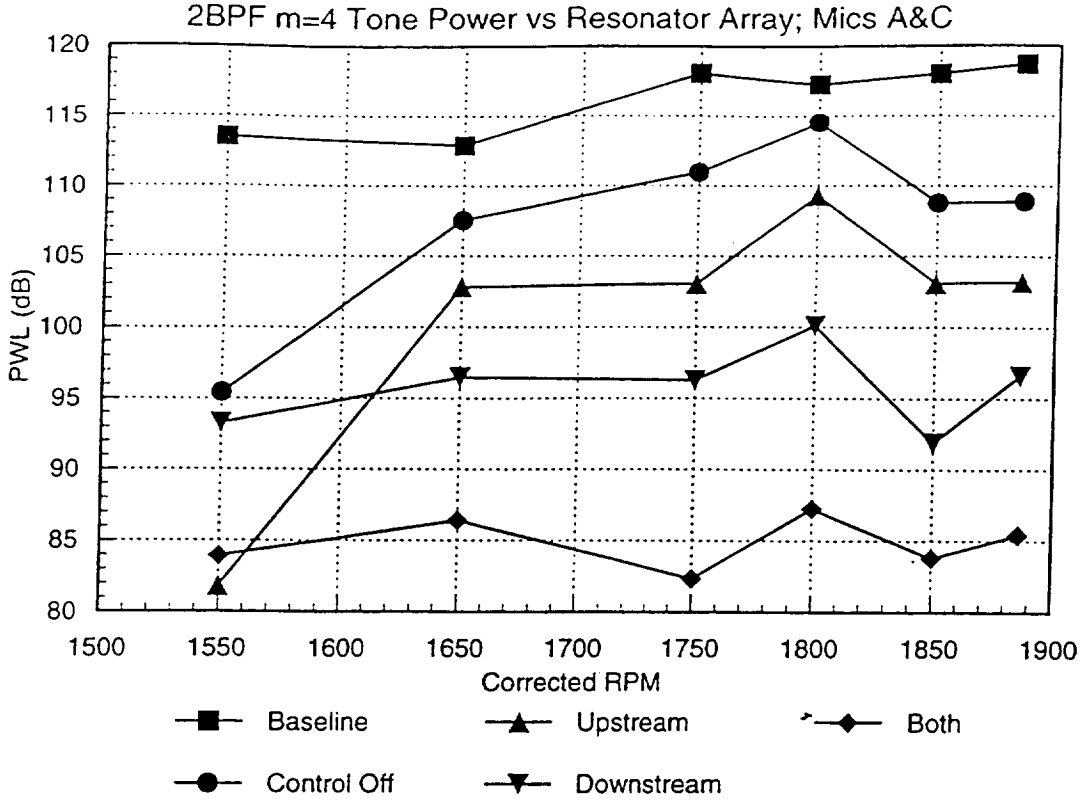

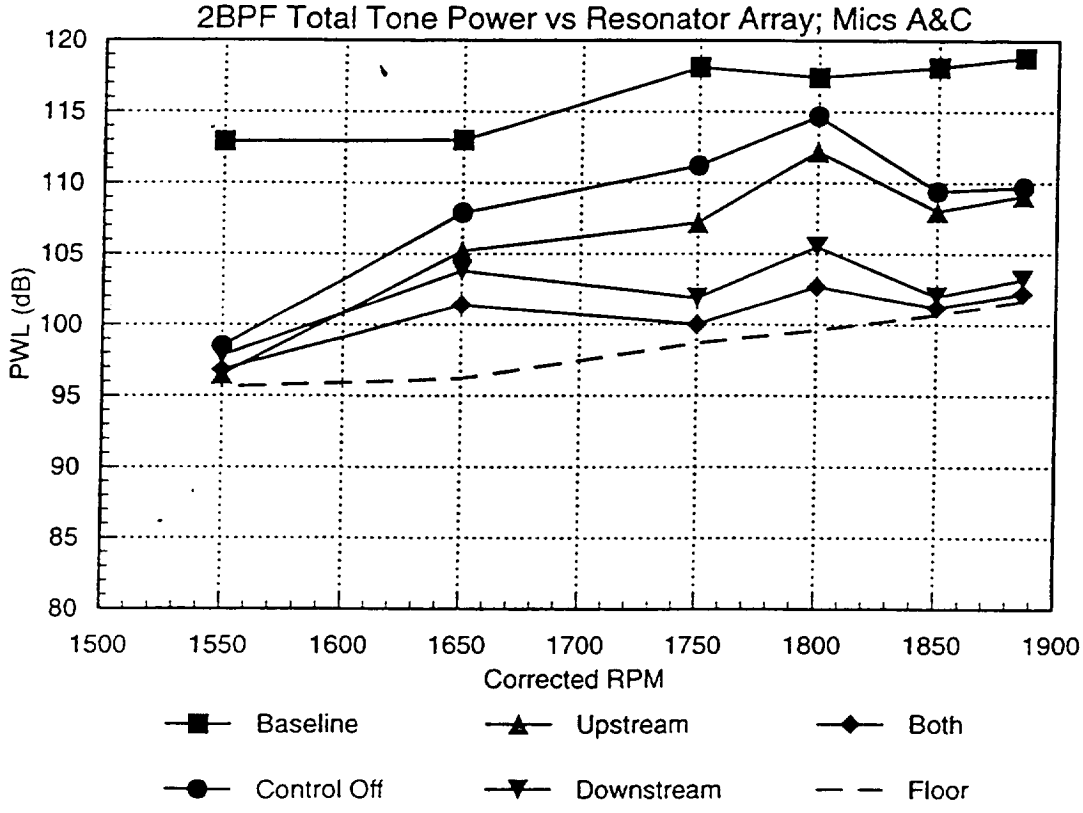

FIGURE 4.39 a,b
NGC/HAE Adaptive Segmented Liner In-Duct Performance Summary
with Passive Segment Exposed in NASA/LeRC ANCF Fan Inlet

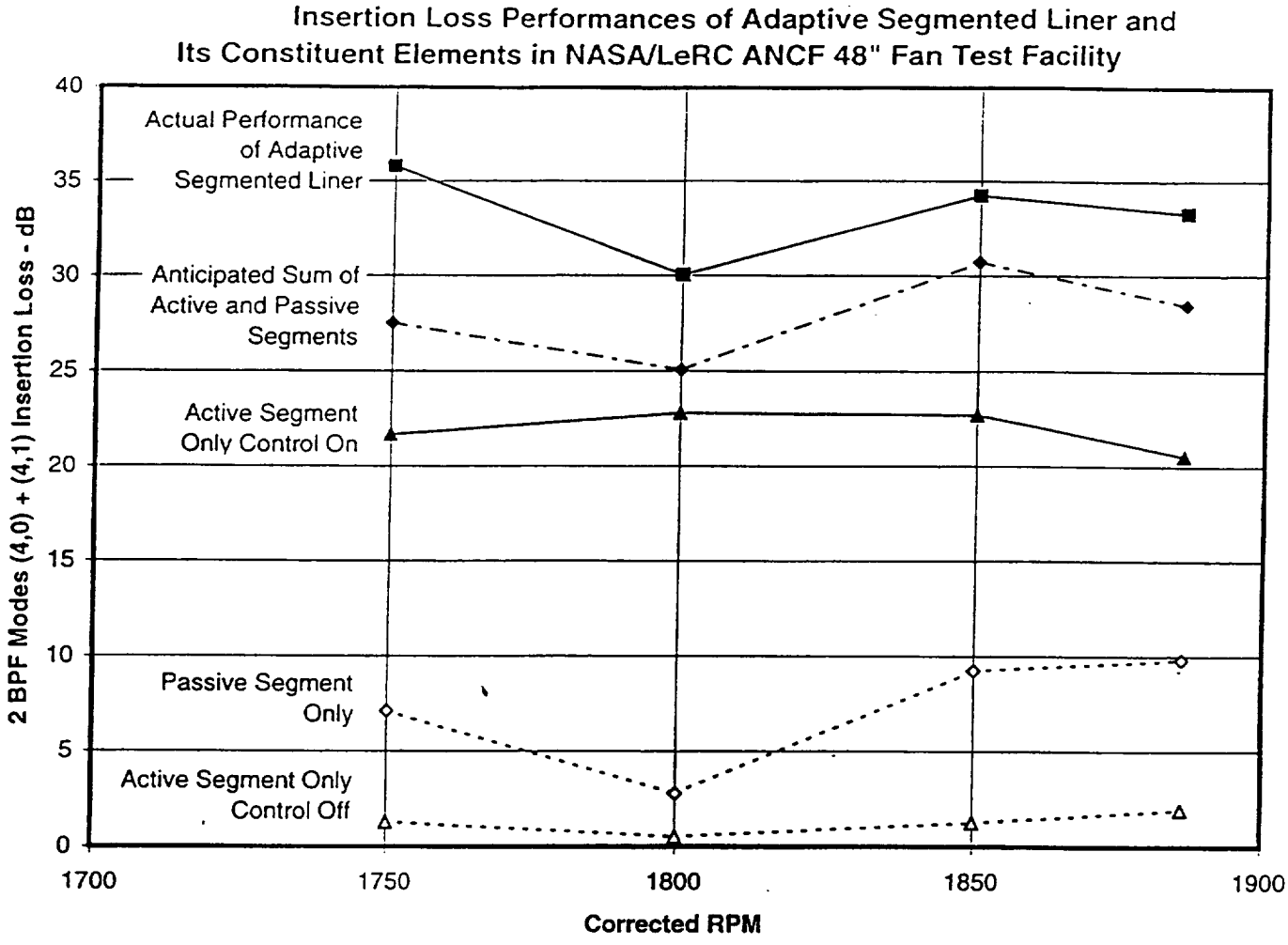

Figure 4.40
Mode m=4 Insertion Loss Performances of Adaptive Segmented Liner and Its Constituent Elements in NASA LeRC ANCF 48" Fan Test Facility

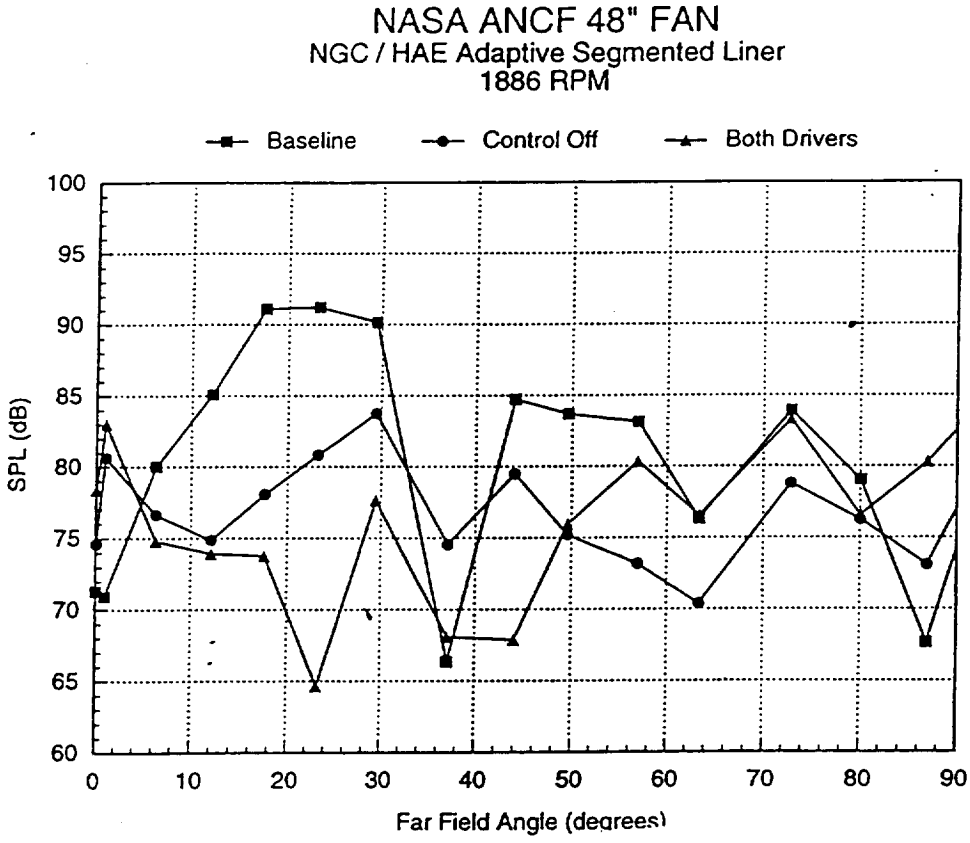

Figure 4.41
Far-Field Forward Directivity for 2BF of NASA LeRC ANCF Fan
1886 RPM, Hardwall and Adaptive Segmented Inlet Liner
With Control Off and On

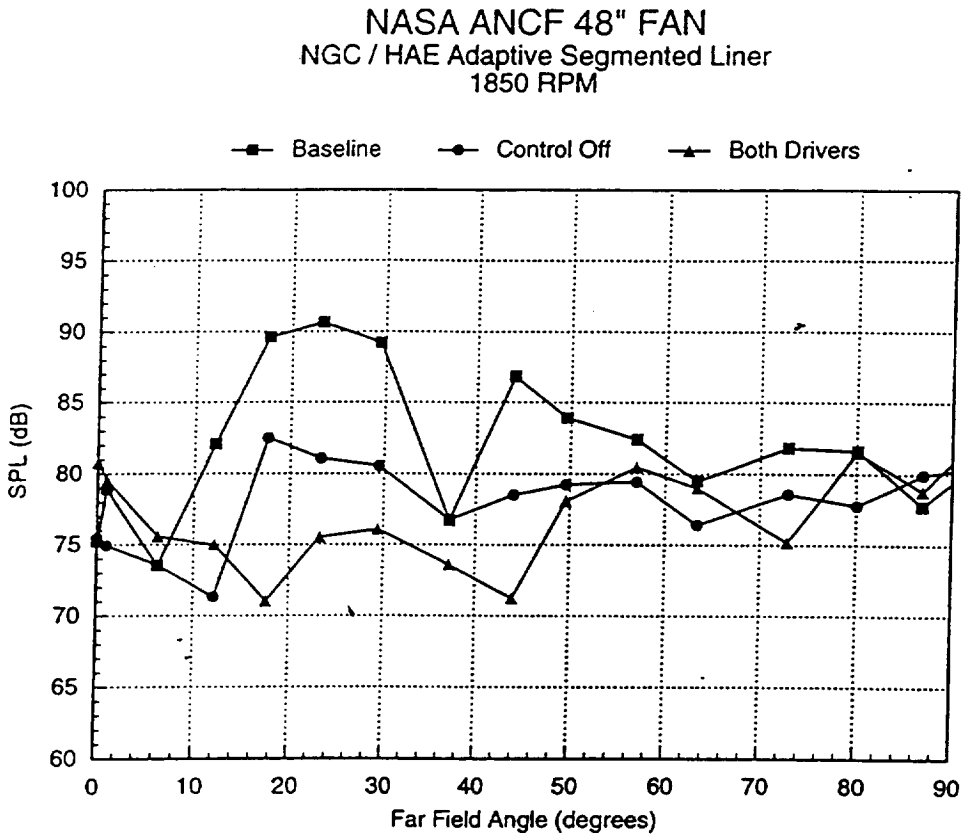

Figure 4.42
Far-Field Forward Directivity for 2BPF of NASA LeRC ANCF Fan
1850 RPM, Hardall and Adaptive Segmented Inlet Liner
With Control Off and On

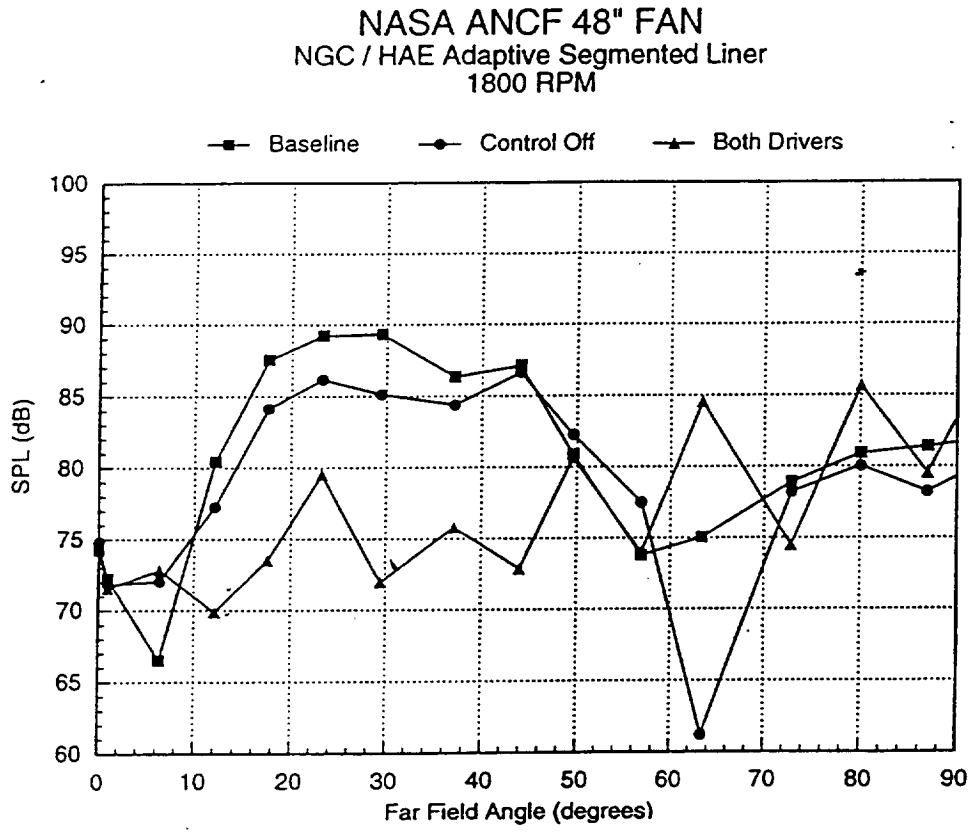

Figure 4.43
Far-Field Forward Directivity for 2BPF of NASA LeRC ANCF Fan
1800 RPM, Hardwall and Adaptive Segmented Inlet Liner
With Control Off and On

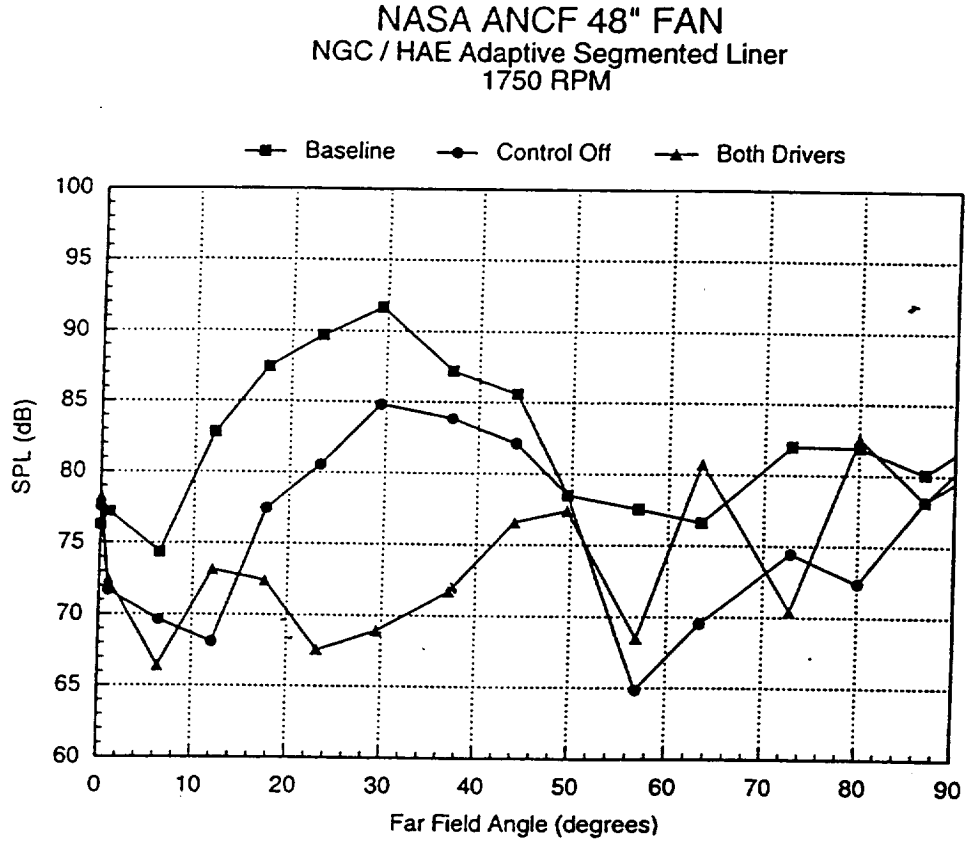

Figure 4.44
Far-Field Forward Directivity for 2BPF of NASA LeRC ANCF Fan
1750 RPM, Hardwall and Adaptive Segmented Inlet Liner
With Control Off and On

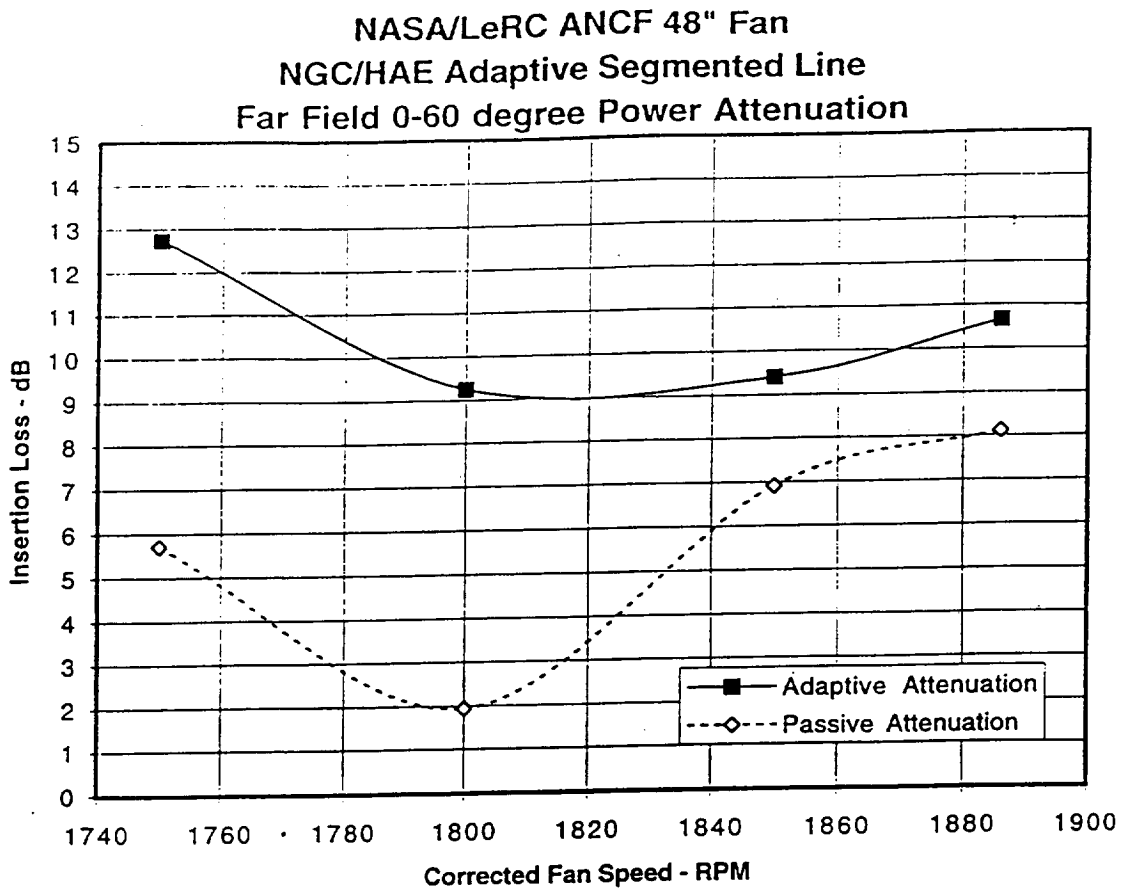

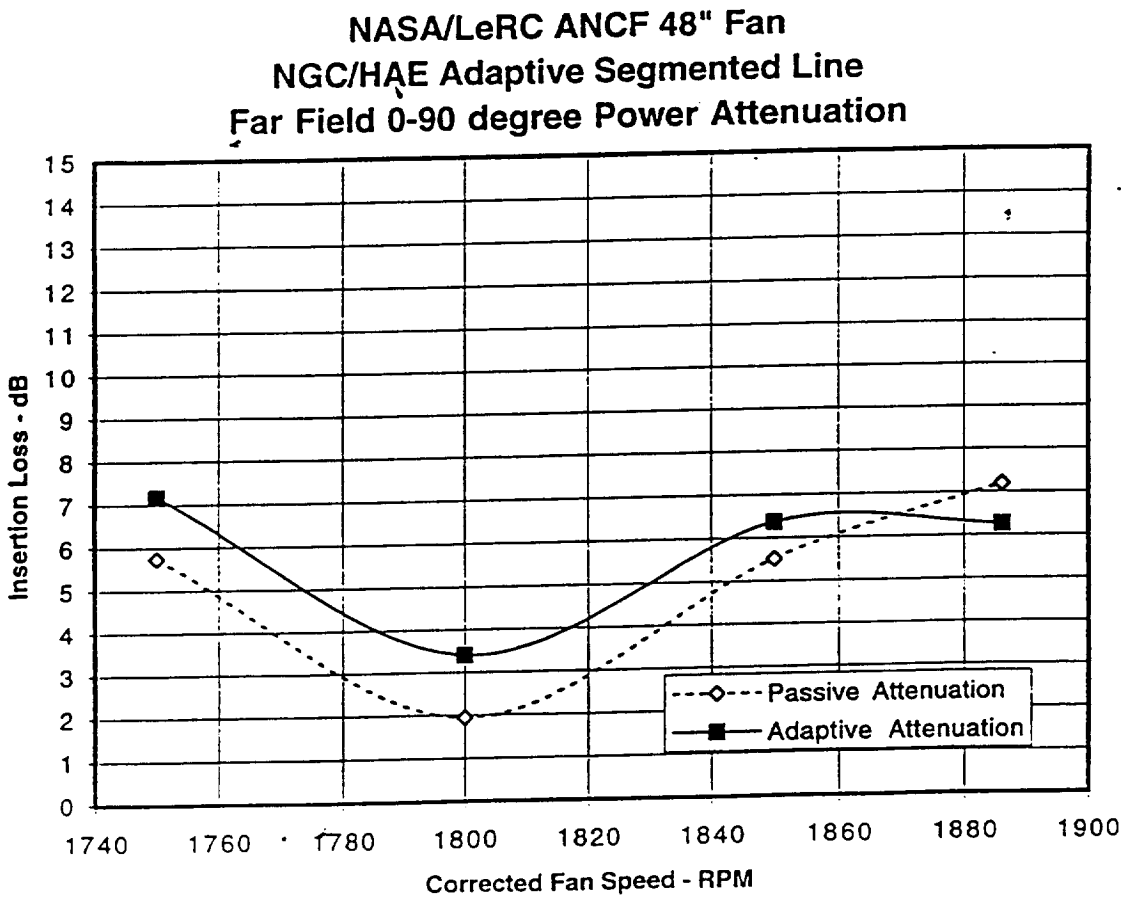

Figure 4.45a, b
NASA/LeRC ANCF 48" Fan - Far-Field 0-60 Degree (a)
and 0-90 Degree Power Attenuation (b)

Figure 5.1a
View of the Hybrid Active/Passive ADP Inlet Mounted for
Far-Field Testing in the LeRC 9x15 ' Wind Tunnel

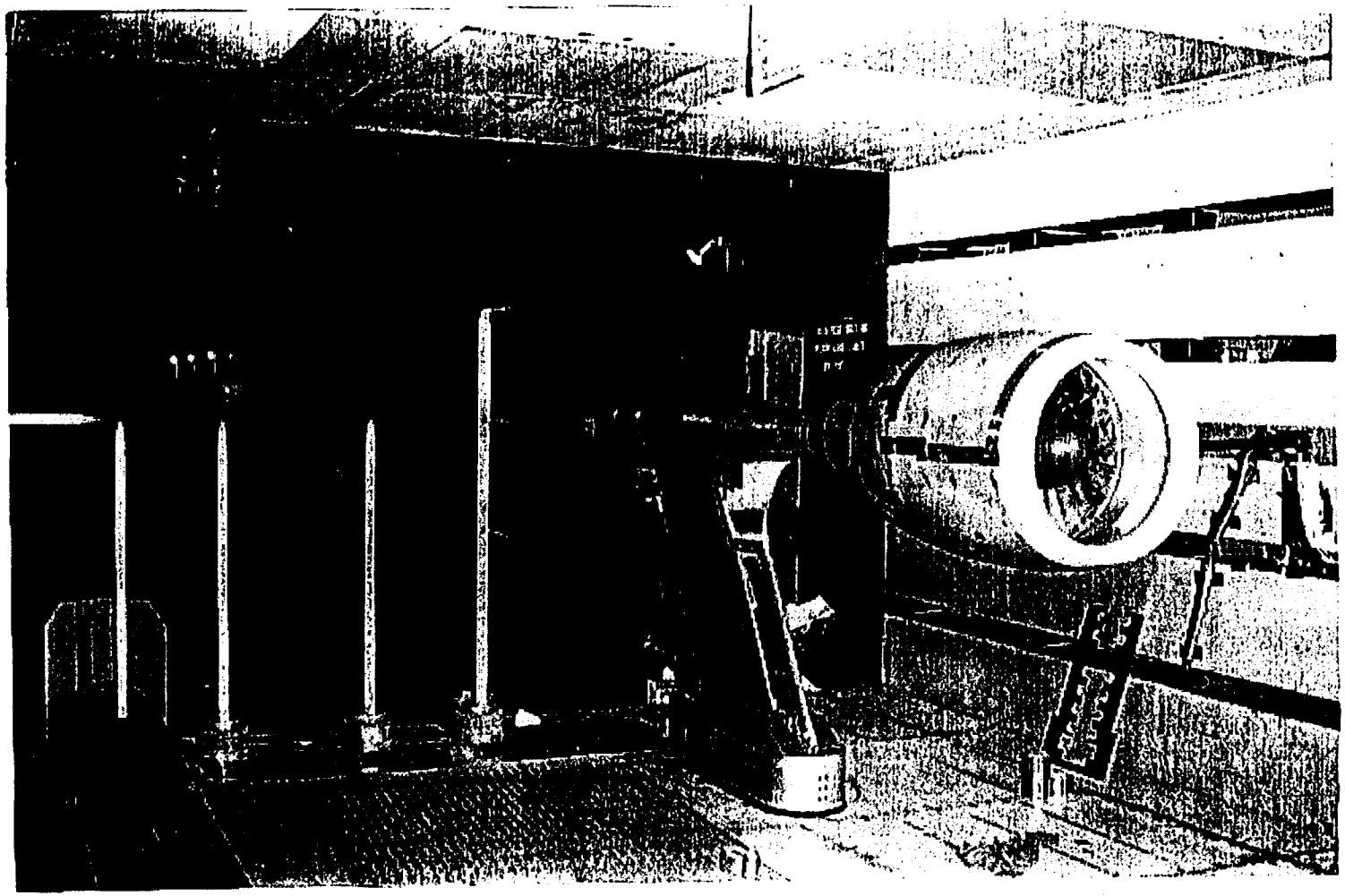

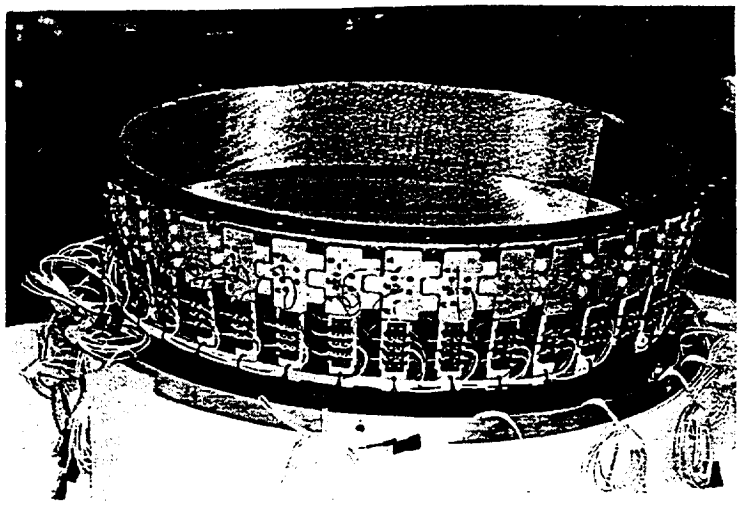

Figure 5.1b
ADP Barrel Shown With Acoustic Drivers Mounted
Near the Barrel Attachment Flange

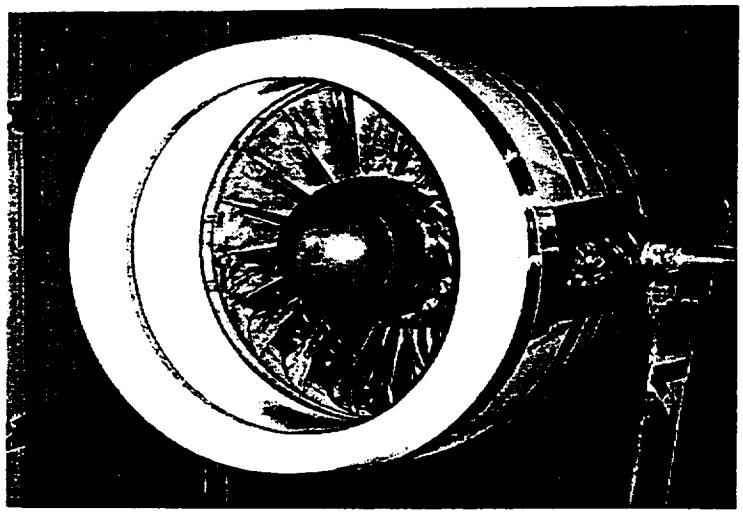

Figure 5.1c
ADP Barrel Mounted on the ADP Engine Core Duct
in the LeRC 9x15 Wind Tunnel for Testing

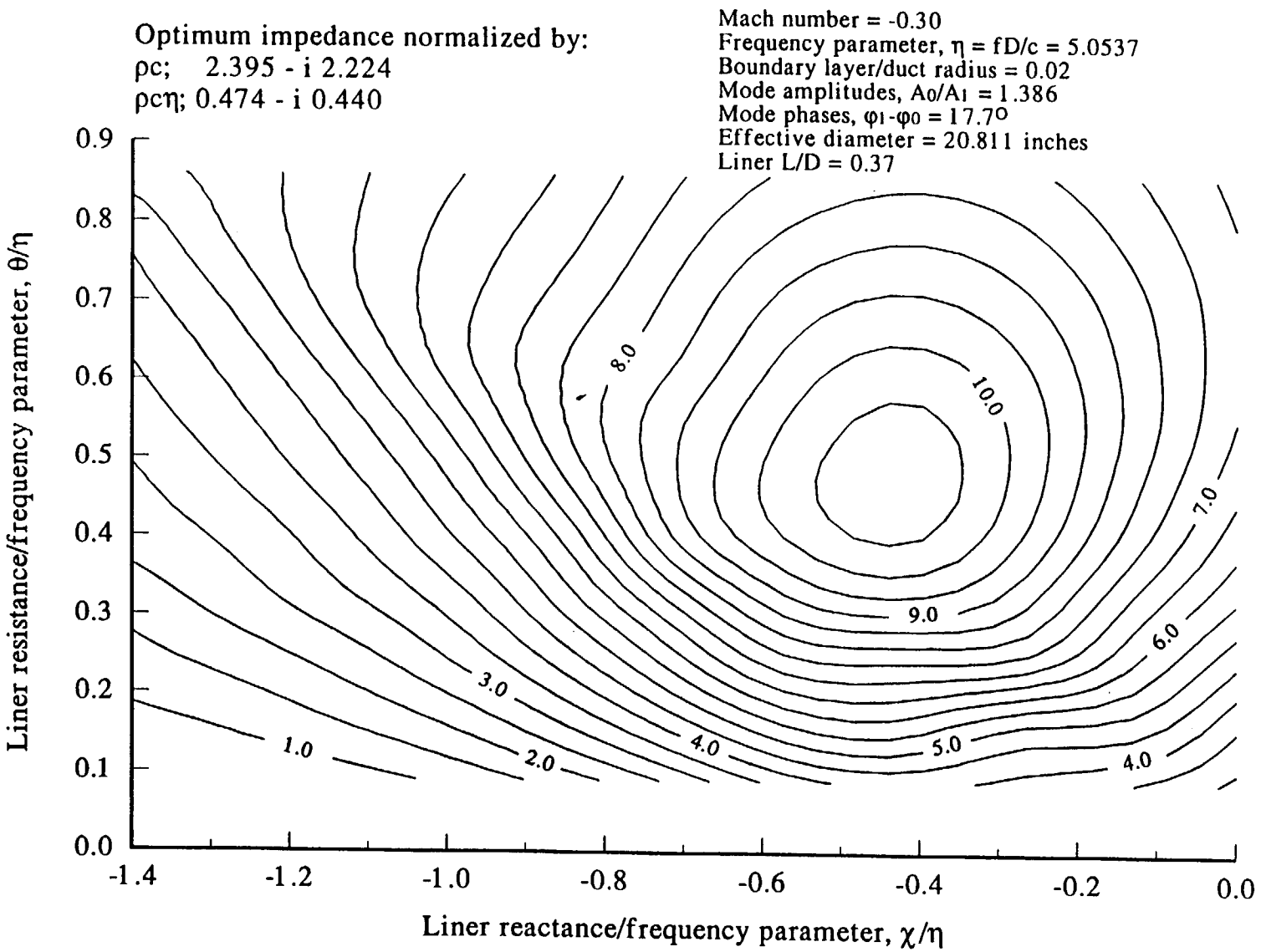

Figure 5.2. Attenuation countours for uniform ADP1 acoustic liner
2BPF = 3255 Hz, 5425 rpm, mode lobes m = 9

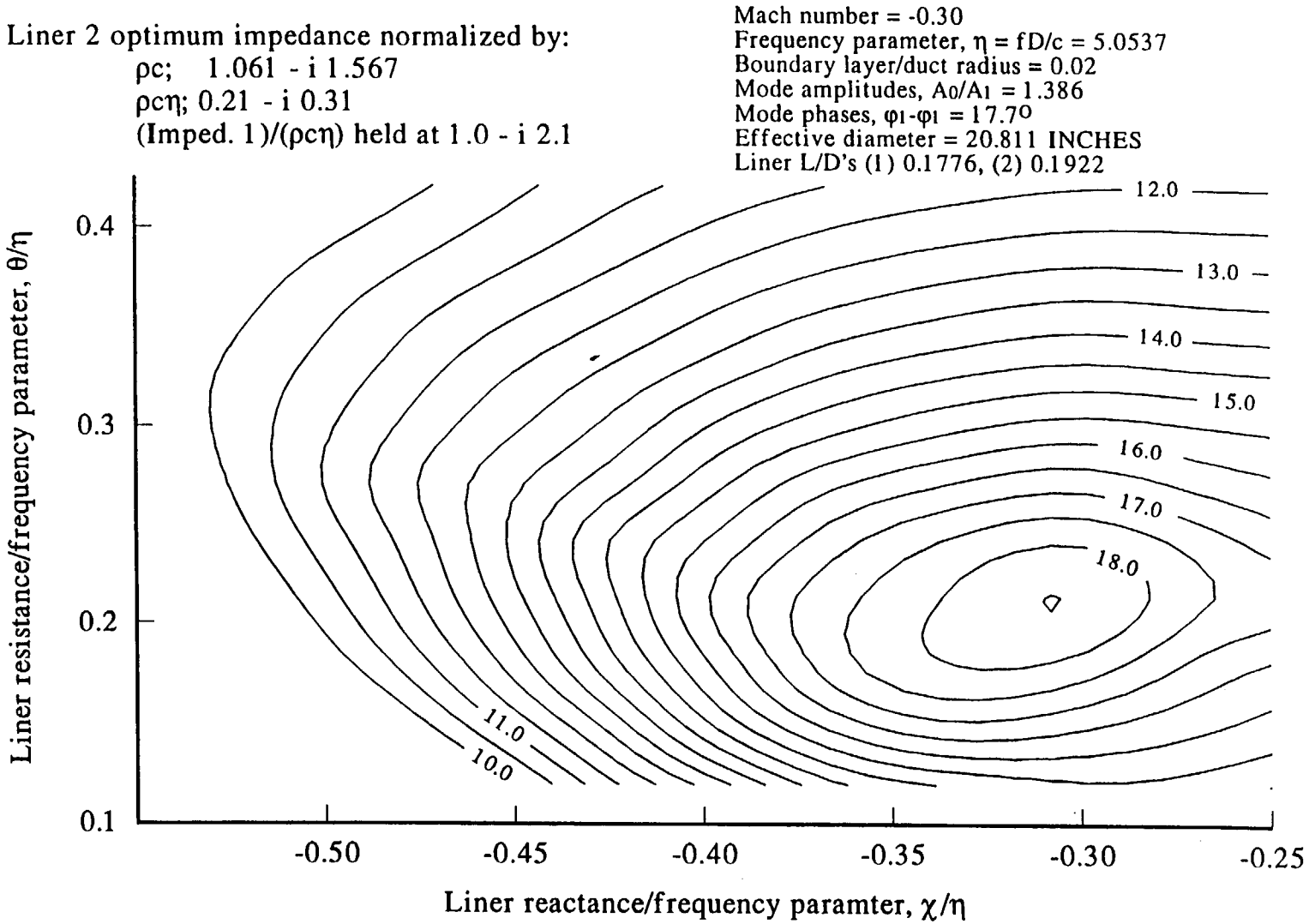

Figure 5.3. Attenuation countours for two segment ADP2 liner
2BPF = 3255 Hz, 5425 rpm, liner (2) nearest inlet lip is varied here, m=9

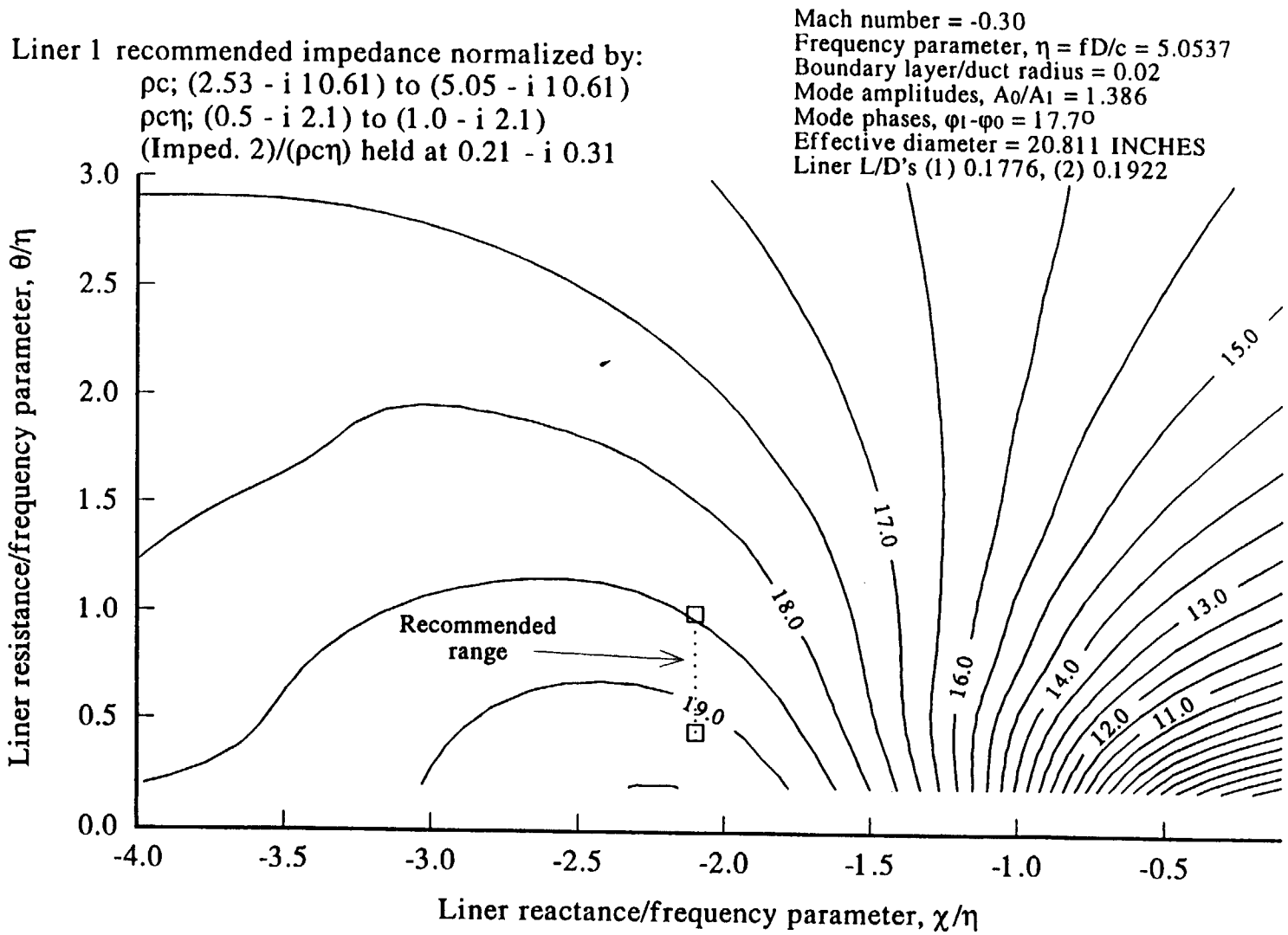

Figure 5.4. Attenuation countours for two segment ADP2 liner
2BPF = 3255 Hz, 5425 rpm, liner (1) nearest rotor is varied here, m=9

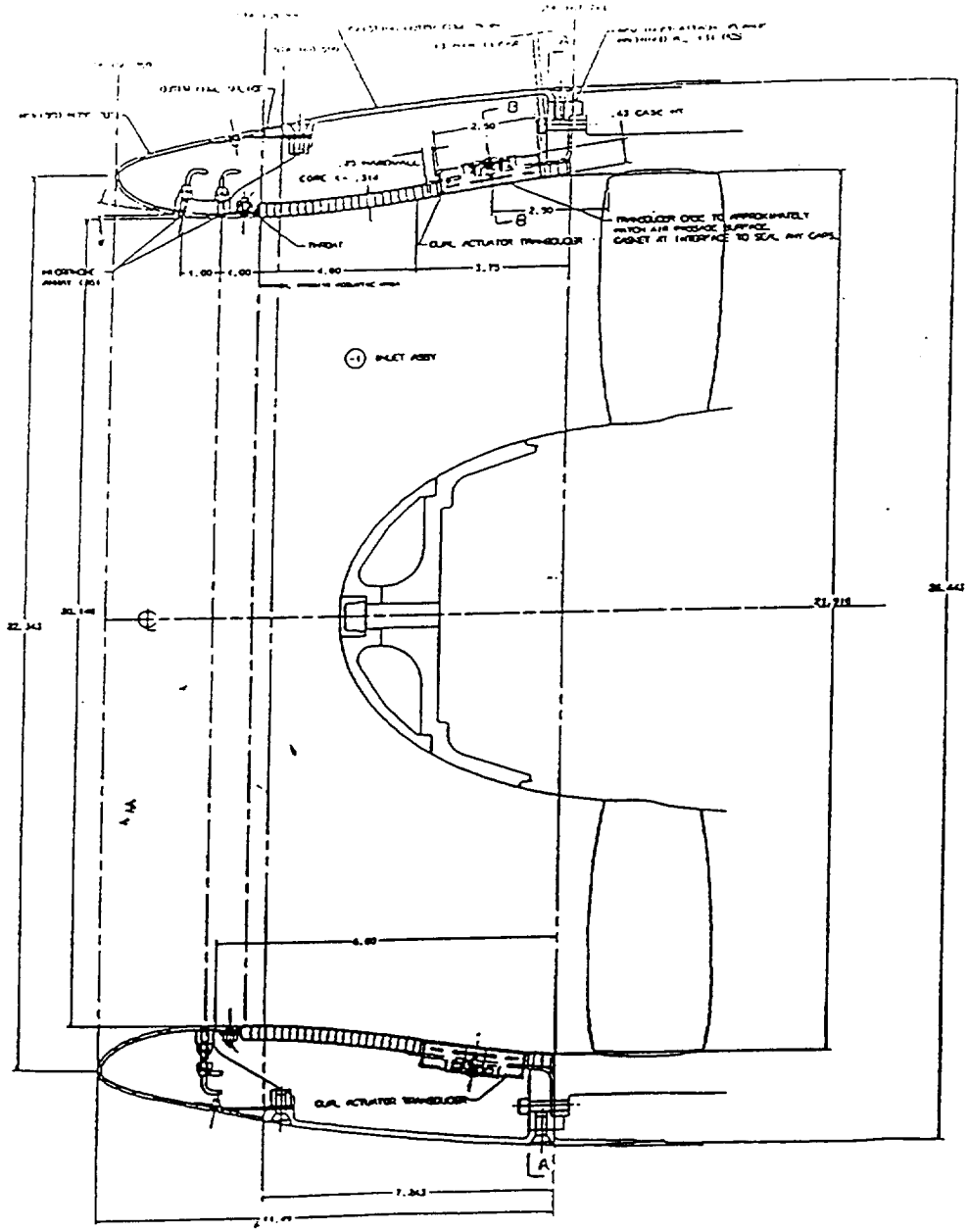

Figure 5.5
Drawing of the ADP Hybrid Active/Passive Barrel
Attached to the ADP Fan Rig

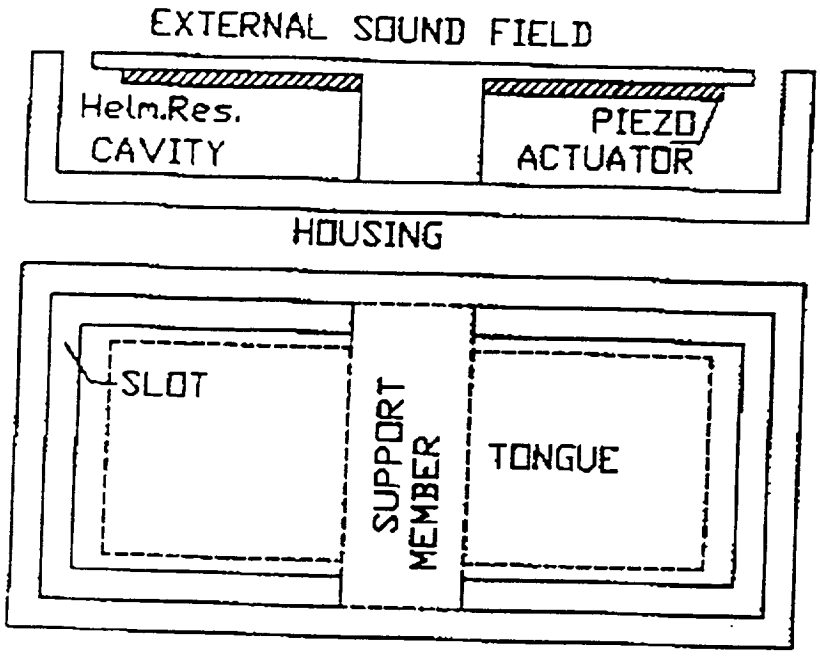

Figure 5.6a

Schematic of the 1 inch x 2 inch Resonator for the ADP Inlet Barrel

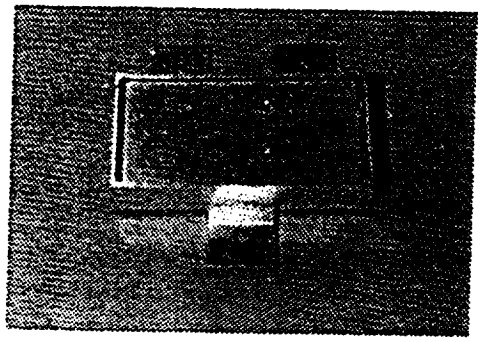

Figure 5.6b

Photograph of an ADP Driver

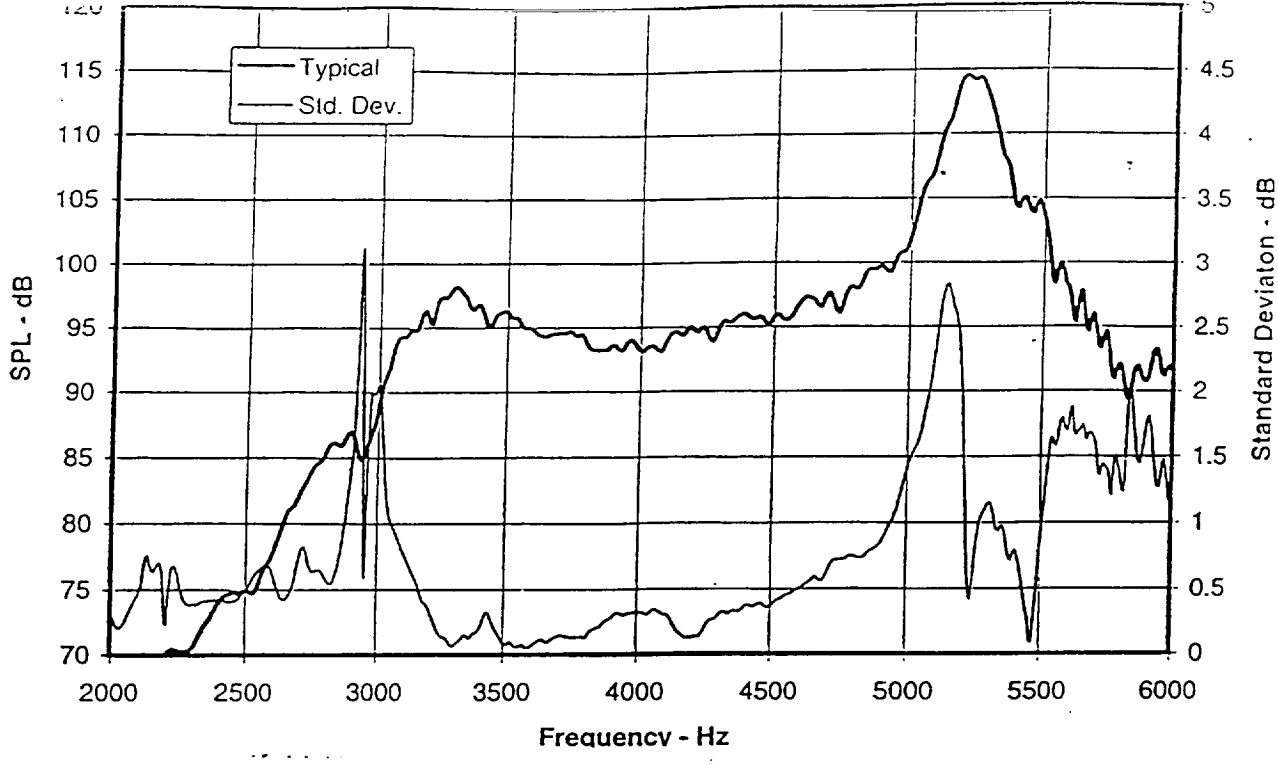

Figure 5.7a

ADP Actuator Free Field Sound Pressure Levels vs. Frequency
on Axis at 12 Inches, 10 Volt Excitation

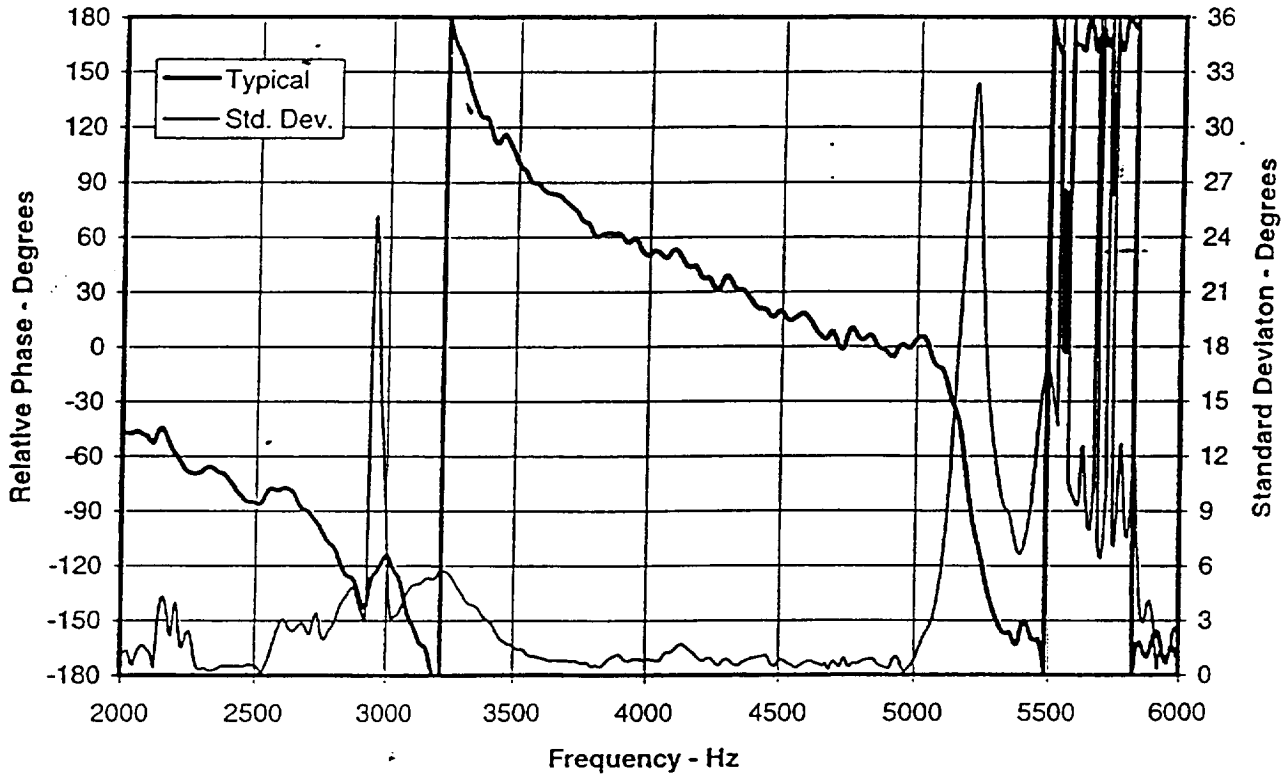

Figure 5.7b

ADP Actuator Free Field Phase Response vs. Frequency
on Axis at 12 Inches, 10 Volt Excitation

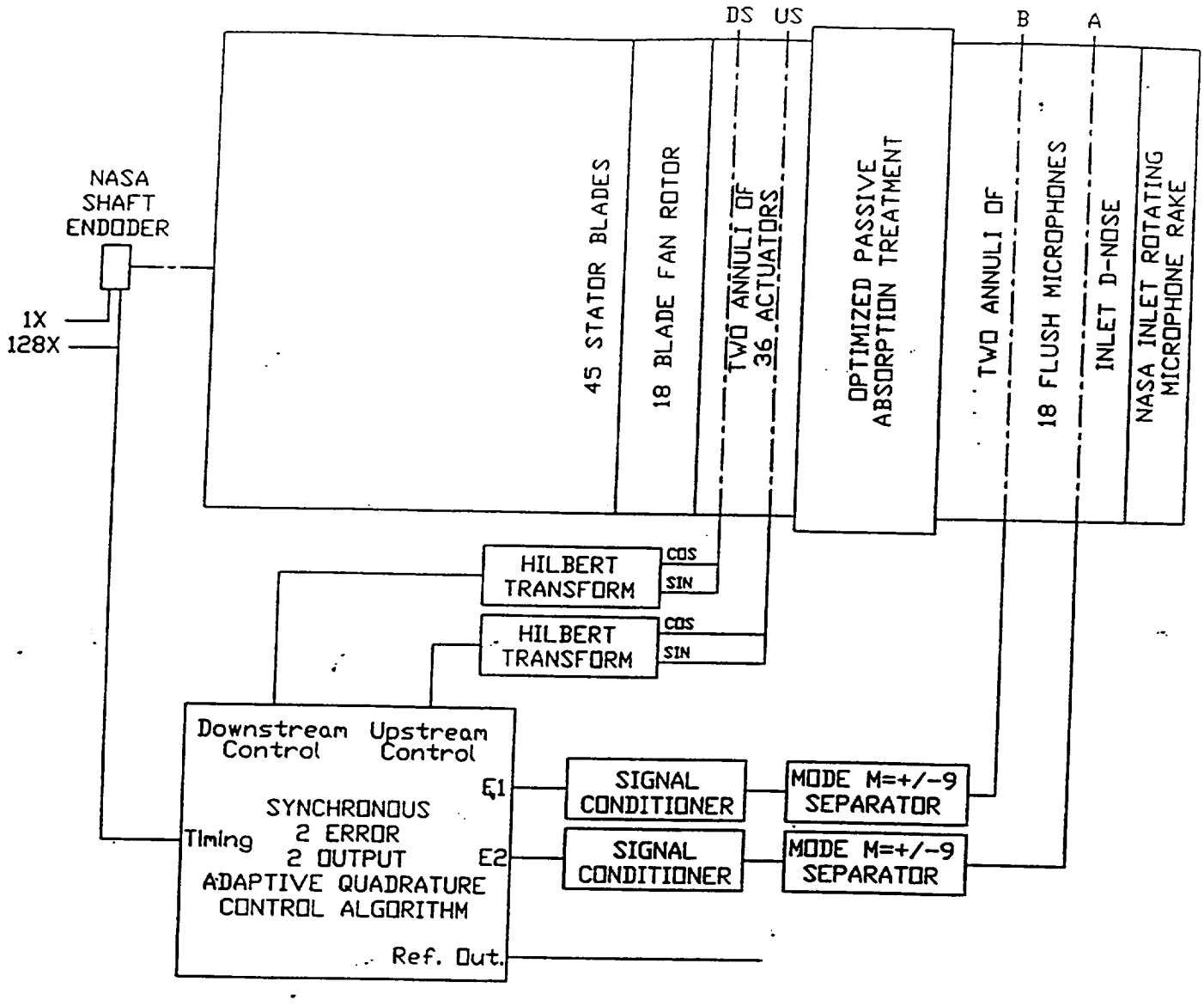

Figure 5.8

Schematic Diagram of Active Passive Segmented Liner Measurements in ADP Fan in the NASA LeRC 9 x 15 Wind Tunnel

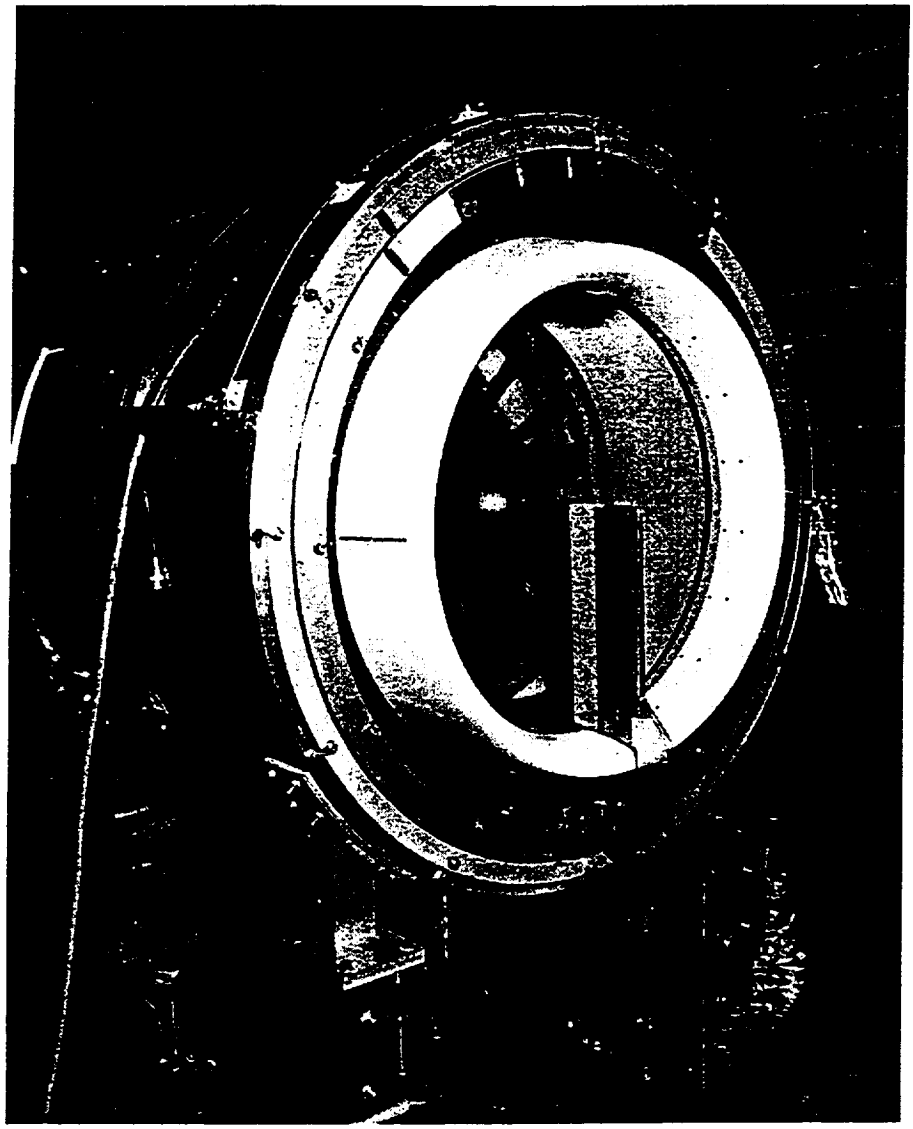

Figure 5.9
Rotating Rake Installed on the ADP Barrel
in the NASA LeRC 9'x15' Wind Tunnel

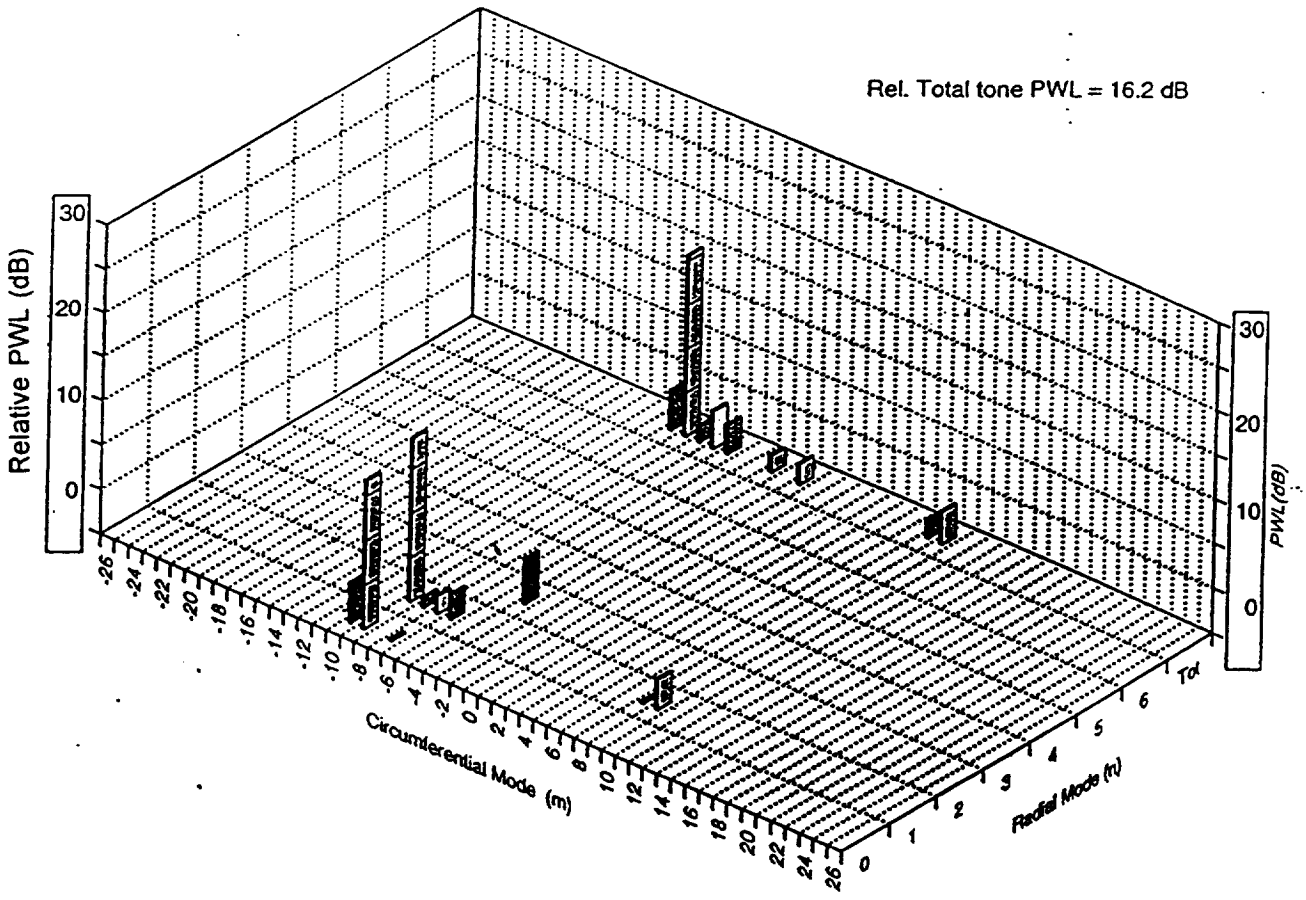

Figure 5.10a

Circumferential and Radial Mode Sound Powers Produced by NGC/HAE Adaptive Segmented Liner in ADP Fan Inlet with Passive Segment Covered

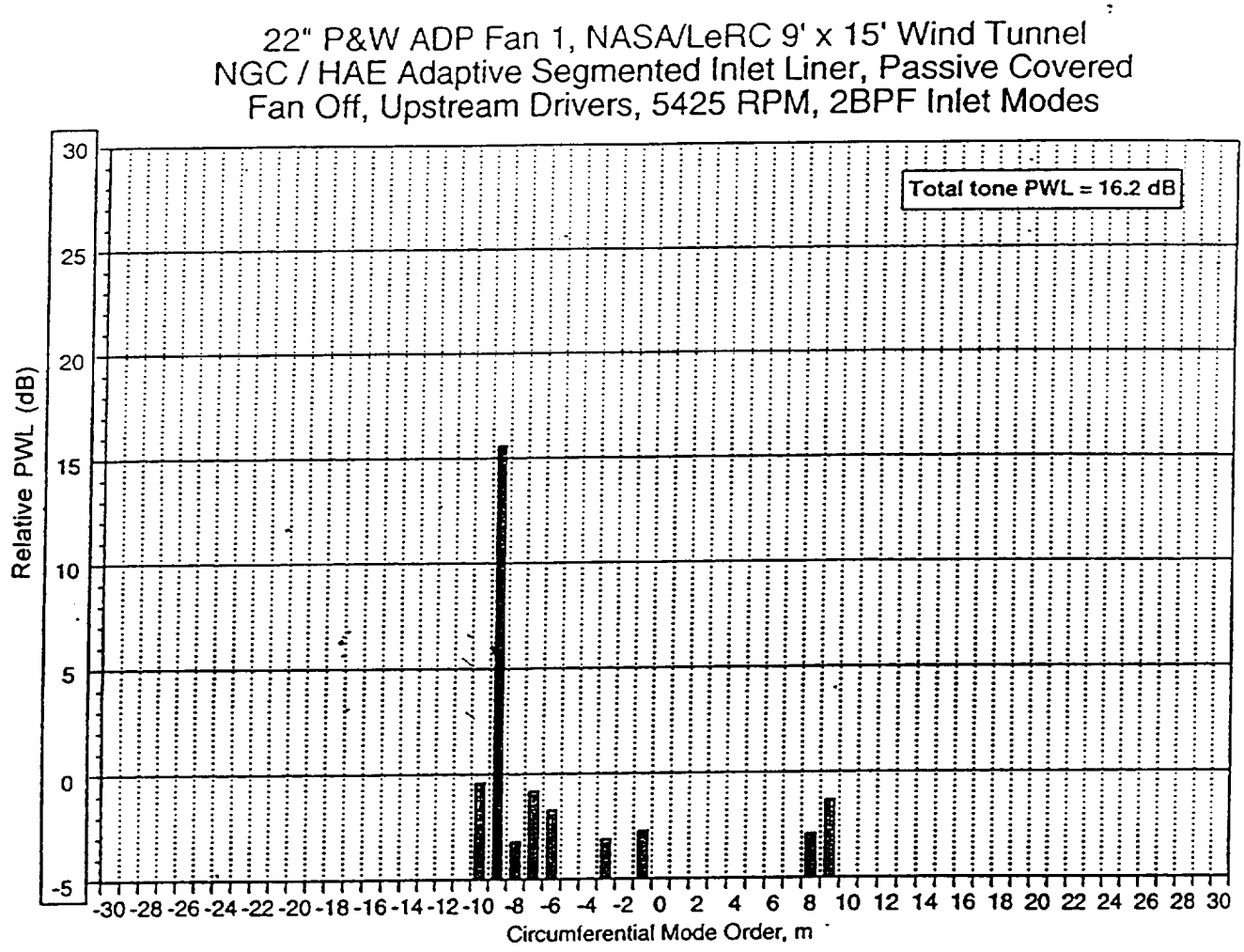

Figure 5.10b

Sum of Radial Mode Relative Sound Powers in Circumferential Modes
Produced by NGC/HAE Adaptive Segmented Liner in
ADP Fan Inlet with Passive Segment Covered

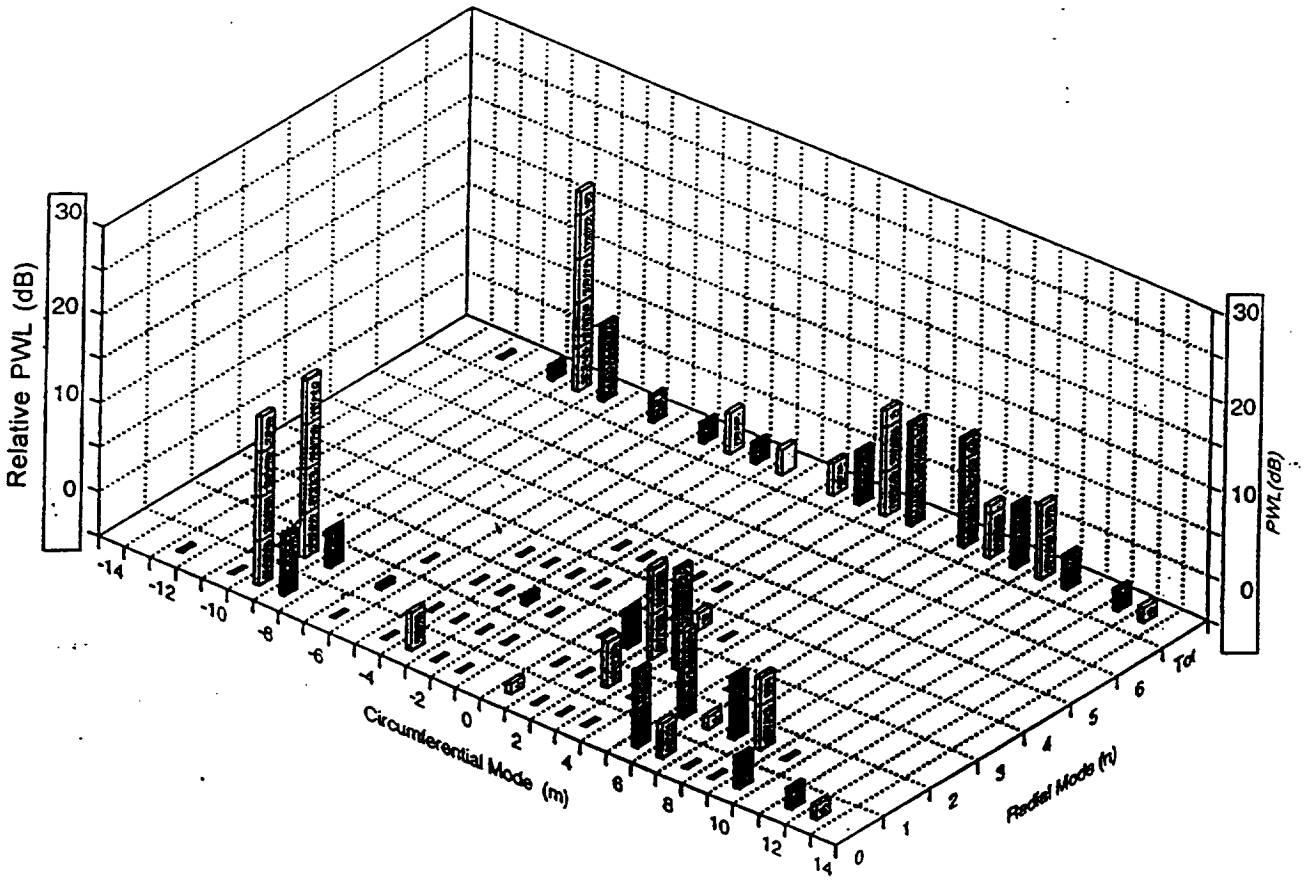

Figure 5.11a

Circumferential and Radial Mode Relative Sound Powers in ADP Fan Inlet with Hardwall Baseline

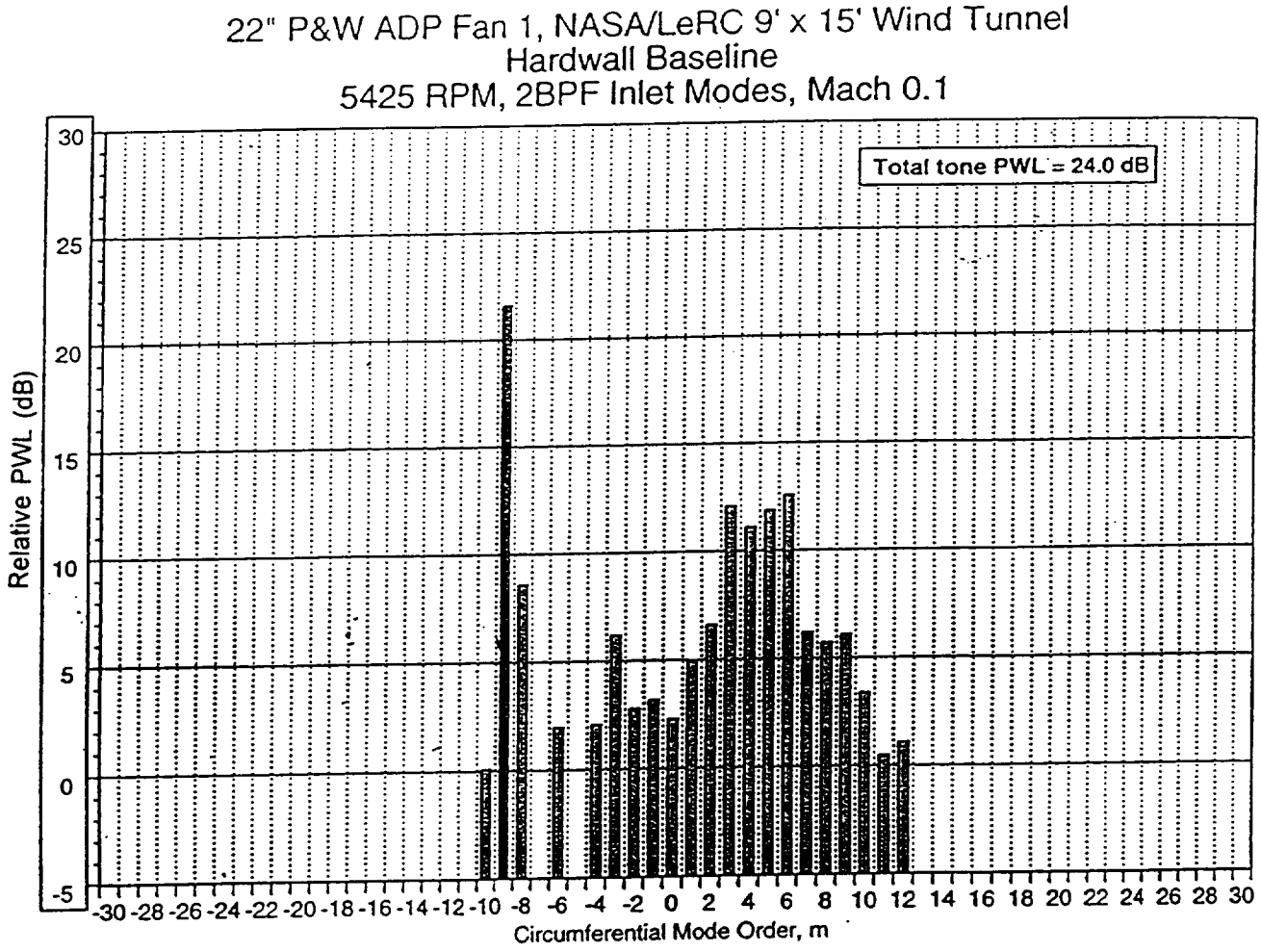

Figure 5.11b

Sum of Radial Mode Relative Sound Powers in Circumferential Modes in ADP Fan Inlet with Hardwall Baseline

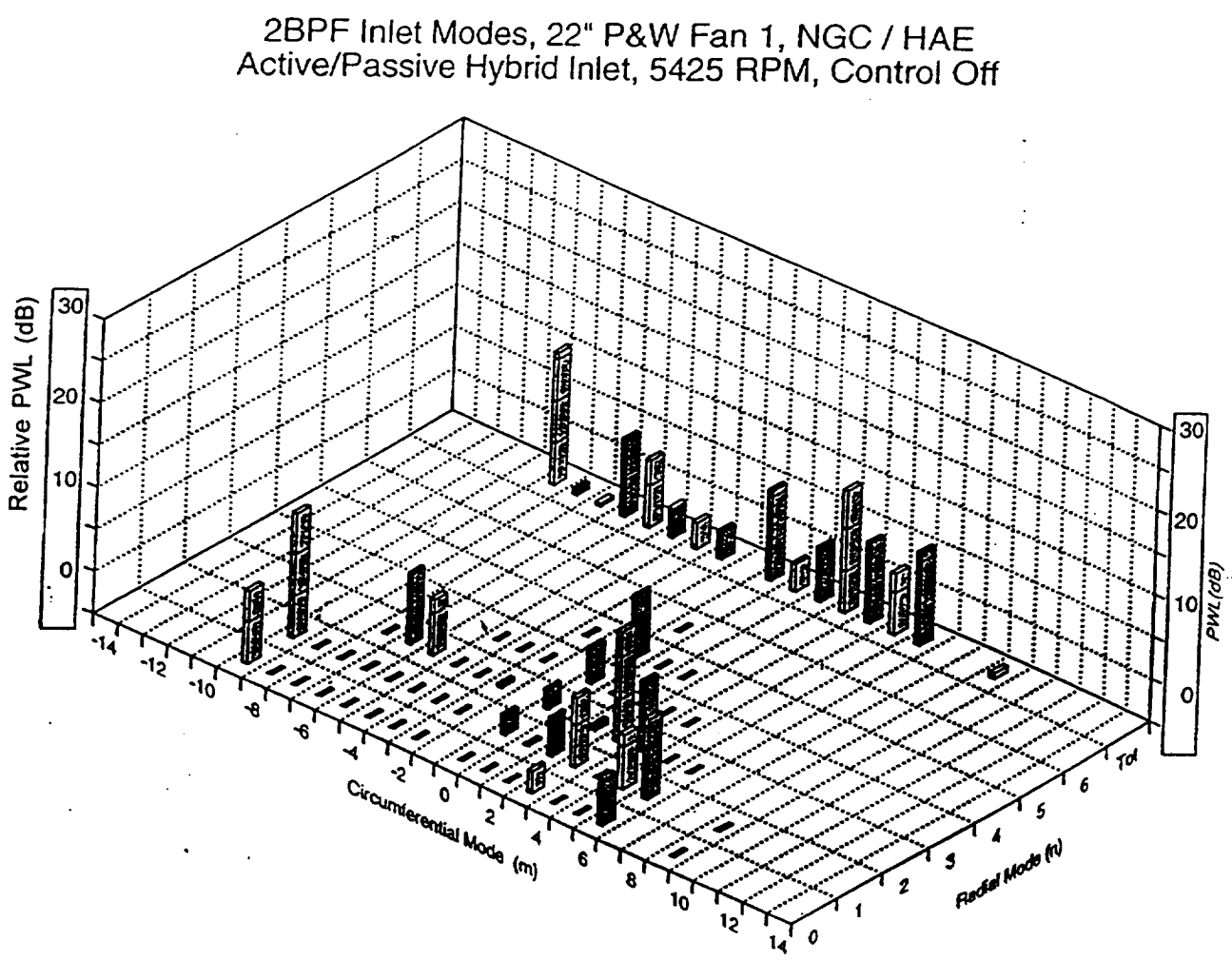

Figure 5.12a

Circumferential and Radial Mode Relative Sound Powers in
ADP Fan Inlet with NGC/HAE Adaptive Segmented Liner, Control Off

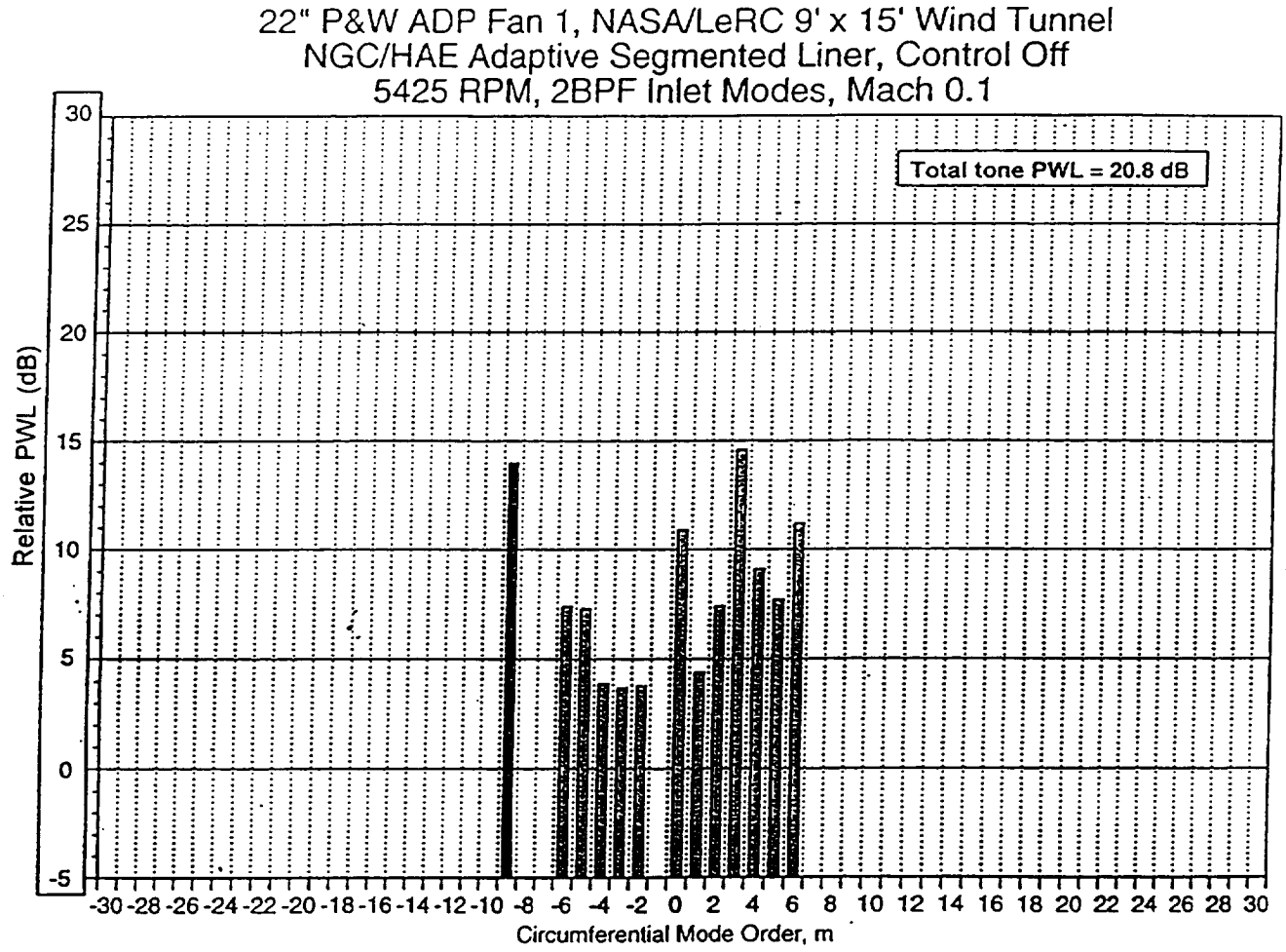

Figure 5.12b

Sum of Radial Mode Relative Sound Powers in Circumferential Modes in ADP Fan Inlet with NGC/HAE Adaptive Segmented Liner, Control Off

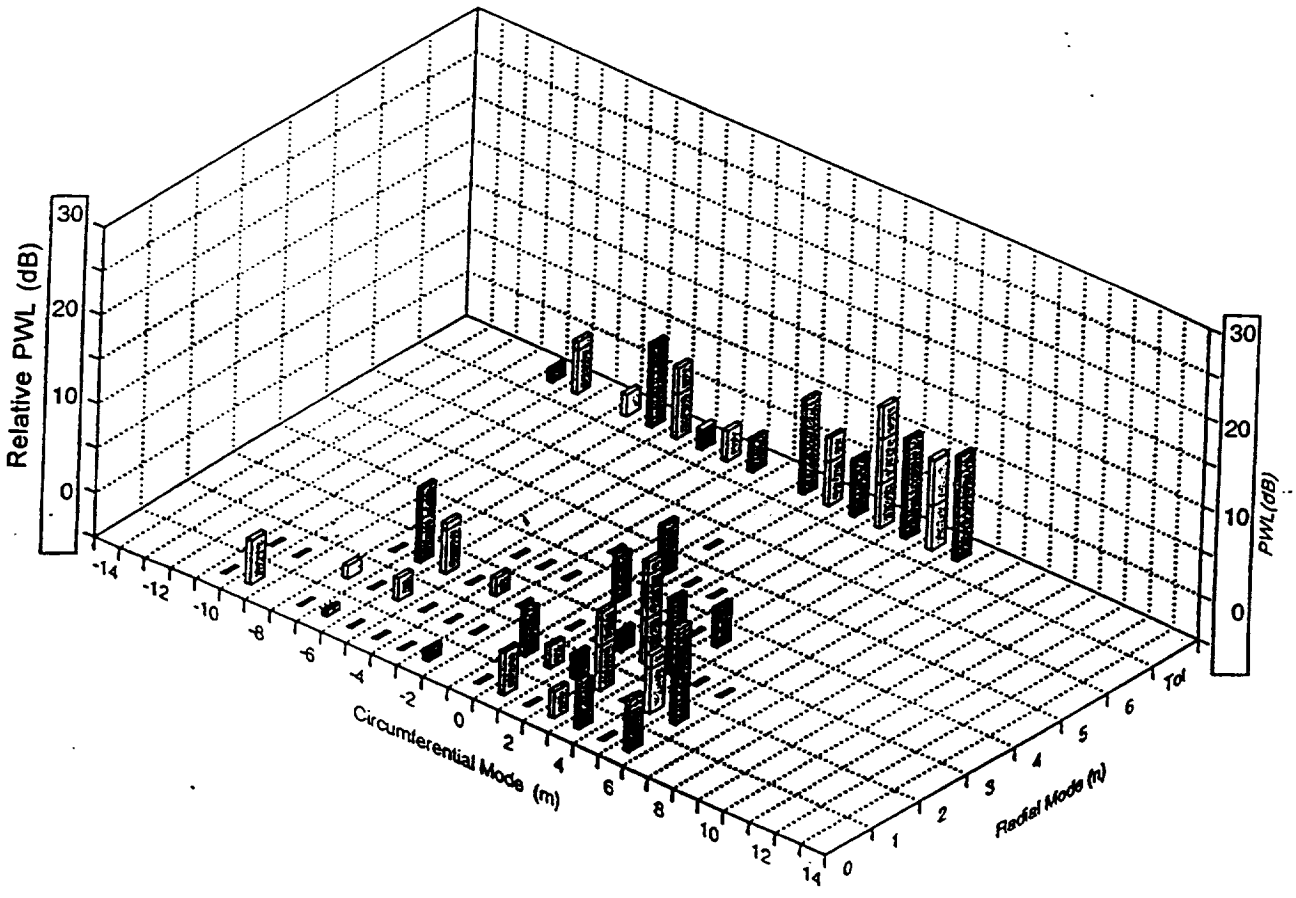

Figure 5.13a

Circumferential and Radial Mode Relative Sound Powers in
ADP Fan Inlet with NGC/HAE Adaptive Segmented Liner, Control On

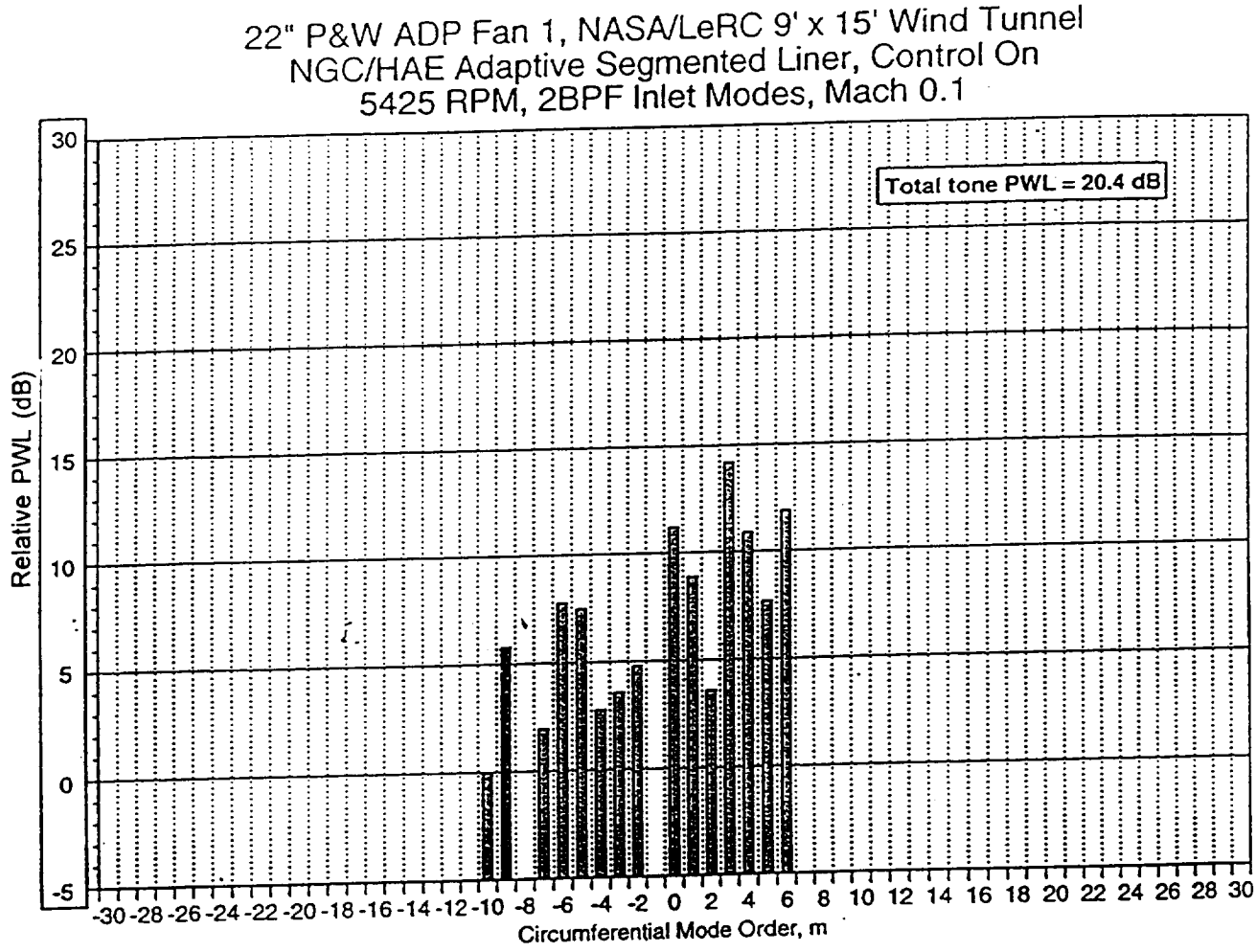

Figure 5.13b

Sum of Radial Mode Relative Sound Powers in Circumferential Modes in ADP Fan Inlet with NGC/HAE Adaptive Segmented Liner, Control On

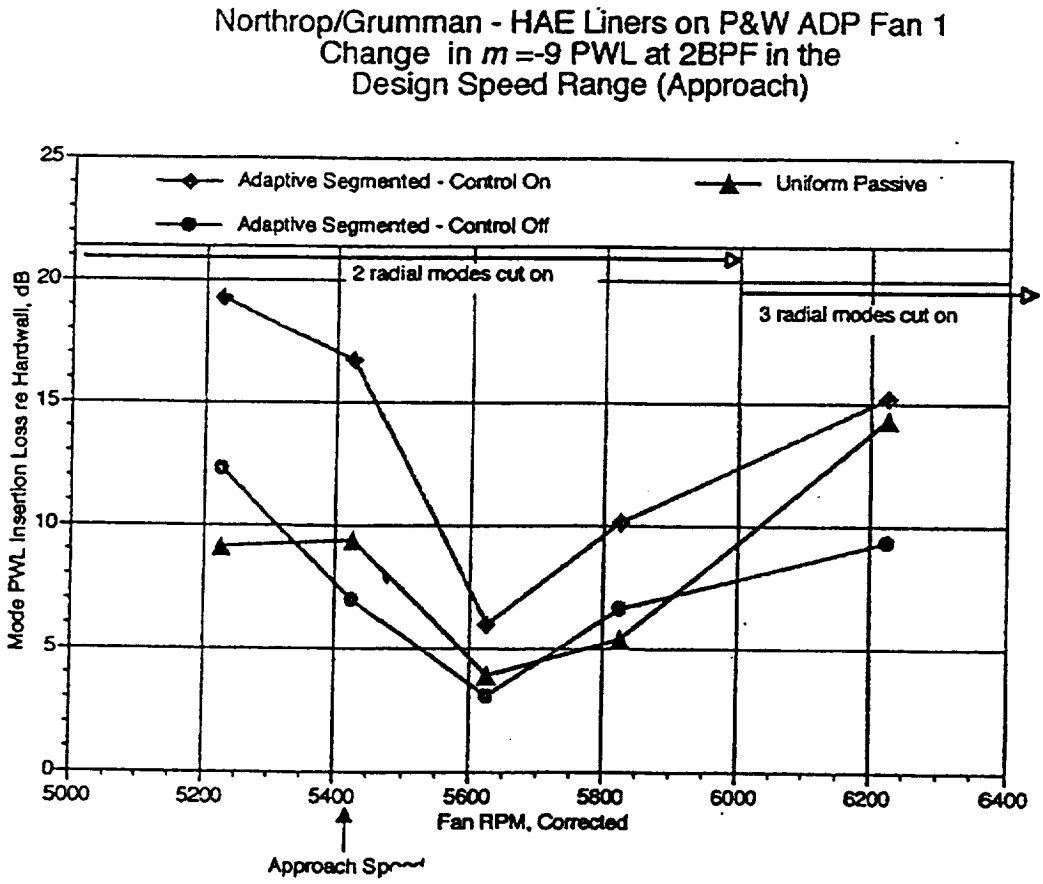

Figure 5.14
Circumferential Mode m=-9 Sound Power Reduction by Uniform Passive, Adaptive Segmented (Control Off) and Adaptive Segmented (Control On) Liners in P&W 22 Inch ADP Fan in NASA LeRC 9 x 15 Wind Tunnel at Mach 0.1 in the Design (Approach) Speed Range

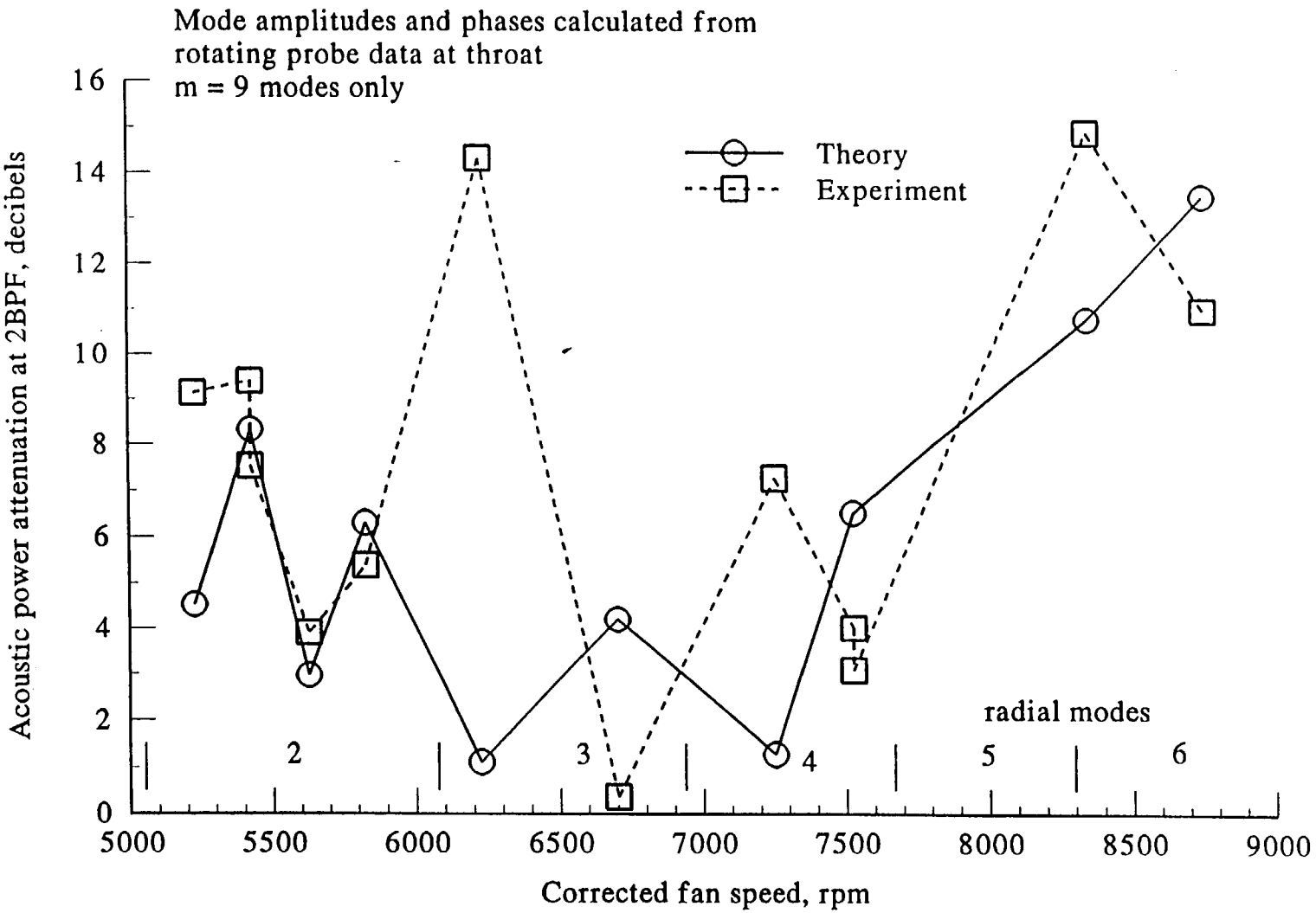

Figure 5.15. Calculated and experimental attenuation of uniform passive acoustic liner ADP1 (NSL96001) at 2BPF, NASA ADP fan, 18 blades, 45 vanes

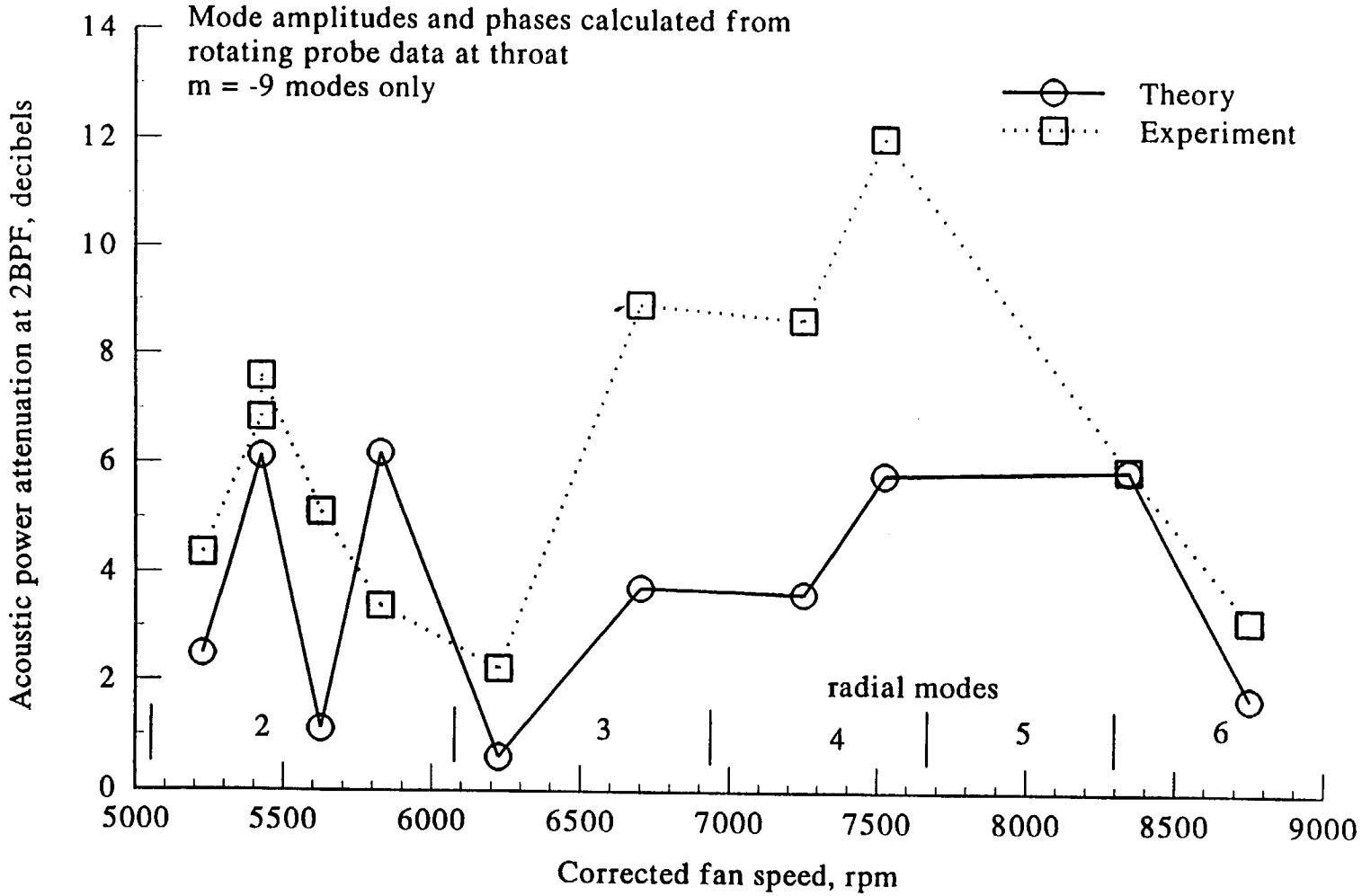

Figure 5.16. Calculated and experimental attenuation of segmented passive acoustic liner ADP2 (NSL96002) at 2BPF, NASA ADP fan, 18 blades, 45 vanes

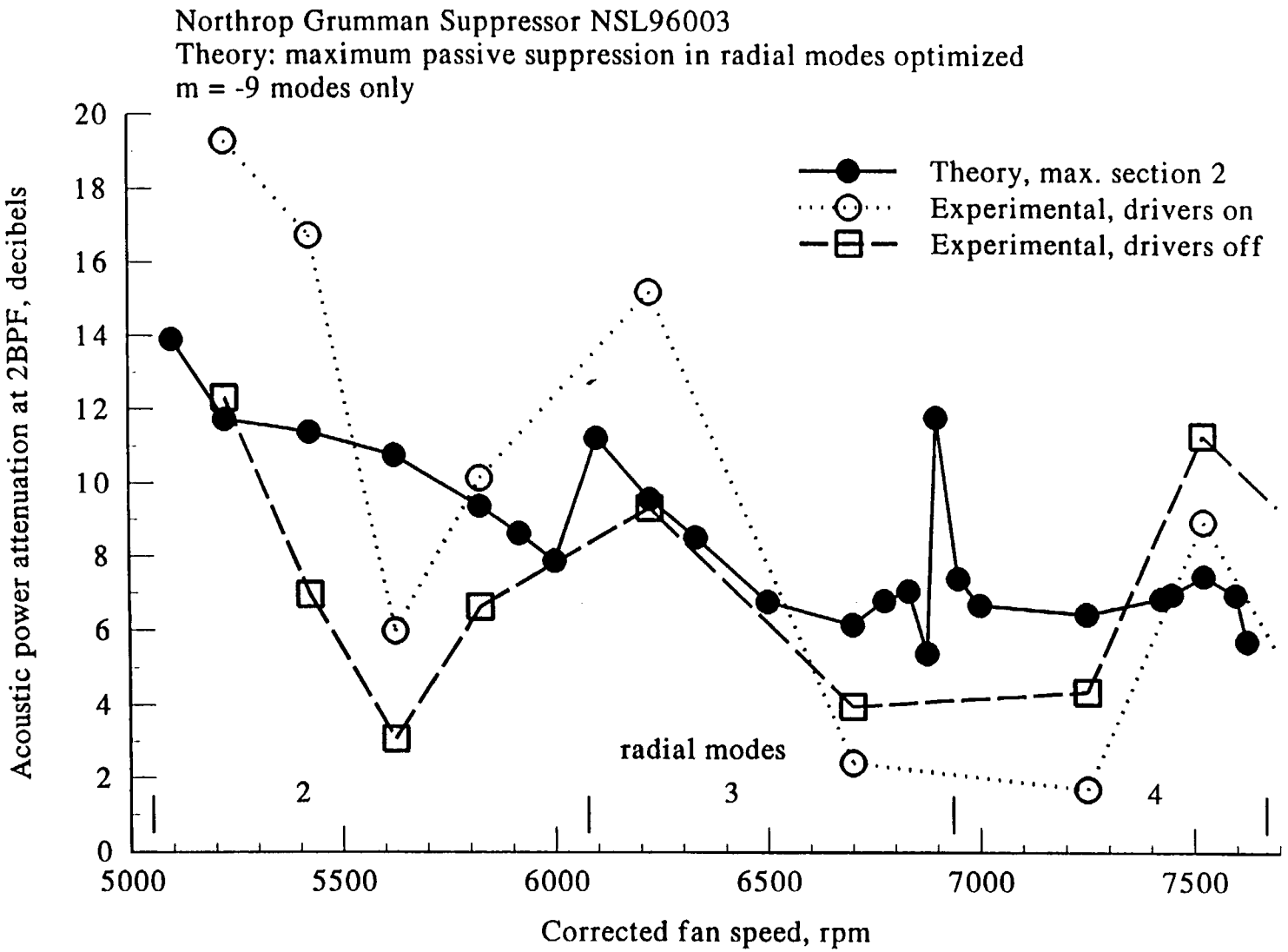

Figure 5.17. Calculated and experimental attenuation of hybrid active-passive liner ADP3, 2BPF, NASA ADP fan, 18 blades, 45 vanes

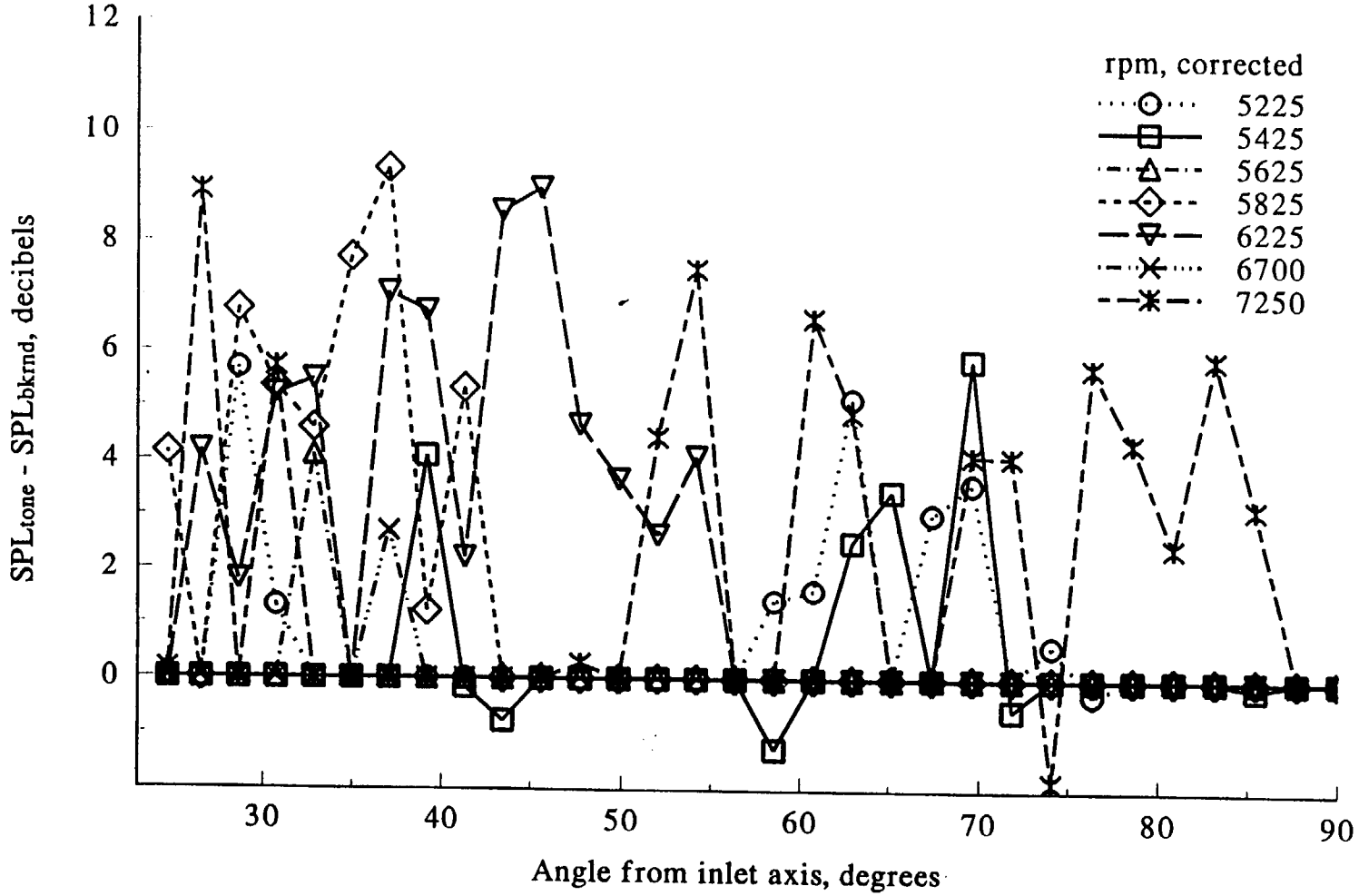

Figure 5.18. Tone protrusion above background, ADP hard wall inlet, 2BPF far-field 9X15 Wind Tunnel tests, aft barrier in place

Appendix

A – REVIEW OF ACTIVE HELMHOLTZ RESONATOR CONCEPT

Combining the recently developed active control Helmholtz resonator concept with advanced broadband passive liner design technology represents the "heart" of the research program. The active control Helmholtz resonator concept is briefly described below to assist the reader in understanding its application to the hybrid liner concept. This is followed by two demonstrations of the concept to provide broadband control of sound in impedance tube and side-branch applications.

A-1 Basic Concept

Consider the Helmholtz resonator shown schematically in Figure A.1. A loudspeaker (or other suitable sound source) is connected to the interior of the active control resonator cavity. The (adiabatic) fluctuations of fluid density within the cavity interior are generated from the two independent sources, one generated by the incident sound field (within the resonator orifice) and the other by the cavity speaker (i.e., the active control sound source). The active control generated interior oscillating volume flow interacts with the acoustic velocity within the orifice to control the resonator impedance. The idea here is that since the impedance of a Helmholtz resonator is defined as the (complex) ratio of the sound pressure incident to its orifice to the average acoustic velocity within its orifice, controlling the acoustic velocity within the orifice (with an independent active control sound source) controls the resonator impedance.

Referring to Figure A.1, the mass of fluid within and surrounding the orifice is assumed to move as a solid mass, the so-called "lumped element" model. Although the "lumped element" model is known to be correct only for very weak incident sound fields, it does, nonetheless, permit a simple explanation of the active control concept.

The motion of the "lumped element" fluid is predicted, using Newton's Second Law,

$$\rho_0 d_e S_0 \ddot{\xi}_0 = \left(P_{inc} - P_{cav}\right) S_0 e^{i\omega t} - R_0 S_0 \dot{\xi}_0 \qquad \text{(A1)}$$

where d_e represents the effective length of the lumped element mass, R_0 the orifice resistive losses, So the orifice cross-sectional area, S_w the orifice wetted area, P_{cav} the resonator cavity acoustic pressure, P_{inc} the incident sound pressure and ξ_o the displacement of the "lumped element" mass from equilibrium.

The cavity pressure P_{cav} is calculated using the following adiabatic connection between oscillating pressure and density within the cavity,

$$P_{cav} = \rho_0 c_0^2 \left(\frac{\xi_0 S_0 + Q_a}{V_{cav}} \right); \qquad Q_a = \left|Q_a\right| e^{i\varphi_a} \qquad \text{(A2)}$$

where $\xi_o S_o$ and Q_a represent orifice and active control driven volumetric displacements respectively and V_{cav} is the cavity volume. It is important to understand that Q_a as used in Eq. (A2) is complex. It will be shown below that

this plays an essential role in the control of resonator impedance and hence absorption.

Substituting Eq. (A2) into Eq. (A1) and solving for the resonator impedance Z yields,

$$\frac{Z}{\rho_0 c_0} = \frac{P_{inc}}{\rho_0 c_0 \sigma \xi_0} = \frac{\frac{R_0}{\rho_0 c_0 \sigma} + i\frac{\omega d_e}{\alpha c_0}\left[1-\left(\frac{\omega_{res}}{\omega}\right)^2\right]}{\left[1-\frac{\rho_0 \omega d_e\left(\frac{\omega_{res}}{\omega}\right)^2\left|\frac{Q_a}{S_0}\right|\cos(\varphi_a)}{P_{inc}}\right]-i\left[\frac{\rho_0 \omega d_e\left(\frac{\omega_{res}}{\omega}\right)^2\left|\frac{Q_a}{S_0}\right|\sin(\varphi_a)}{P_{inc}}\right]} \qquad \text{(A3)}$$

Equation (A3) is interpreted as follows. Since Q_a is complex, the active control volume source provides two "free" parameters $|Q_a|$ and ϕ_a (relative phase between the "lumped element" and active control fluctuating volume flows) which can be used to generate desired values of resistance and reactance as a function of the incident sound pressure

A-2 Experimental Validation of the Active Resonator Concept

An experimental program was undertaken to verify the scheme of injecting acoustic energy into the cavity of Helmholtz resonators to control their impedance over wide frequency ranges above and below their natural or tuned frequencies. Two experiments were conducted, one to provide anechoic termination in an impedance tube application and the other to provide a null or zero impedance in a side-branch application.

A-2.1 Anechoic Termination Demonstration

Figure A2 is a schematic of the test set-up and data acquisition and reduction scheme used in an impedance tube test to demonstrate the active control resonator concept. A Helmholtz resonator was attached to one end of an impedance tube and a primary sound source at the opposite end. An active control sound source was connected to the resonator cavity as shown. The open-loop scheme shown schematically in Figure A2 was used to vary the impedance of the Helmholtz resonator. The signals from the two microphones used to calculate the incident and reflected sound waves were read by the data acquisition system of a MassComp 5400 minicomputer, Fourier decomposed to determine amplitude and phase and then processed algebraically to determine the acoustic absorption coefficient.

If one-dimensional sound is generated within the impedance tube, then the following theoretical estimate of the fraction of incident sound energy α absorbed by the resonator can be derived,

$$\alpha \equiv 1-\frac{\left(\frac{R}{\rho_0 c_0}-1\right)^2+\left(\frac{X}{\rho_0 c_0}\right)^2}{\left(\frac{R}{\rho_0 c_0}+1\right)^2+\left(\frac{X}{\rho_0 c_0}\right)^2} \qquad \text{(A4)}$$

The computer code then adjusts the amplitude and phase of the cavity speaker until α is maximized. It follows from Eq. (A4) that maximum absorption (i.e., $\alpha = 1$) occurs when

$$\frac{R}{\rho_0 c_0} = 1; \qquad \frac{X}{\rho_0 c_0} = 0 \qquad \text{(A5a,b)}$$

Referring to Eq. (A3), the amplitude and phase of the active control fluctuating volume sound source Q_a provides the two "free" parameters to satisfy Eq. (A5a,b). The required amplitude and phase generated from the active control sound source can be determined from Eq. (A3) and Eq. (A5). In practical applications, however, this is accomplished experimentally as discussed below.

Figure A3 displays the measured normal incident absorption coefficient with and without active control. Note that except near resonance (260 Hz), the non-controlled absorption coefficient is very small. With near optimized control applied to the cavity source, the absorption coefficient exceeded 99% (i.e., greater than 20 dB) over a wide frequency range. Although it is difficult to see from Figure A3, some of the measured absorption coefficient were larger than 0.999 which corresponds to over 30 dB absorption. It is important to understand, however, that the amplitude and phase of the active control sound energy introduced into the cavity must be very accurately controlled to achieve $\alpha > 0.999$.

Referring to Figure A3, observe that efficient absorption was achieved with active control over a bandwidth extending from approximately 200 - 760 Hz, a ratio of 3.8. The important point to be made here in terms of the objectives of this study is that the above tests were not designed to maximize absorption bandwidth in terms of maximum/minimum operational frequency ranges. The low frequency range was limited by the low frequency performance of the particular active control speaker used in the tests and the high frequency range was limited by restricting the sound field in the impedance tube to be plane-wave. Thus the bandwidth test results displayed in Figure A3 were not caused by limitations of the active control scheme - only imposed by operational constraints.

The following discussion explains how active controlled Helmholtz resonators achieve efficient broadband sound absorption. A properly designed passive Helmholtz resonator efficiently absorbs sound at its tuned or resonant frequency because its reactance vanishes. At frequencies very much higher than its tuned frequency, the impedance of a resonator is controlled by large positive inertial reactance which caused the resonator to reflect much of the incident sound and hence absorb poorly. Conversely, at very low frequencies, the resonator impedance is controlled by very large negative stiffness reactance and hence also absorbs poorly. The active controlled resonator introduces a secondary sound field into its cavity having the proper amplitude and phase to cancel or null the resonator reactance regardless of the frequency of the incident sound field. Further, the active control system can

also adjust the resistance of the resonator to achieve efficient sound absorption.

To summarize, the active control resonator achieved excellent sound absorption over the entire frequency range tested - thus behaving as a highly efficient broadband sound absorber! These results are both remarkable and very important because they demonstrate the practicality of applying active control to Helmholtz resonators.

A-2.2 Side-Branch Demonstration

The second application assumes that a Helmholtz resonator is installed on one side of a duct containing an ideal "ρc" termination at one end and a sound source at the opposite end as shown schematically in Figure A4. The interaction of incident sound (P_i) with the resonator generates reflected (P_r) and transmitted (P_t) sound pressure fields. Assuming one-dimensional sound within the duct, the following expression can be derived for the transmitted acoustic energy coefficient (α_t) in terms of the resonator impedance,

$$\alpha_t = \frac{\left[2R_{res}(1+2R_{res}) + 4X_{res}^2\right]^2 + 4X_{res}^2}{\left[(1+2R_{res})^2 + 4X_{res}^2\right]} \qquad \text{(A6)}$$

Equation (6) shows that when the side branch resonator impedance vanishes, all of the incident sound energy is reflected back towards the source and none is transmitted past the side branch resonator. Thus, the desired impedance of the side-branch resonator is

$$R_{RES} = X_{RES} = 0 \qquad \text{(A7a,b)}$$

- Figure A4 is a schematic of the basic experimental setup of the active resonator side-branch application. The setup is similar to the anechoic termination setup with the following exceptions:
- The signals from microphones 1 and 2 signals were processed by an on-line network to separate direct and reflected signal components.
- The active resonator was relocated to the side of the duct and an anechoic termination wedge made of Kevlar was installed at the end of the duct.
- An additional microphone was placed between the resonator and the anechoic wedge to measure the transmitted sound wave.

Figure A5 displays the sound energy transmission loss measured with and without active control applied to the resonator. Note that in the absence of active control, the transmission loss is near zero for all frequencies except at its natural or tuned frequency of 820 Hz where a sound energy transmission loss of about 24 dB was measured. Using the active control system to optimize the amplitude and phase of the sound field injected into the resonator cavity, sound energy transmission losses below 40 dB were achieved over the frequency range 100 - 650 Hz, a 6.5 ratio!

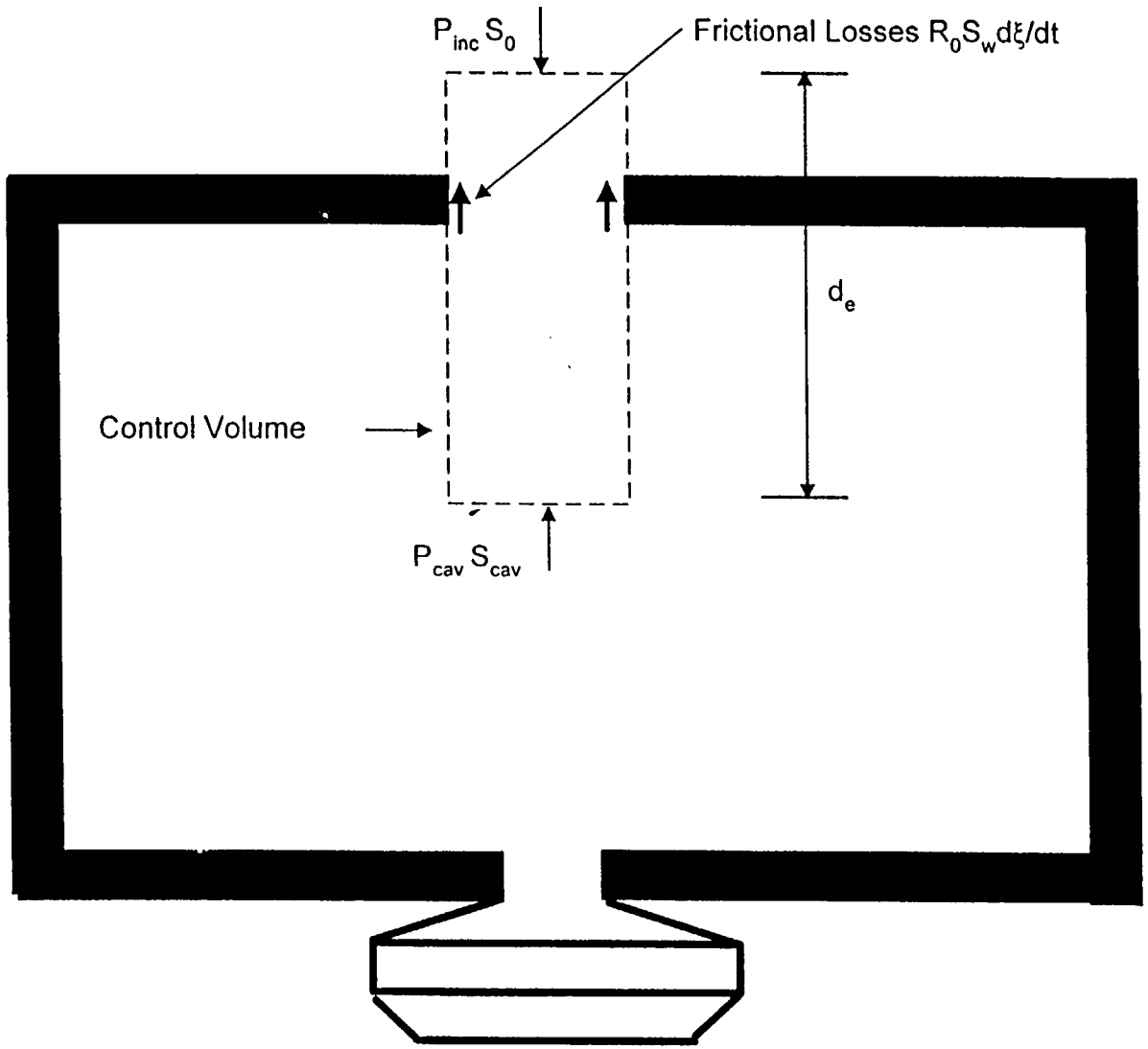

Figure A1. Control Volume Used in Model Derivation of Active Control Helmholtz Resonator Concept

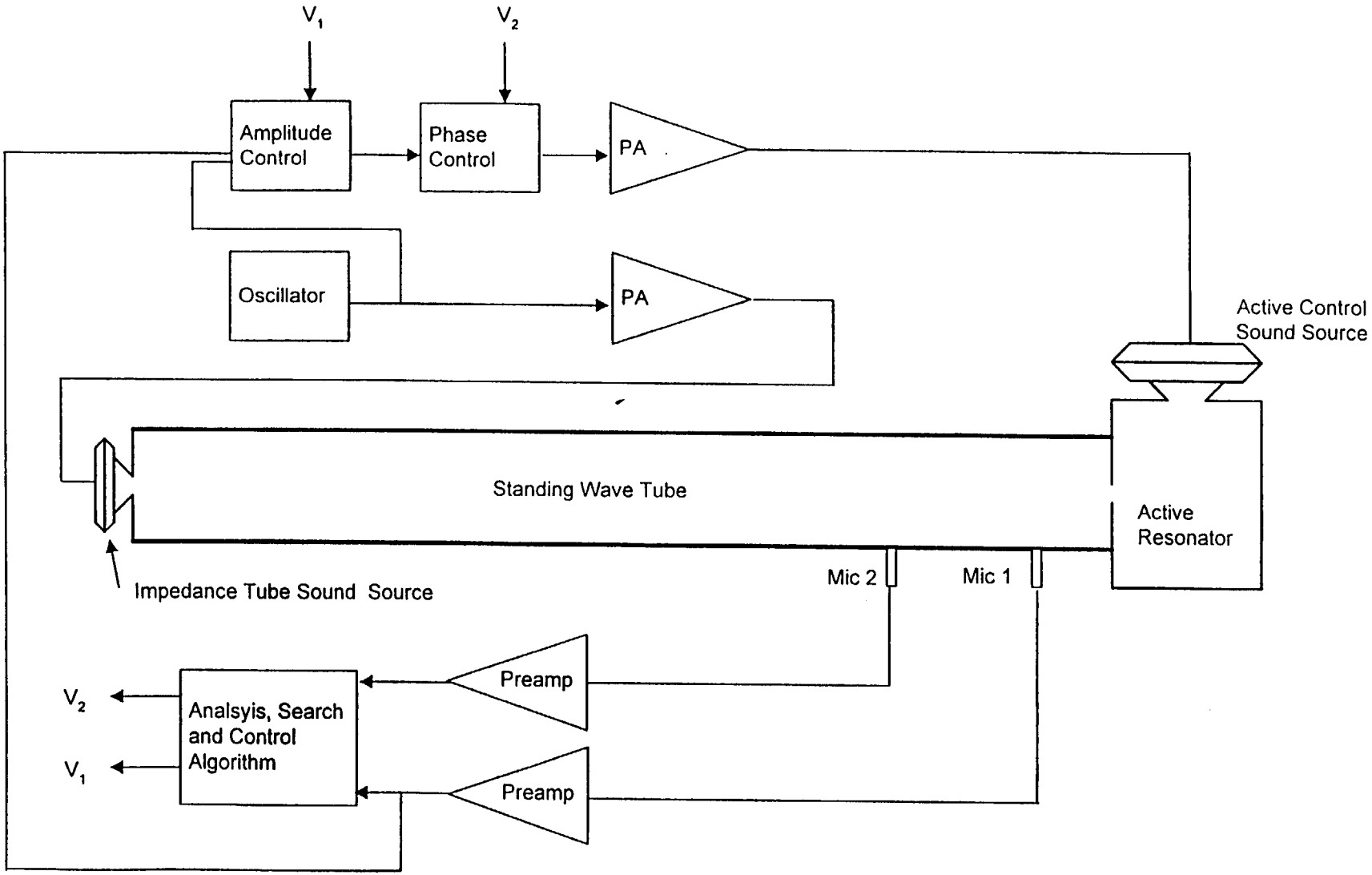

Figure A2. Schematic Diagram of Active Control Resonator Calibration Experiment

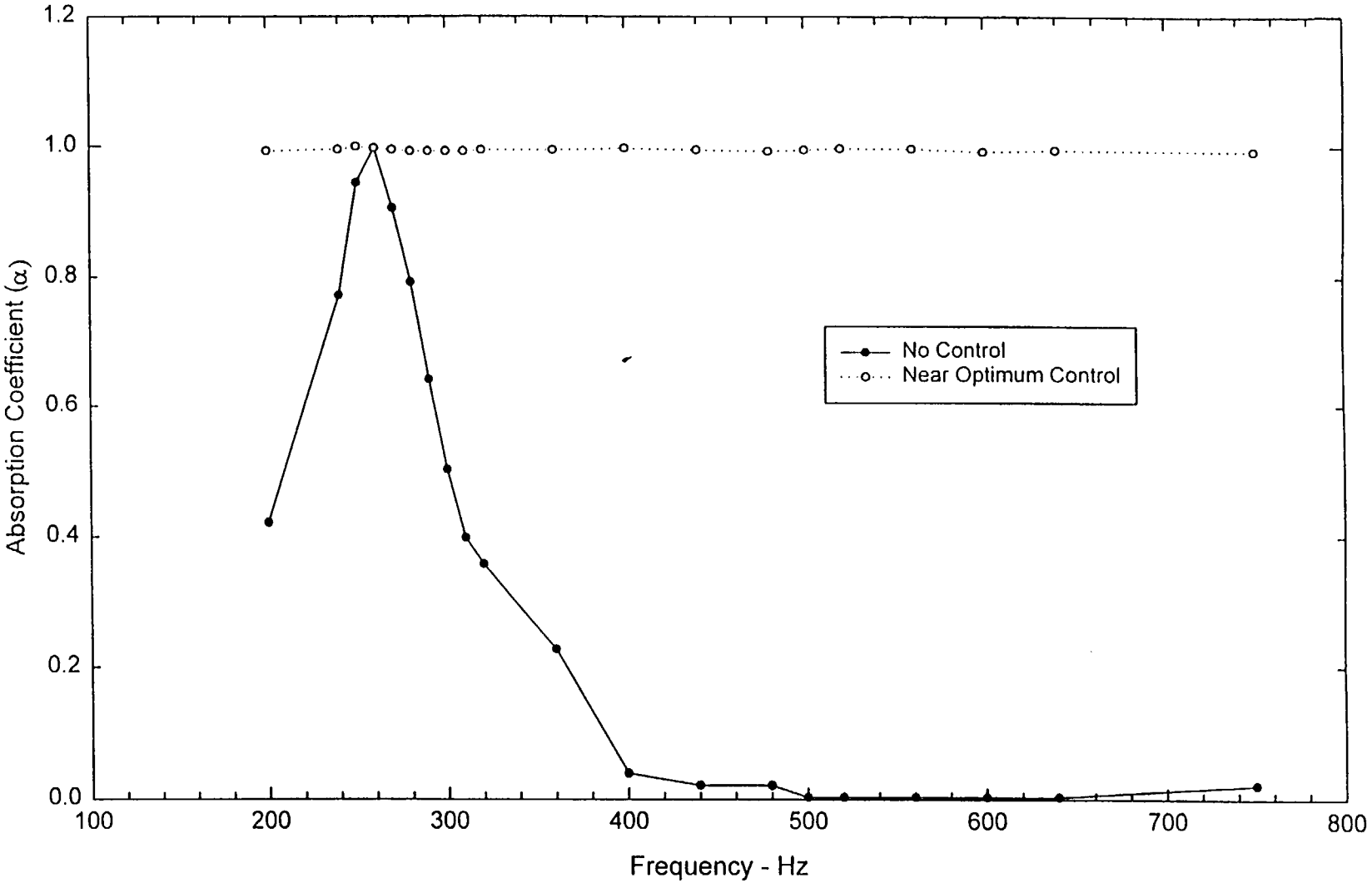

Figure A3. Absorption Coefficient Performance Improvement Achieved with Active Control Resonator

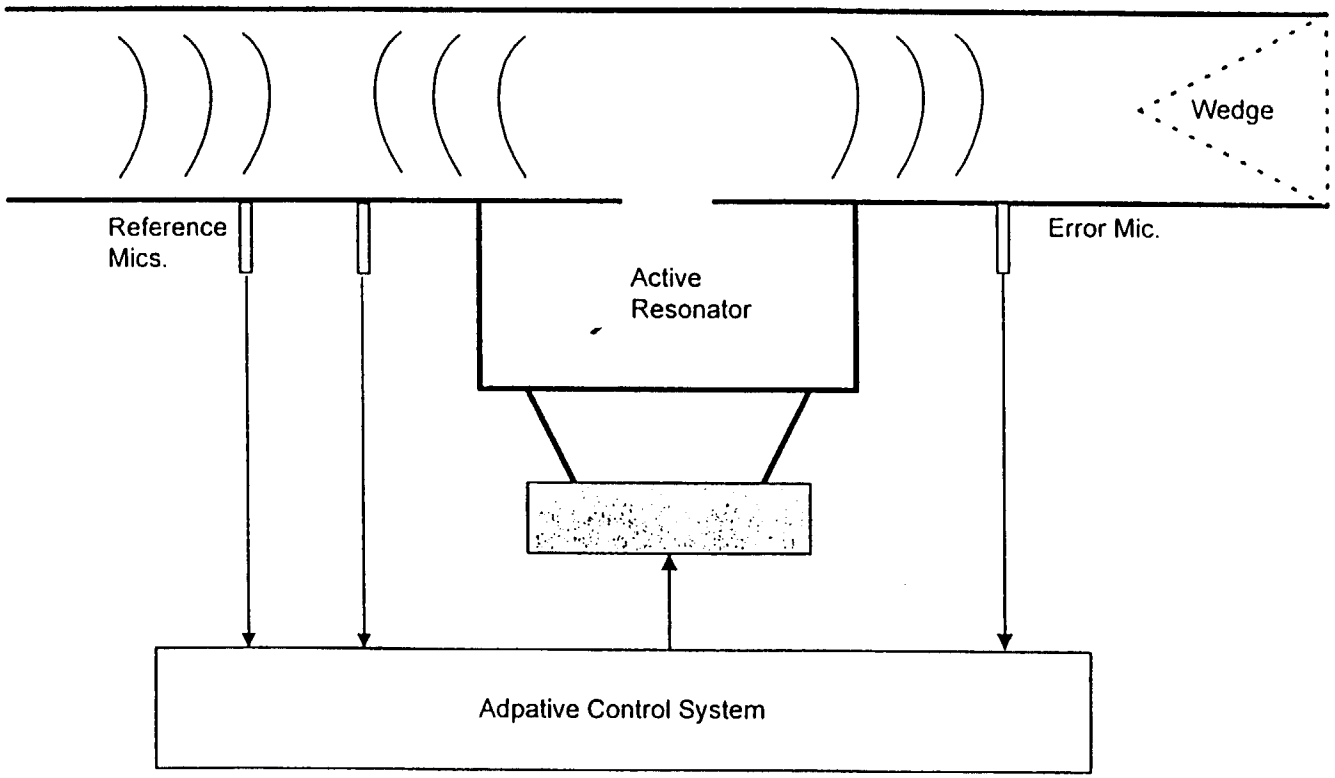

Figure A4. Schematic of Active Resonator Side-Branch Attenuation Test Setup

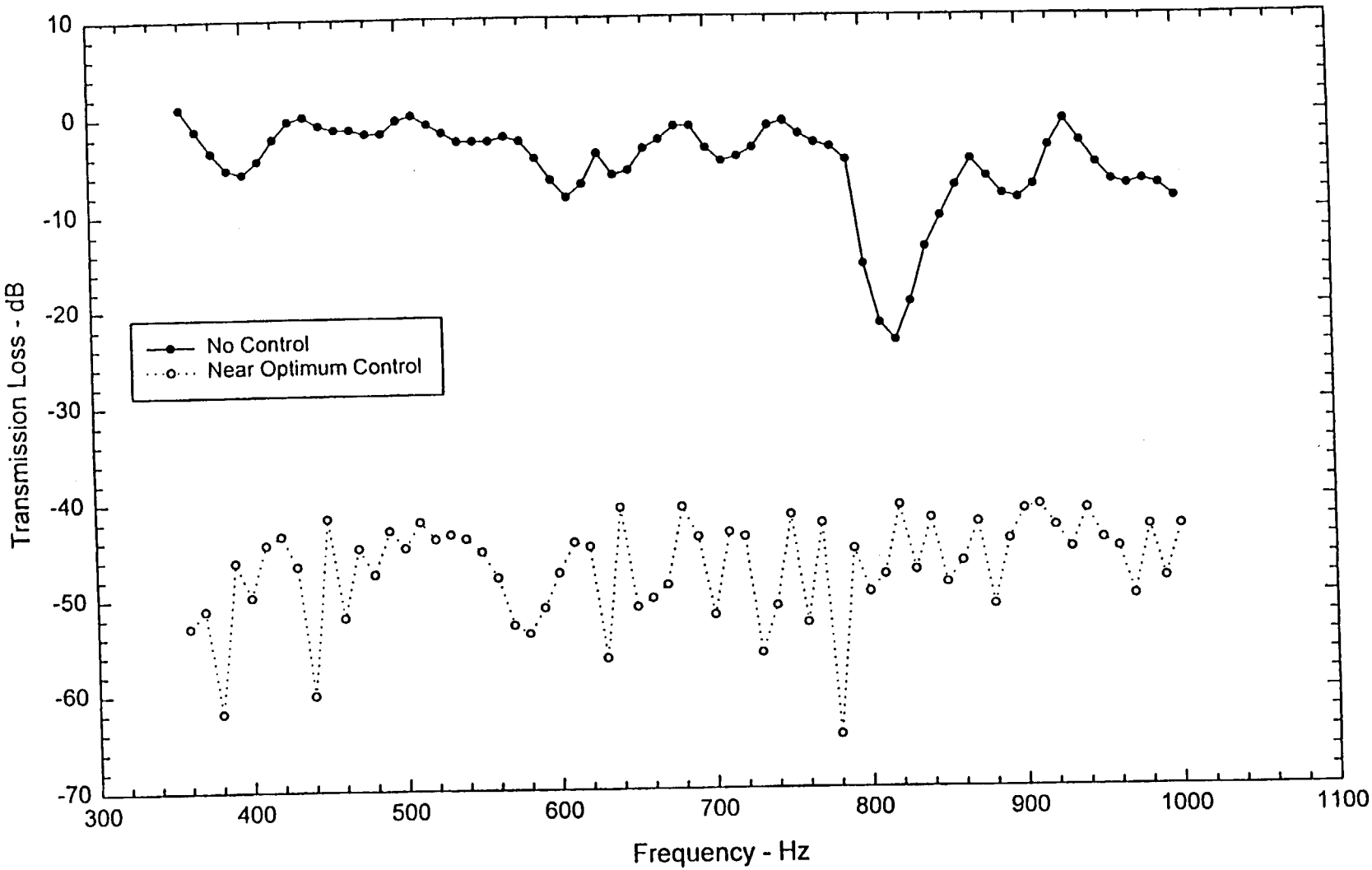

Figure A5. Transmission Loss Performance Improvement Achieved with Side Branch Active Control Resonator

REPORT DOCUMENTATION PAGE

Form Approved
OMB No. 0704-0188

1. AGENCY USE ONLY (*Leave blank*)	2. REPORT DATE	3. REPORT TYPE AND DATES COVERED
	February 1999	Final Contractor Report

4. TITLE AND SUBTITLE

Hybrid Active/Passive Jet Engine Noises Suppression System

5. FUNDING NUMBERS

WU–538–03–11–00
NCC3–379

6. AUTHOR(S)

C.A. Parente, N. Arcas, B.E. Walker, A.S. Hersh, and E.J. Rice

7. PERFORMING ORGANIZATION NAME(S) AND ADDRESS(ES)

Northrop Grumman Corporation
Advanced Systems & Technology
S. Oyster Bay Road
Bethpage, New York 11714

8. PERFORMING ORGANIZATION REPORT NUMBER

E–11570

9. SPONSORING/MONITORING AGENCY NAME(S) AND ADDRESS(ES)

National Aeronautics and Space Administration
Lewis Research Center
Cleveland, Ohio 44135–3191

10. SPONSORING/MONITORING AGENCY REPORT NUMBER

NASA CR—1999-208875
NSL–RPT–98–002

11. SUPPLEMENTARY NOTES

C.A. Parente and N. Arcas, Northrop Grumman Corporation, Bethpage, New York; B.E. Walker and A.S. Hersh, Hersh Acoustical Engineering, Inc., Westlake Village, California; E.J. Rice, E.J. Rice Consulting, Westlake, Ohio. Project Manager, Dennis L. Huff, NASA Lewis Research Center, organization code 5940, (216) 433–3913.

12a. DISTRIBUTION/AVAILABILITY STATEMENT

Unclassified - Unlimited
Subject Category: 71 Distribution: Nonstandard

This publication is available from the NASA Center for AeroSpace Information, (301) 621–0390.

12b. DISTRIBUTION CODE

13. ABSTRACT (*Maximum 200 words*)

A novel *adaptive segmented* liner concept has been developed that employs active control elements to modify the in-duct sound field to enhance the tone-suppressing performance of passive liner elements. This could potentially allow engine designs that inherently produce more tone noise but less broadband noise, or could allow passive liner designs to more optimally address high frequency broadband noise. A proof-of-concept validation program was undertaken, consisting of the development of an adaptive segmented liner that would maximize attenuation of two radial modes in a circular or annular duct. The liner consisted of a leading active segment with dual annuli of axially spaced active Helmholtz resonators, followed by an optimized passive liner and then an array of sensing microphones. Three successively complex versions of the adaptive liner were constructed and their performances tested relative to the performance of optimized uniform passive and segmented passive liners. The salient results of the tests were: *The adaptive segmented liner performed well in a high flow speed model fan inlet environment, was successfully scaled to a high sound frequency and successfully attenuated three radial modes using sensor and active resonator arrays that were designed for a two mode, lower frequency environment.*

14. SUBJECT TERMS	15. NUMBER OF PAGES
Acoustics; Fan noise; Active noise control; Turbomachinery	166
	16. PRICE CODE: A09

17. SECURITY CLASSIFICATION OF REPORT	18. SECURITY CLASSIFICATION OF THIS PAGE	19. SECURITY CLASSIFICATION OF ABSTRACT	20. LIMITATION OF ABSTRACT
Unclassified	Unclassified	Unclassified	